2015

# Mitigation of liquefaction hazards using the combined biodesaturation and bioclogging method

Shifan Wu
*Iowa State University*

# Mitigation of liquefaction hazards using the combined biodesaturation and bioclogging method

by

**Shifan Wu**

A dissertation submitted to the graduate faculty

in partial fulfillment of the requirements for the degree of

DOCTOR OF PHILOSOPHY

Major: Civil Engineering (Geotechnical Engineering)

Program of Study Committee:
Jian Chu, Major Professor
James Alleman
Jeramy Ashlock
David White
Thomas Loynachan

Iowa State University

Ames, Iowa

2015

# TABLE OF CONTENTS

# LIST OF FIGURES

# LIST OF TABLES

# ACKNOWLEDGMENTS

I would like to express my greatest gratitude and appreciation to my advisor Dr. Jian Chu for his inspiration, patience and kindly guidance throughout the research work. His passion and wisdom inspired me not only within academic area, but also in daily life. Without his continuous support and constructive suggestions, this research would not have been possible.

I would like to thank my PhD program committee, Dr. James Alleman, Dr. Jeramy Ashlock, Dr. David White and Dr. Thomas Loynachan for their valuable advices and guidance through this research. I would also like to thank Dr. Volodymyr Ivanov for his helpful advices on microbiology studies in the research.

I would like to extend my thanks to Mr. Bruce Erikson and Mr. Bill Halterman from Iowa State machine shop for fabricating testing models. Assistance from Dr. Warren Straszheim for scanning electron microscope test is appreciated.

My thanks goes to all my friends and colleagues at the Iowa State University and Nanyang Technological University. I would like to acknowledge Dr. Jia He, Dr. Bing Li, Dr. Guanghui Meng, Mr. Seth Hansen for their suggestions and help on laboratory tests.

Finally, I would like to express my deepest appreciation and love to my parents. Their endless encouragement and support provided me the power and energy to finish my study.

# ABSTRACT

Conventional soil improvement methods for mitigation of liquefaction can be costly for large-scale applications. A study to establish a more cost-effective method for mitigation of liquefaction hazard is presented in this thesis. The so-called "combined biodesaturation and bioclogging method" is to produce biogas ($N_2$) in sand to reduce the degree of saturation of sand and sustain the desaturation by immobilizing the gas bubbles through bioclogging. The biogas is produced via a denitrification process and bioclogging is from a microbial induced calcium carbonate precipitation (MICP) process. Shaking table model testing results indicate that as the degree of saturation reduces to less than 90 percent, the generation of pore pressure and potential to liquefaction is largely contained. This phenomenon is also observed in the triaxial compression test. Seepage flow in sand may lead to the mobilization of biogas bubbles in sand. Introduction of a weak bioclogging effect may reduce considerably the tendency for gas bubbles to be displaced. Permeability measured using the sand column tests indicate that when the bioclogging is applied together with the biogas method, gas bubbles generated in sand can sustain for the whole testing duration under a seepage flow. CT images illustrate that gas bubbles are either in the single bubble form or in the form of gas pocket with small gas bubbles aggregating together. SEM images reveal that for sand with low calcium carbonate content produced through the bioclogging method, majority of the calcite precipitation is formed as a single crystal on the surface of sand grain.

# CHAPTER 1

# INTRODUCTION

## 1.1 Background and Motivation

Earthquakes are one of the most devastating natural disasters on earth. The damage caused by earthquakes include the loss of human lives, destructions to various infrastructures such as buildings, bridges, transportation facilities, pipelines, and etc. According to the US Geological Survey for the years from 2000 to 2011, there has been an average of 66, 000 deaths per year due to earthquakes globally (USGS 2013). Among the many effects of earthquakes, liquefaction is one of the most catastrophic geo-hazards. The rapid cyclic loading produced by an earthquake causes the pore pressure to rise more quickly than it can be dissipated, and reduces the effective stress applied to a soil deposit. Once the effective stress approaches zero, the ability of the soil to resist shear loading is lost, resulting in significant soil deformations thus triggering the complete failure of the soil.

As liquefaction normally takes place over a large area, the scale of mitigation works for liquefaction must be extensive. Conventional techniques usually are not cost-effective on a large scale. It is necessary to develop methods for liquefaction mitigation to be effective as well as economical for large area applications.

It has been observed that a certain range of gas bubbles present in sand leads to an increase of shear strength in cyclic triaxial test (Martin *et al*. 1975; Sherif *et al*. 1977; Yoshimi *et al*. 1989; Xia and Hu 1991). This phenomena inspired researchers exploring the potential of using desaturation method which turns saturated sand into partially saturated

sand as a means to enhance its resistance to liquefaction (Yang *et al*. 2004; Okamura *et al*. 2006; Okamura and Soga 2006; Yegian *et al*. 2007; He *et al*. 2013).

A biogas-desaturation method is developed in this study as a liquefaction mitigation approach. In this method, the microbial denitrification process is adopted to generate nitrogen gas bubbles in sand grains to reduce the degree of saturation of the originally fully saturated sand and thus increase its resistance against liquefaction. Embracing microbial technology in geotechnical engineering is one of cutting edge research topics in recent years (Mitchell and Santamarina 2005; Ivanov and Chu 2008; DeJong *et al*. 2013). The rapid development of bio-mediated soil improvement methods over the last decade has generated exciting advances in geotechnology. Microbial Induced Calcite Precipitation (MICP) has evidently been the primary focus of efforts to employ biogeotechnical technology to date (Whiffin *et al*. 2007; van Paassen 2009; DeJong *et al*. 2010; Harkes *et al*. 2010; Chu *et al*. 2012). Enzymatic hydrolysis of urea by microbes is one of the most energy efficient MICP process. A new study has also found that denitrification is also beneficial for the suitability and sustainability of the MICP process since the denitrifying organisms gain energy from the catabolic reaction while producing $CaCO_3$ (van Paassen *et al*. 2010). Usually a MICP process involves a large quantity of calcium source to produce a considerable amount of calcium carbonate as binding bridges between sand grains to increase shear strength. However, such a resource consuming approach is not a sustainable strategy for liquefaction mitigation alone. In this research, a reduced usage of MICP process which named as bioclogging for mainly reducing the permeability of sand is developed. An attempt to integrate the biogas and bioclogging process is also investigated in this study.

## 1.2 Objectives

The objectives of this study are:

1) To better understand the mechanism of liquefaction and investigate the potential of applying microbial geotechnologies for mitigating liquefaction hazard.

2) To study the mechanisms of biogas desaturation and bioclogging method and their effects on sand engineering properties.

3) To develop a combined biogas desaturation method that incorporates both denitrification and microbial bioclogging process through laboratory experiments.

4) To investigate the distribution and sustainability of biogas bubbles in sand under various seepage flow conditions. Explore the potential of increased biogas bubble stability by using the bioclogging method.

5) To evaluate the effectiveness of the combined biogas desaturation method for liquefaction mitigation through analyzing seismic responses of biogas desaturated sand.

## 1.3 Scope of Research

The scope of research is listed as follows

1) Cultivate denitrifying bacteria in conditions that favor the denitrification process in sand. Adopt centrifuging and freeze dried technique in a large quantity fermentation process to cultivate urease-producing bacteria (UPB) for bioclogging.

2) Conduct biogas generation and biocementation tests to examine the effectiveness of microbial activities in sand.

3) Set up sand column tests to investigate the sustainability of biogas trapped in sand with presence of the seepage flow.

4) Investigate microscopic characteristics of biogas and bioclogging treated sand specimens through computer tomography (CT) and scanning electron microscope (SEM) techniques.

5) Design and fabricate a fully-instrumented laminar box and shaking table testing system to conduct a series of model tests on biogas desaturated sand samples with different degrees of saturation and relative densities.

6) Use the denitrification process to produce nitrogen gas and de-saturate loose and medium dense triaxial sand specimens. Carry out monotonic compression tests to study the undrained shear behavior of biogas desaturated sand.

## 1.4 Outline of Dissertation

This dissertation is comprised of seven chapters. Chapter 2 is a literature review on liquefaction studies including the liquefaction mechanism and approaches for liquefaction mitigation. The application of microbial techniques in geotechnical engineering is another focus in the review. The potential improvement of engineering properties of granular soil brought by microbial techniques is also introduced. A preliminary study on biogas and bioclogging process and cultivation of microbes is presented in Chapter 3. Chapter 4 investigates biogas stability and microscopic characteristics of sand treated with the bioclogging method. Chapter 5 covers a series of model tests using a fully instrumented laminar box and shaking table testing system to study seismic response of biogas desaturated

sand. Chapter 6 discusses the undrained shear behavior of biogas desaturated sand by performing monotonic compression tests. The conclusions and recommendations for future studies are presented in Chapter 7.

# CHAPTER 2

# LITERATURE REVIEW

## 2.1 Introduction

This chapter reviews three major research topics. One is the development of the study on soil liquefaction susceptibility and its countermeasures. The second one relates to the newly emerged microbial geotechnologies and their processes and applications. The last part is a brief introduction of soil engineering properties and its potential improvement through bio-geotechnical processes.

## 2.2 Liquefaction Susceptibility and Mitigation Methods

Soil liquefaction is a major concern for structures and engineering activities on liquefiable soils. The phenomenon has been recognized for a long period. The progress of work on soil liquefaction has been described in detail in a series of state-of-art reports or technical papers, such as Yoshimi *et al*. (1978), Finn (1981), Iwasaki (1986), Ishihara (1993), Robertson and Fear (1995), and Youd *et al*. (2001).

### 2.2.1 Liquefaction terminology

The term soil liquefaction is commonly used to define a condition in which a saturated cohesionless soil is transformed from a solid state into a liquid state by static or cyclic loading. Terzaghi and Peck (1948) proposed a concept of "spontaneous liquefaction" to indicate a sudden state change of soil deposits in the early development stage of soil

mechanics. It was not until 1960s that the problem of liquefaction started attracting engineering concerns. The 1964 Niigata earthquake can be cited symbolically as the first event in the world where all kinds of modern infrastructure were destroyed by what came to be well known later as soil liquefaction (Ishihara 1993). Since then, significant research focuses and resources have been heavily invested in topics concerning liquefaction. Studies include but are not limited to the mechanism of liquefaction, assessment of liquefaction potential, prevention or mitigation of liquefaction, consequence of liquefaction. Case history, cyclic shear tests, shaking model tests and numerical tests are some typical approaches adopted in liquefaction research. Castro (1969) defined liquefaction as the strain softening and collapse of loose sand to an ultimate state of constant effective stress and deformation. Robertson (1994) suggested liquefaction terminology based on the differing mechanisms of liquefaction. Two main groups are created to describe different liquefaction phenomena, flow liquefaction and cyclic mobility.

Flow liquefaction occurs when the static shear stress of the soil is greater than the shear strength of the soil in its liquefied state (Kramer 1996). It produces a large deformation under both monotonic loading and cyclic loading. In contrast of flow liquefaction, cyclic mobility occurs when the static shear stress is less than the shear strength of the liquefied soil. The deformation produced by the cyclic mobility is actually an accumulation of shear strain that developed during cyclic loading. Figure 2.1 displays the behavior of the flow liquefaction and cyclic mobility.

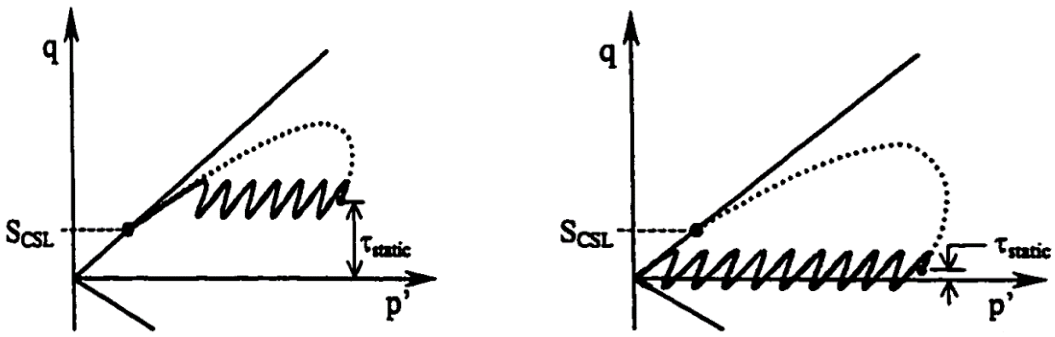


*Figure 2.1 Behavior of flow liquefaction and cyclic mobility (modified from Cho 2001)*

### 2.2.2 Liquefaction susceptibility assessment

Since the liquefaction poses a significant damage to a particular site, a complete evaluation of liquefaction hazards must be conducted. Not all soils are susceptible to liquefaction, the first step for researchers or engineers usually is to evaluate the liquefaction susceptibility. Considerable studies have been done for liquefaction susceptibility assessment and various criteria have been proposed to judge the liquefaction potential.

Youd and Hoose (1977) pointed out that the depositional environment, hydrological environment, and age of a soil deposit all contribute to its liquefaction susceptibility. Particle size, shape and gradation associated with high volume change potential are found to be related to high liquefaction susceptibility. Well-graded soils are generally less susceptible to liquefaction than poorly graded soils. Soils with rounded particle shapes are known to densify more easily than soils with angular grains. Consequently, they are usually more susceptible to liquefaction than angular-grained soils (Kramer 1996).

In addition to the criteria mentioned above, liquefaction susceptibility strongly depends on the initial state of the soil. One of the most important achievements for such

criteria is the finding of the "simplified method" or "simplified procedure". Seed and Idriss (1971) first proposed this concept and many researchers modified and improved it continuously until today. The simplified procedure was developed from empirical evaluation of field observations and field and laboratory test data. There are two major factors in the simplified procedure. One is the Cyclic Stress Ratio (CSR) induced by cyclic loading, for instance, by an earthquake or laboratory test drive. The other one is the Cyclic Resistance Ratio (CRR) from cyclic triaxial test or cyclic simple shear test. The comparison of CRR to CSR (factor of safety F) is employed to assess the liquefaction potential. Usually a factor of safety greater than unity means that the soil will not liquefy. Otherwise the soil is liable to develop liquefaction. The CSR is determined by the following equation

$$CSR = 0.65 \frac{a_{\max}}{g} \frac{\sigma_{v_0}}{\sigma'_{v_0}} \gamma_d \tag{2.1}$$

where $a_{max}$ is the peak horizontal acceleration at the ground surface during an earthquake; $g$ is gravitational acceleration; $\sigma_{v_0}$ and $\sigma'_{v_0}$ are total and effective overburden stress, respectively; $r_d$ is a stress reduction coefficient that is a function of depth. Based on the past research, Youd *et al* (2001) summarized a few methods to determine CRR, including laboratory cyclic triaxial test, CPT, SPT and geophysical methods.

Dobry *et al* (1982) modified the cyclic stress criterion and proposed the cyclic strain criterion based on the following equation

$$\gamma_c = 0.65 \frac{a_{\max}}{g} \frac{\sigma_v \gamma_d}{G_{\max} (G / G_{\max})_{\gamma_c}} \tag{2.2}$$

Comparing $\gamma_c$ with the threshold strain of the soil. If the $\gamma_c$ is smaller than the threshold strain, no liquefaction will occur. Otherwise, verify whether $\Delta u / \sigma_v^{'}$ equals to unity. If the excess pore pressure increase equals to current effective stress, the soil is liable to liquefaction due to the loss of shear resistance.

Thanks to the large quantity of laboratory and *in situ* data in the literature, it is possible for mapping methods to determine a site's liquefaction susceptibility. For example, as shown in Figure 2.2a, the steady state line can be used to distinguish liquefiable and non-liquefiable soil according to the initial void ratio and stress (Castro 1969; Casagrande 1971; Been and Jefferies 1985; Poulos *et al*. 1985). Another criterion benefits from *in situ* data collection is the back analysis method (Seed 1979; Seed *et al*. 1983; Robertson *et al*. 1995). By using *in situ* measurement data from CPT or SPT, engineers are able to judge the liquefaction susceptibility of the current site because the liquefaction often recurs at locations where soil and groundwater conditions have remained unchanged.

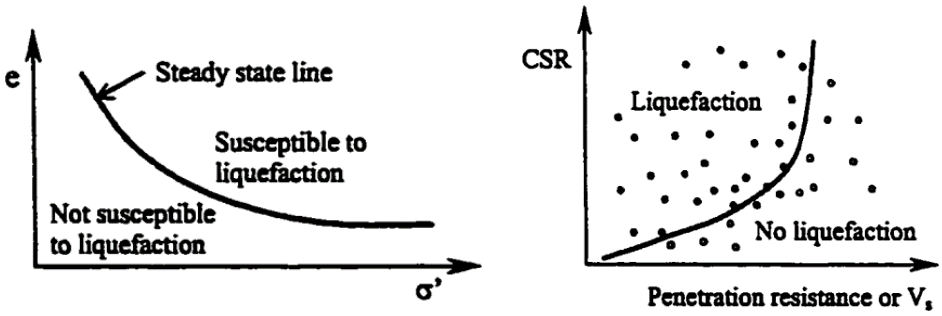


(a) Steady state criteria (b) Back analysis criteria

*Figure 2.2 State criteria for liquefaction susceptibility (modified from Cho 2001)*

### 2.2.3 Liquefaction mitigation methods

Intensive efforts have been devoted to the understanding of the mechanism of liquefaction, and to develop procedures for analyzing the liquefaction potential at a site during a given event. When a construction site is found to have liquefaction potential, proper mitigation measures must be taken to avoid the damage to structures. Liquefaction hazards have typically been mitigated through in situ soil improvement. The geotechnical engineering practice has developed various techniques for soil improvement that can mitigate the potential effects of liquefaction as shown in Figure 2.3. Conventional techniques of liquefaction mitigation include but are not limited to densification, solidification and pore pressure dissipation.

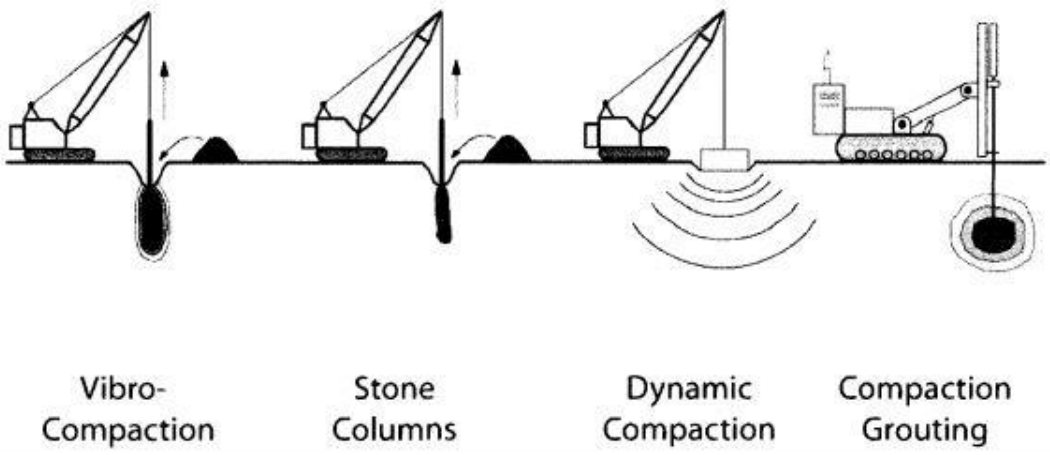


*Figure 2.3 Typical soil improvement techniques for liquefaction mitigation (www.haywardbaker.com)*

Soil compaction is considered as one of the most fundamental types of mitigation. Compaction of soil reduces the pore space between soil particles. As a result, compacted soil behaves rather dilative tendency than contractive tendency under the monotonic and cyclic loading. Soil solidification is to induce cementation into soil particles and directly increase

the shear strength of soil skeletons. The pore water pressure build-up in the cohesionless soil is a key factor to liquefaction potential. The generation of excess pore water pressure under undrained loading conditions is a hallmark of all liquefaction phenomena (Kramer 1996). Effectively dissipating excess pore pressure, usually through vertical drains, is proven to be quite helpful for liquefaction mitigation. Seed and Booker (1977) proposed by using vertical gravel drains to provide rapid pore pressure dissipation channels to prevent liquefaction. It is expected that the drain will effectively dissipate the excess pore pressure generated, at the same time, leading to an increase in the liquefaction resistance of the soil adjacent to the drain (Yamamoto *et al*. 2009). For the same reason, lowering the groundwater table is another way to reduce the liquefaction susceptibility.

All of these conventional approaches show positive effects on liquefaction mitigation. However, they have their own limitations. For instance, these remediation techniques are usually expensive for a large area application and they require professional equipment to deliver. Also, these methods can hardly be applied to liquefiable regions where existing structures are present. Unconventional liquefaction remediation gradually becomes a research focus and some innovative techniques against liquefaction have emerged in the last decade. Such as bio-cementation and biogas desaturation method. Both involve microbial knowledge and techniques for developing promising applications in the geotechnical engineering field. Such a highly integrated discipline attracts not only geotechnical or civil engineering researchers and professionals, but also microbiologists to dedicate their expertise to extensive research work.

### 2.2.4 Desaturation method for liquefaction mitigation

2.2.4.1 Relationship between the degree of saturation and liquefaction resistance

It has been realized for a long time that a small reduction of degree of saturation can lead to a significant improvement of liquefaction resistance. Rocker (1968) reported that partial saturation would have a very large effect on liquefaction, even at levels of saturation near 99%. The effect would be to increase the number of cycles required for failure at a given cyclic deviator stress. Chaney (1978) found that the resistance to liquefaction was about two times that of fully saturated samples when the degree of saturation reduced to 90%. According to Yoshimi *et al*. (1989), the liquefaction resistance increased significantly with a decrease in degree of saturation to such an extent that the liquefaction resistance at 70 percent saturation was about three times that at full saturation. The position of the drained strength plotted at zero saturation suggests, however, that one cannot expect too great a strength gain by further reduction of the degree of saturation (Figure 2.4). As shown in Figure 2.5, Xia and Hu (1991) observed an apparent effect of the degrees of saturation on the liquefaction resistance of the tested sand.

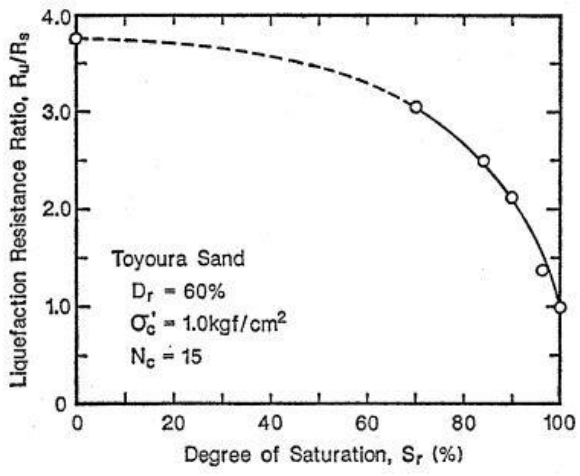


*Figure 2.4 Relationship between the degree of saturation and liquefaction resistance ratio (Yoshimi et al. 1989)*

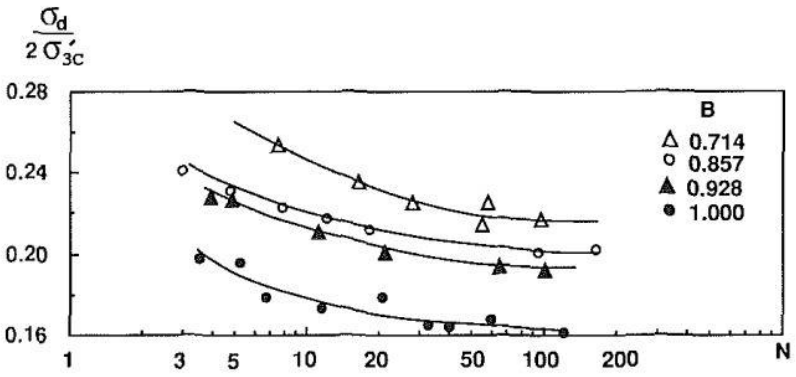


*Figure 2.5 Effect of the degree of saturation on liquefaction strength from laboratory tests (Xia and Hu 1991)*

These early findings inspired the following researchers to focus on the potential of de-saturating soil as an effective liquefaction countermeasure. Grozic *et al*. (2000) conducted triaxial tests on specimens of reconstituted Ottawa sand which were prepared with various gas contents and densities. The results of laboratory program showed that the cyclic resistance ratio increases as gas content and density increases. Results obtained by Yang *et al*. (2003) showed that the reduction in saturation by 1% led to a decrease in the excess pore pressure ratio from 0.6 to 0.15 under pure horizontal excitation. Altun and Goktepe (2006) investigated the stress-strain behavior and the strain softening response of partially saturated cohesive soil and found the partial saturation of soil gave higher strength and lower compressibility. Another encouraging finding comes from Yegian *et al.* (2007). As curves of pressure head shown in Figure 2.6, the introduced small amount of gas/air in loose sand led to a significant reduction in the excess pore pressure and thus increased the liquefaction resistance.

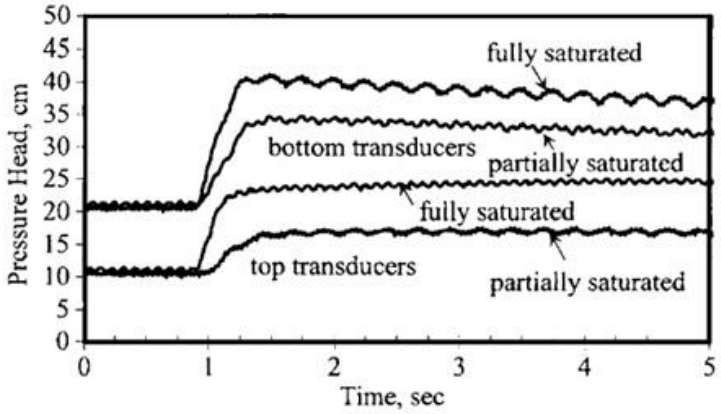


*Figure 2.6 Effect of entrapped air on the excess pore water pressure generation (Yegian et al. 2007)*

2.2.4.2 Evaluating the degree of saturation

The B-value, defined as the ratio of the induced pore water pressure to the applied effective confining stress, has been widely used in laboratory soil testing for evaluating the degree of saturation of a sand specimen (Chaney 1978; Yoshimi *et al* 1989). Skempton (1954) proposed the pore water pressure coefficient *A* and *B* as

$$\Delta u = B\Delta\sigma_3 + A(\Delta\sigma_1 - \Delta\sigma_3) \tag{2.3}$$

When the deviatoric stress $\Delta\sigma_1 - \Delta\sigma_3$ is zero, the B-value equals to

$$B = \frac{\Delta u}{\Delta\sigma_3} \tag{2.4}$$

According to Bishop (1973), the pore water pressure coefficient *B* can be obtained by

$$B = \frac{1}{1 + \dfrac{n(1/K_{wa} - 1/K_s)}{(1/K_d - 1/K_s)}} \tag{2.5}$$

Where $K_{wa}$ = bulk modulus of water-air mixture, $K_s$ = bulk modulus of soil particle, *n*=porosity and $K_d$ = bulk modulus of soil skeleton. Considering $K_s/K_{wa} \gg 1$ and $K_s/K_d \gg 1$, Equation 1.3 becomes

$$B = \frac{1}{1 + nK_d / K_{wa}} \tag{2.6}$$

The bulk modulus of a water-air mixture developed by Koning (1963) using Boyle's law is given by

$$\frac{1}{K_{wa}} = \frac{S_r}{K_w} + \frac{1 - S_r}{K_a} \tag{2.7}$$

in which $K_w$ = bulk modulus of water, $K_a$ = bulk modulus of air and $S_r$ = degree of saturation. Combine equation 2.4 and 2.5, get the following equation (Lade and Hernandez 1977)

$$B = \frac{1}{1 + nK_d(S_r / K_w + (1 - S_r) / K_a)} \tag{2.8}$$

Thus, the degree of saturation can be expressed by *B*-value. Figure 2.7 illustrates the theoretical curve obtained from the above equation.

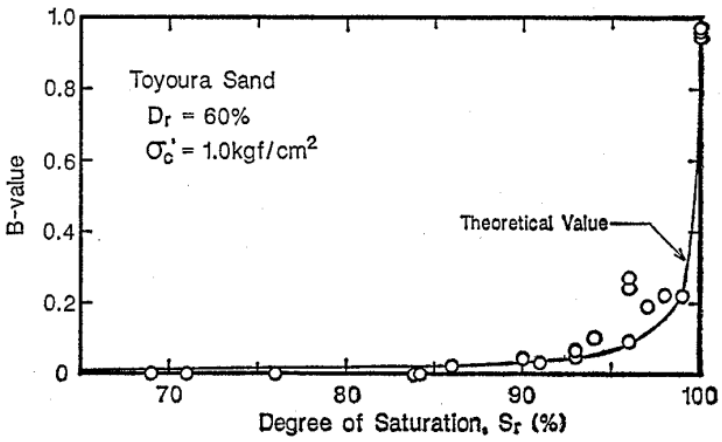


*Figure 2.7 Relationship between degree of saturation and B-value (Yoshimi et al. 1989)*

It must be noted that this relationship is only available in the situation of nearly full saturation scenario. Because when the degree of saturation is quite low, even a small magnitude of effective stress can cause a large compression of the gas, and hence a considerable compression of the soil mass without drainage. It has been known in tests that when the saturation ratio $S_r$ of a soil drops to a value close to 90%, the *B*-value becomes practically equal to zero. Black and Lee (1973) performed measurements of the degree of saturation by means of *B*-value in Ottawa sand specimens and found very low value (B<0.1) for degree of saturation even close to 90% (Figure 2.8). This tendency is also verified by other researchers (Tsukamoto *et al*. 2002; Yang *et al*. 2004).

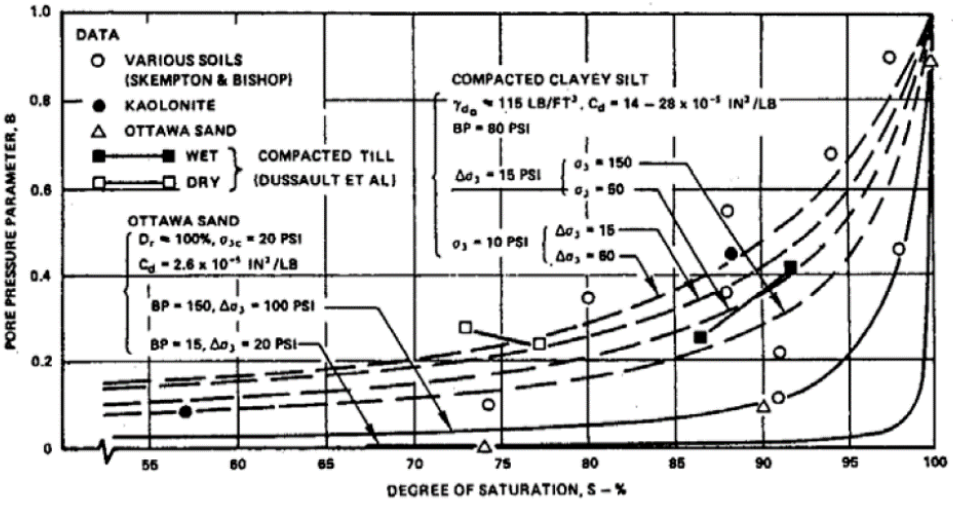


*Figure 2.8 Degree of saturation related to B-value (Black and Lee 1973)*

However, using this method in the field to determine in situ states of saturation is impracticable due to the difficulty of measuring techniques. An alternative method that can be employed in both laboratory and field to determine the saturation state of soil is therefore desirable. The seismic method through measuring the compression wave, or P wave, is proved to be an effective way to evaluate the saturation states of soil. There have been some

techniques and instruments developed in laboratory tests to measure the compression wave and shear wave velocity in soil specimens. One of the most widely adopted methods is through piezoelectric disks and bender elements to detect P-wave and S-wave, respectively (Brignoli *et al*. 1996; Fioravante and Capoferri 2001; Lee *et al*. 2008; Montoya *et al*. 2012; Valle-Molina and Stokoe 2012; Suwal and Kuwano 2013). Figure 2.9 shows some typical arrangement of wave measurement instruments employed by different researchers.

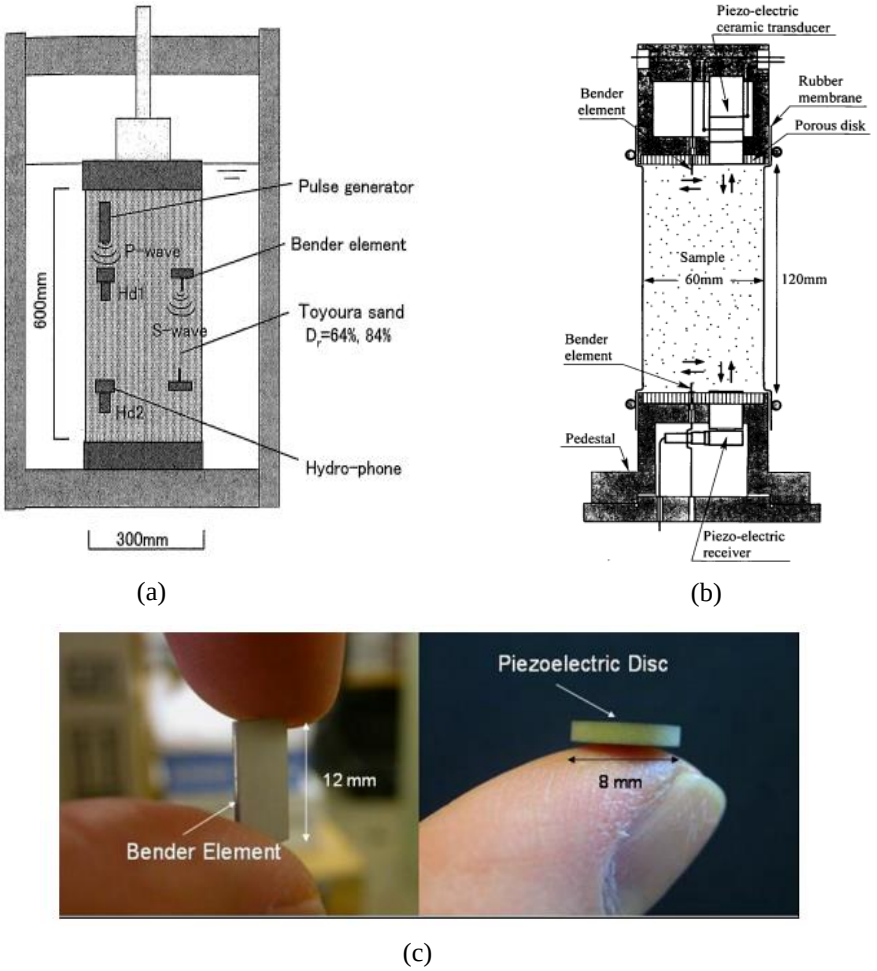


(a) (b)

(c)

*Figure 2.9 Wave instruments in a triaxial system (a) Modified cyclic triaxial apparatus (Tamura et al. 2002); (b) Cross section of the cap, samples and pedestal with transducers (Tsukamoto et al. 2002); (c) Bender element and piezoelectric disc (Valle-Molina 2006)*

Typical test results of the P- and S-wave velocity measurements on samples produced by instruments mentioned above are presented in Figure 2.10. The outcomes suggest that the value of $V_p$ tends to increase significantly with an increase in the $B$ value from a value of about $V_p$ = 500m/sec at $B$ = 0 to $V_p$ = 1500m/sec at $B$ = 0.9 (Tamura *et al*. 2002; Tsukamoto *et al*. 2002). Thus, it is clearly observed that the measurement of $V_p$ can be very useful in determining whether a soil specimen is nearly or completely saturated. In contrast, it has been observed that the velocity of shear wave propagation remains unchanged with an increase in the *B*-value. A relationship between *B*-value and P-wave velocity has been presented by Rebata-Landa and Santamarina (2012) in Figure 2.11.

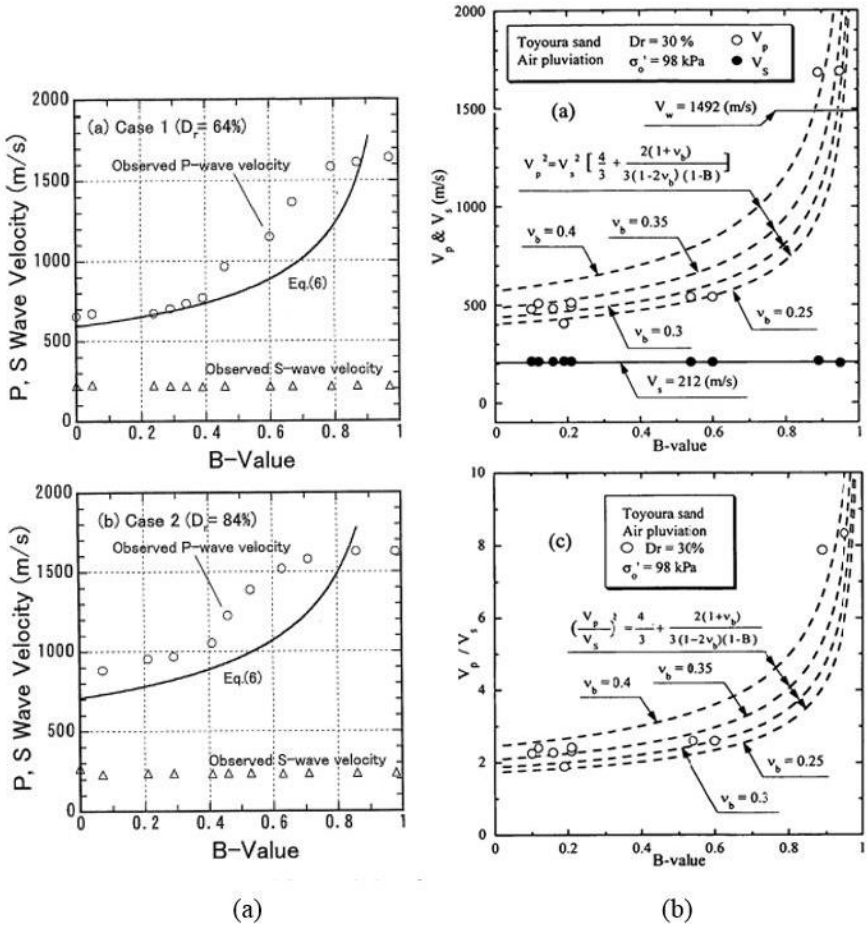


*Figure 2.10 Wave velocity versus B-value (a) Data from Tamura et al. (2002); (b) Data from Tsukamoto et al. (2002)*

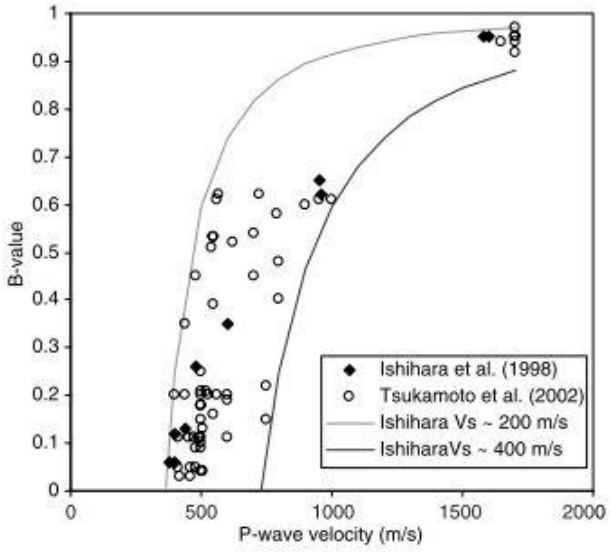


*Figure 2.11 Relationship between B-value and P-wave velocity (after Rebata-Landa and Santamarina 2012)*

2.2.4.3 Desaturation techniques

For the application of desaturation method as a means of mitigating liquefaction potential, several essentials must be born in mind. First of all, the magnitude of saturation reduction cannot be unlimited. Otherwise, not only the purpose of mitigation fails, the stability of existing soil may also be harmed. Next, gas bubbles are able to distribute uniformly in the soil which helps improve the effectiveness of the treatment. Last but not the least, gas bubbles are able to stay in soil for a long time. A number of techniques have been reported and some results are quite promising.

The most direct approach to de-saturate soil is injecting air into soil directly. Yasuhara *et al*. (2008) injected air into different sizes of soil containers to examine the nominal rates and magnitudes of the soil desaturation driven by air injection. The results indicate that the evolution of desaturation is strongly controlled by the injecting air pressures and the soil permeability. In October 2007, a field test was conducted on ground desaturation

through air injection (Okamura *et al*. 2011). Observations revealed that the air-flow rate increased linearly with rising air-injection pressure and the desaturated zone was generated within 4m from the injection point. The degree of saturation ranged from 68-98%, which was almost low enough to double the cyclic strength. Results of degree of saturation measurement from the 3D electric resistivity tomography are quantitatively compatible with the ones obtained indirectly from *in situ* frozen soil samples.

Another used *in situ* technique, the sand compaction pile, is also efficient to improve the liquefaction resistance. Accompanying the installation of sand compaction pile, a large amount of air bubbles are brought into the ground through the casing pipe. Okamura *et al*. (2003) found that the degree of saturation measured from high quality freezing samples was lower than 77% in the sand piles and 91% in the improved sand layers.

Researchers from Northeastern University have tried to de-saturate sand through a water electrolysis method (Yegian *et al*. 2007). They successfully reduced the degree of saturation to 96.3% in 3 to 5 hours. However, this method could not ensure the uniformity of the generated hydrogen and oxygen gas. Alternatively, a chemical method by using sodium perborate ($NaBO_3$) is adopted in later studies to generate oxygen gas. Eseller-Bayat (2009) found that the degree of saturation could be controlled by adjusting the amount of sodium perborate added. To verify the effectiveness of the desaturation, strain-controlled shaking table tests were performed for both saturated sand and desaturated sand. Results confirmed that the desaturated sand had a higher liquefaction resistance than the fully saturated sand.

One of a recent innovative desaturation methods is to produce gases within the soil via microbial processes. Several microbial processes are able to produce different types of gases, such as nitrogen gas ($N_2$), carbon dioxide ($CO_2$), methane gas ($CH_4$) and hydrogen gas

($H_2$). Among these gases, hydrogen gas is a potential detonation and poses a number of hazards to human safety; methane gas with a low solubility coefficient of approximately 0.034L/L in fresh water (Yamamoto *et al*. 1976) is also explosive; carbon dioxide, a well-known greenhouse gas, with a solubility coefficient of approximately 0.86L/L (Rad and Lunne 1994) is moderately to highly soluble in water and not suitable for high pressure application. Thus, nitrogen gas presents several advantages to serve the desaturation purpose. It is neither corrosive or flammable nor a greenhouse gas and its solubility in water is extremely low under the atmospheric pressure. Plus the nitrogen gas is inert and thus it can stay in the soil for a long period of time without reacting with other chemical compound. Considering all these positive advantages, the denitrification process which produces nitrogen gas is the most favorable candidate for desaturation approach.

As mentioned before, the longevity of gas trapped in the soil is another pivotal factor for the desaturation process. Recently, several studies have evaluated the persistence of gas below the groundwater table by measuring the degree of saturation in the ground at sites that have been improved by the sand compaction pile technique. Large amounts of air are introduced in the soil during the installation process (Okamura *et al*. 2006; Okamura *et al*. 2009; Okamura *et al*. 2011). As shown in Figure 2.12, it is found that air was present at all sites and stayed more than several years after the sand compaction piles were installed. Yegian *et al* (2007) used a more than 1 meter partially saturated sand column to verify the long term stability of trapped air under different hydraulic gradient drainage conditions. Results show that the degree of saturation remained mostly constant for more than a year. Since the nitrogen gas is a major component of air, it is reasonable to expect that it can be reserved in the soil for a considerable long term once generated.

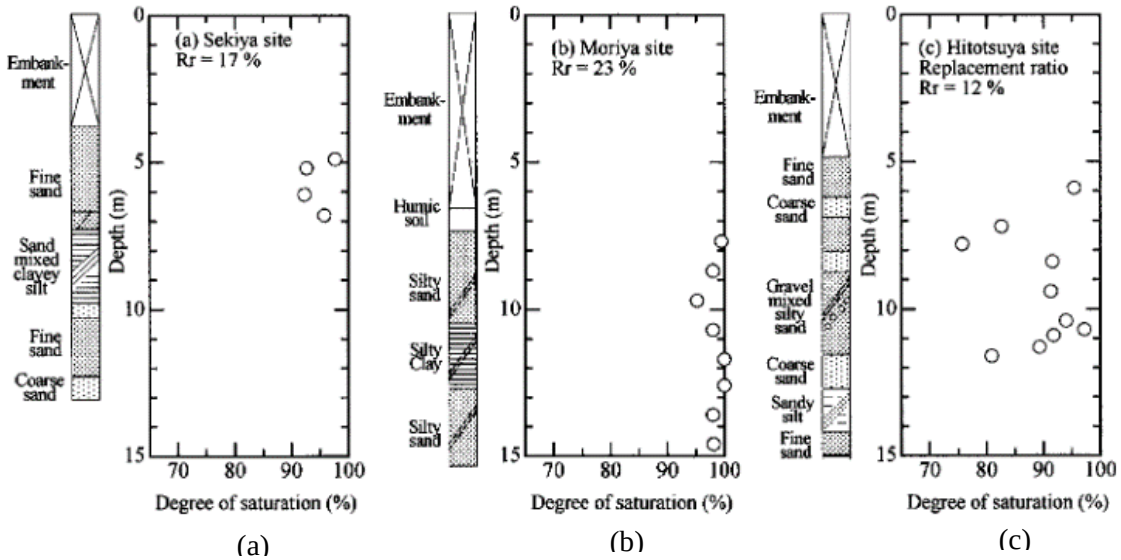


*Figure 2.12 Degree of saturation of soils at different improved sites (a)26 years, (b) 8 years, and (c) 4 years (after Okamura et al. 2006)*

## 2.3 Microbial Geotechnology Process and Application

Soils are ecosystems. There are typically 40 million bacterial cells in a gram of soil and a million bacterial cells in a milliliter of fresh water. There are approximately 5 x $10^{30}$ bacteria on Earth, forming a biomass which exceeds that of all plants and animals (Whitman *et al*. 1998). Great microbial diversity and the fast reproduction rate of microorganisms are responsible for their ubiquitous presence in the geoenvironment. Realizing the potential of integrating microbiological concepts with geotechnical practice is good for advancing the state of knowledge in geotechnical engineering. A proper understanding of biological principles will lead to improved soil characterization, enhanced understanding of soil behavior, and even alternative geotechnical engineering solutions (Mitchell and Santamarina 2005). Numerous effects have been made in the past decade on this emerging inter-discipline. The United States National Research Council (NCR, 2006) recognized the

application of biological processes in geotechnical engineering as one of the priority research areas in the new millennium.

### 2.3.1 Bio-mediated soil improvement

Soil, contrary to conventional civil engineering thought, is a living system host to multiple simultaneous processes (DeJong *et al*. 2011). The natural capacity of soil may provide innovative and sustainable solutions to engineering demands. A bio-mediated soil improvement is distinct from traditional soil improvement. It spontaneously involves biological processes to manage and execute physical or chemical reactions and thus alternates the engineering properties of soil. An overview of bio-mediated soil improvement system is presented schematically in Figure 2.13. Bearing this fundamental understanding in mind is benefit of conducting research and exploring potential engineering practices. The current research in the bio-mediated soil improvement area includes biocementation or biomineralization, bioclogging or biosealing and biogas.

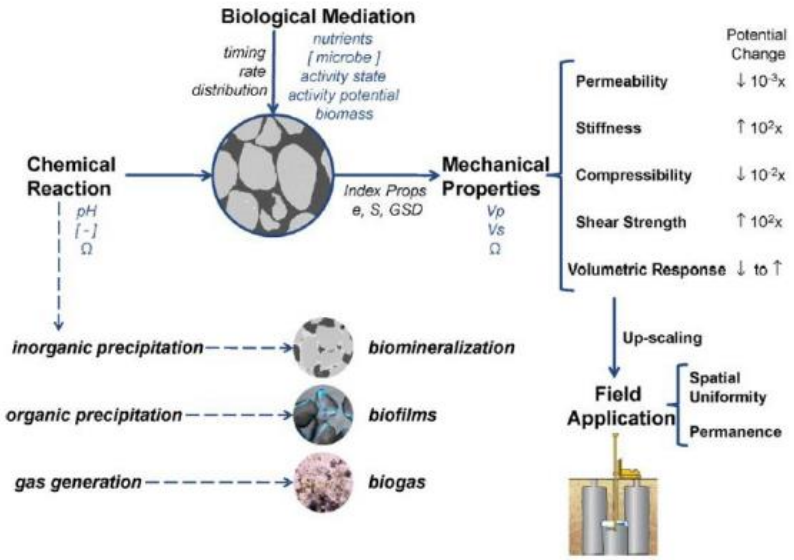


*Figure 2.13 Overview of bio-mediated soil improvement system (DeJong et al. 2010)*

2.3.1.1 Biocementation

Microbially induced calcium carbonate precipitation, or MICP, has been widely studied over the world in recent years (Whiffin *et al*. 2007; Van Paassen *et al*. 2009; Banagan *et al*. 2010; Harkes *et al*. 2010; Al Qabany *et al*. 2012; Cheng and Cord-Ruwisch 2012; Chu *et al*. 2012; Cheng *et al*. 2013; Chu *et al*. 2013; DeJong *et al*. 2013; Onal Okyay and Frigi Rodrigues 2014). Four groups of microorganisms are currently involved in the process, photosynthetic organisms, sulfate reducing bacteria, organisms utilizing organic acids and organisms that are involved in the nitrogen cycle either ammonification of amino acids, nitrate reduction or hydrolysis of urea (Dhami *et al*. 2013). *Bacillus pasteurii* (American Type Culture Collection 6453), which has been recently reclassified as *Sporosarcina pasteurii* (ATCC 11859), an alkalophilic bacterium with a highly active urease enzyme has been the most used microorganism in laboratory studies for the MICP. Using urea hydrolyzing process, calcium carbonate ($CaCO_3$) is produced and crystallized on the surface of soil particles which can bind adjacent particles together to increase the shear strength and reduce the permeability as well. Bacteria produce enzyme urease that hydrolyzes urea by the following reaction:

$$(NH_2)_2CO + 3H_2O \xrightarrow{Urease} 2NH_4^+ + HCO_3^- + OH^- \tag{2.9}$$

Then with the presence of $Ca^{2+}$, the precipitation and crystallization of calcite formed:

$$Ca^{2+} + HCO_3^- + OH^- \rightarrow CaCO_3 \downarrow + H_2O \tag{2.10}$$

$$Ca^{2+} + 2HCO_3^- \leftrightarrow CaCO_3 \downarrow + CO_2 \uparrow + H_2O \tag{2.11}$$

The primary role of urease producing bacteria has been ascribed to their ability of creating an alkaline environment through various physiological activities (Figure 2.14).

Bacteria surface also plays an important role in the calcium precipitation process (Fortin *et al*. 1997; Stocks-Fischer *et al*. 1999). Because the bacteria surface is usually negatively charged. Under a neutral pH environment, positively charged metal ions are able to bond on bacteria surfaces, favoring heterogenous nucleation (Douglas and Beveridge 1998; Bäuerlein 2003). An example of sand filled with calcite crystals generated through the microbial processes is shown in Figure 2.15. Unlike chemically-induced precipitation, the microbiologically-induced calcite precipitation is a far more complicated process (Stocks-Fischer *et al*. 1999). The whole process can be summarized as follows

$$Ca^{2+} + Cell \rightarrow Cell - Ca^{2+} \tag{2.12}$$

$$HCO_3^- + NH_3 \leftrightarrow NH_4^+ + CO_3^{2-} \tag{2.13}$$

$$Cell - Ca^{2+} + CO_3^{2-} \rightarrow Cell - CaCO_3 \tag{2.14}$$

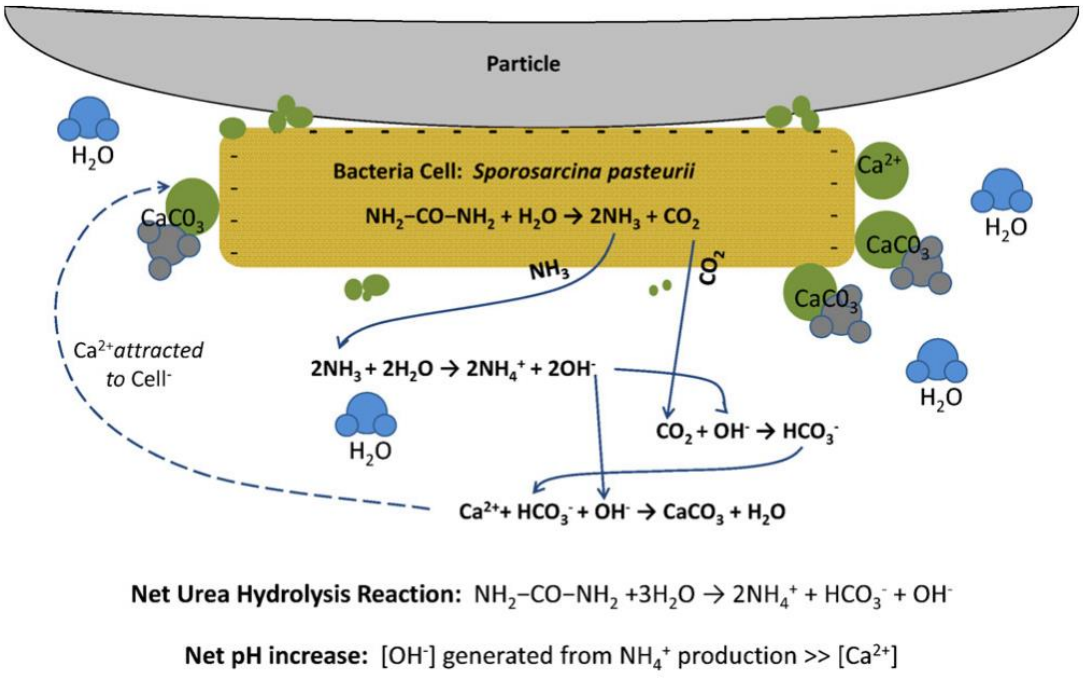


*Figure 2.14 Overview of bio-mediated calcite precipitation using ureolysis (Dejong et al. 2010)*

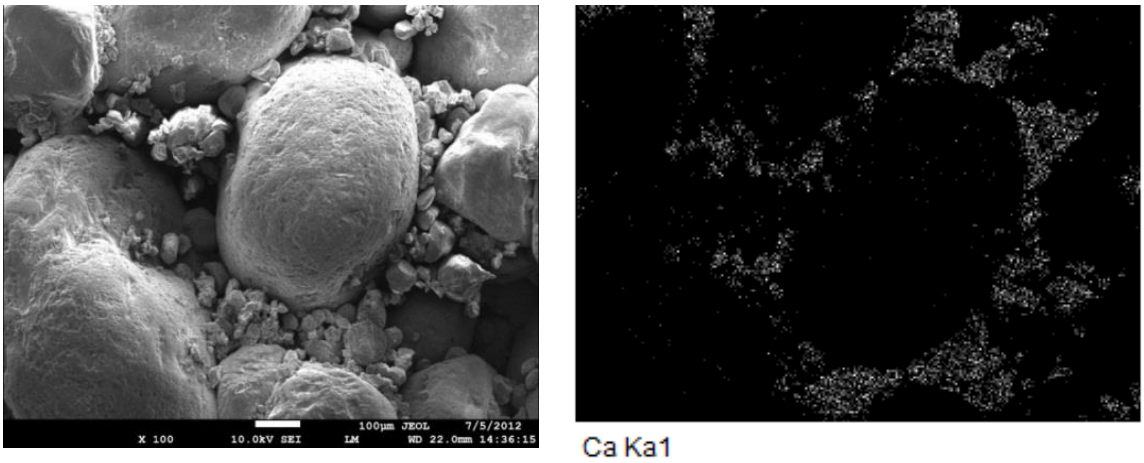


(a) (b)

*Figure 2.15 Microscopic images of biotreated sand (a) SEM image of pores in sand filled with calcite crystals and (b) DESEM/FDX image of calcite crystals around sand grains (after Chu et al. 2012)*

In addition to urea hydrolysis, denitrification (van Paassen *et al*. 2010), sulfate reduction (Warthmann *et al*. 2000) and iron reduction (Roden *et al*. 2002; Ivanov *et al*. 2012) can also produce calcite precipitation. It is worthy of noting that except calcium carbonate, some alternative bonding substances for performing MICP are also reported. Yu *et al* (2015) found that barium hydrogen phosphate by microbial deposition can well bind loose sand particles into bio-sandstone.

Now MICP has been widely explored and promising with potential in various technical and engineering applications. Except ground improvement, MICP can also contribute to the removal of heavy metals and calcium ions in soil and wastewater (Warren *et al*. 2001; Fujita *et al*. 2008); carbon dioxide sequestration (Jansson and Northen 2010; Mitchell *et al*. 2010); repair cracks in rocks and rebabilitation of concrete (Bang *et al*. 2010; Jonkers *et al*. 2010; Van Tittelboom *et al*. 2010; Sangadji and Schlangen 2012; Amidi and Wang 2015); dust suppression (Bang *et al*. 2009); even remediation of historical heritages (González and Saiz-Jiménez 2005; Anderle *et al*. 2006; Shen and Cheng 2008).

2.3.1.2 Bioclogging and biosealing

Bacteria are the dominant microorganisms in soils. The common cell diameter of bacteria is usually in the range of 0.5-3 μm. The transportation of bacteria is largely controlled by the relative size (pore throat relative to a single bacteria or bacterial aggregations), electrical interactions, surface roughness and cell shape (Mitchell and Santamarina 2005). The void size between soil particles will be the first emerging subject relates to clogging, especially when the clogging is caused by biological activities. Figure 2.16 identifies the boundaries and main regions where clogging can take place. It shows bioclogging is liable to occur in silt and sand. For clay, due to its own tiny pore voids and low permeability, transportation of bacteria and nutrients as well as other substrates is hugely limited.

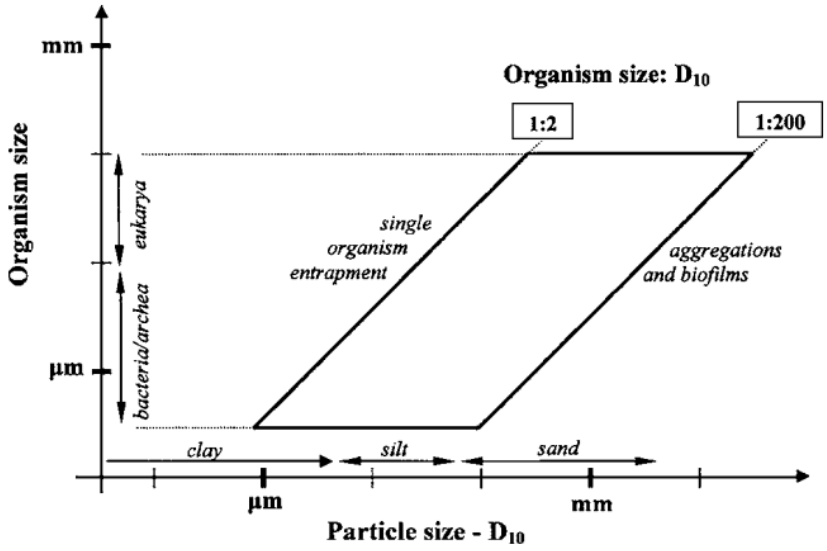


*Figure 2.16 Potential regions of particle size for bioclogging events (adapt from Mitchell and Santamarina 2005)*

Suitable microorganisms could be applied to soil to form and accumulate bacterial biomass or insoluble bacterial slime, for example, exopolysaccharides or extracellular polymeric substances (EPS). The slimy EPS enhances further attachment of more microorganisms and other particles, thereby forming a biofilm that can affect the physical properties of soils, for example, permeability (Ivanov and Chu 2008; DeJong *et al*. 2013). In that case, those microbial process products make the soil less permeable for water. Therefore, bioclogging could be used to seal leakage in a construction site, landfill, or levee. And organic wastes can be nutrient source for both bacteria growth and fermenting of EPS-producing microorganisms in large-scale applications to diminish the cost of soil clogging. The growth of microorganisms and accumulation of insoluble microbial slime from cheap raw materials will give great economical credits to the engineering application of bioclogging.

By using the halotolerant, alkaliphilic *Bacillus sp. VS1*, Stabnikov *et al*. (2011) successfully sealed a sand-lined model pond. Bouwer (2002) found a clogging layer of silt on basin bottom with the exopolysaccharides presence. Bioclogging due to the precipitation of minerals from an aqueous system has also been proposed to enhance the recovery of oil from oil reservoirs or to control the flow of a spilled contaminant in a reservoir (Ferris *et al*. 1996; Fortin *et al*. 1997; Fujita *et al*. 2000). Successful field trials of bioclogging also have been reported in the Netherlands and Austria, with the objective of reducing leakage through water-retaining constructions (Van Meurs *et al*. 2006; Blauw *et al*. 2009).

2.3.1.3 Biogas

Many studies (Rad and Lunne 1994; Grozic *et al*. 2000; Fourie *et al*. 2001; Amaratunga and Grozic 2009; He and Chu 2014) have shown that the mechanical behavior of soil is significantly affected by the presence of gas in either dissolved or free form. Due to

numerous microbial processes, biogas or biogenic gas universally existed in wide soil profiles. Biogas is typically produced by the breakdown of organic or inorganic matter through microbial processes, for example, anaerobic digestion with anaerobic bacteria or fermentation with biodegradable materials. The most common biogenic gases found in subsurface soils are methane ($CH_4$), carbon dioxide ($CO_2$), hydrogen ($H_2$) and nitrogen ($N_2$). Methane and hydrogen are combustible or oxidized with oxygen. Carbon dioxide has high solubility in water under normal pressure condition. Both methane and carbon dioxide are greenhouse gas which requires regulation. They are all not suitable for large engineering application. Nitrogen, on the other hand, shows up several advantages and potential of being the eligible candidate of the study conducted in this research. It is neither explosive nor corrosive. Due to its low solubility in the water, it will remain undissolved for a prolonged period. It is an inert gas and thus will not react with other gases or chemicals in the field.

Biogas can be used to reduce liquefaction potential of sand by making it slightly unsaturated using gas. There is no effective way yet to inject gas bubbles uniformly into soil and keep the bubbles in soil for a long time. Biogas is a promising alternative as very tiny gas bubbles can be produced and the distribution of the bacteria (or bubbles) can be more uniform compare to the injection method.

There are different ways to introduce nitrogen gas into soils. The easiest method is just inject air directly since dry air contains huge amount of nitrogen (78.09% by volume). Considering the energy consumption, the air injection method is not a cost effective approach. Generating nitrogen through microbial processes, such as denitrification, can be worth trying as an alternative. The denitrification process will be reviewed in the following section.

### 2.3.2 Biogas ($N_2$) generation through biological denitrification process

2.3.2.1 Overview of denitrification process

Denitrification is a microbially facilitated process of nitrate reduction that ultimately produce nitrogen through a series of intermediate steps. The complete denitrification process can be expresses as a redox reaction:

$$2NO_3^- + 10e^- + 12H^+ \rightarrow N_2 + 6H_2O \quad (2.15)$$

General requirements for biological denitrification are 1) the presence of denitrifying bacteria; 2) electron donors are available, such as available organic C compounds; 3) anaerobic conditions or restricted supply of oxygen; 4) availability of N oxides as terminal electron acceptors (Saggar *et al*. 2012).

Denitrifying bacteria utilize N oxides as the electron acceptor in the denitrification process. They exist in three kingdoms: bacteria, archaea, and eukarya. Only bacteria are capable of anaerobic respiration. There are two distinct pathways of nitrate metabolism in bacteria. Nitrate can be reduced to ammonia, which is assimilated by the cell, or under certain conditions it can be used in place of oxygen as terminal electron acceptor in respiration. To ultimately diverse nitrate to nitrogen, four independent intracellular enzymes shall be present in denitrifying bacteria: Nitrate reductase (Nar), Nitrite reductase (Nir), Nitric-oxide reductase (Nor) and Nitrous oxide reductase (Nos). As shown in equation 2.6, the denitrification process relies on these enzymes to proceed step by step.

$$NO_3^- \xrightarrow{Nar} NO_2^- \xrightarrow{Nir} NO \xrightarrow{Nor} N_2O \xrightarrow{Nos} N_2 \quad (2.16)$$

Denitrifying bacteria can be isolated from various sources, for example, waste water, soils and meadows. Most of them are heterotrophic bacteria, such as *Paracoccus denitrificans* and various pseudomonads (Carlson and Ingraham 1983).

2.3.2.2 Factors affecting denitrification in the environment

As many other biological activities, denitrification is a high environment-interactive process. Environmental factors ineluctably affect the occurrence and effectiveness of the process. In general, complete denitrification is promoted by high soil moisture content, neutral to slightly soil pH, high soil temperature, low rates of $O_2$ diffusion and the presence of labile carbon source (Saggar *et al*. 2012). Some major factors are discussed here.

The availability of nitrogen source (N), especially in the form of nitrate ($NO_3^-$), is a major source for denitrification and thus its concentration can be one of the primary factors limiting denitrification. The impact of different nitrate concentration is significant (Arah and Smith 1990; Luo *et al*. 1996; Senbayram *et al*. 2012). A high level of $NO_3^-$ concentration is known to result in incomplete denitrification because of the relative high $N_2O/N_2$ ratio. (Bremner and Blackmer 1978; Weier *et al*. 1993; Cho *et al*. 1997; Stevens and Laughlin 1998). Studies have found that as $NO_3^-$ decreases, a greater proportion of the N is emitted as $N_2$ due to the stimulation of *Nos*, where $N_2O$ acts as a major electron acceptor (Swerts *et al*. 1996; Dendooven *et al*. 1997). Mycielski *et al*. (1982) reported that approximately 1 g/L nitrite was accumulated as the initial nitrate concentration was above 3 g/L. van Paassen *et al*. (2010) pointed out that nitrite accumulation was detected when the initial nitrate concentration was higher than 120mM. The $NO_3^-$ concentration applied in this study is 10mM

(0.62g/L) so that there will be barely nitrite presence in the final product according to previous researches.

Soil pH value is another key regulator of the microbial denitrification process. The effect of pH on denitrification is controversial. Common opinion is that denitrification process is slower in acid conditions (Bremner and Shaw 1958; Nägele and Conrad 1990; Fageria and Baligar 2008; Saleh-Lakha *et al*. 2009). According to Šimek and Cooper (2002), there is no significant relationship between soil pH and denitrification activity. They suggested it is not necessary to optimize pH for denitrification. However, the final products of denitrification seems to be affected by pH condition. Šimek *et al*. (2002) found that nitrogen gas ($N_2$) is the major product rather than nitrous oxide ($N_2O$) when the pH value is above 7. Čuhel *et al*. (2010) also found that the amount of generated nitrogen gas ($N_2$) benefits from the pH increase. Based on these results, it is wise to apply the microbial denitrification process into geotechnical practice, a neutral or alkaline environment is preferred since the major target biogas is nitrogen gas.

Available carbon source benefits the denitrification as well. Heterotrophic denitrification is limited by labile carbon source in soils. Any process prohibits the rate of carbon mineralization in soils can have a major impact on the denitrification rate (Saggar *et al*. 2012). Not only as electron donors, but also a necessity for organism's metabolism, carbon plays a critical role in the entire ecosystem. The availability of carbon in soil affects the denitrification enzyme activity and microbial community composition. It is generally agreed that increase the carbon concentration will decrease the ratio of $N_2O/N_2$, in other words, pushes the denitrification process into a complete end stage - more $N_2$ generated (Smith and Tiedje 1979; Arah and Smith 1990; Dendooven *et al*. 1998).

Temperature and anaerobic condition can also affect the rate and product of microbial denitrification process. Although the denitrification can occur over a wide range of soil temperatures ranging from sub-zero to 75 °C (Knowles 1982), low temperature condition results in incomplete denitrification. Studies have found more $N_2O$ is produced at low temperatures (Keeney *et al*. 1979; Avalakki *et al*. 1995). It is necessary to point out that besides the denitrifying bacteria activity, the temperature effects the substrate supply, gas solubility, $NO_3^-$ availability as well (Saggar *et al*. 2012). As denitrification is an anaerobic reaction, the presence of oxygen is apparently undesired for the denitrification process. Even small quantities of $O_2$ can cause large decreases in denitrification enzyme activities (Firestone *et al*. 1979). Oxygen availability also causes a higher $N_2O/N_2$ ratio than in an anaerobic condition. However, usually the underground water is considered as an anaerobic environment which is favorable by the denitrifying bacteria.

Given all factors mentioned above, the potential of adapting denitrification process as an alternative for generating nitrogen gas within soil is sound.

### 2.3.3 Challenges and recommendations for microbial geotechnology

As an emerging and promising research area, microbial geotechnology has already attracted vast initiatives from both scientific researchers and industrial professionals. A number of findings mentioned above really promise an exciting future for this technique. However, all new solutions to persistent traditional problems always come with challenges. Despite considerable exciting and positive achievements obtained so far, there is still huge space for improvement. Take the most widely studied technique MICP as an example, almost

all research work are still concentrated on lab scale. Further *in situ* tests are required to continue the exploration. And either research or education in such a highly integrated discipline demands a comprehensive corporation between researchers, students and professionals from microbiological, chemical and geotechnical engineering.

2.3.3.1 From lab to field

Successful implement microbial geotechnical technique in the field is the goal of current research work. To fulfill this purpose, based on the elementary and bench scale tests, up-scaling biological, chemical and geotechnical system must be established and examined. To date, only a limited number of field trails have been performed.

A 1000 $m^3$ volume of soil at a depth of 3 and 20m below the surface treated by MICP technique was reported (Van Paassen 2011). Contractor Visser & Smit Hanab applied MICP on gravels and successfully stabilized the loose gravel deposit in the horizontal direction of the drilling. Following a 14-day treatment of 1000 $m^3$ gravel site, two 48 inch steel gas pipelines with a length of 600 and 900 meters respectively were successfully installed (Van der Star *et al*. 2011). Another trial was conducted at a mine site in the province of Saskatchewan, Canada during summer 2012 (Gomez *et al*. 2014). A treatment depth of nearly 30 cm was verified via dynamic cone penetration test and calcite content measurement. Figure 2.17 shows some photos of field applications.

(a) Biogrout in Netherland (Van Paassen 2011)

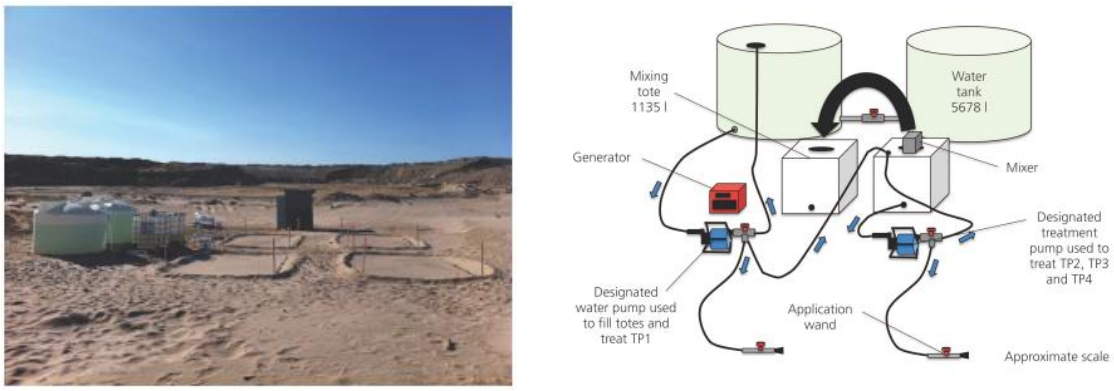


(b) Biocementation site in Saskatchewan, Canada (Gomez *et al*. 2014)

*Figure 2.17 MICP field implementations*

Successful field trials of bioclogging have also been reported in the Netherlands and Austria, with the objective of reducing leakage through water-retaining constructions (Van Meurs *et al*. 2006; Blauw *et al.* 2009).

The adoption of bio-geotechnical methods into industry will take time. Field implementation of microbial geotechniques raises new research topics for lab work. Such as the uniformity of the bacteria and cementation source; how to successfully deliver the bacteria and calcium source to a desired depth for biogrouting; reduce the cycles of MICP treatments for economic concerns and ease the impact of MICP byproducts to the environment. Still, numerous opportunities for adaptation of the engineering approach may be uncovered as the research and experimentation goes on.

2.3.3.2 Research and education

The rapid development of biogeotechnical methods over the last decade has generated exciting advances in geotechnology. Research in this area is truly dynamic. Three important workshop and symposium related to the bio-chemo-soil interaction has been organized (2008 Delft, The Netherlands; 2011 Cambridge, The Great Britain; 2013 Lausanne, Switzerland). Two special issues are published in the Journal Géotechnique and Ecological Engineering, respectively. Positive outcomes of these studies lay a steady foundation for further studies. More efforts are required to integrate analytical work, numerical modeling and experimentation. Key areas like optimization of the bio-geo application process, management of treatment byproducts, development of economical and reliable monitoring technique, verification of soil mechanical properties in the post-treatment stage. Few alternative biogeochemical processes have yet received as much attention as MICP, and there are undoubtedly other processes that have yet to be discovered (DeJong *et al*. 2013). Another area that needs to draw attention is the numerical modeling and simulation about bio-chemo-geo integration. Few researches (Mostafa and Van Geel 2007; Soleimani *et al*. 2009; Fauriel and Laloui 2012; Wijngaarden *et al*. 2012) were reported due to the difficulties of applying existing models to such a multiple phases coupling system. All these fields require sustained research investment.

In addition to strong initiative of performing this integrated disciplinary research, both instructors and students are required to equip with biological, geochemical and geotechnical knowledge. Given such a high demand for research, it is essential to recruit graduate students with a diverse background. Conventional single background students will find difficulty to comprehend knowledge out of his/her field thus requiring remedial training.

To develop such a new workforce, education and training must include fundamentals of biology, chemistry and geotechnical engineering. It is also essential to encourage cross-disciplinary collaboration between researchers and industry practitioners. Those who can intelligibly integrate and engage with experts from diverse disciplines will be the most valuable treasures in future.

## 2.4 Engineering Property of Granular Soil

### 2.4.1 Critical state soil mechanics framework

It is well-known in the soil mechanics that soil element can be seen as a three-phase combination. The voids among the soil skeleton plays a critical role in the mechanical behavior of soils. The early investigation of volume change and shearing under confining stress can be traced back to Casagrande's work in 1930s. Based on the results of drained direct shear tests, he found there is a critical void ratio for a given type of sand, depend only on confining stress imposed during shearing (Casagrande 1936). This finding lays the foundation of critical state soil mechanics. Roscoe, Schofield and Worth later proposed the critical state concept based on much more extensive data of triaxial test results (Roscoe *et al*. 1958). The publication of textbook "Critical State Soil Mechanics" represents the establishment of a Critical State Soil Mechanics (CSSM) framework. Critical state refers to a state when the soil continues to deform without any further changes in mean effective stress, deviator stress or specific volume. In the CSSM, following stress and strain parameters are defined:

$$p' = (\sigma_1' + 2\sigma_3')/3 \tag{2.17}$$

$$q = \sigma_1 - \sigma_3 = \sigma_1^{'} - \sigma_3^{'} \tag{2.18}$$

$$\varepsilon_v = \varepsilon_1 + \varepsilon_2 + \varepsilon_3 = \varepsilon_1 + 2\varepsilon_3 \tag{2.19}$$

$$\varepsilon_s = 2(\varepsilon_1 - \varepsilon_3)/3 \tag{2.20}$$

Where $p'$ and $q$ are the mean effective stress and deviator stress, $\varepsilon_v$ and $\varepsilon_s$ are the volumetric strain and deviator strain, respectively. Mathematically, the critical state can be defined as:

$$\frac{\partial p'}{\partial \varepsilon_s} = \frac{\partial q}{\partial \varepsilon_s} = \frac{\partial \varepsilon_v}{\partial \varepsilon_s} \tag{2.21}$$

There exists a unique critical state line (CSL) in the $q' : p' : \nu$ space on which all shearing test paths terminate. For a given soil, the CSL is independent of the stress paths and initial state of the soil (Atkinson and Bransby 1978). The projections of the CSL onto the $q - p'$ space and $\nu - \ln(p')$ show a linear relationship

$$q = Mp' \tag{2.22}$$

$$\Gamma = \nu + \lambda \ln(p') \tag{2.23}$$

Where $\nu$ is the specific volume ($\nu = 1 + e$), $M$, $\lambda$ and $\Gamma$ are critical state parameters. From the one-dimensional consolidation theory, the normal consolidation line (NCL) and the swelling line ($\kappa$-line) can be expressed as

$$\nu = N - \lambda \ln(p') \tag{2.24}$$

$$\nu = \nu_\kappa - \kappa \ln(p') \tag{2.25}$$

The meanings of N, $\Gamma$, $\lambda$, $\lambda_\kappa$ and $\kappa$ can be found in Figure 2.18.

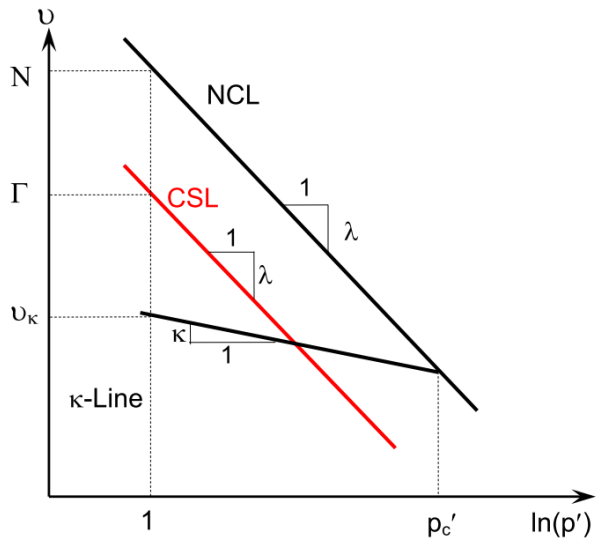


*Figure 2.18 The CSL, NCL and* κ-line *in the* $v-\ln(p')$ *space (after Meng 2010)*

Under the CSSM framework, whether soil behaves a contractive or dilative manner in compression test can be expected according to the initial void ratio of the soil in the $e-\ln(p')$ space. Been and Jefferies (1985) pointed out that the nature of the CSL implies the limited applicability for characterizing a potentially liquefiable soil. They introduced a state parameter, $\psi$ to express the initial state of soil in terms of its density

$$\psi = e - e_{cr} \tag{2.26}$$

Where $e$ is the void ratio at the initial state and $e_{cr}$ is the void ratio at the critical state at the same mean effective stress. As shown in Figure 2.19, if $\psi > 0$, which locates above the CSL, defines contractive behavior. To the contrary, when $\psi < 0$, the point falls below the CSL, the dilative behavior of granular soil is likely to happen.

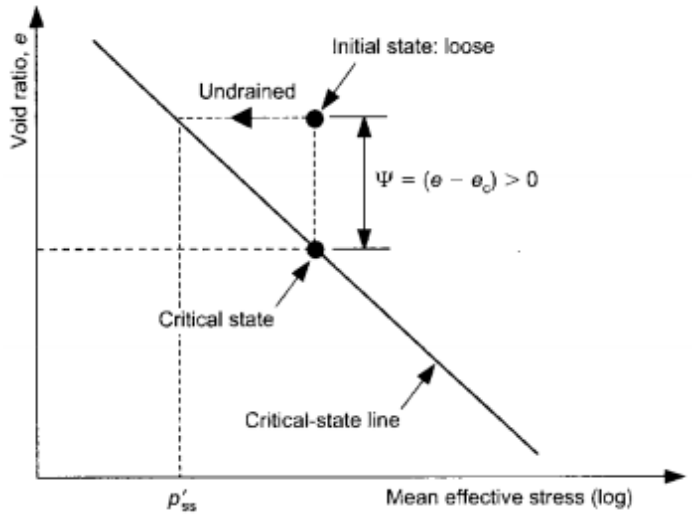


*Figure 2.19 Definition of state parameter (after Yang 2002)*

### 2.4.2 Undrained behavior of sand under monotonic loading

Liquefaction usually occurs when excess pore pressure reaches the amount of effective overburden stress and results in considerable deformation taking place. It is reasonable to investigate the undrained response of sand for liquefaction study since pore pressure is involved.

Figure 2.20 illustrates three different types of stress-strain relations obtained from undrained shear tests on saturated sand. It is clear that strain-hardening takes place for dense sand while the loose sand shows a strain-softening behavior. When the density is moderate, the sand first exhibits the strain-softening at moderate shear strains but it starts to show the strain-hardening behavior as the strain increases.

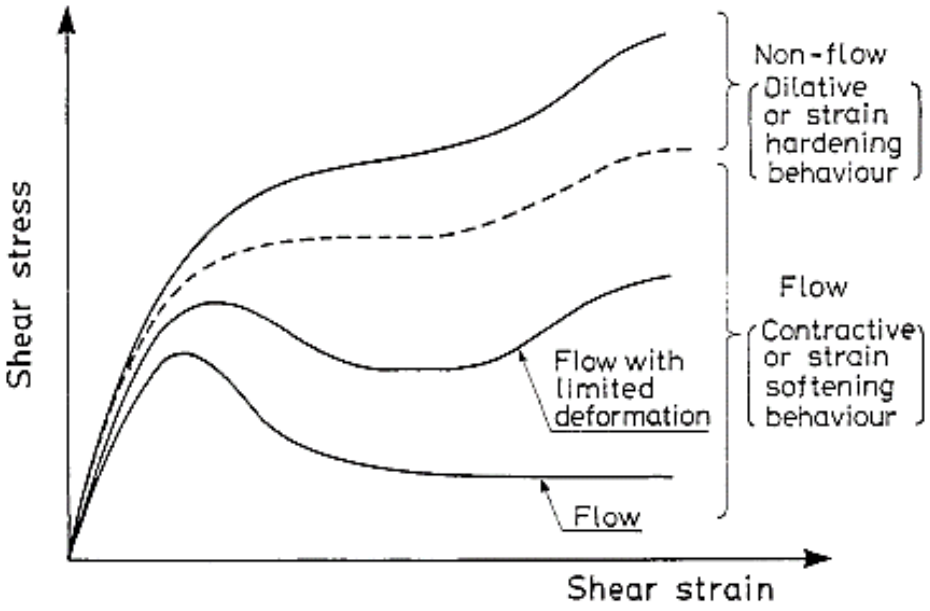


*Figure 2.20 Classification of undrained behavior of sandy soils (after Ishihara 1996)*

Robertson and Wride (1998) also summarized the behavior of a granular soil loaded in undrained monotonic triaxial compression tests. As shown in Figure 2.21, in the $e-p'$ space, a soil with an initial void ratio higher than the ultimate state line (USL) will strain soften (SS) at large strains and a soil with an initial void ratio lower than the USL will strain harden (SH) at large strains until its ultimate state is reached. If a soil with an initial void ratio higher than but close to the USL, the response will show limited strain softening (LSS) to a quasi-steady state (QSS) (Ishihara 1993).

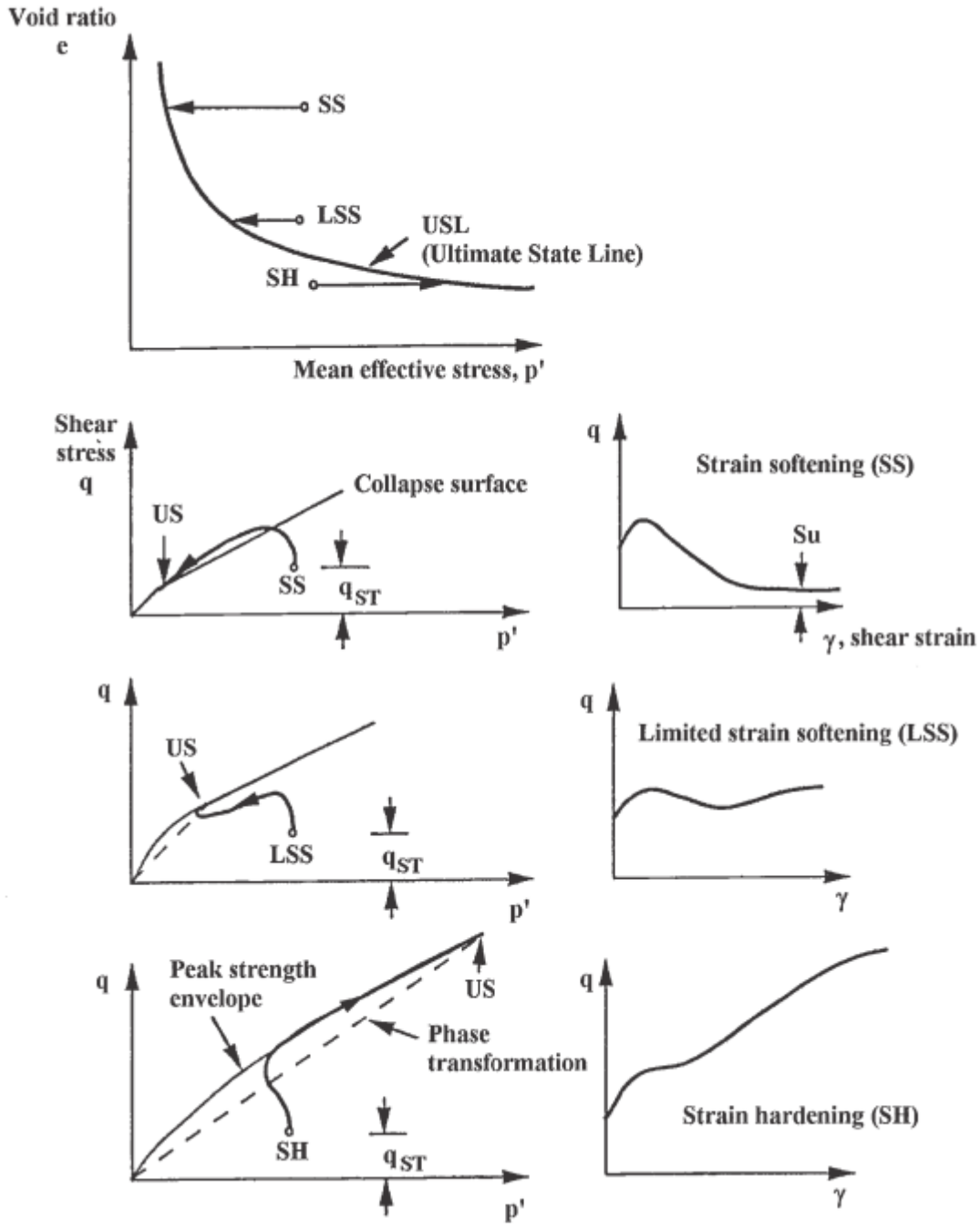


*Figure 2.21 Undrained behavior of sand under monotonic loading (after Robertson 1994)*

### 2.4.3 Undrained behavior of sand under cyclic loading

Sand under seismic loading conditions has been extensively investigated by many researchers by means of cyclic triaxial tests, cyclic simple shear tests and cyclic torsional tests. Outcomes have generally confirmed that the cyclic resistance of sand to liquefaction is influenced primarily by its initial confining stress, initial void ratio or relative density, intensity of the cyclic shear stress and the number of cyclic stress application (Ishihara 1996). Cyclic stress ratio $\sigma_d / (2\sigma_0^{'})$ in terms of the combined effect of cyclic shear stress and initial confining stress was defined to describe the cyclic resistance. Usually, given a void ratio or relative density, the cyclic stress ratio required to cause 5% D.A. axial strain under 20 load cycles as a factor quantifying the liquefaction resistance of sand (Ishihara *et al*. 1975). Another commonly adopted failure criterion in cyclic triaxial test is when the pore pressure reaching effective confining pressure. Figure 2.22 shows a typical undrained behavior of sand under cyclic loading.

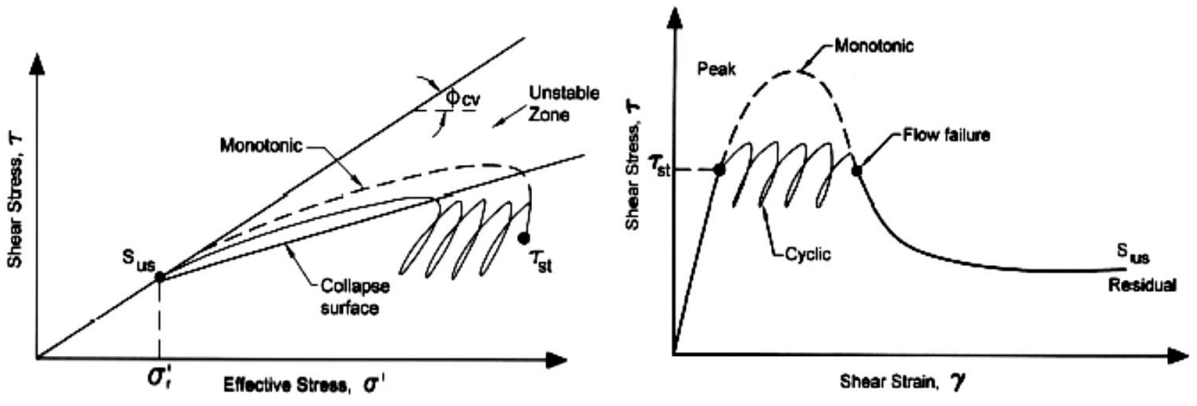


*Figure 2.22 Undrained behavior of sand under cycling loading (after Davis et al. 2002)*

### 2.4.4 Instability of sand

A number of studies (Lade *et al*. 1987; Lade *et al*. 1988; Lade and Pradel 1990; Chu *et al*. 1993; Yamamuro and Lade 1997; Chu and Leong 2001; Chu and Wanatowski 2008) have found for granular materials, large plastic strains will develop while they carry or sustain a given load. However, such a large strain is different from that caused by failure because it can occur inside the established failure surface. This phenomena is defined as instability. The zone of instability is defined by the zone in between the failure line and the instability line. As shown in Figure 2.23, the instability line is obtained by connecting the peak points of the effective stress paths of undrained tests. Instability of soils occurs when strain goes beyond the peak deviator stress. Unlike critical state line, Chu *et al* (2003) pointed out that the instability line varies with void ratio and the initial stress state (Figure 2.24).

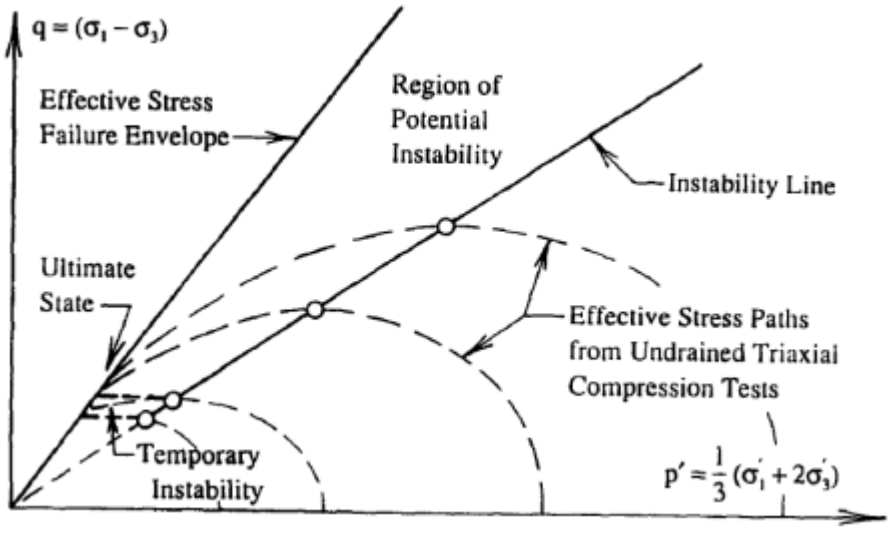


*Figure 2.23 Schematic diagram of location of instability line in q-p' space (after Lade 1993)*

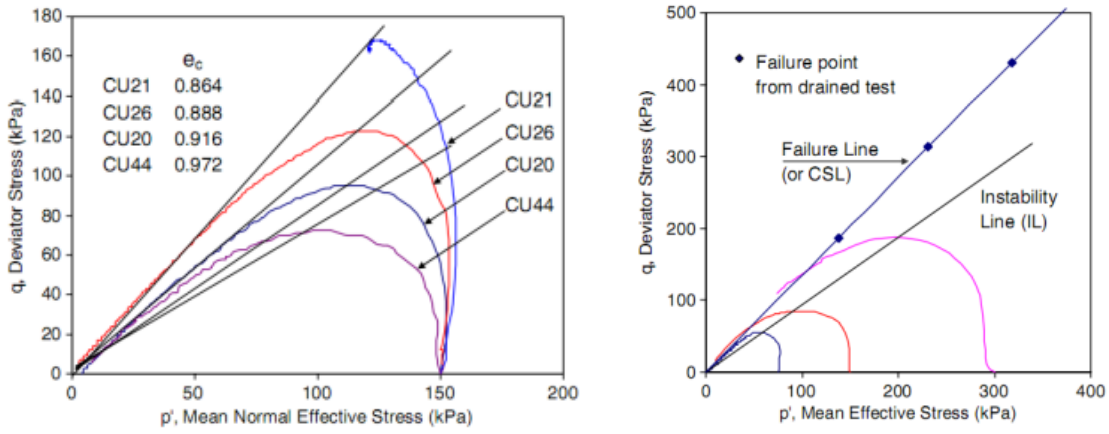


*Figure 2.24 Influence of void ratio and effective confining stress on instability line (after Chu et al. 2003)*

Notice should be taken that the instability is not the same as strain softening. Strain softening often depicts the reduction in the shear stress with increase of the shear strain after the deviator stress reaches its peak value. In contrast, instability refers to the inability of a soil sustaining a constant load and thus leading to a large strain development. During the strain softening, the deviator stress reduces gradually without observation of specimen collapse while the instability generally accompanied by a sudden collapse. Based on the difference, Chu and Wanatowski (2009) suggested studying the instability behavior under stress-controlled tests and investigating the strain softening through stain-controlled tests.

### 2.4.5 Improvement of engineering properties of soil through microbial process

Microbial activity and its product can directly or indirectly influence the physical and engineering properties of the soil on a permanent or a temporary basis.

2.4.5.1 Shear strength

Shear strength is one of the most important engineering properties of soil. Results of many laboratory scale MICP tests have shown substantial increases in soil strength as the microbial induced calcium carbonate accumulates. (DeJong *et al*. 2006; Van Paassen *et al*. 2009; Chu *et al*. 2012; Chu *et al*. 2012; Qabany and Soga 2013; Montory and DeJong 2015). Li (2014) summarized the relationship between the calcite contents and the UC strength of soil treated by MICP and other binders in the Figure 2.25.

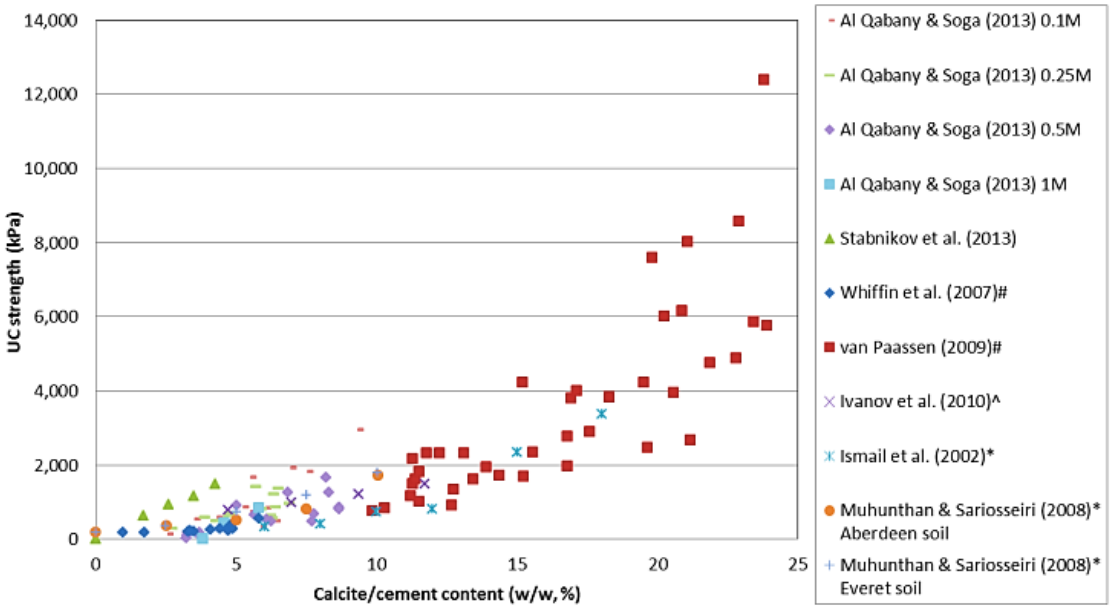


*Figure 2.25 Relationship between UC strength and calcite content in the literature (after Li 2014)*

Based on test results in Figure 2.26, DeJong *et al*. (2006) proposed to ascribe the response of MICP treated sand to undrained shearing to two effects – densification and cementation. MICP binds sand particles together like cement and actually reduces the void ratio at the same time. Both effects contribute to the increase of the shear resistance. Due to the densification, the failure envelope of the MICP treated sand is higher than that clean sand.

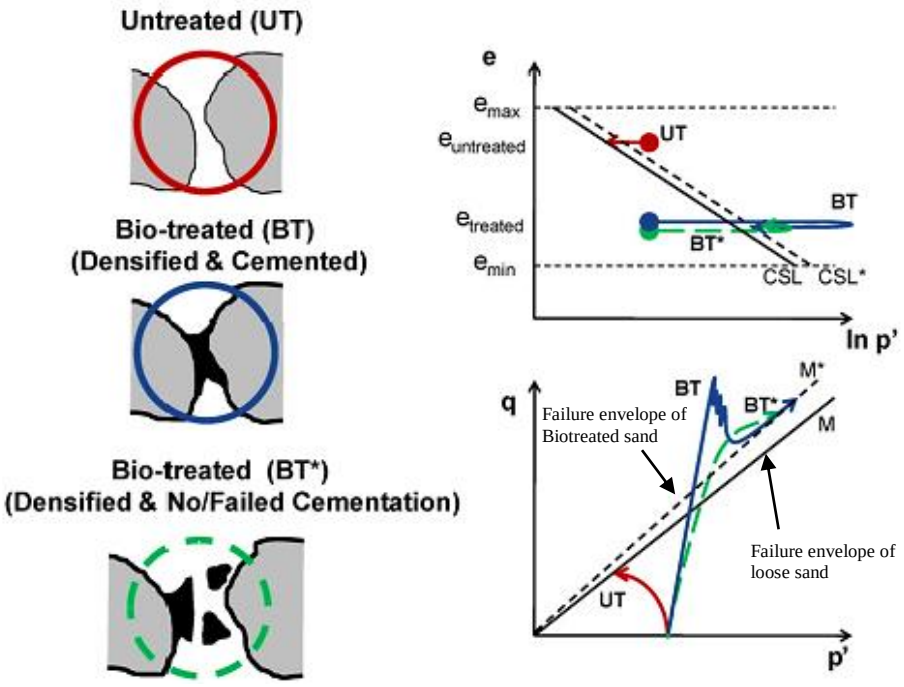


*Figure 2.26 Illustration of impact of MICP on shear response of loose sand (after DeJong et al 2009)*

Montoya *et al* (2013) investigated the dynamic response of MICP treated sand specimen through centrifuge tests and cyclic direct simple shear tests. They found that the MICP treated sand reduced both pore pressure generation and ground settlement at all levels of shaking. The CRR ratio of the sand sample gained a substantial increase, about 30% after the treatment.

He and Chu (2014) first conducted a series of undrained shear test on sand specimens with biogas generated by denitrifying bacteria. Results shown in Figure 2.27 clearly proves that the partially biogas ($N_2$) saturated sand exhibits greater resistance under both compression and extension conditions. It also suppress the excess pore pressure generation as investigators expected.

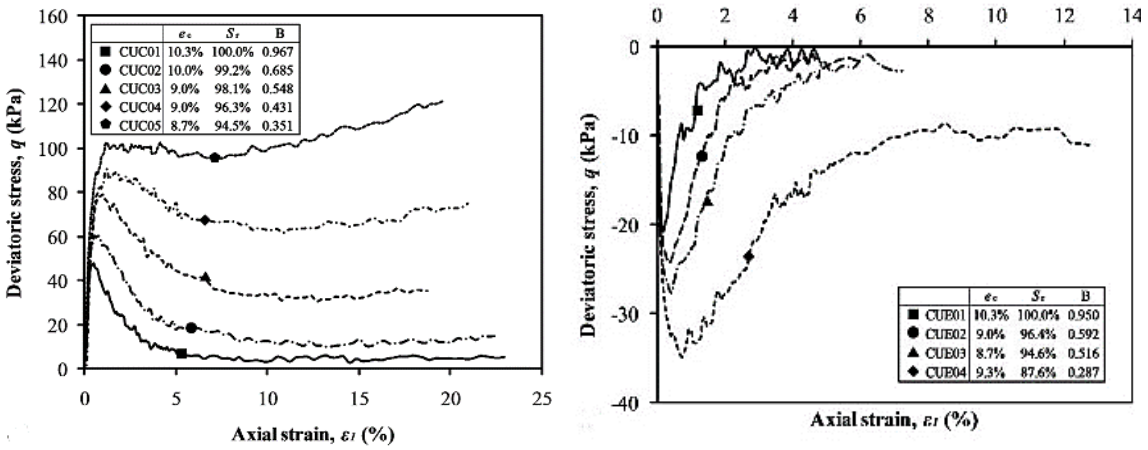


(a) Compression test (b) Extension test

*Figure 2.27 Undrained triaxial test results of biogas desaturated sand (He and Chu 2014)*

2.4.5.2 Stiffness

Soil stiffness determines the relationship between changes of stress and changes of strain. Bulk modulus, shear modulus, Young's modulus and Poisson's ratio are all important parameters for soil stiffness measurement. Recent years, the non-destructive measurement technique such as geophysical measurement has been widely adopted as a reliable and economical approach for soil stiffness determination. At the same time, application of microbial geotechnical process is a 'live' progress. It is not enough to just examine the soil properties after microbial treatments. Techniques which can monitor the intermediate stage are also required in the investigation. To this end, researchers have employed bender elements and piezo discs to measure shear wave (S-wave) and compression wave (P-wave) in most of microbiological geotechnology studies.

Wave measurements are effective in monitoring the incremental cementation that occurs with MICP. Weil *et al.* (2012) detected shear wave velocity of Ottawa sand increased

from 180m/s to about 1100m/s after MICP treatment. A linear relationship between calcium carbonate content and shear wave velocity in the Figure 2.28 was established by Martinez *et al*. (2013) based on their experiments. It confirmed an earlier similar trend found by Al Qabany *et al*. (2011).

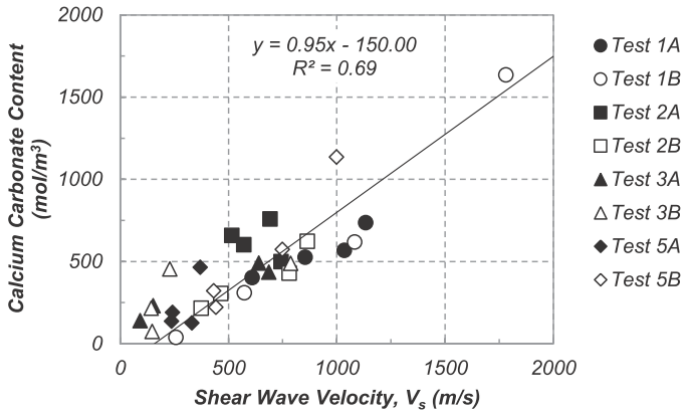


*Figure 2.28 Calcite content versus shear wave velocity (after Martinez et al. 2013)*

Although P-wave velocity is unaffected during MICP treatment, it is found to be an effective means to measure the degree of saturation. A slight change from fully saturation to partially saturation is able to decrease the P-wave velocity from 1500m/s to below 1000m/s. Some details were reviewed in Section 2.2.4.

2.4.5.3 Permeability

Soil permeability can be heavily altered by microbial activity and related mineralization or precipitation process. It has been observed that accumulation of bacterial biomass, insoluble bacterial slime, and poorly soluble biogenic gas bubbles in soil will make the soil less permeable for water (Ivanov and Chu, 2008). Microbial cells and their synthesized products exist on soil surface by forming biofilms or microcolony.

Experimentally, Kantzas *et al.* (1992) observed porosity reductions of up to 50% and permeability reductions of up to 90% when bacteria growth medium and a $CaCl_2$ and $NaHCO_3$ combined solution flushed through either sand columns or glass beads. Whiffin *et al.* (2007) similarly observed a reduction in permeability due to the MICP treatment from 22% to 75% of the initial value. Recently, researches have shown that the decrease in permeability was greater than two orders of magnitude after biological treatment (Rusu *et al*. 2011; Al Qabany *et al*. 2012; Chu *et al*. 2013; Martinez *et al*. 2013). Chu *et al*. (2012) successfully built an aquaculture pond in sand through a microbial method in the laboratory. The test results demonstared in Figure 2.29 indicated that the permeability of sand was reduced from the order of $10^{-4}$ m/s to $10^{-7}$ m/s.

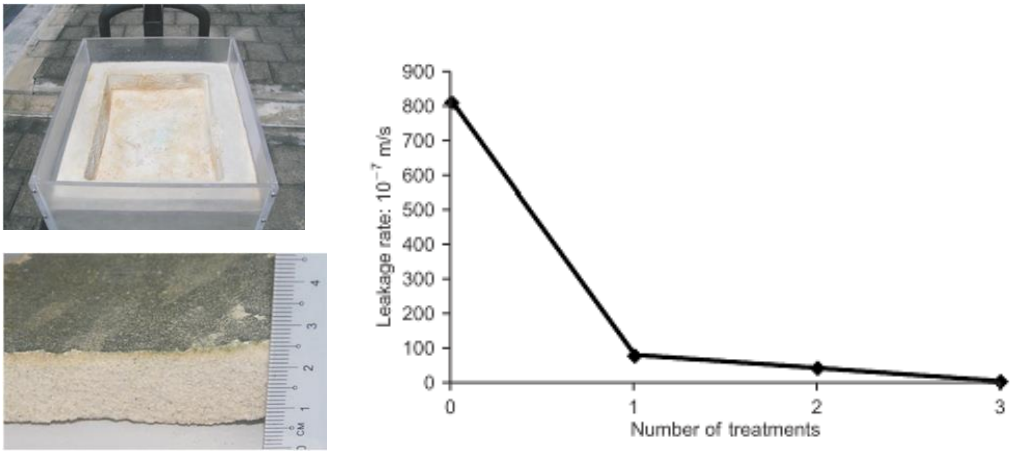


*Figure 2.29 An aquaculture pond built through microbial method (after Chu et al. 2012)*

It is reasonable to believe that an impereable layer either on surface or within soil can be artificially formed through appropriate treatment. However, it should also be recognized that permeability may not be unifrom through the whole treating soil sample or area.

## 2.5 Summary

Since the 1964 Niigata earthquake and Alaska earthquake, liquefaction has become a focus in the geotechnical and earthquake engineering. Extensive studies have greatly improved our understanding of its mechanism and trigger condition. Liquefaction susceptibility assessment relies on both historical data and current laboratory and site investigation. Cyclic triaxial test, SPT, CPT and elastic waves all can be empolyed as liuqefaction assessment approach based on given site conditions. Thanks to intellectual efforts of researchers and engineers, considerable liquefaction countermeasures have been developed and achieved certain success. However, as liuqefaction normally takes place over a large area. Most of the existing liuqefaction mitigation methods are not cost effective for vast area application. There is an urgent need to carry out scientific study to develop more cost-effective methods to mitigate the damages due to liquefaction.

In the laboratory, many studies have shown that the presence of gas in the voids or pore fluid will affects the mechanical response of soil during monotonic and cyclic loading. Recent fundamental soil mechanic tests, such as triaxial tests have suggested that inclusion of gas bubbles in saturated sand can reduce its susceptibility for liquefaction substantially. Some field trials have already been implemented in Japan and received positive outcomes. Although there are a few methods available for introducing gas bubble into saturated soils, for example, direct air injection, water electrolysis, using chemical reagent and sand compaction pile method, drawbacks are obvious in some approaches. Considering the energy consumption and uniformity of gas bubble distribution, biogas produced from microbial activity is a promising candidate for desaturation purpose.

Microbial denitrification process is adopted in this study to produce tiny nitrogen ($N_2$) gas bubbles from nitrate solution as a liquefaction mitigation method. Previous studies suggests that denitrification is an effecitve process for generating inert $N_2$ gas at given conditions such as availability of nutrient source, pH, ambient temperature and nitrate concentration. A slight reduciton of degree of saturation caused by nitrogen gas is going to significantly increase sand liquefaction resistance. To monitor the change of the degree of saturion, compressive wave (P-wave) method seems to be a wise option. The relationship between velocity of P-wave and the Skeptom pore pressure ratio B has been established. It is possible to evaluate the real time degree of saturation accoring to the P-wave velocity measurement.

The application of microbial process in the geotechnology engineering has been attracting great attentions in the past decade. A major research has been conducted on biocementation, bioclogging or biofilm and biogas approach as bio-mediated soil improvement means. The mechanisms behind these processes include: 1) binding soil particles with biomass and crystals; 2) filling voids and channels in soil and 3) both aspects combined. Despite encouraging results gained so far, extensive research is still required for better understanding of mechanisms and effectively applying the microbial process in the field. From microbiology to geotechnology, from government agencies to universities to industrial communities, exchanges and cooperation will be the main stream and key factor to push forward interdisciplinary research and application.

Critical state soil mechanics provides a theoretical basis to learn the fundamental mechanism of undrained behavior of sand and liquefaction hazards. The effectiveness of desaturation method for liquefaction mitigation can be verified under the CSSM frame. Basic

soil engineering properties in the CSSM frame can be improved thanks to certain microbial biological processes. Biocementation is capable of substantially enhancing soil shear strength and stiffness. Bioclogging and biofilm manages the seepage and permeability. Biogas contributes to the improvement of the resistance to the liquefaction and thus reduce the liquefaction potential.

# CHAPTER 3

# BACTERIA CULTIVATION, BIOGAS GENERATION AND BIOCLOGGING PROCESSES

## 3.1 Introduction

As reviewed in chapter 2, microbial geotechnology is a highly integrated discipline which requires multi-discipline knowledge. This chapter focuses mainly on the microbiological aspects, including bacteria cultivation, biogas generation process, microbial induced calcium carbonate precipitation (MICP) process and their integration. Batch experiments were performed by using enrichment culture to produce denitrifying bacteria. Strain culture purchased from Leibniz-Institut DSMZ was employed in producing large quantity of urease producing bacteria for MICP. Bench scale tests were conducted to study the influence of different carbon source to the denitrification process and the rates of biogas generation. Upon completion of MICP treatment, permeability and unconfined compression tests were performed to study the microbial treatment effects to sand engineering properties.

## 3.2 Cultivation of Bacteria

### 3.2.1 Cultivation of denitrifying bacteria

All organisms need complements of nutrients for growth. Carbon, hydrogen, oxygen and nitrogen are four basic element for organic compounds. Phosphates are required by the cell for synthesis of nucleic acids and phospholipids. Potassium is necessary for enzymes' activities. Calcium helps stabilize cell walls in many microorganisms and plays a key role in

the heat stability of endospores. Sulfur is required because of its structural role in the amino acids cysteine and methionine and because it is present in several vitamins. Microorganisms also require various metals for growth, such as iron and trace metals. The growth medium used in this study for cultivating denitrifying bacteria is consisted of ($L^{-1}$) 1.01g potassium nitrate ($KNO_3$), 0.66g glucose ($C_6H_{12}O_6$), 0.12g ammonium chloride ($NH_4Cl$), 0.75g monopotassium phosphate ($KH_2PO_4$), 2.5g dipotassium phosphate ($K_2HPO_4$), 0.1g magnesium sulfate heptahydrate ($MgSO_4 \cdot 7H_2O$), 0.01g ferrous sulfate heptahydrate ($FeSO_4 \cdot 7H_2O$), 0.015g calcium chloride dihydrate ($CaCl_2 \cdot 2H_2O$), 1 ml trace element (DSMZ SL-12 B) and 1L distilled water. Here $KH_2PO_4$ and $K_2HPO_4$ works as a pH buffer. A similar receipt was adopted by He and Chu (2014) before.

The source of denitrifying bacteria was anaerobic digester found in the soils which collected from different spots around the Iowa State University campus, Ames, IA. Batch experiments were performed to obtain the enrichment culture. Fifty grams of soil was first mixed with the growth medium in a 1 L glass bottle and left on a shaker for 15 minutes. Then the liquid culture was purged with nitrogen gas and transferred to a light-proof environment for 48 hours (Figure 3.1a). After the first batch, 200 ml of the culture was kept to mix with 800 ml growth medium for a second batch. The same process was repeated until the third batch was complete. Figure 3.1b shows gas bubbles were found at the surface of the culture media. The obtained enrichment culture was kept in the fridge for up to two weeks for further application.

(a) Dark room

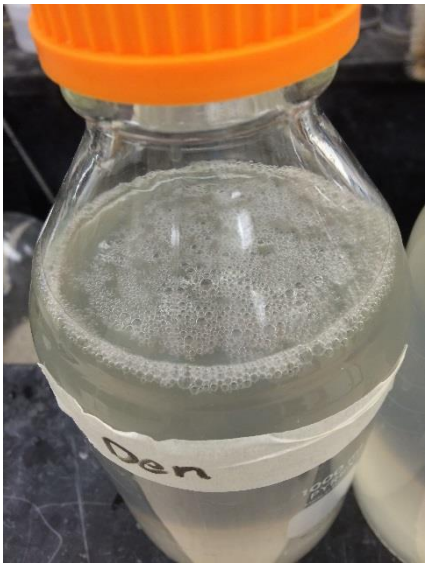

(b) $N_2$ gas bubbles

*Figure 3.1 Enrichment culture batch test*

Pure culture of denitrifying bacteria was isolated from the colony on solid medium which contained the suspension of enrichment culture. At first, the enrichment culture was diluted ten-fold with sterilized 1% NaCl solution. And then the diluted suspensions were spread uniformly on plates filled with agar. The inoculation process took 5 days until there were colonies found on the agar plate as shown in Figure 3.2. To cultivate pure culture, cells were collected from a single colony on the petri dish and then transferred to a sterilized liquid medium. In addition to chemical components mentioned before in the cultivation medium, Bacto Difco® Agar in a concentration of 12 g/L was used to solidify the liquid medium. The biomass in the suspension after cultivation was collected by filtration of 50 ml of bacteria suspension through a membrane with 0.2 μm pores and drying of the filter at 60°C for 12 hours. The pure culture was harvested and stored in fridge at 4°C.

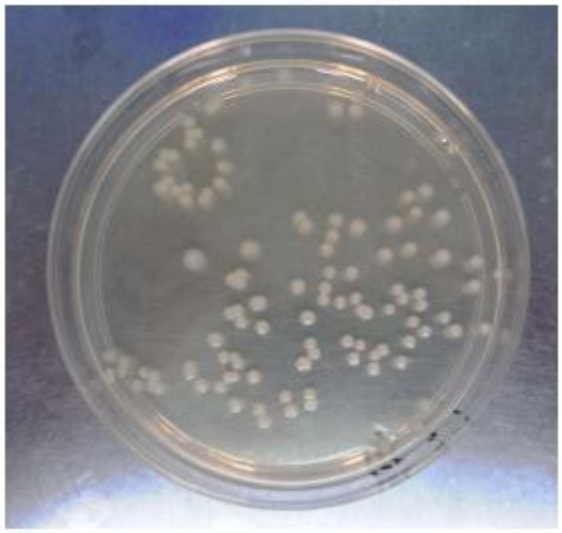

*Figure 3.2 Colony of denitrifying bacteria*

### 3.2.2 Cultivation of urease producing bacteria

The urease producing bacteria strain used in this study was *Sporosarcina pasteurii*, formerly known as *Bacillus psteurii*. The pure freeze dried culture (DSM 33) was purchased from DSMZ, Germany. Medium for the cultivation of urease producing bacteria (UPB) contains following components: Trypic Soy Broth DIFCO$^{TM}$, 20 g; Yeast Extract 10 g; NaCl 10 g; $MgSO_4$ $H_2O$ 12 mg, $NiCl_2$ $6H_2O$ 24 mg and 1 L distilled water. Adjust pH to 7.3. All components of the medium, except urea, were sterilized at 121°C for 30 minutes. Urea solution with a concentration of 20 g/L was sterilized through a 0.2 μm Whatman$^{TM}$ nitrocellulose membrane because heating would decompose the urea. Figure 3.3 shows the colony of the *Sporosarcina pasteurii* (DSM 33) cultivated in this study.

*Figure 3.3 Colony of Sporosarcina pasteurii (DSM 33)*

The cultivation of the bacteria *Sporosarcina pasteurii* was conducted in a 50 L sterilizable-in-place fermenter (Figure 3.4) in the Fermentation Facility at the Center for Corps Utilization Research, Iowa State University. The cultivation process maintained aerobically in an ambient 30°C condition. Silicone antifoam was injected for preventing of form accumulation. The pH was adjusted to 7.3 by using hydrochloride acid with a concentration of 1 M. As shown in Figure 3.5, the consumption of oxygen started about 6 hours after inoculation and stopped almost 24 hours later. The increase in pH indicated the hydrolysis of urea which also meant the urease producing bacteria had been releasing urease continually. The organisms were allowed to grow to the stationary phase before harvest. In other words, most of readily available nutrients were consumed from the medium.

*Figure 3.4 A 50 Liter sterilizable-in-place fermentor (Fermentation facility, ISU)*

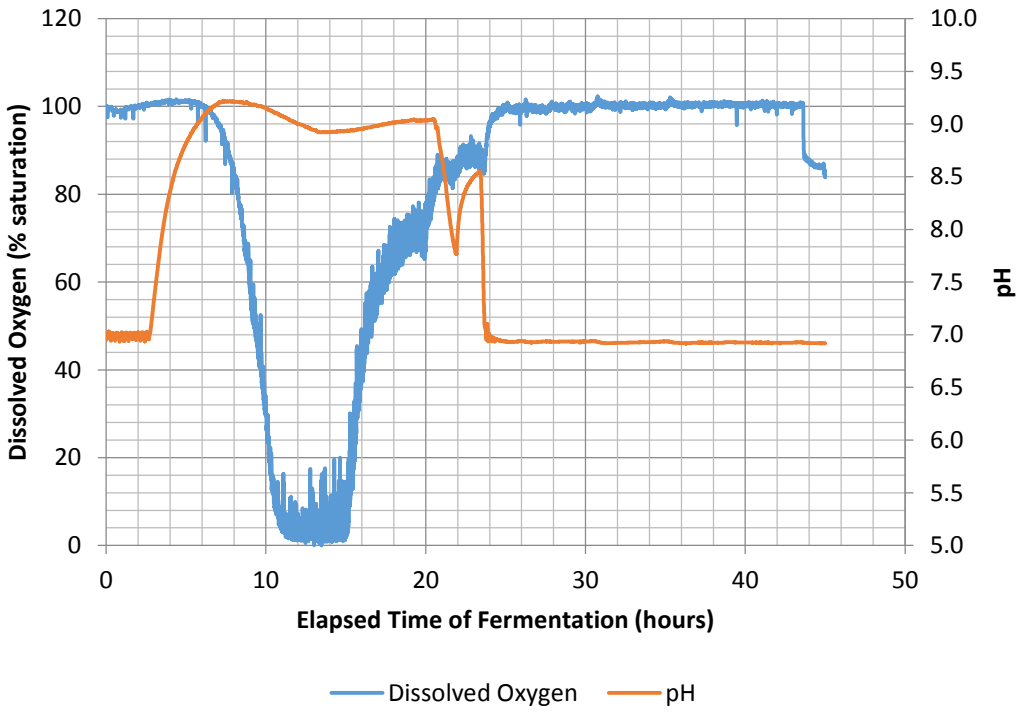


*Figure 3.5 Dynamics of dissolved oxygen concentration and pH value change during the cultivation of UPB*

In order to separate cells of UPB from its cultivation solution upon the completion of cultivation, the biomass was collected through a CEPA Z-41 high speed centrifuge (Eppendorf AG, Hamburg, Germany) as shown in Figure 3.6. The centrifuging process had effectively reduced the odor of ammonia due to the hydrolysis of urea during the cultivation stage. Another positive contribution of centrifuging UPB is that it can stabilize urease inside the cells and make the release of urease slower and steadier to form uniform biocementation (Li, 2014). Then the biomass was suspended in 10 g/L sodium chloride (NaCl) solution (Figure 3.7a). The usage of salinity solution was to prevent osmotic shock of cell and stop urease being released from cell to its solvent. Then the biomass was freeze dried in a VirTis Ultra 35 L Pilot Lyophilizer (VirTis Sp Scientific, Stone Ridge, NY, USA). Figure 3.7b shows a freeze dried UPB sample used in this research.

*Figure 3.6 CEPA Z-41 high speed centrifuge*

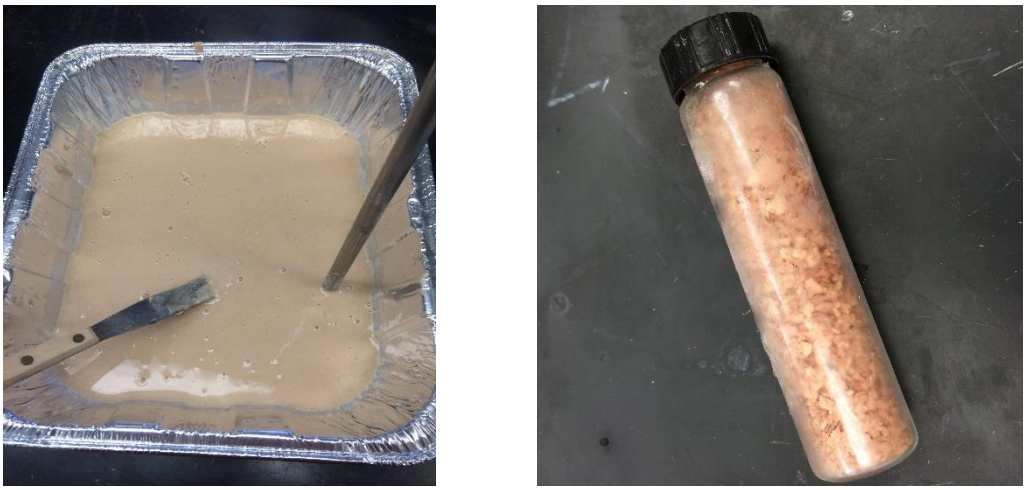

(a) (b)

*Figure 3.7 Images of UPB (a) UPB biomass suspension in NaCl; (b) Freeze dried UPB biomass*

## 3.3 Biogas Generation Test

A series of preliminary tests were conducted to investigate the nitrogen gas generation potential of the denitrifying bacteria. As a redox reaction, denitrification process can be expresses as a following reaction

$$2NO_3^- + 10e^- + 12H^+ \rightarrow N_2 + 6H_2O \quad (3.1)$$

The quantity of nitrogen gas generated by the denitrifying bacteria is mainly determined by nitrogen source in the liquid medium. It is possible to quantify the output of nitrogen gas by adjusting the amount of nitrogen source, the potassium nitrate in this case, for the purpose of producing desired gas volume.

Another factor restricts the biogenic gas production is the carbon availability. Four different carbon sources, ethanol, dextrose (glucose), glycerol and methanol, were employed

to study the feasibility of their roles in producing biogenic nitrogen gas through denitrification. Their reaction with nitrate are listed below

$$
\begin{aligned}
&5C_2H_5OH + 12NO_3^- \rightarrow 6N_2 \uparrow + 10CO_2 + 9H_2O + 12OH^- \\
&5C_6H_{12}O_6 + 24NO_3^- \rightarrow 12N_2 \uparrow + 30CO_2 + 18H_2O + 24OH^- \\
&5C_3H_8O_3 + 14NO_3^- \rightarrow 7N_2 \uparrow + 15CO_2 + 13H_2O + 14OH^- \\
&5CH_3OH + 6NO_3^- \rightarrow 3N_2 \uparrow + 5CO_2 + 7H_2O + 6OH^-
\end{aligned}
\tag{3.2}
$$

A fixed carbon versus nitrogen mole ratio of 3 was maintained in all batch tests. The concentration of potassium nitrate was 1.01g/L (0.01M) and the accordingly carbon source was added into the liquid medium with other components mentioned in the section 3.2.1.

### 3.3.1 Test setup

The test set-up is illustrated in the Figure 3.8. Four capacity of 60 ml syringes were filled with sand and treatment solution. The initial void ratio of sand column was about 0.7. The syringe had a diameter of 2.5 cm and the sand column height was 10.7 cm. The total void volume can be obtained via phase calculation. The treatment solution consisted of 10% (V/V) of denitrifying bacteria suspension and 90% of liquid medium. One end of the syringe was sealed by paraffin and the other end was connected to a 50 cm height U-shape manometer. The manometer was partially filled with distilled water and open to air. As the denitrification process took place, nitrogen gas was generated within the sand in the syringe. Since the nitrogen gas is hardly dissolvable, the accumulated gas bubbles would push the fluid in the voids out of the sand and into the manometer. The water level change in the manometer thus indicates the volume of nitrogen gas trapped in the sand column. When the generation of gas stopped, the test setup was disassembled and the pH value and nitrate

concentration of the treatment solution was measured through Accumet® AP85 pH Meter and Accumet® nitrate probe, respectively.

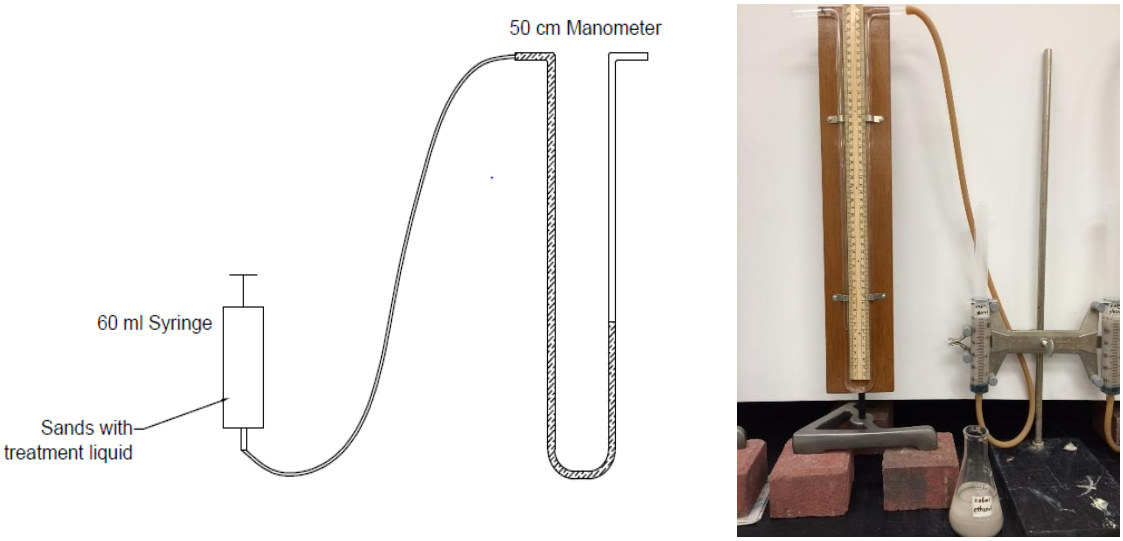


*Figure 3.8 Gas generation test set-up*

### 3.3.2 Results and discussion

The entire testing process took about 2 days. Test results are summarized in Table 3.1. The generated nitrogen gas volume was obtained through monitoring the water head change in the manometer. The nitrate conversion rate can be calculated via the following formula

$$\text{Nitrate conversion rate (\%)} = \frac{V_{N_2} / V_m}{C_{NO_3^-} \times V_{NO_3^-}} \tag{3.3}$$

In the equation, $V_{N_2}$ is the volume of the generated nitrogen gas, $V_m = 22.4L/mol$ is the molar volume of an ideal gas, $C_{NO_3^-}$ is the nitrate concentration of the liquid medium and $V_{NO_3^-}$ is the

volume of the liquid medium. Table 3.1 shows that not all nitrate was converted to nitrogen gas. The percentage of conversion varies as different carbon sources present.

*Table 3.1 Results of gas generation test with various carbon sources*

| Carbon source of medium | Void ratio of sand column | Initial nitrate source ($KNO_3$) concentration (M) | Initial carbon source concentration (M) | $N_2$ induced water level change (cm) | Nitrate conversion rate | Post-test pH value |
|---|---|---|---|---|---|---|
| Ethanol | 0.69 | 0.01 | 0.015 | 1.46 | 69.8% | 7.58 |
| Glycerol | 0.69 | 0.01 | 0.010 | 0.92 | 41.1% | 7.41 |
| Methanol | 0.68 | 0.01 | 0.030 | 0.99 | 44.2% | 7.45 |
| Glucose | 0.70 | 0.01 | 0.005 | 1.79 | 79.6% | 7.65 |

Figure 3.9 shows four curves that represent the generation of gas volume with different carbon sources. The liquid medium with glucose obviously produced the most nitrogen gas and the one with glycerol generated the least. There were almost no gas bubbles observed in the first 6 hours in all conditions. After that, all four groups started generating gas bubbles gradually and until 30 hours later all four curves showed no sign of increasing. Although the sample with methanol and glycerol had a relatively high rate for producing gas bubbles at the beginning. They ended up with less total volume of gas. Initially, the rate of gas generation from media with glucose was slower than other media. This may due to the availability of the aerobic bacteria activity of consuming oxygen. The anaerobic denitrifying bacteria was dominant later as all the soluble oxygen was consumed which resulted a faster rate of gas generation compared with other carbon sources.

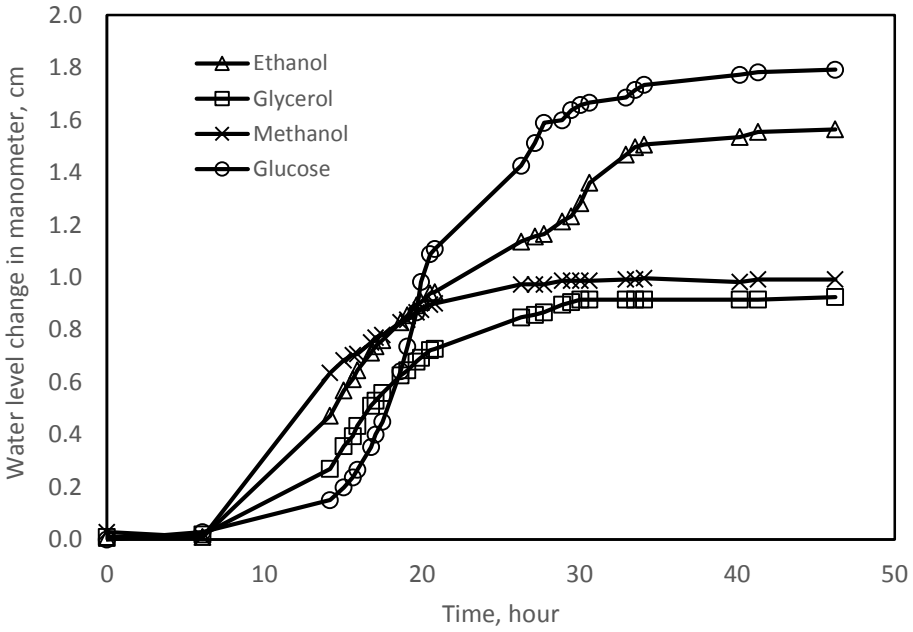


*Figure 3.9 Gas generation curve*

Additional tests using the same test setup were conducted to compare the effectiveness of denitrification process with ethanol and glucose. Figure 3.10 shows that in a same C:N ratio condition, glucose and ethanol yields similar production of nitrogen gas. T1 set had the same content of nitrogen and carbon source as previous four tests. T2 set contained as twice of nitrogen and carbon source content as T1 set. Similar trend was observed that ethanol based liquid medium produced nitrogen gas in a faster rate at the early stage of denitrification process than its glucose counterpart did. The final quantity of gas volume was quite close for both carbon source, although glucose may be a little bit more than ethanol. Considering glucose may also be consumed by other bacteria and generated carbon dioxide, the difference was not significant. Although today non-food based ethanol has been a widely used biofuel, its potential impact to the environment is still controversy. Given the fact that both carbon source produces similar amount of nitrogen gas at final, glucose is employed as a carbon source in the liquid medium in the following study. As addressed by

many researchers, denitrification does not always reaches the last step of $N_2$ formation with 100% percent efficiency (Firestone *et al*. 1980; Barnes *et al*. 1995; Chung and Chung 2000; Rebata-Linda and Santamarina 2012). According to equation 3.3, for the glucose case, the nitrate conversion rate had an average value of 0.8. It is necessary to take the value of 80% as a conversion rate for preparing nitrate source in the subsequent studies.

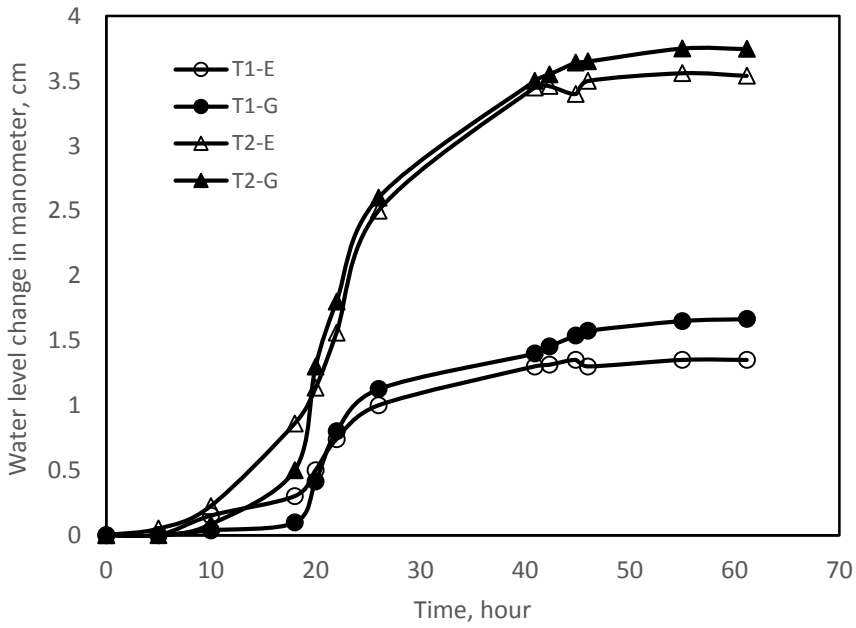


*Figure 3.10 Gas generation tests with different nitrogen and carbon content*

The post-test pH increased from their initial values for all tests. Similar trends were reported by Akunna *et al* (1993). As shown in the Table 3.2, the highest pH was found at the high concentration of ethanol based medium. The solution became slightly alkaline since the denitrification leads to ammonification which would increase the pH value. Table 3.2 also reveals that double the initial nitrate concentration of the treatment solution resulted a higher production of nitrogen gas, which suggests that the denitrification activity relates to the initial nitrate concentration. At the same time, the conversion rate of nitrate to nitrogen did not

change as much as the production. There was a certain percentage of nitrate left or converted to other formation such as nitrite or even nitric oxide at the end of the test. Either NO or $N_2O$ contributes to the global warming effect, ozone depletion, and other atmosphere pollution (Bremner and Blackmer 1978; Kester *et al*. 1997; Senbayram *et al*. 2012). Measures must be taken to avoid these intermediates when applying the *in situ* denitrification method. The process of the reaction should be closely monitored to ensure the emission of undesired byproduct meets the requirement of the environmental safety.

*Table 3.2 Test results of denitrification process with ethanol- and glucose-based medium*

| Test No. | Initial nitrate concentration (M) | Initial carbon source concentration (M) | $N_2$ induced water level change (cm) | Nitrate conversion rate | Degree of saturation (%) | Post-test pH value |
|---|---|---|---|---|---|---|
| T1-Ethanol | 0.01 | 0.015 | 1.35 | 60.3% | 94.6 | 7.65 |
| T1-Glucose | 0.01 | 0.005 | 1.67 | 74.3% | 93.3 | 7.35 |
| T2-Ethanol | 0.02 | 0.030 | 3.54 | 79.0% | 85.9 | 8.01 |
| T2-Glucose | 0.02 | 0.010 | 3.75 | 83.6% | 85 | 7.93 |

## 3.4 Microbially Induced Calcium Carbonate Precipitation (MICP) in Sand

The microbially induced calcium carbonate precipitation (MICP) process is one of the key processes behind biocementation and bioclogging. The hydrolysis of urea provides carbonate ions, with the presence of dissolved calcium ions, the produced carbonate ions will precipitate and form calcium carbonate crystals. These crystals are able to build bridges between sand grains or coat on sand particles directly and thus increase the strength and stiffness properties of the material. Urease producing bacterial (UPB) plays a key role in this process since they are in charge of releasing urease to hydrolyze urea. To verify the effectiveness of UPB cultivated in this study, a series of sand column tests were performed.

### 3.4.1 Test setup

The sand used for testing MICP process was a graded fine natural silica sand which meets ASTM C778. The $D_{50}$ of the sand is 0.36 mm and the specific gravity is 2.65. Dry sand samples were packed into a cylindrical PVC. Figure 3.11 presents a typical test setup in this study. The mold has a diameter of 50 mm. All solution including UPB and cementation fluid were injected from the bottom of the mold and flew out from the top. To prevent clogging at the inlet and outlet, drainage layers were prepared to separate sand and mold openings. At first there was a scouring pad attached to the inlet and a layer of approximately 2 cm filter gravel was then placed with another scouring pad covered it. Based on phase calculation, the sand was packed by targeting an initial void ratio of 0.65. Water sedimentation method was employed when preparing the sand column. The mold was half-filled with de-aired water. Raining the sand in a circular motion 5 mm above the water surface. After completion of the sand placement, laid another drainage layer with the same combination as in the bottom of the mold. A peristaltic pump (Cole Parmer FH100) was connected to an injection point at the bottom of the mold to regulate the flow rate.

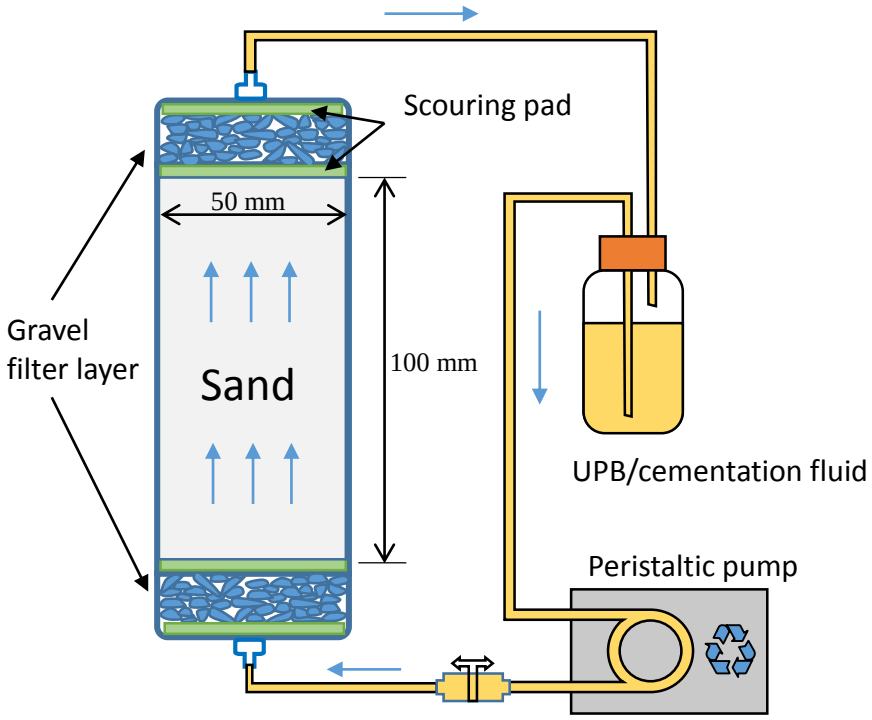


*Figure 3.11 Schematic of sand column test setup*

### 3.4.2 Treatment procedure

The UPB solution was made of 1 gram dry biomass (Figure 3.7b) dissolved in 1 L sodium chloride solution (10g/L). Depending on the quantity, one to two hours shaking time on a shaker could help improve the uniformity of biomass in the UPB solution. The cementation fluid consisted of 1.5 M urea and 1 M $CaCl_2$. Unless otherwise stated, the MICP treatment processed in the following steps:

(1) Introducing UPB into the sand column from the bottom of the cylindrical mold. The volume of the solution was 2 times of the pore volume. Keep circulating for 30 minutes and stop the peristaltic pump to retain the solution for 2 to 3 hours. This attachment period could allow the bacteria to diffuse in the sand voids and adhere to sand particles.

(2) Drain out all UPB solution, injecting calcium rich cementation fluid via the bottom port to initiate biocementation. The volume of cementation fluid injected was the same as UPB solution. Keep circulating for an hour and then close the bottom valve to retain the cementation fluid in the sand column.

(3) Restart circulating cementation fluid 4 hours later and carry on for an hour. Then stop the peristaltic pump and let the cementation fluid left in the mold to remain static for 12 hours.

(4) Drain out cementation fluid and repeat step (1) to (3).

Steps (1) to (3) can be seen as one batch of MICP treatment. Increase amount of calcium source input result in accumulation of calcite which can bond sand particles together. Usually more treatment batches contributes to a higher shear strength goal.

### 3.4.3 Monitoring and sampling methods

After re-suspending the dry UPB biomass in the fresh sterile saline prior to injection into sand columns, the urease activity was first measured for selection of a proper UPB solution. The urease catalyzes the hydrolysis of urea to $CO_2$ and $NH_3$ with a reaction mechanism based on the formation of carbonate as an intermediate. Urea hydrolysis will generate an increase in overall electrical conductivity of the solution. The rate of urease activity is obtained by measuring the rate of conductivity increase in a test sample against standards containing certain concentration of ammonium ion ($NH_4^+$).

To assess the ongoing and aftermath of the MICP process, it is necessary to monitor and measure a few parameters on both cementation solution and sand sample itself. Column

effluent was collected and tested for ammonium and residual calcium concentration after each batch. The ammonium concentration was determined relied on an ammonia electrode (ORION® 9512HPBNWP) and the Accumet® AR25 dual channel pH/Ion meter. Residual calcium concentration was measured by using the calcium titration method.

Upon completion of the treatment, the PVC mold was disassembled and sand columns were taken out for shear strength and permeability test. Figure 3.12 shows photos of two post-treatment sand specimens. The T1 sample did not form a strong texture and failed during the cutting because of limited treatment batches. The permeability of the sand column was determined by employing falling head permeability method and measured directly in the PVC mold. All sand columns' ends were trimmed by a grinder to create a flat surface without any irregularities to maintain a full contact during UC strength tests. A GeoTAC® automatic UCS machine was used for testing. After crushing sand columns, all pieces of samples were collected in plastic bags and different fragments of the sand specimen were picked for calcite content determination. There were two techniques involved. One was the titration and the other was so called "washing method". A piece of weighed sand fragment (1 to 4g) was washed in 10 ml 1 M hydrochloride acid. The mix resulted in acid dissolution of the sample and carbon dioxide generation. The remaining sand was then oven-dried and weighed again. The loss of weight before and after acid washing was seen to be the calcite formed in the original sand fragments since the sand itself was silica and immune of dissolving in acid.

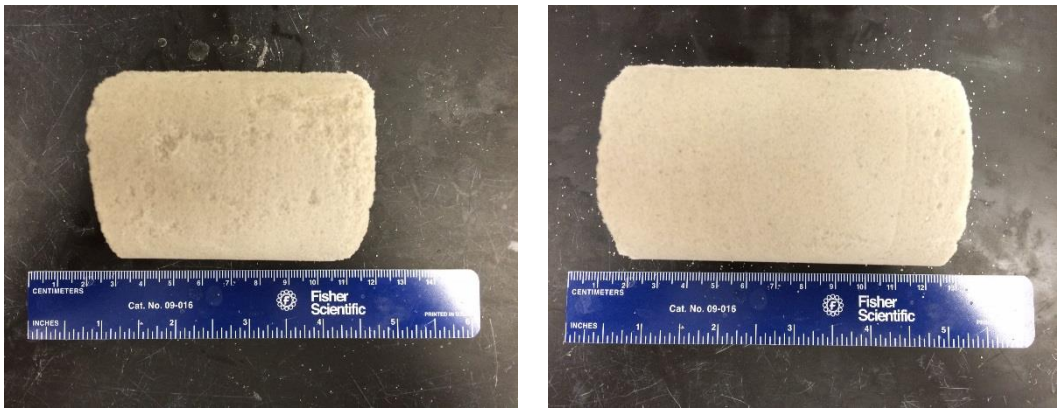


(a) T2 sample, 10 treatment batches

(b) T3 sample, 20 treatment batches

*Figure 3.12 Sand specimens after MICP treatment*

### 3.4.4 Results and discussion

Various batches of treatment were applied to different sand column specimens. Table 3.3 presents major results of all MICP tests. These results will be exemplified in this section under the general headings of urease activity, pH value, ammonia and residual calcium concentration, permeability and unconfined compression strength.

*Table 3.3 Summary of MICP test results*

| Test No. | Initial void ratio ($e_0$) | Relative density (%) | Treatment batch | Calcite content (w/w, %) | UC strength (kPa) | Permeability ($\times 10^{-4}$ m/s) |
|---|---|---|---|---|---|---|
| T1 | 0.68 | 40.51 | 5 | 1.24 | 449.25 | 6.79 |
| T2 | 0.65 | 49.39 | 10 | 6.12 | 1267.33 | 2.03 |
| T3 | 0.67 | 44.1 | 20 | 10.28 | 2339.36 | 0.85 |

*Urease activity*

Figure 3.13 plots urease activity change against time. The results illustrate that the initial urease activity of the UPB solution increased with time. Both sample UPB-1 and UPB-2 were made from the same dry biomass with a different concentration of 1 g/L and 1.5 g/L, respectively. After nearly 20 minutes of continues increase, the urease activity transferred to a stable status which keeps the activity value between ranges of 2 mM/min and 2.5 mM/min. It is worth noting that increase the biomass content, from UPB-1 1 g/L to UPB-2 1.5 g/L did result in a quicker rate of urease activity increase at the beginning and yield a higher final activity value. However, the difference is not significant. This finding is consistent with the claim made by Alef and Nannipieri (1995) that urease activity was not significantly correlated with microbial biomass and was affected differently by heavy metal, oxygen concentrations and nitrogen availability in different circumstances.

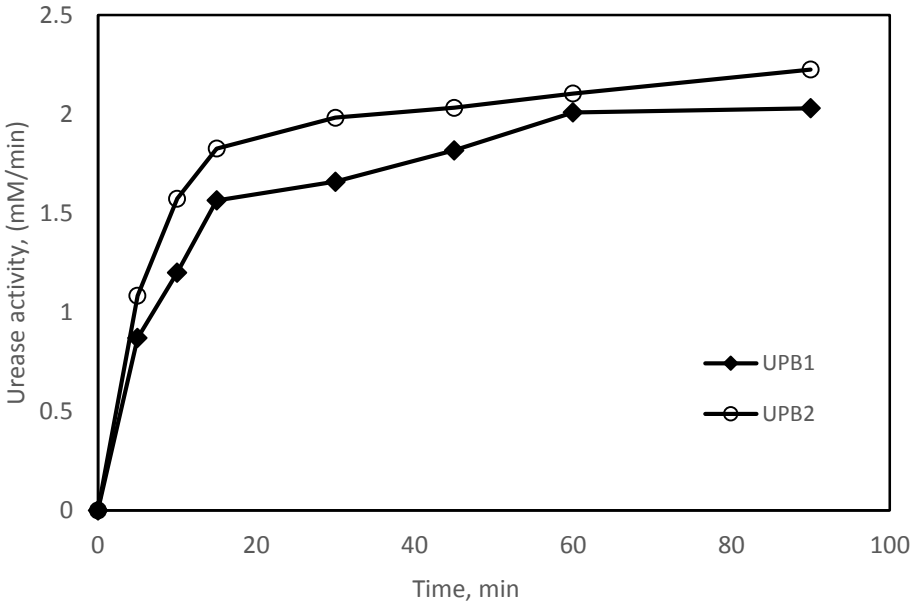


*Figure 3.13 Measurement of urease activity of UPB made from dry biomass*

*pH value*

The pH value is one of key indications for the MICP performance evaluation. Urea hydrolysis reaction produces hydroxyl ($OH^-$) which contributes to the alkalinity of ambient circumstance. Figure 3.14 presents the pH variation in a typical MICP treatment batch. A clear trend reveals the separation of UPB attachment period and treatment period. It can be seen that pH value of all samples kept almost constant during the UPB attachment period. Such a behavior indicates that the UPB solution prepared from freeze dried biomass was free of urea and bicarbonate. It attributed to previous procedures of filtration and effective centrifugation. Otherwise, an alkaline condition would inhibit the delivery of calcium and cause clogging in the injection channel. The pH value of the effluent started to rise in the treatment period due to the hydrolysis of urea. All three sand columns shared a similar pH variation trend. At the first hour of cementation fluid injection, the pH value was still steady. And then it increased gradually until a stationary period was reached. When the pH value reached a range of 8.5 to 8.9, a significant decrease of residual calcium in the effluent was observed. Previous studies also reported similar pH measurement in treatments (Whiffin 2004; van Paassen 2009; Li 2014). It is reasonable to speculate that after 8 hours' reaction, most urea injected was already consumed and the alkaline condition was preferred by the MICP process. It also found in most treatment batches that high initial pH value doesn't necessary yield high final pH values.

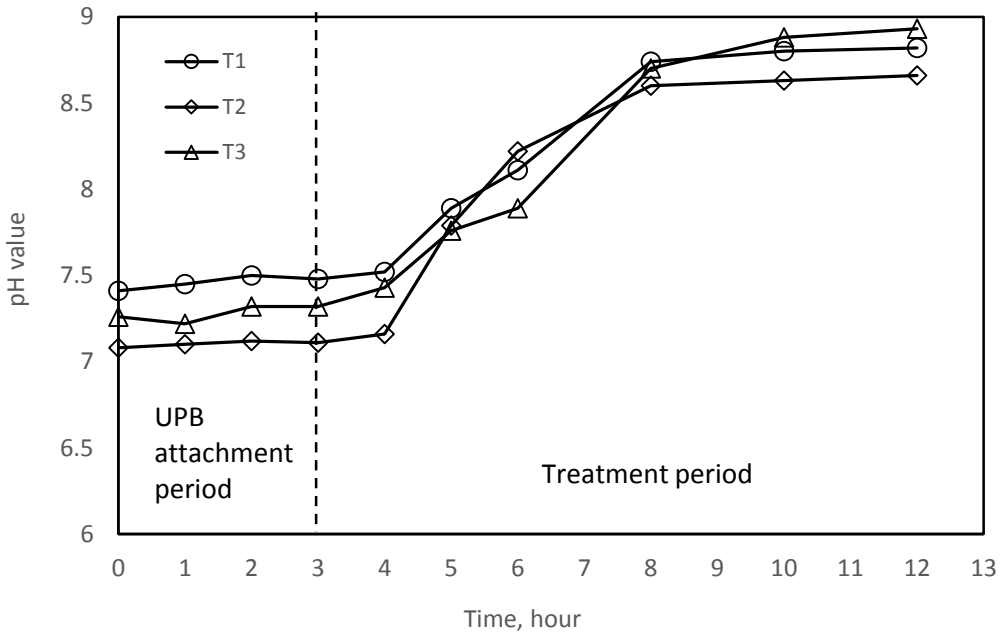


*Figure 3.14 The pH variation in a MICP batch*

*Ammonium and residual calcium concentration*

Figure 3.15 reveals the relationship between ammonium and residual calcium concentration in the effluent solution. Assume the effluent was drained out completely from a sand column, the fluid that came out at about 70 mL represented a treatment batch. The ammonium profiles indicates that the conversion rate of urea hydrolysis at beginning batches was not as high as later ones. Correspondingly, the residual calcium concentration was also significant in those batches. This suggests that the microbial calcium precipitation is not as fast as normal chemical precipitation. Even in a relative high pH environment (pH > 8.5) which benefits the activity of UPB (Whiffin, 2004), calcite formation is not straightforward as other factors might step in, such as mineral saturation status (Phillips *et al.* 2013). However, for a long term treatment, it is clear that a high ammonium concentration was maintained and resulted in a high pH environment. Under such an alkaline circumstance,

residual calcium concentration quickly dropped to below 0.2 M. The reason could be most of calcium injected reacted with carbonate ($CO_3^{2-}$) or bicarbonate ($HCO_3^-$) and contributed to forming calcium carbonate ($CaCO_3$) precipitation.

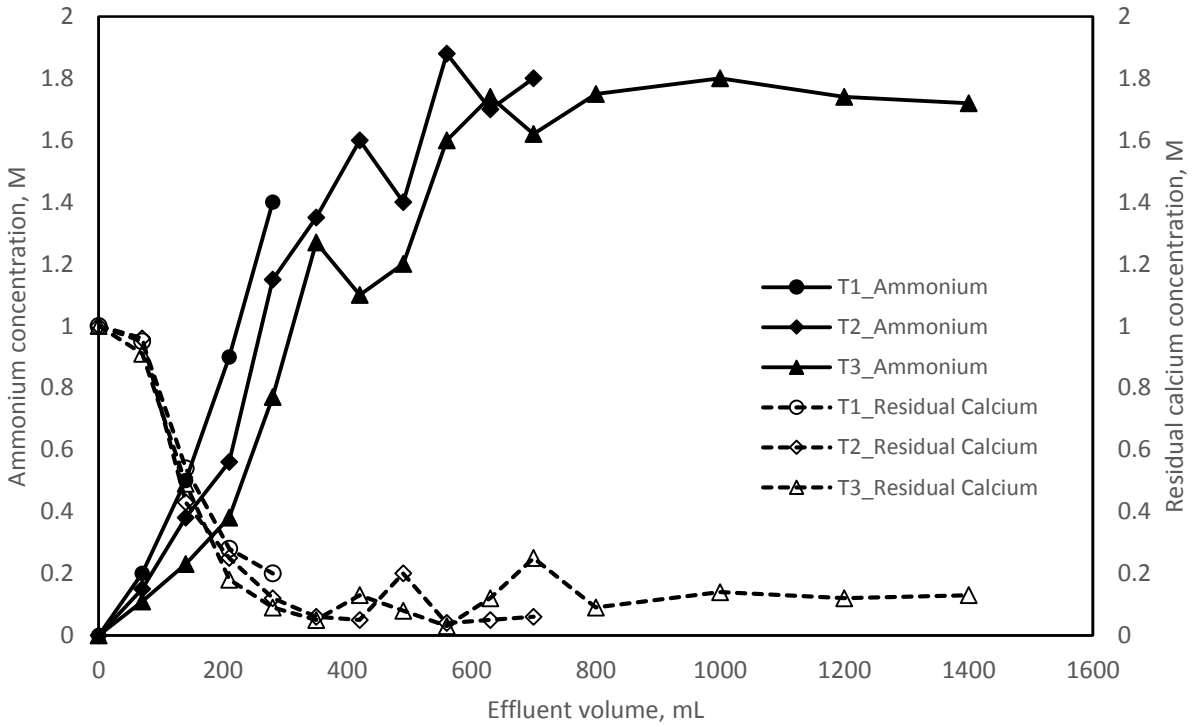


*Figure 3.15 Ammonium and residual calcium concentration in the effluent fluid*

*Permeability and unconfined compression strength*

The measurement of permeability after each treatment in three tests were plotted in Figure 3.16. As expected, the permeability reduced as the number of treatment batches increased. All three tests show that the permeability fell quickly even only after just a few treatment batches were performed. It can be seen from curves that after 4 to 6 treatments, the permeability already dived down to more than half of original values. The final permeability measured in Test 3 almost decreased a magnitude. However, it was merely different from the

one obtained in Test 2 regardless double treatment batches were involved. This phenomenon indicated that larger pores are easier to be 'sealed' by calcium carbonate precipitated through microbial activities. More details will be discussed later in this section.

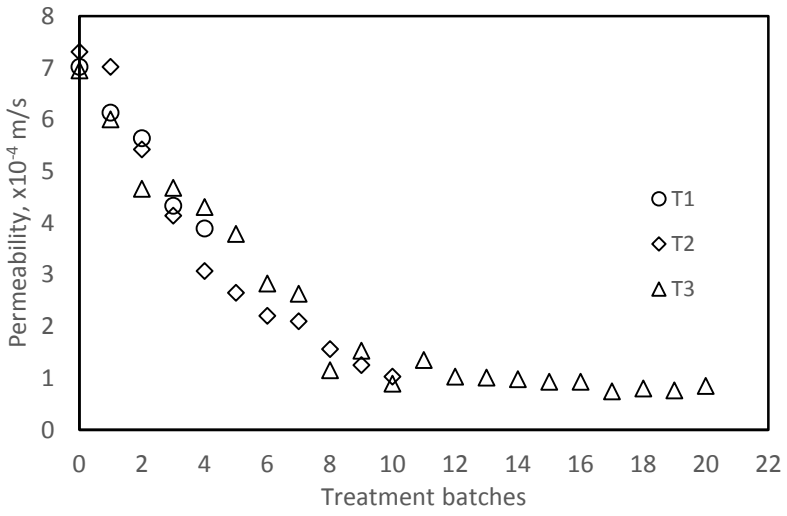


*Figure 3.16 Permeability variation with MICP treatment batches*

Unconfined compression test results were reported in Figure 3.17. All three tests showed that MICP treatments effectively improved the sand shear strength. The strength climbed quickly as the strain developed and reached highest value in a strain range of 1 to 1.5 percent. As expected, the highest strength was obtained in Test 3 which most treatment batches were given and resulted in the highest calcite content. For the Test 1, a limited numbers of MICP treatments still enabled an obvious improvement of the shear strength compared with loose sand. The results also indicated that the stiffness of sand increased with the number of treatment batches, in other words, the content of calcium carbonate precipitated in sand. The rate of stress rising in Test 3 was much higher than other two tests when small strain was developed. Figure 3.18 presents imagines of samples' failure in the unconfined compression test. Unlike the specimen in Test 1 whose major pieces were found

collapsed, specimens in Test 2 and Test 3 did not fail completely even when a big crack developed like in Test 3. The failure mode suggested that sand specimen treated by MICP behaves as brittle material which also is supported by the stress-strain relationship that the shear stress plumbed sharply after the peak stress.

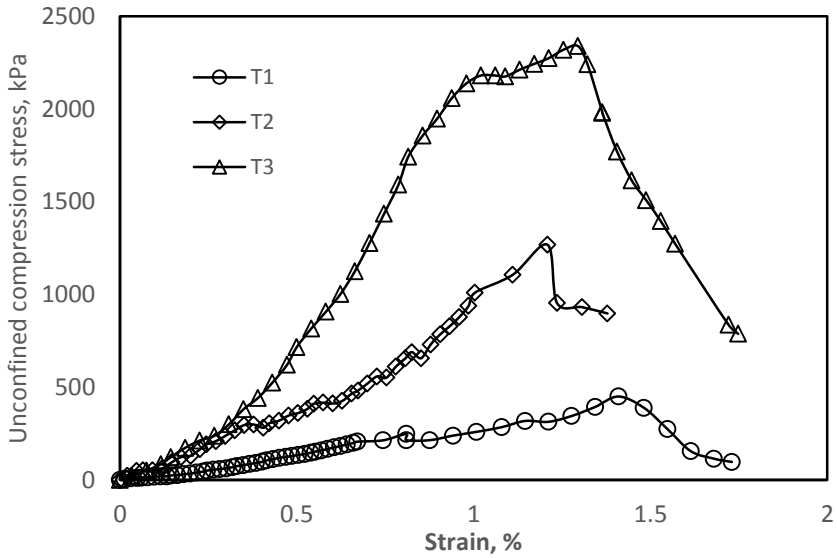


*Figure 3.17 Unconfined compression strength of MICP treated sand specimens*

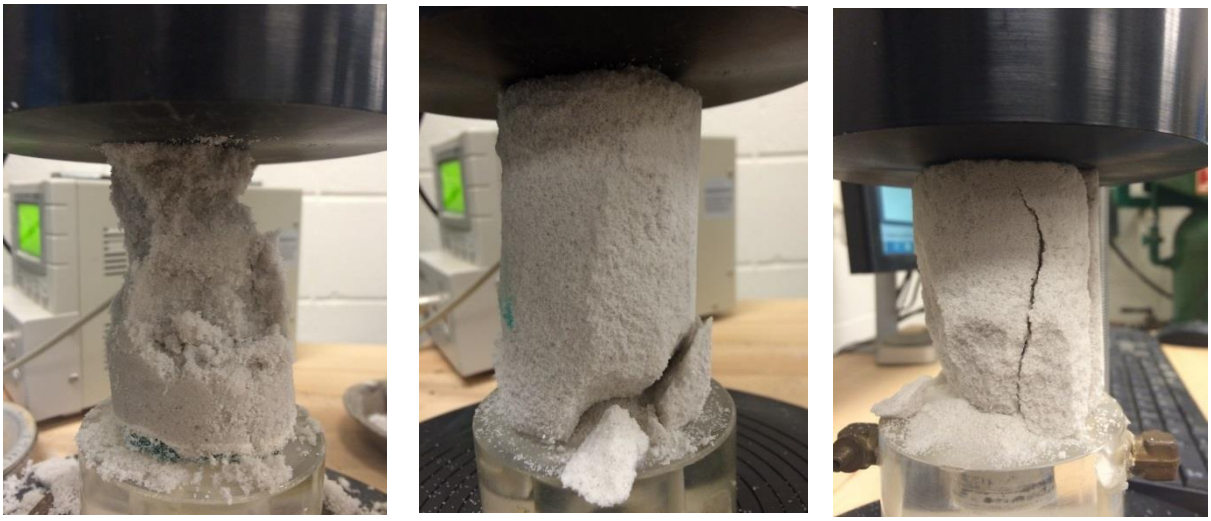

(a) T1 (b) T2 (c) T3

*Figure 3.18 Images of sand specimens in the failure phase of UC test*

Figure 3.19 summarized the relationship of calcite content with permeability and unconfined compression strength. It shows that permeability decreases with increasing calcium carbonate precipitation and unconfined compression stress rises as the calcite accumulates in the sand specimen.

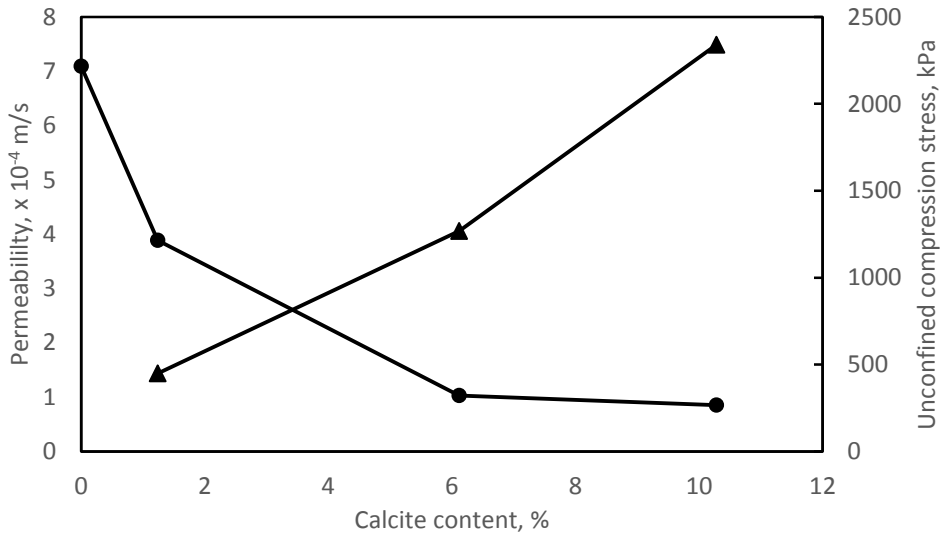


*Figure 3.19 Summary of permeability and UC strength, versus calcite content*

Low calcite content which below 1% did not significantly improve the strength of the samples. However, it did reduce permeability considerably. With a higher calcite content there was a significant improvement in strength compare to pure sand which cannot form sand columns by itself. Similar results were reported by von Paassen (2009) and Ivanov *et al*. (2010). The reason for this phenomenon may be attributed to two aspects, one is that the initial high presence of bacteria, urea/$Ca^{2+}$ in the large voids among sand particles easily caused calcite precipitation formation. Given the same concentration, bacteria and solutes were distributed sufficiently in those big voids at first when sand were loosely parked. The microbial calcium carbonate precipitated easier and quicker when more resources were

available. Because of the limited pore volume, UBP and solutes were relatively less distributed in those space and thus a slower rate of MICP resulted less nucleation of new crystals formation. It was easier for the plugging to take place in large pore voids because of more calcium carbonate precipitated. As those big pore voids were sealed, the permeability dropped dramatically. However, these plugging did not provide strong bindings because the shear resistance was still low. With the developing of calcite precipitation, free space in large voids was gradually occupied and big pore voids turned into small ones. This transformation balanced the UPB, urea and calcium source distribution in pore voids. If pore voids are tiny, the growth of existed calcite crystals prevails in the nucleation of new crystals, which strengthen the binding bridge between sand particles instead of clogging pore voids.

Another possibility of explaining the reduction of permeability at the early stage of MICP treatment without improving shear resistance could be as Stewart and Fogler (2001) described that the biomass accumulation closed some flow channels. The micro-organisms are keen to adhere to a surface and excrete extracellular polymeric substances (EPS) as product of their metabolism. This film-like EPS would further attack more micro-organisms and other particles attach on it. As a result, the formation of micro-organisms aggregation and EPS biofilm in those large pore voids altered the flow within the whole sand structure and reduced the permeability. However, those slimy biofilms did not function as a strong binder and provide enough strength to resist shear force.

## 3.5 Conclusions

Denitrification is a naturally occurring process which produces nitrogen gas through several intermediate steps. It poses less negative impact on environment compared to other

chemical or artificial activities to generate gas *in situ*. Enrichment culture was successfully cultivated via batch experiments in this study. A favored condition for the growth of denitrifying bacteria and the progress of denitrification reaction was selected. Various carbon source were investigated for the effectiveness of the denitrification process. The media with glucose or ethanol had higher nitrate conversion rate (nitrate to nitrogen gas) than ones with glycerol or methanol. Further testing results revealed that by using glucose instead of ethanol as the electron donor seemed benefiting the activity of denitrifying bacteria because of higher production of nitrogen gas when the same amount of nitrate was available. Moreover, glucose is environmental friendly compared with the application of ethanol. Lower pH value was measured in the media with glucose than its counterpart in the media with ethanol during the gas generation test. Some environmental concerns should still be taken into account for *in situ* application of denitrification process. First of all, it is necessary to identify the denitrifying bacteria strain to exclude disease causing pathogens or other strains may have potential threat to ecosystems. Secondly, use chemical substrates carefully according to the standards to avoid contamination of groundwater and soil. Any byproducts must be neutralized through imperative approaches.

The urease producing bacteria employed in this study was *Sporosarcina pasteurii.* A technique of producing dry UPB biomass was developed. Compare with conventional methods, the dry biomass was much easier to store and transport. The centrifuged UPB was free of chemical precipitation even in an alkaline environment. Otherwise, without proper manners, the clogging may happen in the delivery system and thus inhibit the application of cementation fluid. No chemical precipitation was observed in treatment batches when UPB was injected. The pH value can be seen as an indicator in the MICP process because when

the pH value was higher than 8.5, the permeability reduced significantly even after only a few treatments were performed. A reduction of one magnitude of permeability was observed after the treatment was completed. Unconfined compression tests revealed a remarkable increase of the shear resistance as the calcite accumulated in sand specimens. Sand behaves as brittle material after MICP treatments. Further studies are required to investigate the microbial induced calcium carbonate precipitation pattern and the crystal size, quantity along with their influence in engineering properties.

# CHAPTER 4

# BIOGAS STABILITY AND MICROSCOPIC CHARACTERISTICS OF SAND TREATED WITH BIOCEMENT

## 4.1 Introduction

We discussed the bio-desaturation method for mitigation of liquefaction in Chapter 2. To ensure the effectiveness of this method, the stability of biogas bubbles in sand is one of critical concerns in the study. This chapter discusses two aspects related to the stability issue. One is the permeability variation in a sand column treated by the microbial method. The other is the microscopic characteristics of the sand treated by denitrification and microbial induced calcite precipitation processes. For the former, sand column tests were conducted to measure permeability under different flow conditions for evaluating short- and long-term sustainability of entrapped gas in sand. The results show that the permeability can be an indicator for gas bubble stabilization in sand. For the later, X-ray computed tomography (CT) and Scanning Electron Microscope (SEM) imagines were used to reveal the structure of sand samples at a microscopic level and to provide visual information for understanding the mechanisms of the microbial treatment.

## 4.2 Stability of Biogas in Sand

### 4.2.1 Sand properties

ASTM C778 graded silica sand was used for all sand column tests. Table 4.1 gives typical properties of the silica sand. Figure 4.1 shows the particle size distribution curve. The

silica sand has a mean grain size ($D_{50}$) of 0.36 mm, a coefficient of uniformity ($C_u$) of 1.5, coefficient of curvature of ($C_c$) of 0.95, and a fines content of 0.1 percent. The maximum ($e_{max}$) and minimum ($e_{min}$) void ratios were 0.87 and 0.52, respectively, as determined by ASTM D-4254 and ASTM D-4253. Figure 4.2 demonstrates a SEM image of the clean silica sand.

*Table 4.1 ASTM C778 graded silica sand properties*

| Sand Type | Mean grain size (mm) | Specific gravity | Coefficient of uniformity | Max void ratio | Min void ratio | Minerology |
|---|---|---|---|---|---|---|
| Silica sand | 0.36 | 2.65 | 1.5 | 0.87 | 0.52 | Quartz |

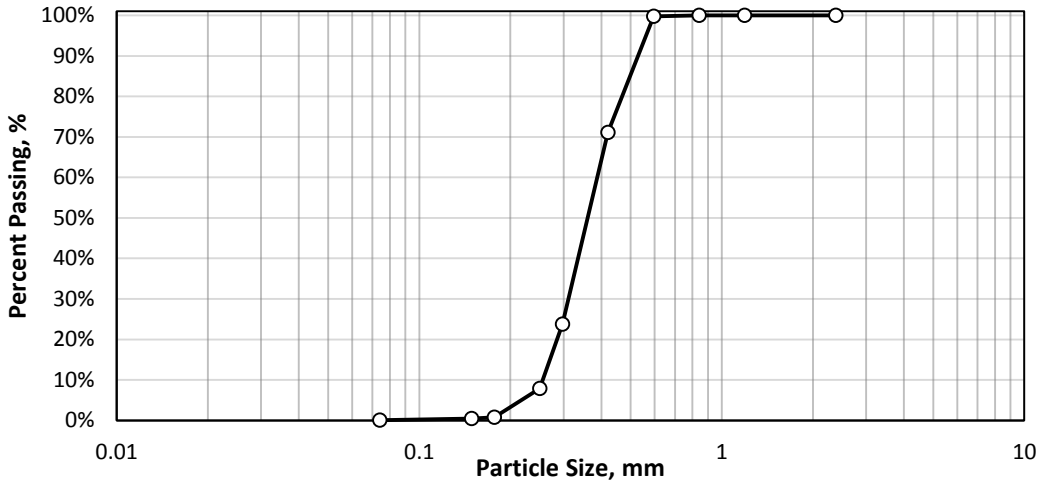


*Figure 4.1 Silica sand particle size distribution curve*

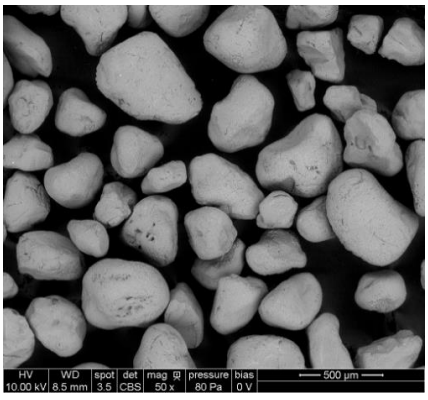

*Figure 4.2 Clean silica sand SEM image*

### 4.2.2 Testing setup

To examine the biogas stability in sand, long sand columns with different flow conditions were adopted. Two different sizes of transparent acrylic columns were designed and fabricated to serve the test purpose. As shown in Figure 4.3, the first one, Column A, had an inner diameter of 7.62 cm (3 inch) and a length of 150 cm. There were two outlets located at the top and bottom of the column, respectively. The second one, Column B, had the same length but a bigger inner diameter of 13.5 cm. Column B had 4 outlets at one side of the wall which connected with 4 graduated standpipes. This design enabled researchers to monitor the total water head changes at different positions of the sand column and thus calculate the water head loss and corresponding permeability.


(a) Column A (d = 7.62 cm) (b) Column B (d = 13.5 cm)

*Figure 4.3 Acrylic pipes used in sand column tests*

Table 4.2 presents the details of all sand column tests. Five Column A type of tests, Ta1H, Ta2U, Ta3D, Ta4UM and Ta5DM were prepared for examination of biogas stability in sand specimens under different flow conditions. Three Column B type of tests, Tb1, Tb2 and Tb3, were carried out to investigate distribution of biogas bubbles in sand.

*Table 4.2 Biogas stability sand column test setup*

| Test No. | Mass of sand (kg) | Height of sand column (cm) | Initial void ratio $e_0$ | Relative density $D_r$ (%) | Targeted degree of saturation (%) | Flow condition | MICP |
|---|---|---|---|---|---|---|---|
| Ta1H | 7 | 97.1 | 0.68 | 41.2 | 85 | Hydrostatic | N.A. |
| Ta2U | 7 | 97.7 | 0.69 | 37.8 | 85 | Upward | N.A. |
| Ta3D | 7 | 96.9 | 0.67 | 42.3 | 85 | Downward | N.A. |
| Ta4UM | 7 | 97 | 0.67 | 41.8 | 85 | Upward | Yes |
| Ta5DM | 7 | 96.6 | 0.67 | 44.1 | 85 | Downward | Yes |
| Tb1 | 15.85 | 70 | 0.68 | 41.6 | 100 | Hydrostatic | N.A. |
| Tb2 | 15.90 | 70 | 0.67 | 43.3 | 90 | Hydrostatic | N.A. |
| Tb3 | 15.83 | 70 | 0.68 | 40.8 | 80 | Hydrostatic | N.A. |

In all Column A type tests, for each column, there was a 10 cm height gravels placed as a drainage layer at the bottom of the acrylic pipe. A scouring pad was put on top of gravels for separation purpose. A total of 500 ml denitrification nutrient medium with 100 ml denitrifying bacterial suspension was poured in first followed by 1 L distilled water. The denitrification nutrient component was same as mentioned in Chapter 3. The total amount of nitrate carbon source was determined based on the desired degree of saturation target which was 85 percent. According to gas generation test results in chapter 3, the real degree of saturation of sand can be determined through the measurement of surface water level change. Next, 7 kilograms sand was dry-pluviated into the transparent acrylic pipe. The falling height was kept constant during the raining process. When all sand was placed, tightly sealed the

pipe with Gripper® mechanical plugs at both ends and flooded the sand column with $CO_2$ gas at atmospheric pressure from the bottom inlet for 20 minutes. This displaces air in sand by $CO_2$, which is about 56 times more soluble in water than is $N_2$ in air. It is advantageous to replace a large fraction of the $N_2$ gas by $CO_2$ to obtain a high degrees of saturation. Kutter (2012) claimed that de-aired water can dissolve about 83% of the volume of $CO_2$, but only 1.5% of the volume of $N_2$. After flushing with $CO_2$, denitrification medium with denitrifying bacteria suspension was injected into the sand column by a peristaltic pump via the bottom inlet to saturate dry sand. The rate was carefully controlled to ensure that the hydraulic gradients were not excessive. In order to improve the uniformity of fluid distribution, three times of void volume denitrification solution was circulated for 2 hours in each sand column. Based on the final height of sand column, the initial void ratio and relative density achieved was around 0.65 and 40 percent, respectively.

When the denitrification process was taking place, nitrogen gas bubbles were produced within pore fluids. Due to its extremely low solubility under the atmospheric pressure, when nitrogen gas bubbles generated in sand, the water level would be lift up. During the denitrification process, gas bubbles were observed on the wall of the transparent acrylic pipe as well as water above sand as shown in Figure 4.4. Gas bubbles appeared on the water surface were relatively big which could be a result of gas bubble aggregation. In contrast, gas bubbles found on the wall of acrylic pipe were in tiny size.

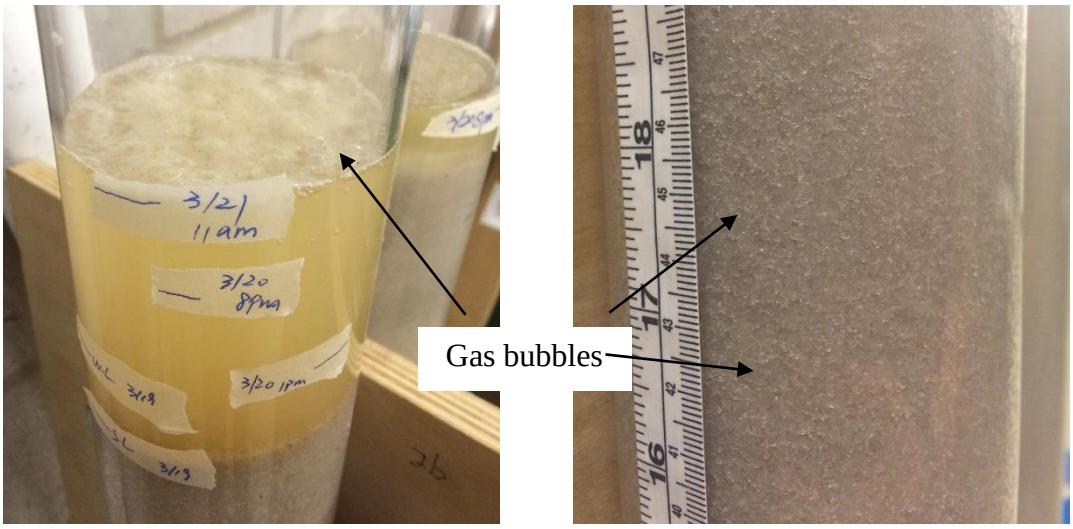


*Figure 4.4 Observed gas bubbles in sand column tests*

Upon the completion of denitrification process, the water level stopped rising. A closed-loop of flow stream was introduced into sand columns via a peristaltic pump in a considerable low rate (10 ml/min). Figure 4.5 was a schematic of test setup for two flow directions and sand permeability measurement. The variation of degrees of saturation during the whole seepage flow process could be monitored and assessed in an assumption that water flow through pore voids and replace some biogas bubbles trapped inside. A weighing balance was used in flow test to measure the difference of water weight between sand column inlet and outlet. Thus the water flow in or out of the tube can be recorded and as an indicator for how much water replaced the biogas bubbles and stay in sand pore voids. The permeability was measured by adopting constant head method. As shown in Figure 4.5(c), $\Delta h$ represents the constant water head difference between a water tank and the sand column. Knowing the height of the sand sample column $L$, the sample cross section area $A$, the volume of discharge $Q$, and the time interval t, the permeability $k = \frac{QL}{A \cdot \Delta h \cdot t}$.

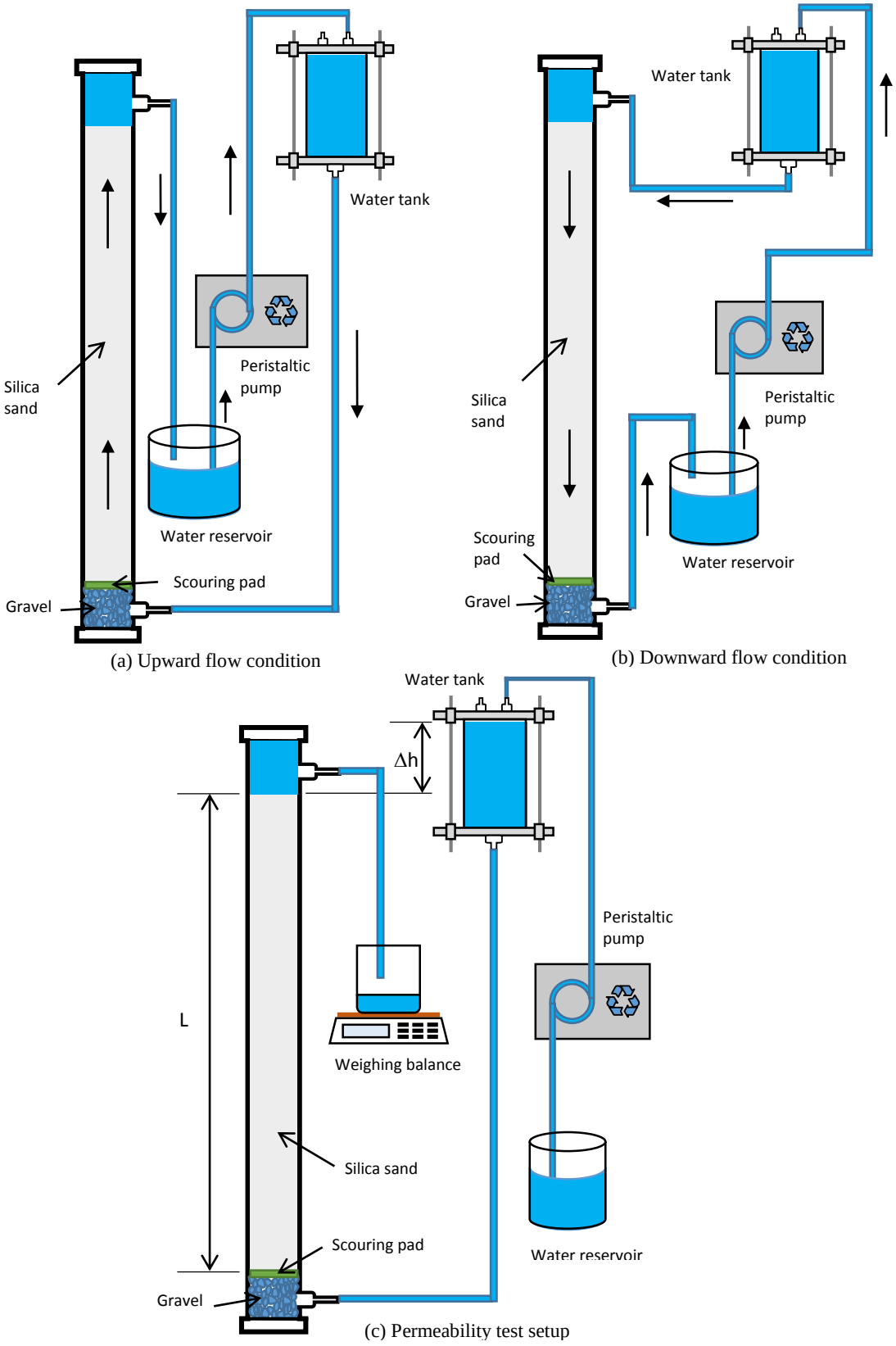


*Figure 4.5 Schematic of biogas stability test with different flow directions*

Three Column B type tests were employed to investigate the distribution of gas bubbles along the depth of sand columns with different degrees of saturation. Following the same procedure adopted for the Column A type of tests, a length of 70 cm sand column with a relative density of roughly 45 percent was obtained. Four liters of denitrification solution, with a nitrate source concentration of 0.01 M was then infiltrated from the bottom to top. Caution was excised to avoid disturbing the specimen due to excessive pressure gradients and erosion. Since the grain size of silica sand used in all test was quite small ($D_{50}$ = 0.36mm), in order to avoid sand grains flow through those outlets into standpipes and impede water heads change, four pieces of thin geosynthetic textile were attached at the inner side of acrylic pipe where each outlet located. No sand grains were found in standpipes in following tests. Finally, close all inlets and outlets and record water surface level change due to the nitrogen gas generated from denitrification process. When the water surface reached a desired height which meant enough nitrogen gas had already been produced to lower the fully saturated sand to de-saturated sand with a controlled degree of saturation, following permeability test were performed. Figure 4.6 illustrates the schematic of sand column test B. Take the highest outlet as a datum, the *h* represents the length of water head in the standpipe. Constant head method was used for permeability measurement. A water tank stand on an adjustable jack platform maintained a constant water head difference between water reservoir and the surface of water level in sand column which was also the place of upper outlet shown in Figure 4.5. A peristaltic pump pumped water into the water reservoir continually to kept a constant water head in every permeability test.

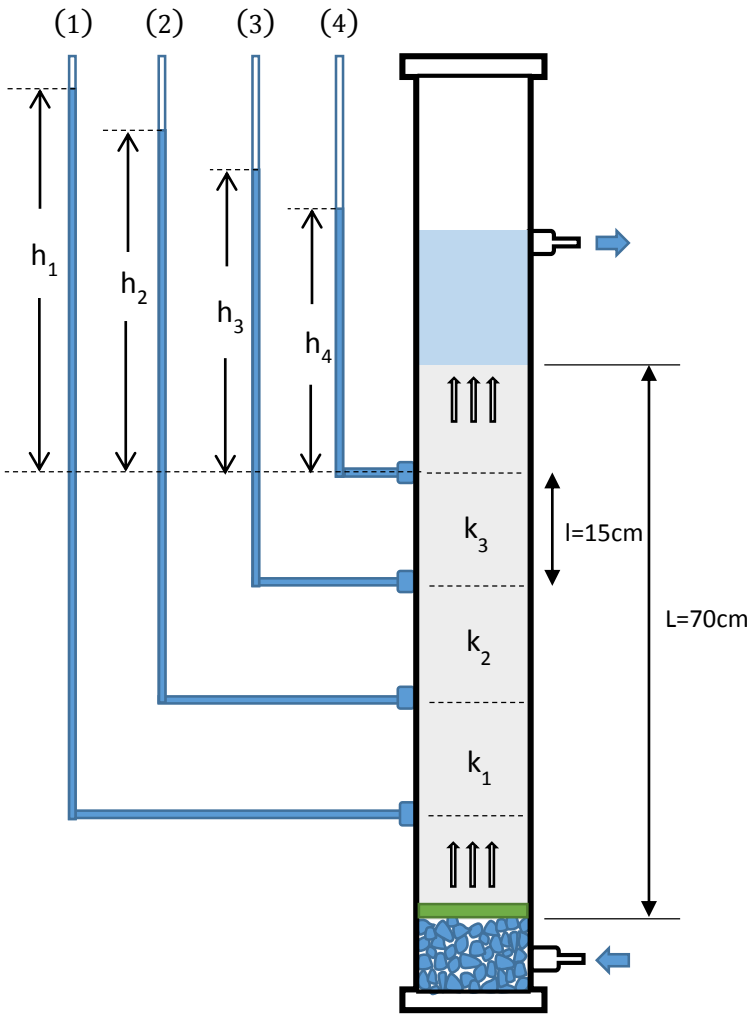


*Figure 4.6 Schematic of biogas distribution test*

### 4.2.3 Test results and discussion

Table 4.3 provides a brief overview of actual degrees of saturation and pH values each sand column achieved after microbial technical treatment. The designed degrees of saturation for small diameter sand columns was 85 percent. The actual results (84.39 – 87.7%) were close to that value which confirmed that as long as the concentration of nitrate and carbon source were controlled in a reasonable C:N ratio, the amount of nitrogen gas generated from the denitrification process can be employed to manipulate degrees of

saturation in sand. Figure 4.7 demonstrates the increase in the water level in the sand column which can be used to calculate the volume of generated biogas bubbles. The ratio of this increased water volume to the initial void volume was an indicator for the current degree of saturation. The denitrification process started to produce nitrogen gas after 20 hours and maintained an efficient biogas generation rate in the following 20 to 30 hours before the water level reached a stable condition when the nitrate source appeared to be fully consumed.

*Table 4.3 Summary of biogas stability test results*

| Test No. | Water surface level change (cm) | Converted volume of biogas (ml) | Actual degrees of saturation (%) | pH value after microbial technique treatment | Seepage flow period (day) | Coefficient of permeability ($\times 10^{-4}$ m/s) | Average calcium carbonate content (w/w, %) |
|---|---|---|---|---|---|---|---|
| Ta1H* | 5.7 | 250.8 | 85.44 | 7.71 | - | 3.44 | - |
| Ta2U | 5.8 | 214.3 | 87.78 | 7.79 | 10 | 3.15 | - |
| Ta3D | 5.7 | 237.1 | 86.20 | 7.82 | 10 | 3.23 | - |
| Ta4UM | 6.1 | 278.2 | 84.39 | 8.67 | 40 | 1.65 | 0.83 |
| Ta5DM | 5.4 | 246.3 | 86.04 | 8.79 | 40 | 1.11 | 0.79 |
| Tb1 | 0 | 0 | 100 | 6.84 | - | 6.64 | - |
| Tb2 | 2.5 | 357.8 | 91.14 | 7.73 | - | 4.96 | - |
| Tb3 | 5.5 | 787.3 | 80.50 | 7.85 | - | 2.86 | - |

*: a, d =7.62 cm; b, d = 13.5 cm; U, upward flow; D, downward flow; M, MICP.

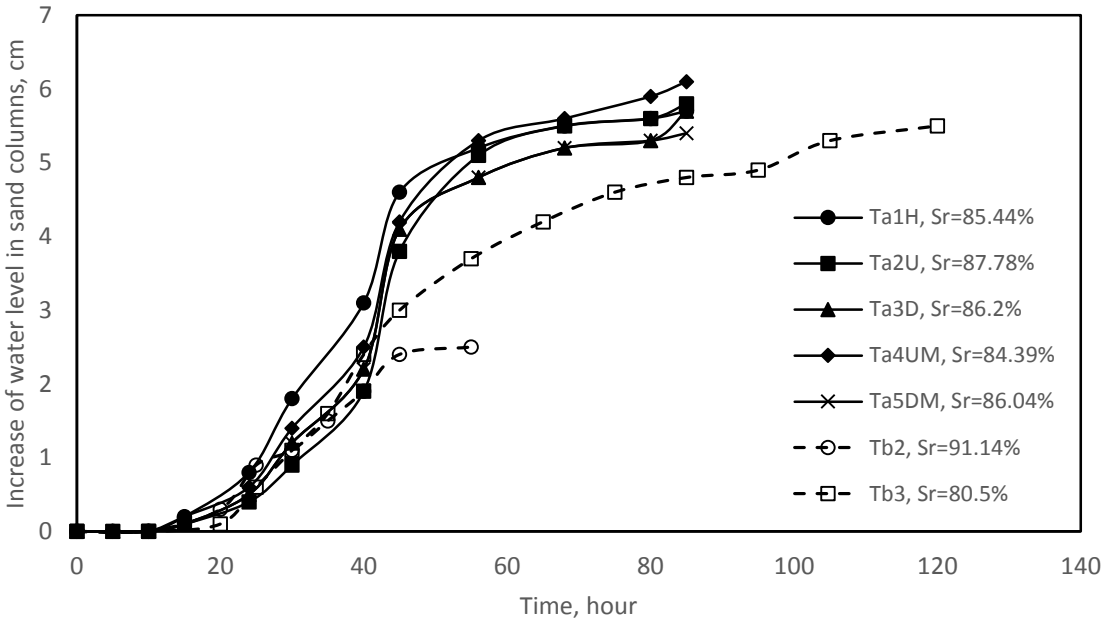


*Figure 4.7 Increase of water level in sand columns during denitrification process*

For sand specimens under the upward or downward flow condition, the variation of the degree of saturation can be obtained through the measurement of weight difference between water flowed in and out of sand columns. Figure 4.8 indicates that for the first 2 days, degrees of saturation kept constant in the upward flow case and changed only 2 percent in the downward flow condition. However, as flow continued through the sand column, the degree of saturation increased quickly in both tests. Especially for the downward flow condition, almost a 10 percent increase in the degree of saturation was observed after 100 hours of flow. After 150 hours flow, the sand specimens in both tests became fully saturated as their degrees of saturation were above 99 percent. The soar in degrees of saturation indicate that the flow had either taken out or dissolved biogas bubbles trapped inside the sand column.

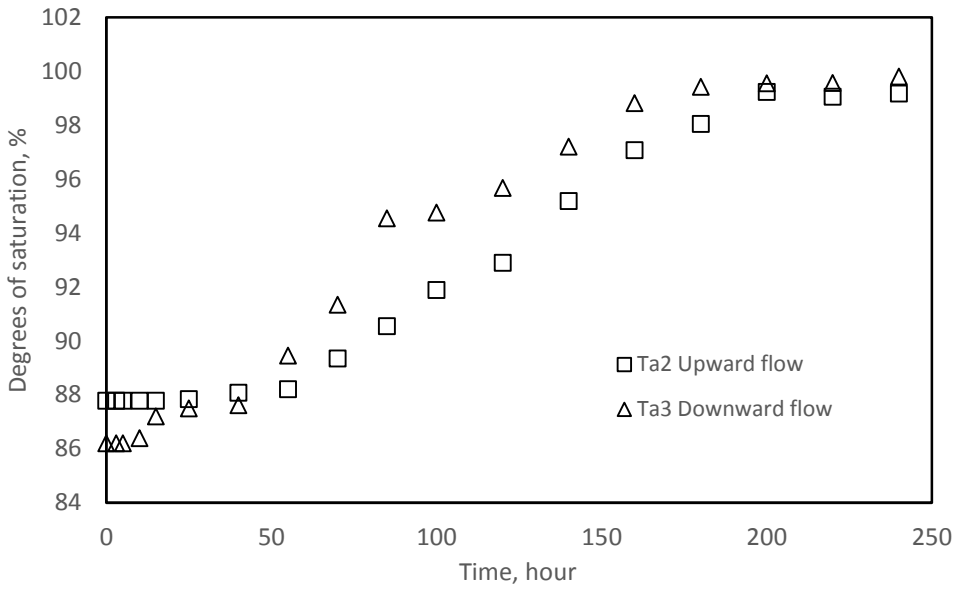


*Figure 4.8 Variation of degrees of saturation in short term flow conditions*

Fredlund and Rahardjo (1993) suggested that Darcy's Law is still valid for partially saturated soils. However, the permeability in partially saturated sand is expected to be lower than that in fully saturated sand and also related to other factors such as degrees of saturation and water content. The permeability of sand was obtained by measuring the water flow out of the sand column in a time interval. A constant water head with a hydraulic gradient of 0.1 was maintained in the permeability test. Figure 4.9 compares test results among three flow conditions – hydrostatic (Ta1H), upward flow (Ta2U) and downward flow (Ta2D).

The permeability of sand in the hydrostatic condition was stable indicating that without the seepage flow, the biogas trapped in the sand column was likely to be stationary. By contrast, the permeability of sand changed when a flow was introduced. The increase in permeability (from about $2 \times 10^{-4}$ m/s to $3 \times 10^{-4}$ m/s) suggests that the biogas bubbles in the sand columns were carried out by flow. A similar observation was also reported by He (2013): within 4 days' seepage flow, a biogas desaturated sand column became fully

saturated. It should also be pointed out that the pattern of change in the curves of Ta2 and Ta3 in Figure 4.9 is consistent with trends variation in Figure 4.8. When the specimen became fully saturated as shown in Fig. 4.8, the permeability also turned to be steady.

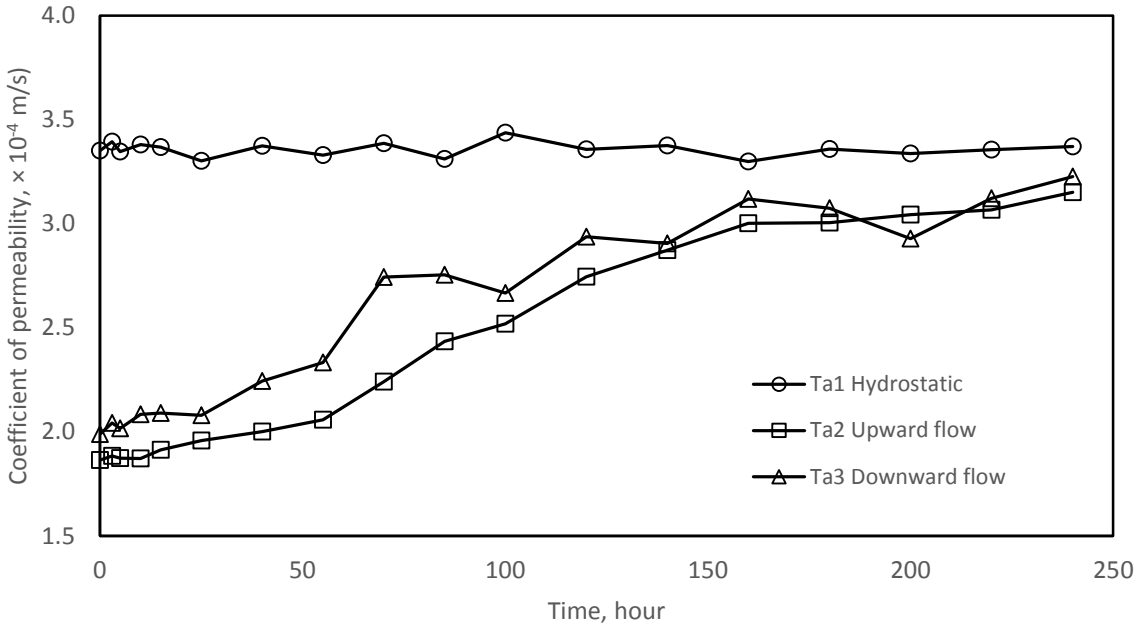


*Figure 4.9 Change of coefficient of permeability in sand in a short term flow condition*

In this study, it was proposed to combine bioclogging together with biogas generation to enhance the stability of the gas bubbles or the degree of saturation. Bioclogging or cementation using the MICP process was incorporated into Test Ta4UM and Ta4DM after the microbial denitrification process to investigate the effectiveness of trapping biogas bubbles using the bioclogging effect under a seepage flow condition. After the denitrification process finished, the bacterial suspension and biocement fluid flew through sand columns from bottom to top in a hydraulic gradient of 0.1. As a very slow flow was used, this flow process did not affect much the degree of saturation of the sand column. After the bioclogging process completed, upward or downward flow was introduced and permeability

measurements were also carried out. The results of the permeability tests are given in Figure 4.10. It can be seen that there is a gradual decrease in permeability with time. In contrast to the data shown in Figure 4.9, the permeability would increase if the degree of saturation would have increased. Thus, the seepage flow in sand that has been treated using bioclogging may not affect the stability of the gas bubbles much. The small decrease in the permeability might be related to the presence of calcite crystals formed among sand grains which was roughly 0.8 percent w/w of calcite content in this case.

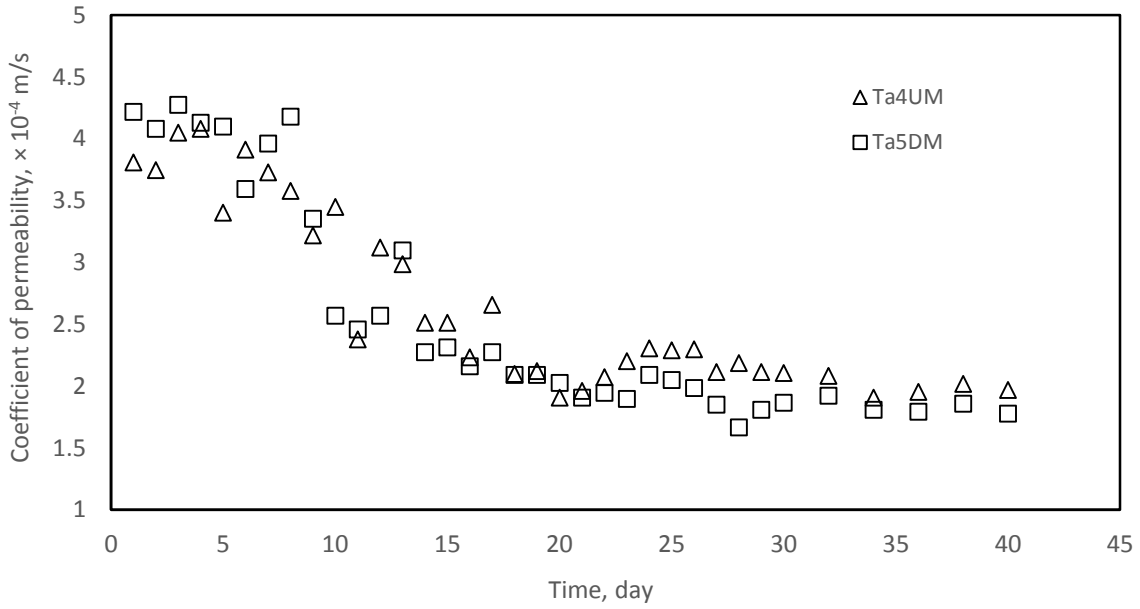


*Figure 4.10 Change of coefficient of permeability in MICP treated sand in a long term flow condition*

The permeability versus time curves for sand columns desaturated using biogas and treated using bioclogging under different hydraulic gradients are shown in Figure 4.11. An interval of one day was used for the first 30 days and after that the permeability was recorded every two days. As can be seen from Figure 4.11, for a flow lasted for 40 days, the low hydraulic gradient had yielded with a higher permeability measurement, especially at the initial stage. The lowest hydraulic gradient i = 0.1 has apparently resulted in the highest

permeability in both the upward and downward flow cases. The difference among tests with the different hydraulic gradients was not significant. The overall permeability of sand under the upward flow condition was higher than its counterpart under downward flow condition. Especially after 10 days of flow, the permeability data obtained in Ta5D plunged with a steeper scope although they all ended up within a small range. Based on the observation, it is possible to hypothesize that when a fast flow rate induced by a high hydraulic gradient passes through sand pores, due to the existence of barriers formed by calcite crystals, the flow stream has to squeeze through fewer effective flow paths in pore voids and in a consequence that the volume of water infiltrates sand layers is reduced. As a result, instead of increase, the permeability decreases when a higher hydraulic gradient is applied.

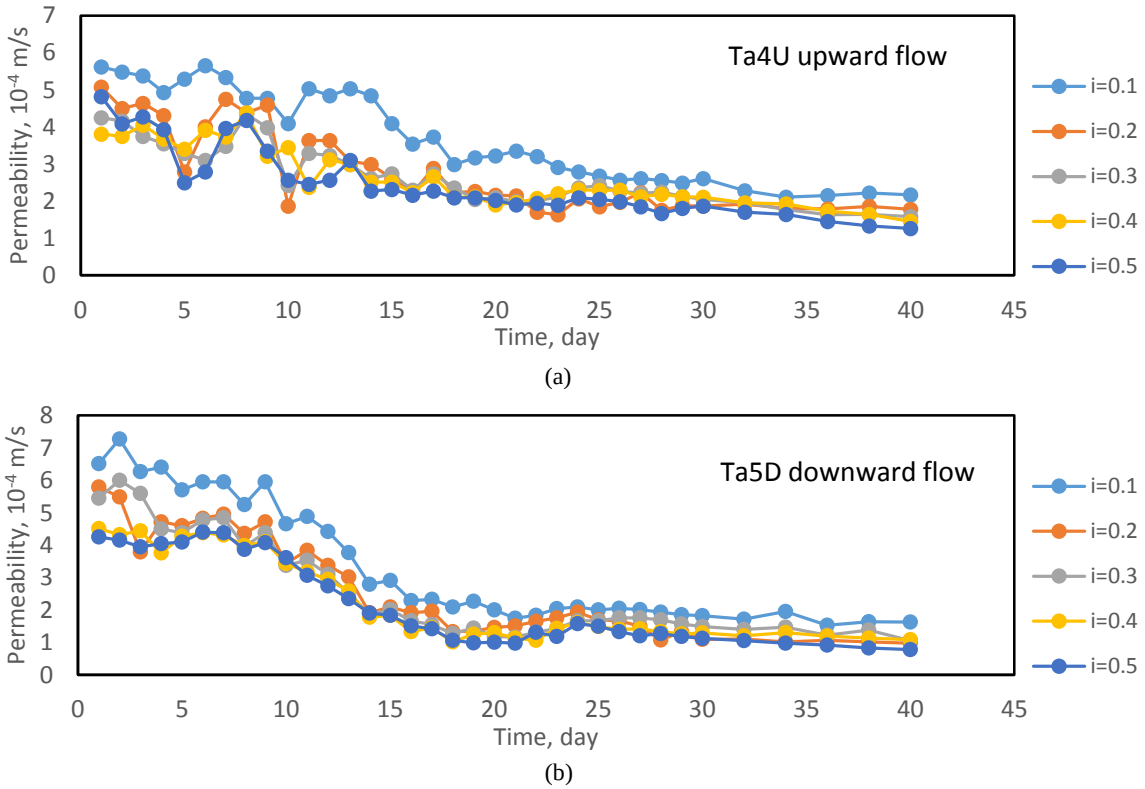


*Figure 4.11 Coefficient of permeability with different hydraulic gradient in a long term flow condition (a) Upward flow; (b) Downward flow*

A large diameter (D = 13.5 cm) sand column was adopted to study the uniformity of biogas distribution in sand. The volume of the biogas in sand increased with time since the denitrifying bacteria gradually turned nitrate into nitrogen gas and reached a maximum value when all nitrate source was consumed. Some part of the nitrogen gas was released into air or flowed away with the water stream. Still, a large quantity of biogas was retained in the sand pores as bubbles and occluded the pathways of water, resulting in the decrease in permeability. Figure 4.12 presents a comparison of the rate of flow versus hydraulic gradient relationships of sand with three different degrees of saturation. The unsaturated samples were biogas desaturated. It can be seen from Fig. 4.12 that the fully saturated sand had the highest coefficient of permeability ($k = 6.635 \times 10^{-4}$ m/s) and the biogas desaturated sand had a lower value of permeability: $k = 4.9554 \times 10^{-4}$ m/s for $S_r = 91.14\%$ and $k = 6.635 \times 10^{-4}$ m/s for $S_r = 80.5\%$. These results are in agreement with the previous reported data (Eseller-Bayat, 2009; He, 2013). Fredlud and Rahardjo (1993) claimed that the coefficient of permeability of partially saturated sand ($K_{PS}$) can be estimated from the coefficient of permeability of fully saturated sand ($K_{FS}$) given that the same void ratio. The relationship between the permeability of partially saturated and fully saturated can be taken as $K_{PS} = K_{FS} S^{\delta}$, where $\delta = 3$ for clean sand is obtained.

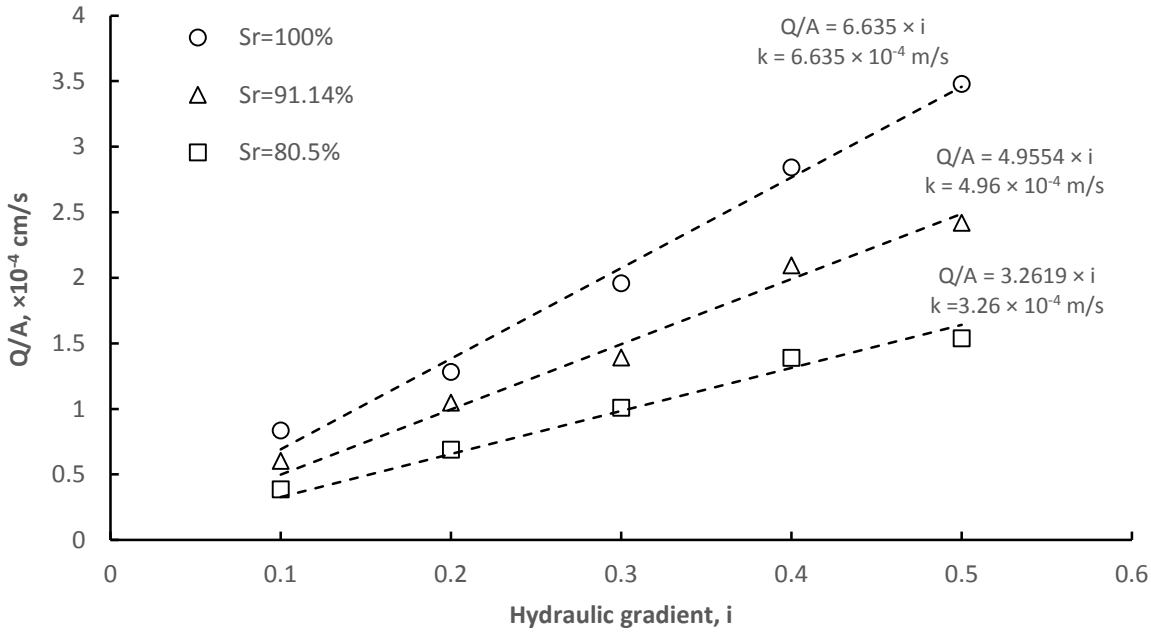


*Figure 4.12 Coefficient of permeability of fully saturated and partially saturated sand*

The water head versus piezometer readings at different locations for sand columns with different degrees of saturation or different hydraulic gradients are shown in Figure 4.13. It can be seen that overall, the greater the hydraulic gradient, the higher the water heads in piezometers. From the data in Figure 4.13(a), it can be seen that linear lines can be drew through the data points. It indicates that the rate of water head loss along the height of the fully saturated sand column is uniform. After the sand was desaturated by biogas bubbles, the linear relationship between piezometers was not consistent, especially when the hydraulic gradient was low. Figure 4.13(b) and (c) illustrates that under a low hydraulic gradient, i = 0.1 to 0.3, reductions of water head between piezometer 1 and 2 were more than those between piezometer 2 and 3 or piezometer 3 and 4. It implies that the coefficient of permeability at the bottom might be lower than that at the upper part of the sand column. This may be explained by the trapping of more biogas bubbles at the bottom than at the top.

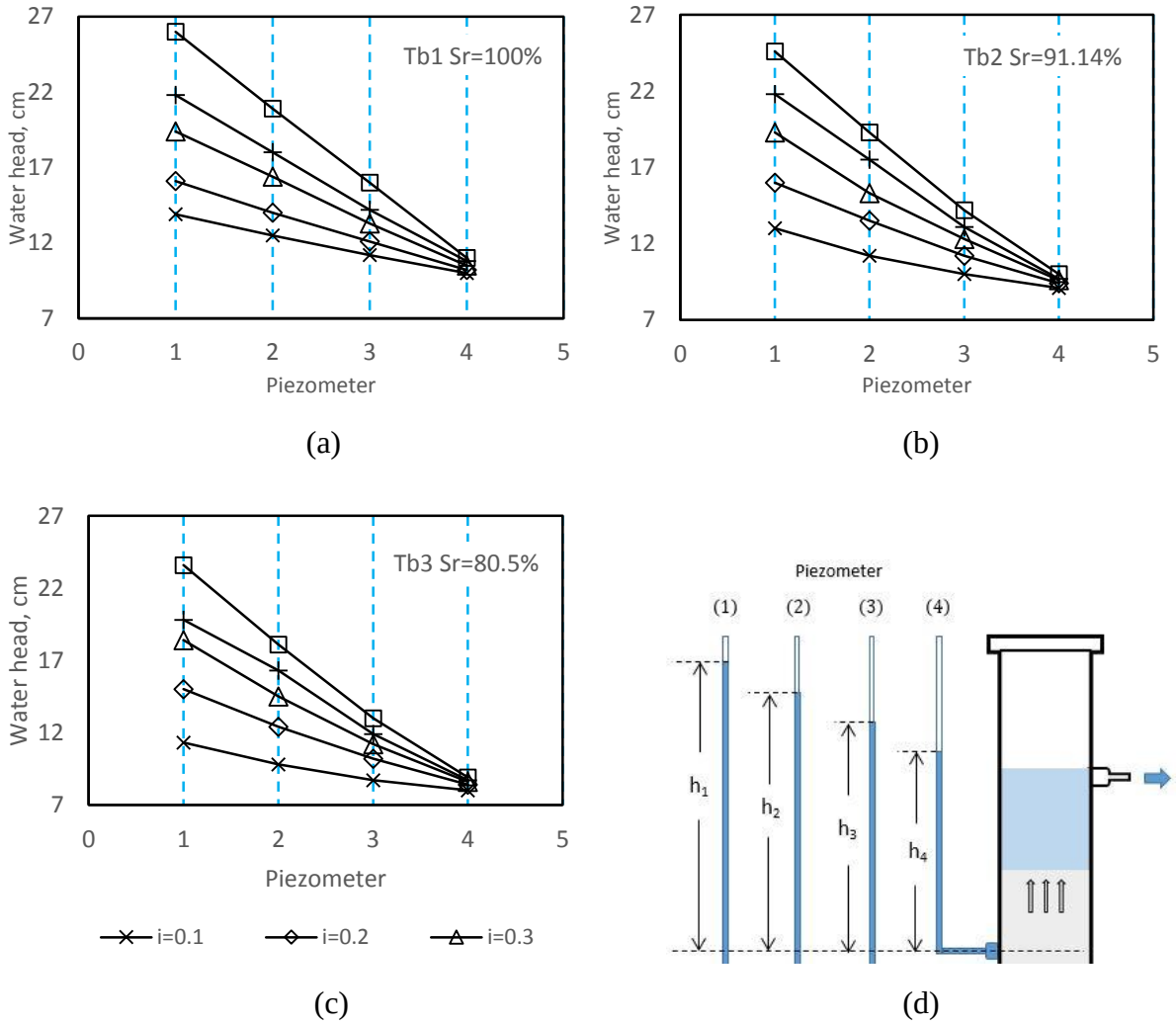


*Figure 4.13 Water head change in piezometers*

*(a) $S_r$ = 100 %; (b) $S_r$ = 91.14 %; (c) $S_r$= 80.5 %; (d) Water heads in piezometers*

Interestingly, a visual observation of the column wall suggests that more biogas bubbles may be seen at the upper section of the column, see Figure 4.14. This is not surprising as the bubbles at the top subjected to a less overburden pressure and thus tended to aggregate into bigger bubbles. This is particularly the case when an upward seepage is applied. Furthermore, it needs to be pointed out that the gas bubbles that can be observed

were only the bubbles outside and did not represent the gas bubble distribution inside the sample.

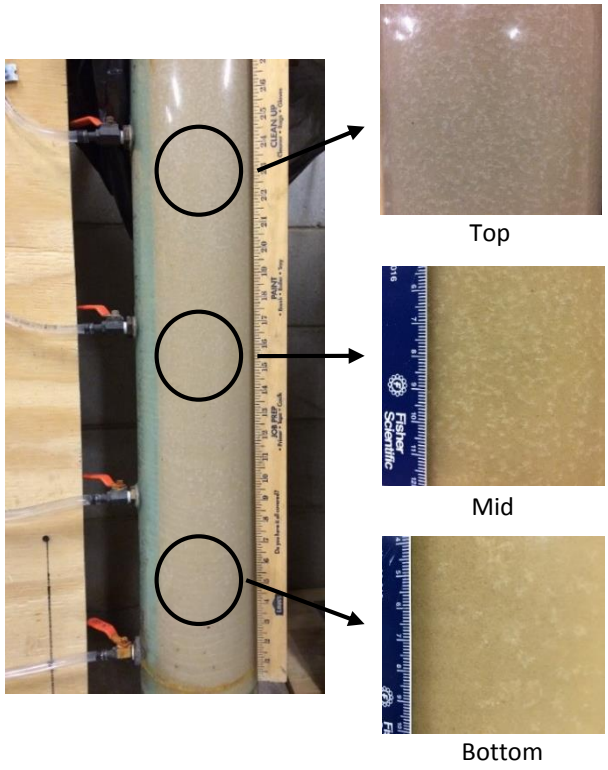


.

*Figure 4.14 Visual observation of biogas trapped in sand columns*

Figure 4.15 illustrates schematically the biogas formation in sand. At the bottom layer, due to a higher overburden stress, gas bubbles can still maintain the tiny sizes and exist separately. When the bubbles go up, the overburden reduces, bubbles have a better chance to collide and aggregate together. At the top layer, large gas bubbles may even form a layer as shown in Figure 4.15.

Factors such as shape of sand particles, packing condition of sand, pore size, viscosity and salinity of fluid, flow rate, and etc., will all affect the bubble formation and distribution. Results and observations in this study suggest with a reasonable amount of overburden, the

gas bubbles can remind tiny and immobile. The combined biogas and bioclogging method can help to stabilize gas bubbles in sand.

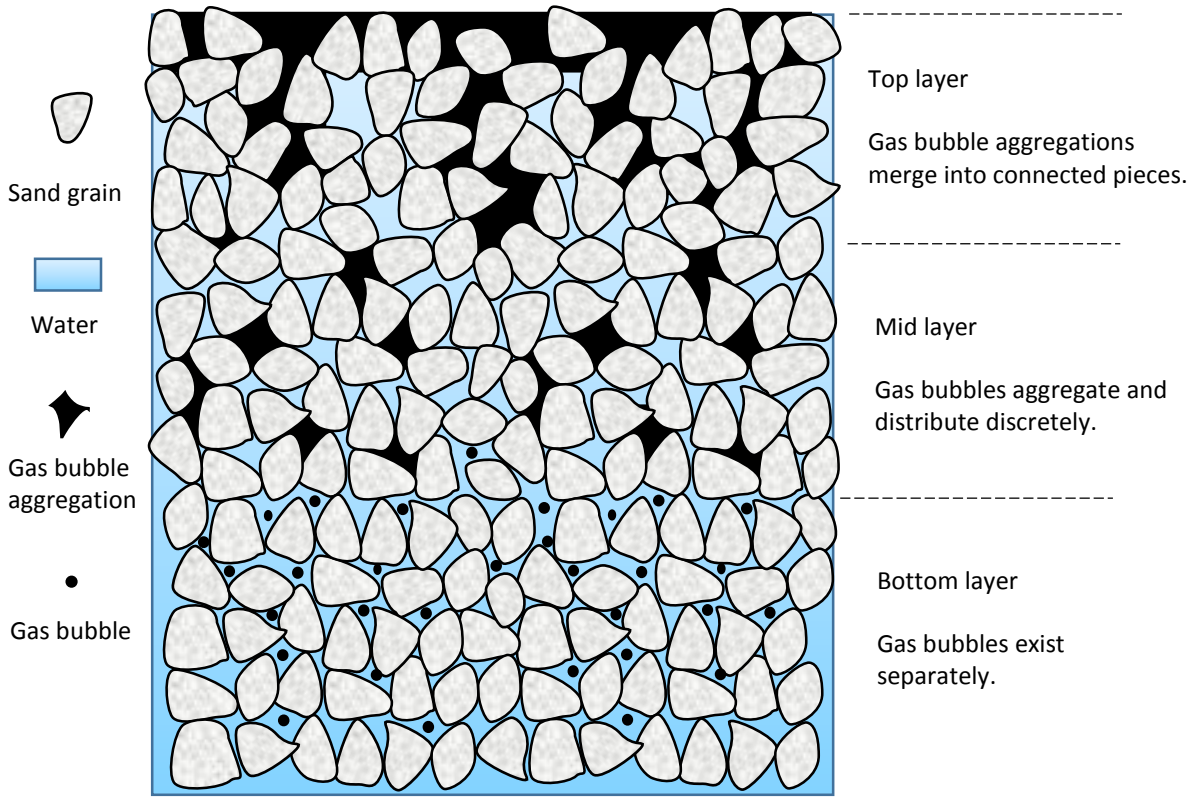


*Figure 4.15 Biogas formation in sand*

## 4.3 Microscopic Characteristics of Microbial Techniques Treated Sand

### 4.3.1 X-ray computed tomography and scanning electron microscope

X-ray computed tomography (CT) is a three-dimensional imaging technique that allows the non-destructive observation of the internal structure of samples in-situ (Viggiani *et al*. 2004). During the process of CT scanning, a cluster of X-ray beams was emitted from a source to the target. Once those beams pass through the material, X-ray is attenuated and the intensity is decreased. Then, based on the amount of attenuated X-ray, a 2D or 3D image is

constructed. CT image is a volumetric map of variation of material density. Brighter pixels represent higher density and vice versa. Since the amount of attenuated X-ray is proportional to the density, higher X-ray tube voltage – the source – is preferred in order to get high quality of CT images. Generally a CT scanning lasts 3 to 10 minutes. In the last decade, micro-computed tomography techniques have been developed to view the inside structures, void spaces and pore water of partially saturated sand with a micron's level of high spatial resolution (Higo *et al*. 2014). The CT tests were conducted at the Center for Nondestructive Evaluation, Iowa State University. A high resolution computed tomography facility with a micro focus x-ray tube (130 kV, 2-micron spot), 4-axis micro step positioner and an amorphous silicon array detector is capable of producing 3D CT images with voxel size as small as 4 microns. Figure 4.16 shows photos of the micro CT system.

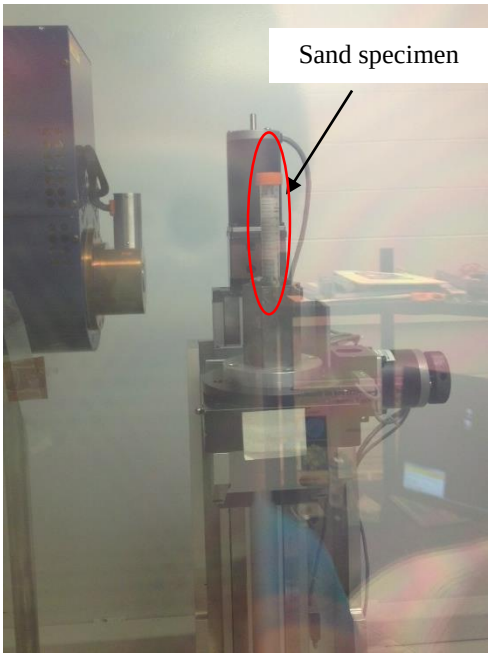


(a) Sand specimen in a CT test

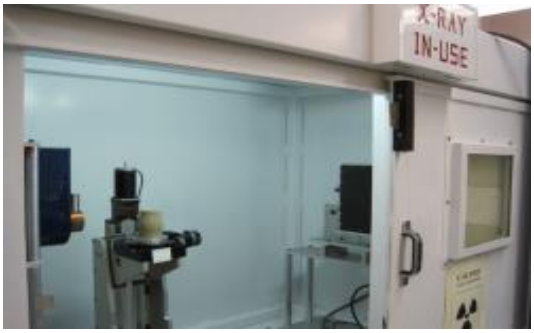


(b) Micro CT room

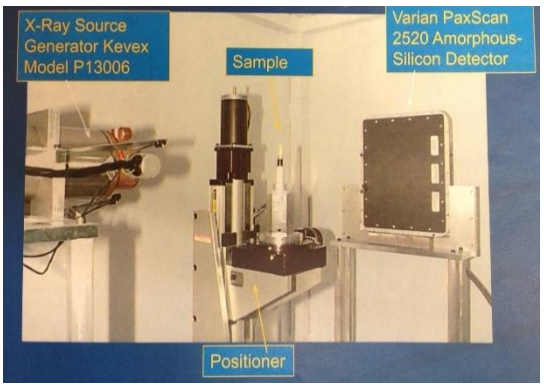


(c) Microfocus high resolution CT system

*Figure 4.16 Photos of ISU micro focus high resolution CT system*

Scanning electron microscope (SEM) is a type of electron microscope that uses electrons instead of light to produce images. A beam of electrons is produced at the top of the microscope by an electron gun. The beam travels through electromagnetic fields and lenses to focus on the sample. Once the beam hits the sample, electrons and X-rays are ejected from the sample. Detectors collect these X-rays and electrons and convert them into a signal that is sent to construct the final image. The SEM has many advantages over traditional microscopes. It has a much higher resolution which allows specimens to be magnified at much higher levels. Characteristic x-rays from the elements in the sample allow investigators to determine the elemental composition of phases as small as a few hundred nm.

The SEM equipment involved in this research is the FEI Quanta-250 SEM from the Materials Analysis and Research Laboratory of the Iowa State University Office of Biotechnology (Figure 4.17). This is a field-emission SEM offering a maximum resolution on the order of 1.0 nm. It is capable of operating in high vacuum for conductive samples. It is capable of variable pressure and extended pressure (i.e., environmental) modes (up to 20 Torr) for observation of non-conductive or moist samples. It is equipped with conventional secondary and backscattered electron detectors but also has two detectors for collecting secondary electrons in variable and extended pressure modes (quote from Iowa State SEM Homepage).


(a) ISU SEM testing system (b) FEI Quanta-250 SEM

*Figure 4.17 Photos of ISU FEI Quanta-250 SEM system*

### 4.3.2 Sand sample preparation

In order to get high quality CT images, multiple sand specimens with different degrees of saturation were prepared in Corning® 15 ml centrifuge plastic tubes. Each tube contained 10 ml silica sand and 5 ml denitrifying medium with 1 ml suspension of denitrifying enrichment bacterial culture. The nitrate concentration in the denitrifying medium was adjustable to produce biogas desaturated sand with a targeted degree of saturation. Figure 4.18 illustrates the procedure of preparing a biogas containing sand specimen. Three sand specimens with biogenic nitrogen gas and a control specimen shared a same dimension of 1.46 cm in diameter and 10 cm in length. Final degrees of saturation of them were 100 percent (control), 94 percent, 88 percent and 81 percent, respectively.

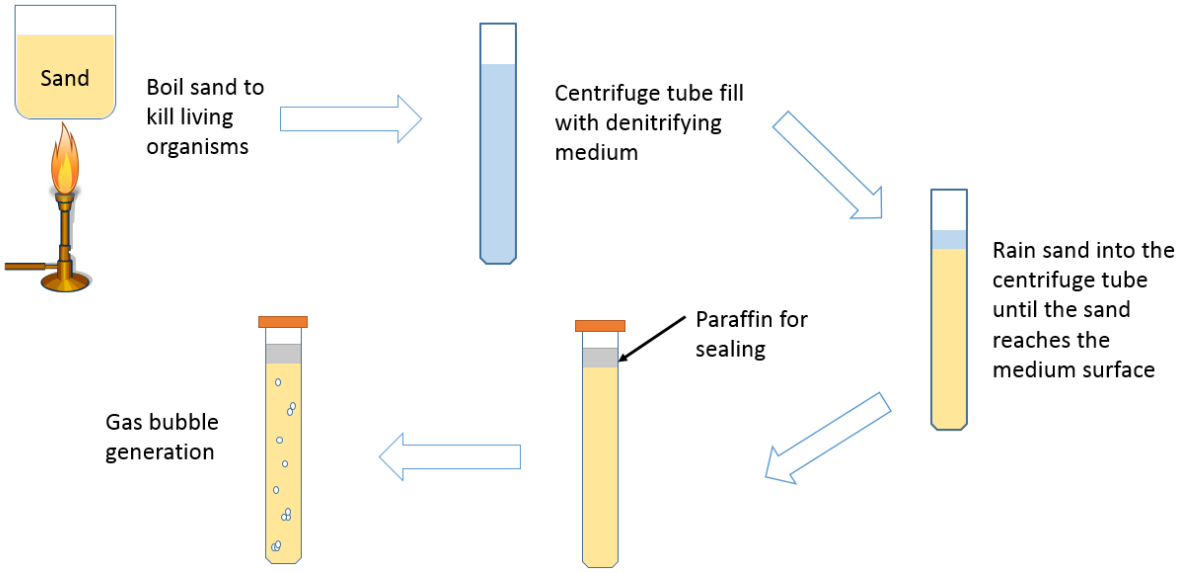


*Figure 4.18 Procedures of biogas containing sand specimen preparation*

The Micro-CT device covered nearly 3 cm length of cylindrical sand sample and gave us both the horizontal and longitudinal profile of samples. For each sample, there were 500 slides of images in XY direction (horizontal cross-section) and 436 slides of images in Z direction (vertical cross-section), as demonstrated in Figure 4.19.

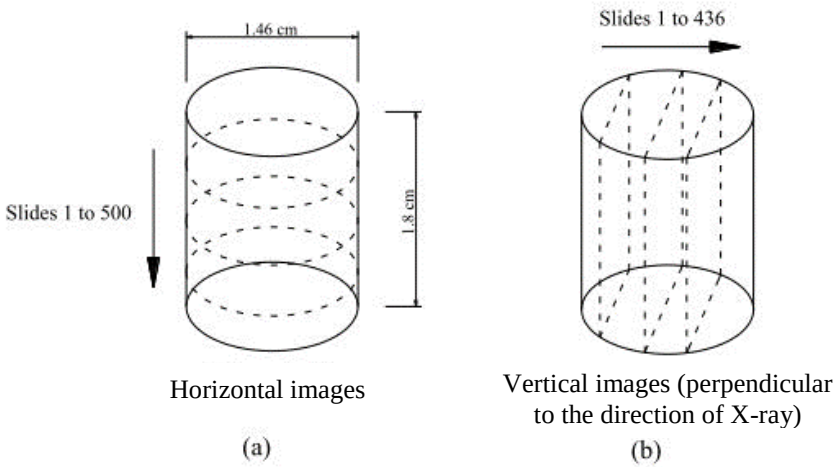


*Figure 4.19 Illustrations of CT images (a) horizontal slides; (b) vertical slides (He, 2013)*

Compare with CT test, the SEM can provide powerful vision on a tiny specimen. In this study, images taken from SEM were employed to investigate crystal characteristics of calcium carbonate crystals induced by microbial hydrolysis of urea. As SEM utilizes vacuum conditions and uses electrons to form images, water will vaporize in a vacuum space and removed from specimens (Lawes 1987). Due to the strong suction force, all SEM samples must be of an appropriate size to fit in the specimen chamber and are generally mounted rigidly on a specimen stub as shown in Figure 4.20.

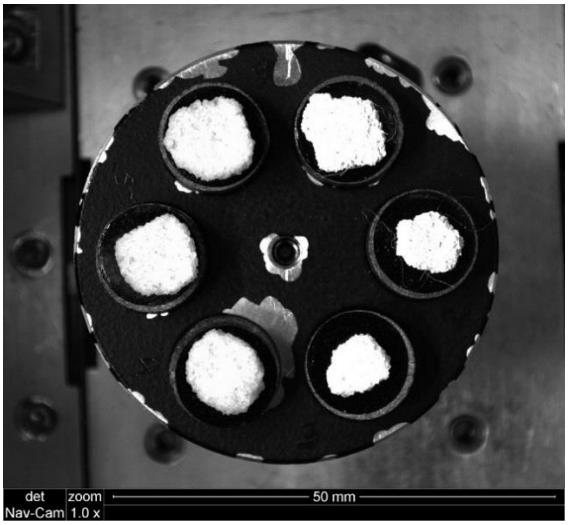


*Figure 4.20 Sand samples on a SEM specimen stub*

Samples in both solid and liquid phases were prepared in this study. Solid sand specimens were directly taken from crushed samples in the unconfined compression test in Chapter 3 and a few samples were collected from sand columns for the long term biogas stability tests (Ta4UM and Ta5DM in Table 4.3). Slices of 1 cm × 1 cm square sample were cut from UC test remnants or dry sand columns and placed into a 105 ℃ furnace for 24 hours to eliminate moisture. Then, all samples were fixed on graphite stubs by double sided tape and transferred into the vacuum chamber of the SEM device for scanning. The MICP

suspension which contained UPB solution, urea and calcium chloride was blended in 50 ml Corning® centrifuge tubes (Figure 4.21). After a week, the suspension transformed from relative clear solution into a turbid mixture as a results of microbial induced calcium carbonate precipitated. Droplets of both suspension were carefully dripped on two SEM specimen stub and left for air dried before SEM scanning.

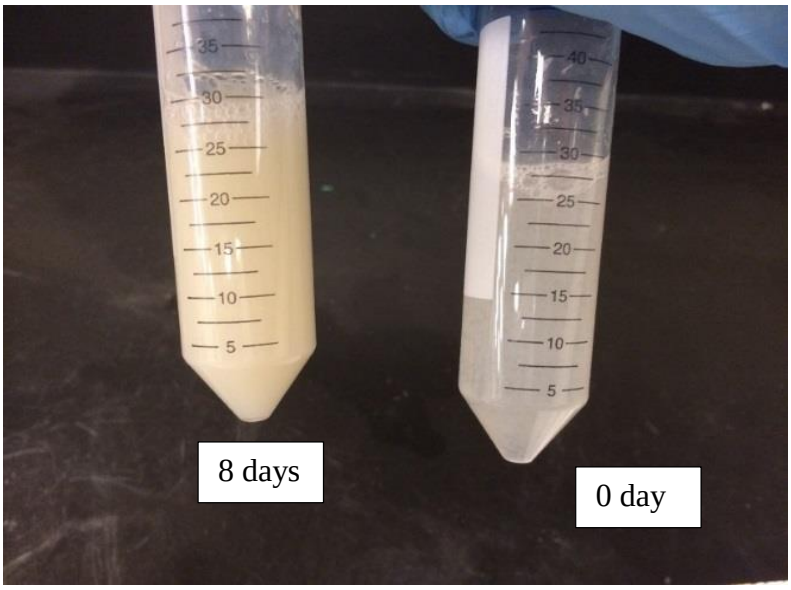


*Figure 4.21 Transformation of MICP suspension in a week*

### 4.3.3 Analysis of test images

Selective X-ray CT horizontal and vertical cross-section images through four specimens with different degrees of saturation are presented in Figure 4.22. Because the density is a key parameter to establish CT images, the brightness contrast reveals the variation of density and offers researchers the inner structure of a sand specimen. The brightest pixels are silica sand particles which have a unit weight of 2.65. Darker space among those bright pixels are pore voids which contains water and gas. It can be seen from

Figure 4.22(a) which taken from the fully saturated sand specimen that the distribution of sand particles and pore voids were quite uniform.

When the degree of saturation dropped to 94 percent, there was a big dark spot appeared in Figure 4.22(b) which highlighted by a yellow square box. Except slight vibration during sample transportation, there was no external loads applied to any sand specimens, the only explanation for this cavity was that biogas bubbles accumulated and combined with pore fluid to form a relatively big gas-liquid phase aggregation.

More of such aggregations were identified in further biogas desaturated sand specimens. A number of big size dark spots can be located in Figure 4.22(c) and (d) when the sand samples' degree of saturation fell below 90 percent. When the degree of saturation close to 80 percent, as shown in Figure 4.22(d), gas-liquid phase aggregations appeared in both core and edge area of the CT image which indicated that the denitrification medium had been transferred through all the sand specimen and gas bubbles tended to merge as the sand specimen was moved. A close examination of those dark pockets suggests that all aggregations had a similar maximum size and they were able to coalesce on both horizontal and vertical direction.

Overall, CT images clearly show that the number of pockets trapped in sand increased as the reduction of the degree of saturation.

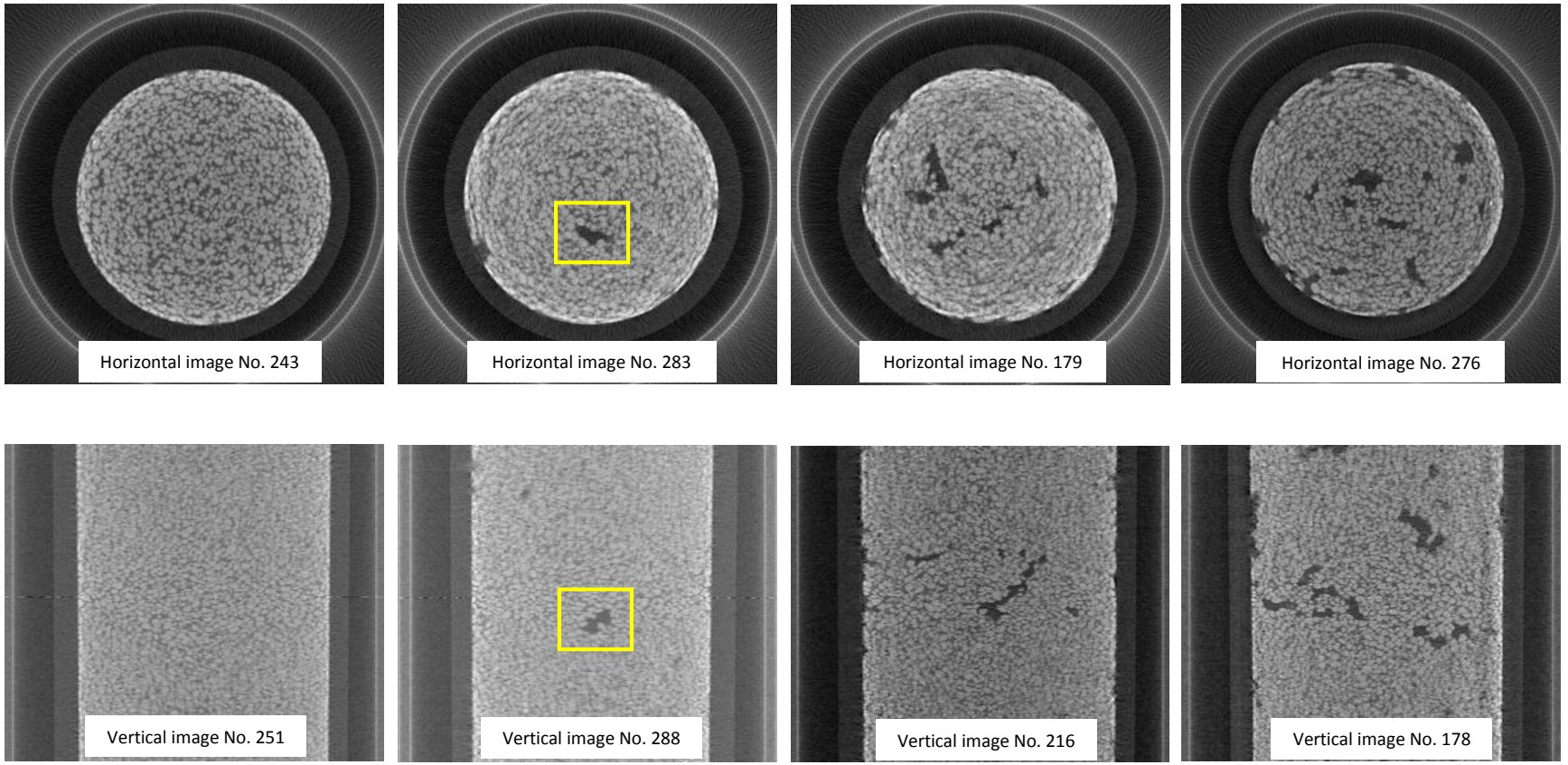


(a) $S_r$=100%, e=0.63 (b) $S_r$=94%, e=0.63 (c) $S_r$=88%, e=0.66 (d) $S_r$=81%, e=0.66

*Figure 4.22 Typical CT images for sand specimens with different degrees of saturation*

SEM images of MICP suspension status at initial and one week later were displaced in Figure 4.23 and Figure 4.24, respectively. Originally, the MICP suspension was free of precipitations. A 500x magnification in Figure 4.23B barely shows any trance of crystals.

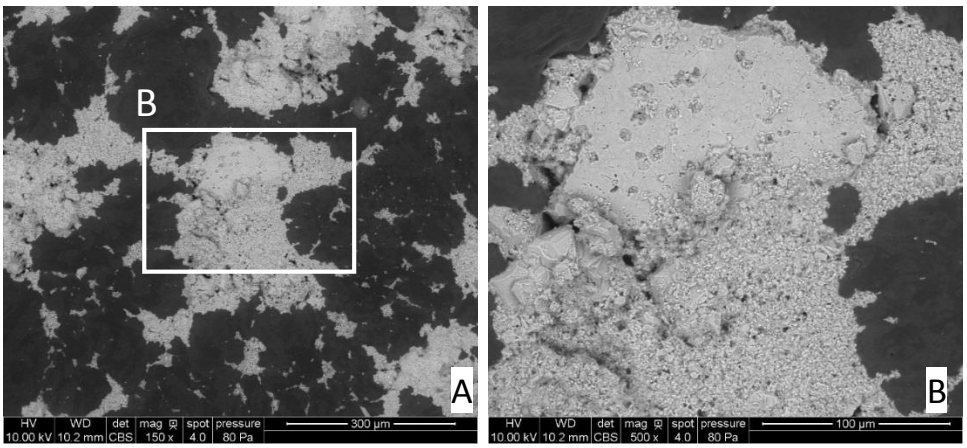


*Figure 4.23 MICP suspension initial status*

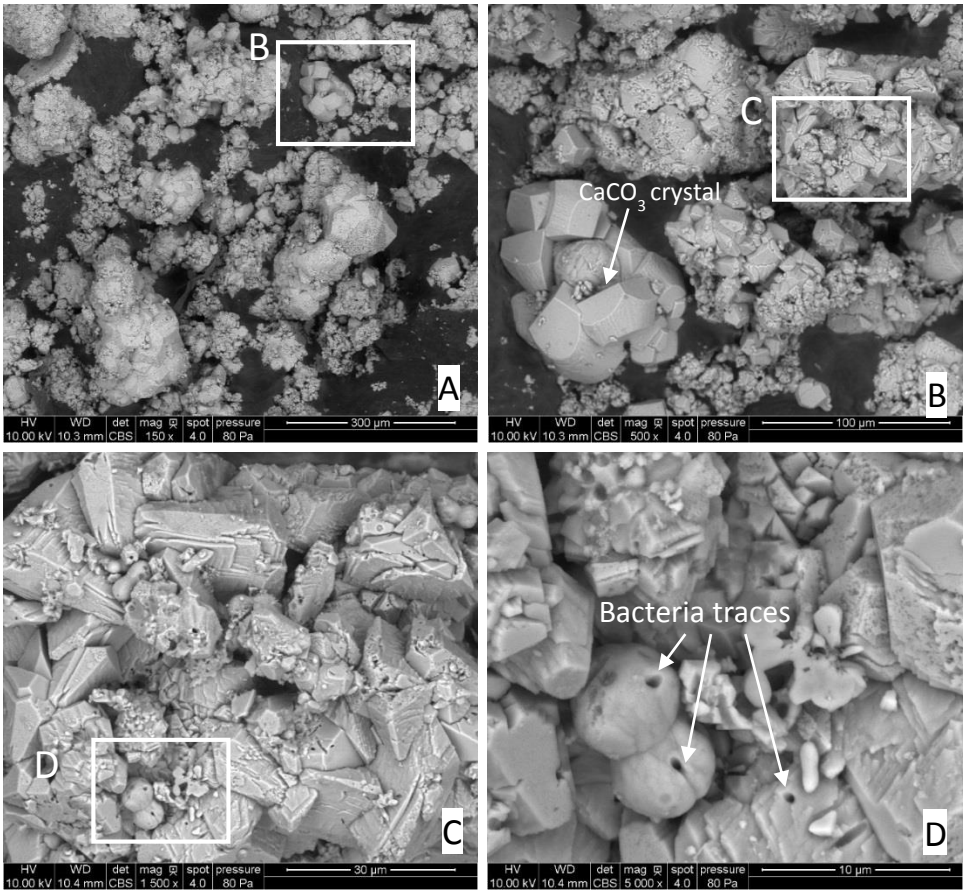


*Figure 4.24 MICP suspension at 8 days*

However, after a week, with plenty supply of calcium source, microbial induced calcium carbonate precipitation caused by UPB produced considerable $CaCO_3$ crystals as one was highlighted in Figure 4.24B. A 1500x magnification shows an agglomerated $CaCO_3$ crystal about 100 μm in size. Various polymorphs including spherical and rhombohedral crystals existed in such an agglomerate. Usually, calcium carbonate ($CaCO_3$) forms three anhydrous polymorphs: calcite, aragonite and vaterite, two hydrated crystalline phases: monohydrocalcite ($CaCO_3 \cdot H_2O$) and ikaite ($CaCO_3 \cdot 6H_2O$), and various amorphous phases (ACC) (Gower 2008; Gebauer *et al*. 2010; Dhami *et al*. 2013) (Figure 4.25). Calcite and vaterite are the most common bacterial activity-associated calcium carbonate polymorphs among those products. Extensive studies suggest that due to influences from various factors (e.g. pH, sand grains, fluid charge, presence of high concentrations of ions, distribution of bacteria cells, organic contents), it is extremely difficult to predict the type and shape or size of crystals formed through biocementation process. At the biggest magnification (5000x) there are some black holes on the surface of a few crystals. These hole may be the bacterial imprints UPB left during the MICP process.

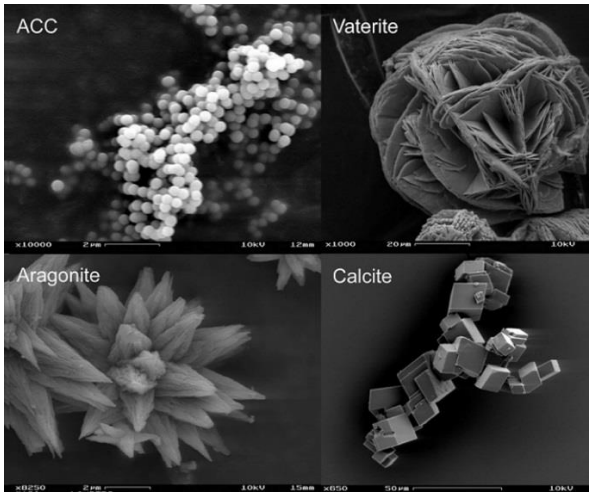


*Figure 4.25 Polymorphs of $CaCO_3$ (http://www.ruhr-uni-bochum.de/sediment/forschung.html)*

Figure 4.26 to Figure 4.28 demonstrate images of biocemented silica sand specimens obtained from crushed UC test remnants. The magnitude of cementation was rated from slight, moderate and heavy. Slight means one percent mass of calcium carbonate in dry sand. Moderate biocemented sample contained calcium carbonate of six percent of dry sand mass. The largest quantity of calcium carbonate precipitation which reached ten percent of dry sand mass were found in the heavily biocemented sand grains.

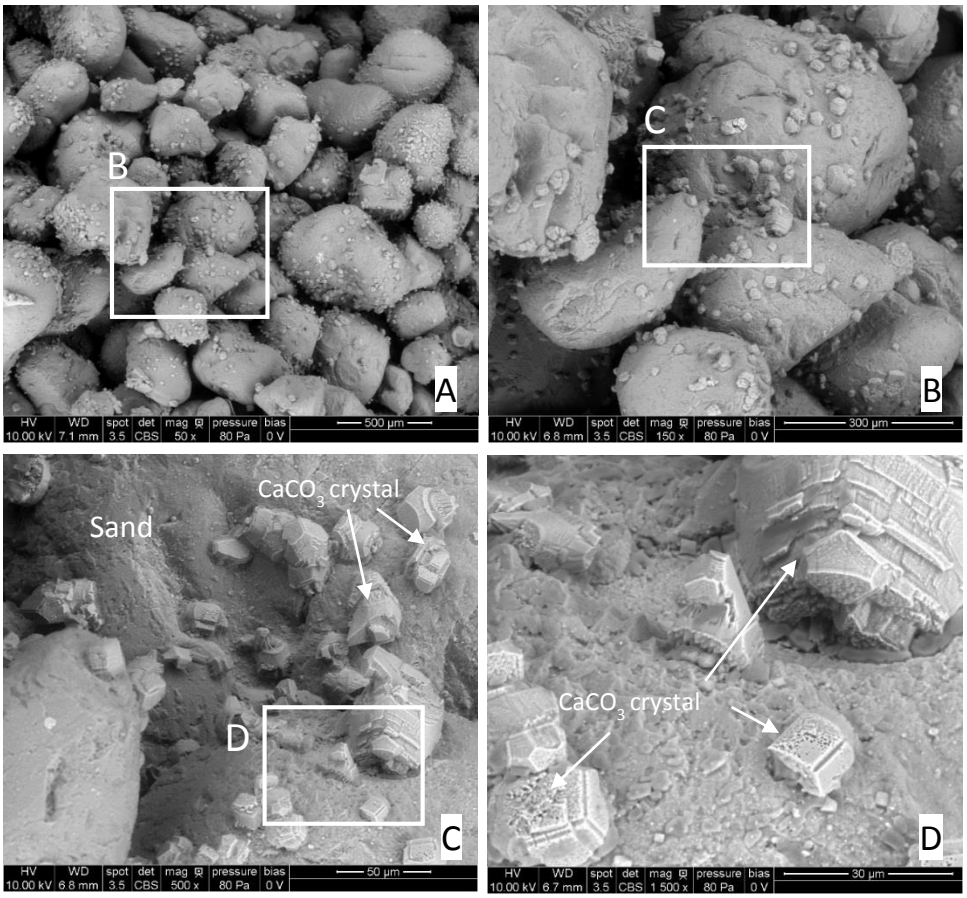


*Figure 4.26 SEM images of slightly biocemented (1%, w/w) sand grains*

In Figure 4.26 A and B, a number of spots can be identified on the surface of some sand grains. Larger magnification shows that $CaCO_3$ crystals formed separately in depressions of the sand grain. Most of $CaCO_3$ crystals with a size from 10 μm up to 40 μm

were in rhomboidal shape as calcite shown in Figure 4.26 C and D. Almost no $CaCO_3$ crystals found between sand grains may explain the low UC strength (<500 kPa, T1 in Table 3.3) obtained from sand under this magnitude of MICP treatment.

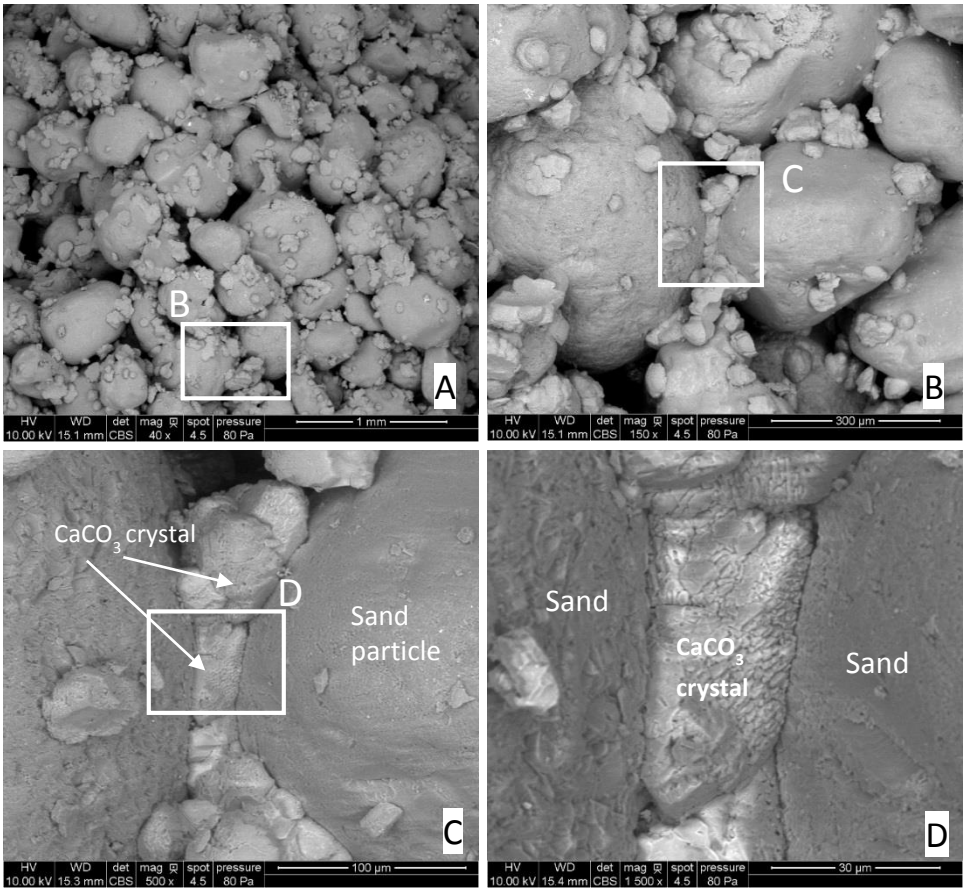


*Figure 4.27 SEM images of moderately biocemented (6%, w/w) sand grains*

In moderately biocemented sand grains, in addition to sand grain surface, $CaCO_3$ crystals were also existed between sand grans. As shown in Figure 4.27 C and D, $CaCO_3$ crystals formed an agglomerate and perfectly shaped around sand grains' edge. Majority of $CaCO_3$ crystals in the agglomerate looked like calcite as they all had a rhomboidal shape. The agglomeration of calcite crystal grew along with sand grain edge and could expend to

adjacent particles. Because $CaCO_3$ crystals bind sand particles together, strong connections were established and the strength improvement was significant.

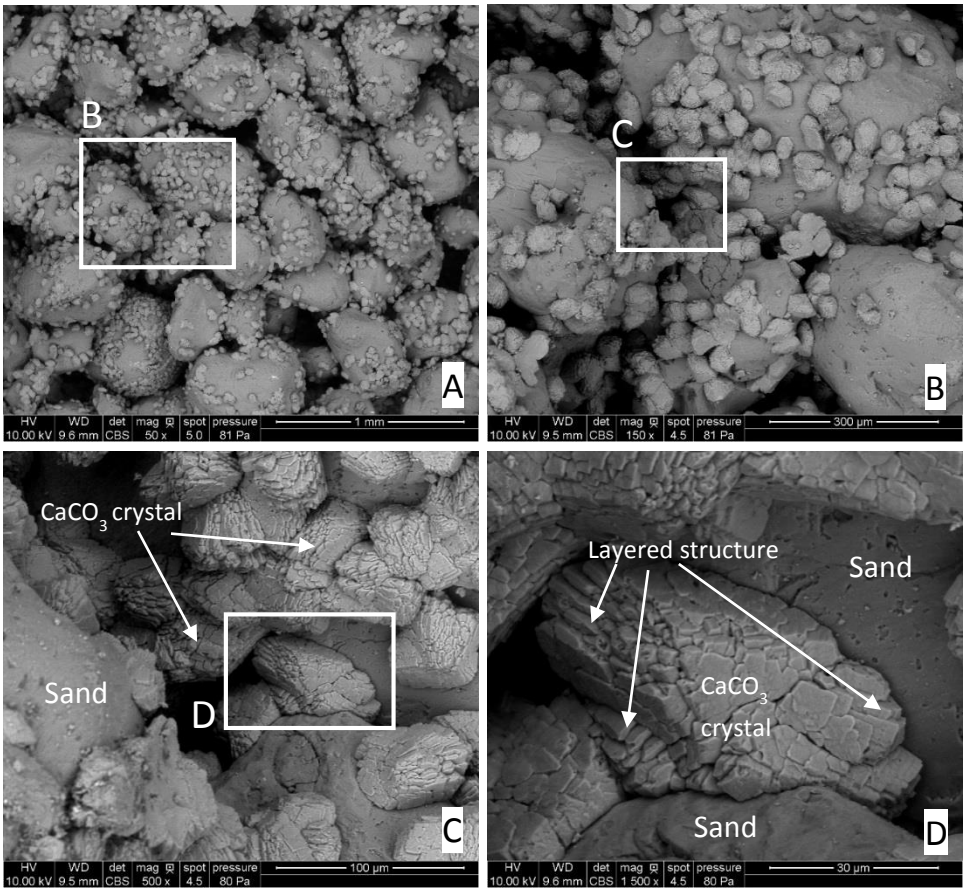


*Figure 4.28 SEM images of heavily biocemented (10%, w/w) sand grains*

Figure 4.28 reveals SEM images of heavily biocemented sand grains. Much more $CaCO_3$ crystals can be identified on both sand surface and gaps among sand grains. Some small size sand grains were almost fully covered by $CaCO_3$ crystals. As in moderately biocemented sand grains, the same agglomeration phenomenon was observed. Most of agglomerates had a size up to about 70 μm. In Figure 4.28 D, a large agglomerate had developed a sort of sheet structure. This highlighted agglomeration of crystals illustrates that the rhomboidal calcite crystals attached to sand grains and grew layer by layer. The boundary

between the agglomerate and sand grain was clear to distinguish from each other. Not only functioned as bridges connecting sand grains, these agglomerations of calcite crystals also successfully filled pore voids and reduced the void ratio of sand. This kind of densification increased the dilatancy of sand. When a shear stress is applied, the shear strength could be improved considerably because of cohesion and dilatancy.

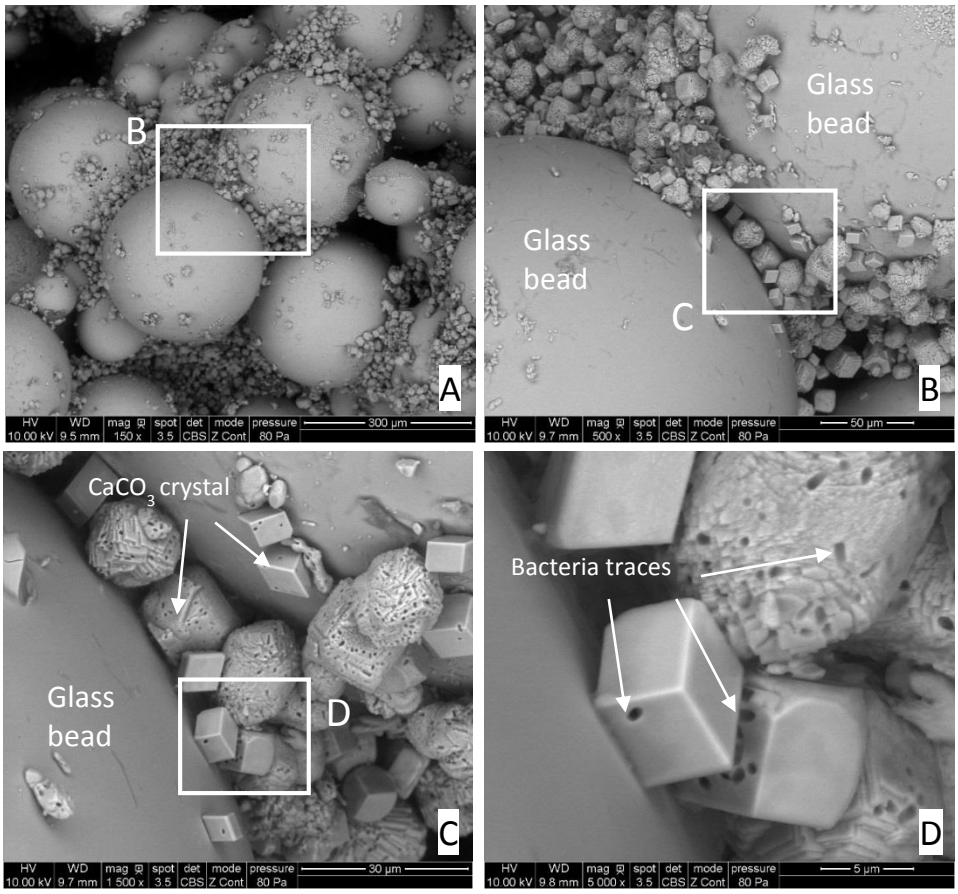


*Figure 4.29 SEM images of biocemented glass beads*

SEM images of glass beads flushed with UPB and cementation solution (1 M $CaCl_2$&Urea) is disclosed in Figure 4.29. Majority of crystals were gathered between gaps of glass beads. Only a few single crystals spotted on the glass beads surface. Rest of the surface was quite clean and smooth. Comparing with images taken from sand grains, the most

interesting finding was that $CaCO_3$ crystals formed as different polymorphs besides calcite. Spherical vaterites with a size of approximately 10 μm were observed in Figure 4.29 C. At the largest magnification (5000x), traces of bacterial imprints appeared again. Black spots on the crystal faces were traces of where bacteria have been encapsulated in the crystal. The mystery raised here is that why there was no bacterial trace found in biocemented sand grains. It has been suggested that bacterial cells themselves can act as nucleation sites for the formation of crystals (Ferris *et al*. 1996). Those crystals with apertures might serve as the inner core of large size $CaCO_3$ crystals. They were covered or wrapped by following crystals as the development of MICP process.

In order to investigate the micro structure of silica sand treated through both denitrification and MICP processes, specimens were collected from sand columns under long term seepage flow test. The calcium carbonate content in taken samples was about 0.8 percent of the dry sand mass. Figure 4.30 provides images of SEM and EDX test results. Energy dispersive X-ray spectroscopy (EDX) is a powerful technique to identify the chemical composition of test subjects. Because of low calcium carbonate content, limited number of $CaCO_3$ crystals were marked on sand grain surface. Figure 4.30 B shows that major $CaCO_3$ crystals were in rhomboidal shapes and less than 70 μm. Although many of them fall into gaps between sand particles, strong bond was unlikely to form due to the limited supply of calcium source. Agglomeration of $CaCO_3$ crystals that connects sand particles requires continuous reaction of microbial induced calcite precipitation which was not guaranteed in the long term seepage flow test. However, according to results of permeability test (Ta4UM and Ta5DM), those dispersed calcites would disturb the slow flow

stream and was capable of detaining a large amount of biogas generated from denitrification process in pore voids.

The EDX analysis results in Figure 4.30 C indicates that the dominant elements in the sample were O, Na, Si, Cl. Few amounts of C, Ca, N, P, S, K, Al were also presented. The main component of silica sand is $SiO_2$. Thus it's reasonable to have Si and O in dominance (orange curve). Sodium and chloride elements were mainly from a NaCl-bearing layer on sand grain which marked in Figure 4.30 B. Calcium and carbon elements were found in carbonate (red curve) produced by MICP process. Other elements such as potassium, sulfur, phosphorus are from components of denitrifying bacteria nutrient.

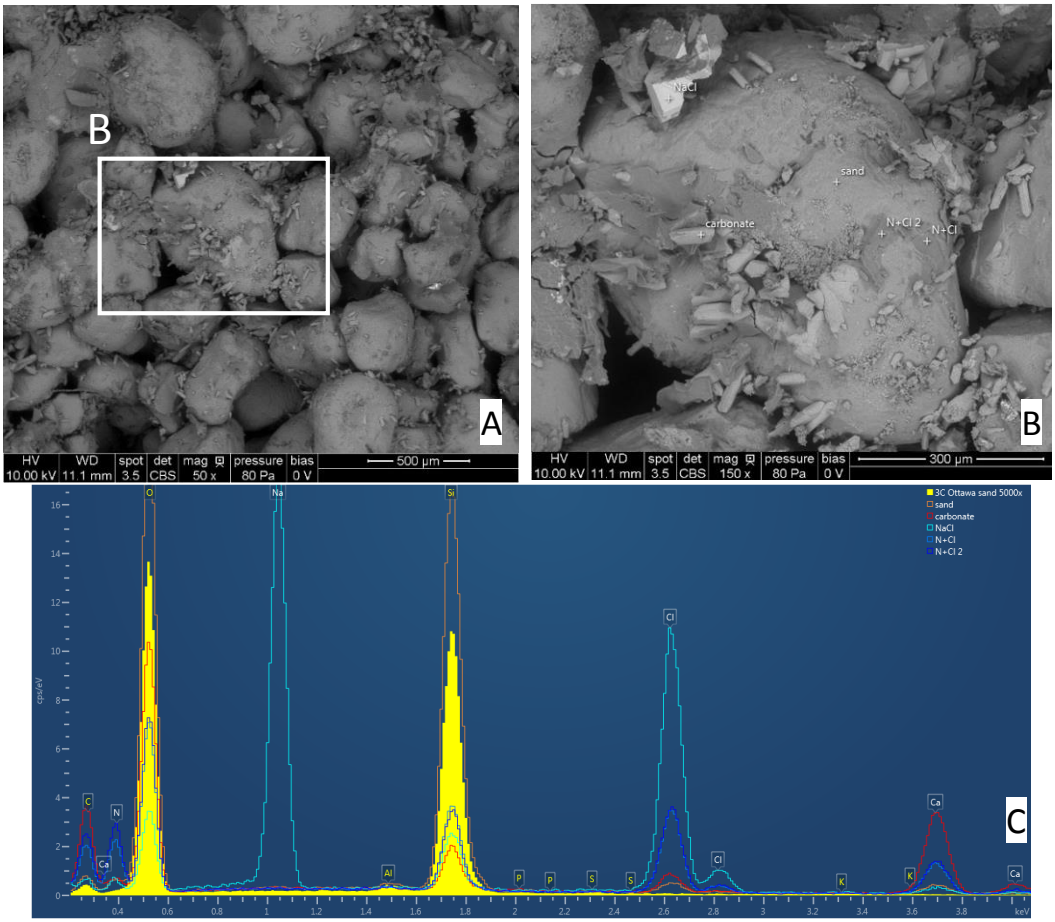


*Figure 4.30 SEM and EDX images of sand treated through denitrification and MICP processes*

## 4.4 Conclusions

Biogas stability tests were carried out using large sand columns. Three seepage flow conditions, hydrostatic, upward flow and downward flow, were applied to the sand columns. The coefficient of permeability measurements indicate that under a hydrostatic condition, almost no change in degree of saturation was found. However, regardless of upward or downward flow, even under a small hydraulic gradient $i = 0.1$, gas bubbles can be carried out by flow in less than 10 days and the degree of saturation gradually turned back to fully saturation status. The testing data indicate that the stability of biogas bubbles appeared to be more vulnerable when a downward flow is applied. Long term flow tests for sand columns treated using the combined biogas and bioclogging method under a hydraulic gradient of 0.1 for up to 40 days with either upward or downward flow show that the combined method is effective in enhancing the stability of the bubbles due to the formation of calcite crystals in sand to act as a sealing wall or barrier to reduce the flow rate.

Tests to study the distribution of biogas bubbles in sand were also carried out. The results reveal that the coefficient of permeability decreased as the reduction in degrees of saturation. Results and observations in this study suggest that with a reasonable amount of overburden stress, the gas bubbles can remain tiny and immobile. The combined biogas and bioclogging method can help to stabilize the gas bubbles in sand.

CT and SEM scan were adopted to study the microscopic structure of the bio-treated sand. The CT scanning shows that for fully saturated sand, the distribution of sand grains and pore voids was uniform through the whole sample. There were some small biogas bubbles observed in a slightly desaturated sand specimen ($S_r = 94\%$). As the degree of saturation

dropped further to 81%, large biogas bubble aggregation formed and created pockets within sand pores. Some pockets expended in both horizontal and vertical directions.

SEM images provide a useful way to visualize the $CaCO_3$ crystals formation and distribution in three sand specimens with different $CaCO_3$ concentrations. For biocemented sand with low $CaCO_3$ concentration (0.8%, w/w), majority of the $CaCO_3$ precipitation was formed as single crystal on top of sand grain.

# CHAPTER 5

# MODEL TESTS TO STUDY THE SEISMIC RESPONSE OF BIOGAS DESATURATED SAND

## 5.1 Introduction

A series of shaking table tests were performed to evaluate the liquefaction potential of biogas desaturated sand and the consequence if liquefaction does occur. The responses of the sand at varying amplitude of seismic motions, including the acceleration response, the pore pressure generation, the sand specimen settlement and its lateral displacement were measured. Comparisons were made between the behavior of biogas desaturated and untreated soil. Furthermore, the different seismic behavior of biogas desaturated sand at both leveled ground and sloping ground conditions were investigated.

A laminar box which consists of multiple layers of laminates was designed and fabricated for the shaking table tests. The need for the use of a laminar box has been explained in Kagawa *et al*. 2004; Ueng *et al*. 2006; Zhou *et al*. 2010; Dobry *et al*. 2011; Ghayoomi *et al*. 2011; Su *et al*. 2013; He and Chu 2014. The benefit for the use of the laminar box is that it minimizes the friction among metal frames and thus allows free movements between two adjacent soil layers during the cyclic motion. As is well known, the seismic response of soil is largely related to ground motions and boundary conditions. The use of a laminar box in shaking table tests can bring the experimental conditions closer to *in situ* conditions imposed during an earthquake.

The combined biodesaturation and bioclogging method was also adopted for some of the model tests. Some studies have found that biocementation alone can increase the resistance to liquefaction (Whiffin *et al*. 2007; Banagan *et al*. 2010; Inagaki *et al*. 2011; Montoya *et al*. 2013). However, the amount of $CaCO_3$ has to be relatively high to increase the liquefaction resistance to the required level. This approach is thus expensive. When the normal MICP process is adopted, it also produces a substantial amount of ammonia. In the combined method adopted in this study, the function of the $CaCO_3$ is only for bioclogging of the biogas bubbles. Thus, the amount of $CaCO_3$ required is much reduced.

## 5.2 Material and Equipment

### 5.2.1 Laminar box

As mentioned in the introduction section of this chapter, the laminar box is an optimal solution because it simulates shear beam conditions in which shear waves propagate uniformly through the whole soil specimen while minimizing end effects (Whitman and Lambe 1986).

The laminar box in this study consists of a stack of 10 rectangular laminate rings separated by linear ball bearings. The rings are 457.2 mm (18 inch) in length, 304.8 mm (12 inch) in width and 25.4 mm (1 inch) in height. They are all made of high strength aluminum alloy. Linear ball bearings created a 1 mm gap between adjacent two rings. Those ball bearings are arranged to permit free lateral movement with minimal friction and prevent vertical displacement or tilt of the rings during the cyclic motion. A relatively big displacement is allowed between adjacent rings. And the design permits an overall shear

strain up to 20%. Figure 5.1 shows the laminar box assembly. It has internal dimensions of 457.2 mm (L) × 304.8 mm (W) × 279.4 mm (H).

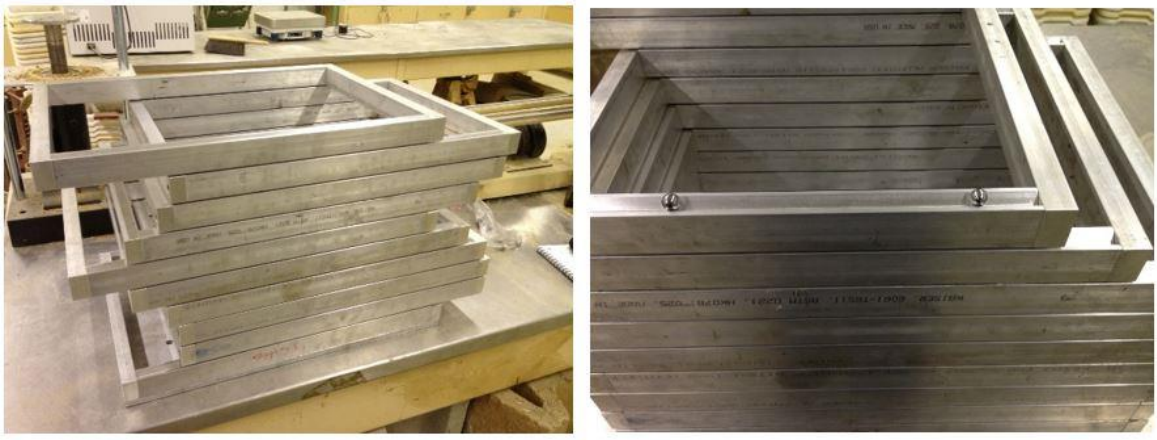

*Figure 5.1 Laminar box assembly*

The laminar box was modified to enable controlling flow of pore fluid through the sand specimen. In order to introduce the flow stream, four outlets were installed at the bottom plate of the laminar box as shown in Figure 5.2. A latex membrane with a thickness of 1 mm was tailored to attach on the inner wall of the laminar box for preventing sand and water from penetrating through the gaps among aluminum rings. The membrane separated the sand specimen from the box and thus provided a watertight box to contain the sand. Thanks to the well flexibility and durability of the latex membrane, aluminum rings can move freely during the cyclic motion. At the open top of the laminar box, four large size clips were used to attach the membrane to four edges. Fixation of the membrane on the top made the laminate to be the boundary of the sand specimen. Otherwise, the membrane itself would restrict the lateral deformation of the sand.

*Figure 5.2 Drainage outlets of the laminar box*

### 5.2.2 Shaking table

In the field of geotechnical earthquake engineering, 1-g shaking table tests have played an important role in exploring the behavior and failure mechanisms of geotechnical structures and soil-structure interactions. Many instructive results obtained from 1-g shaking table tests have enhanced our understanding of the mechanism of liquefaction (Ueng *et al*. 2006; Thevanayagam *et al*. 2009; Rebstock *et al*. 2010; Dobry *et al*. 2011). In this study, a manual shaking table was designed and fabricated to simulate earthquake condition. Two big rectangular wood boards with a same dimension of 1219mm × 812mm × 25.4mm (48 inch × 32 inch × 1 inch, length × width × thickness) were used. As shown in Figure 5.3, the upper piece of board served as a platform for the laminar box. The other piece of board was fixed to the ground as a base. Two wood boards were connected by two mild steel plates of 300 mm long and 2 mm thick through steel bolts and angle sections. Figure 5.4 shows the manual shaker with an aluminum frame which used for instruments arrangement.

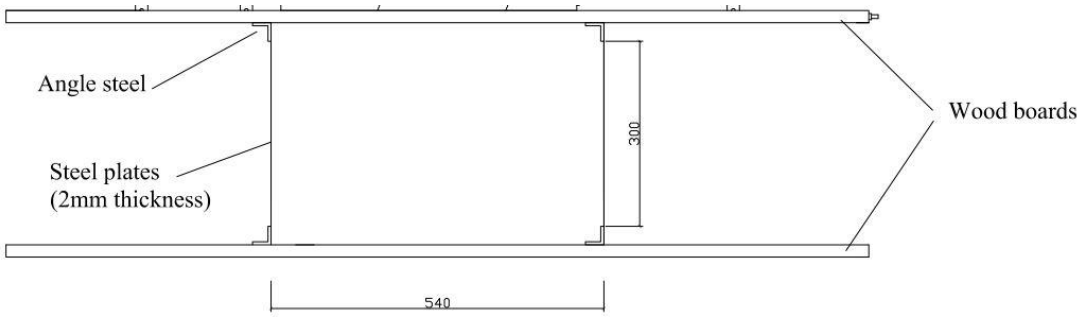


*Figure 5.3 Design sketch of a manual driving shaking table*

*Figure 5.4 Manual driving shaking table with an aluminum frame*

The shaking table used in this study was designed to provide harmonic sinusoidal motion along the horizontal direction and can be treated as a single degree of freedom system in the analysis. Similar one degree of freedom testing device has been used before and was proofed to be reliable (Prasad *et al*. 2004; He *et al*. 2013). By applying a small magnitude of force, it is able to create an acceleration of a = 1.5 m/s$^2$ as recorded in Figure 5.5. Generally

speaking, people lose their balance when the peak acceleration is 0.02g (0.2 m/s$^2$). And depending on the duration, well-designed buildings may be damaged if the peak acceleration hits 0.5g (5 m/s$^2$) (Lorant 2012).

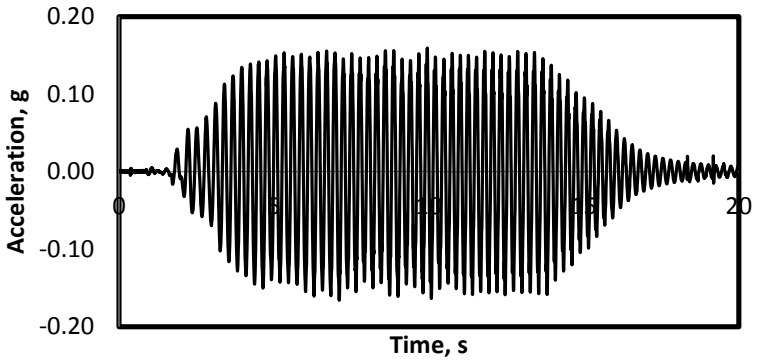


*Figure 5.5 A typical input acceleration*

### 5.2.3 Instrumentation

Different types of instruments were employed to monitor and measure the responses of the sand specimen under the dynamic loading imposed on the shaking table, including accelerometer, pore pressure transducers (PPT), and linear variable differential transformers (LVDT). Figure 5.6 shows the front and side-view of the instruments arrangements in the laminar box. Details of those instruments are shown in Figure 5.7.

Four pieces of Integrated Circuit Piezoelectric (ICP) accelerometers (Model 353B33) manufactured by PCB Piezoelectronics, Inc. were used to measure the induced acceleration time. One of them was attached on the base (upper broad plate) of the shaker. And the other three were installed at different positions of the laminar box. The upper one had a height of 18 cm and the lower one a height of 10 cm. The third one was fixed to the base of the laminar box.

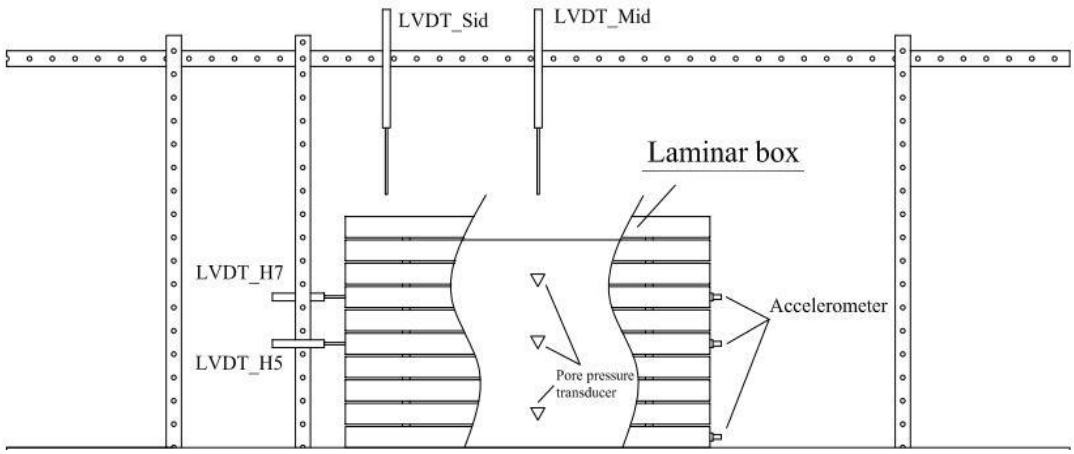


*Figure 5.6 Arrangements of measuring instruments*

In order to measure the pore water pressure development in the shaking, Kulite® XCL-11-250 miniature pore pressure transducers (PPTs) were adopted. Three PPTs were buried at the bottom, 2/3 depth, and 1/3 depth of the sand specimen along the central line, respectively. To prevent the movement of PPTs during shaking stages, all three PPTs were attached to aluminum bars which were fixed on a supporting frame to maintain their original position in the motion. To ensure high quality of measurement, all PPTs were immersed in vacuum applied de-aired water prior to each test for 24 hours.

Four spring return version LVDTs obtained from RDP Group were used for displacement measurement. Two high ranges (±75mm) of DCTH3000A were fixed above the laminar box to monitor the vertical displacement of the sand specimen surface: one in the center and the other in the corner, respectively. For measuring the subsidence of the sand surface, it is necessary to put a piece of acrylic square footing under the LVDT tip to prevent punching of the LVDT core into the sand. The other two low ranges (±7.5mm) of DCTH300AG were responsible for measuring the lateral displacement of the sand specimen.

They were mounted on the supporting frame next to the laminar box at corresponding levels of the buried PPTs.

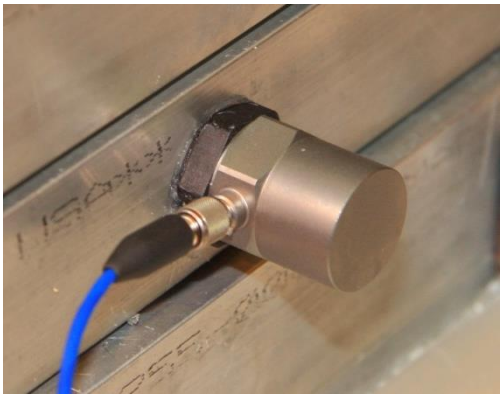

(a) Accelerometer

(b) Pore pressure transducer (PPT)

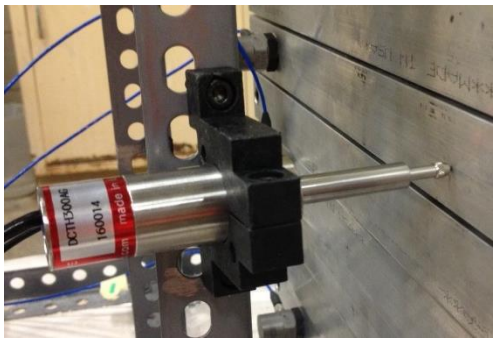

(c) Linear variable differential transformer

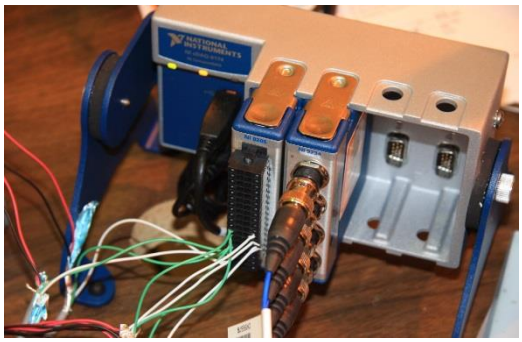

(d) National Instruments data logger

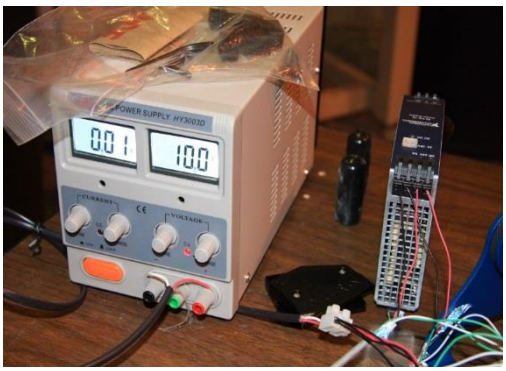

(e) Power supplies

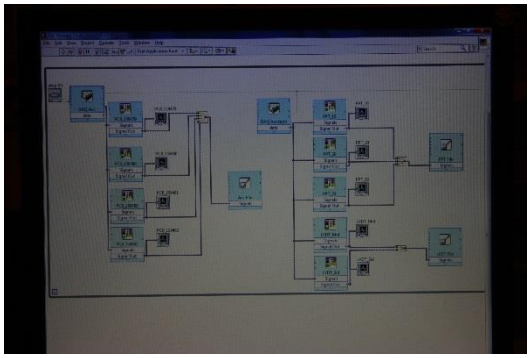

(f) Data collection program

*Figure 5.7 Instrumentations of manual shaker test*

To collect all data from the above mentioned transducers, a National Instrumentation data logger, NI CompactDAQ, was adopted. It included modules of NI9205 and NI9234 to collect and transfer data to a computer. The NI9205 featured 32 single-ended or 16 differential analog inputs, 16-bit resolution, and a maximum sampling rate of 250 kS/s. All readings from PPTs and LVDTs were processed through the NI9205. The NI9234 was a high-accuracy data acquisition module specifically designed for high-channel-count sound and vibration applications and was in charge of processing acceleration data in this study.

### 5.2.4 Sand properties

ASTM graded silica sand was used in all shaking table test had same properties of those employed in previous sand column permeability test. Property details of this silica sand were described in Section 4.2.1.

## 5.3 Test Methodology

### 5.3.1 Test arrangement

Nine shaking table tests were carried out in different setups to study the seismic response of bio-microbiological treated sand specimen. Table 5.1 summarizes all nine test arrangements.

Test 1 to Test 5 were conducted in a leveled ground and Test 6 to Test 9 were performed in a 5-degree sloping ground. As shown in Figure 5.8, the base of the laminar box is parallel to the shaker surface in the leveled ground condition. By contrast, under the

sloping ground condition, one side of the laminar box was raised up and sat on a fixed metal block to create a 5 degrees slope between the container base and the shaker surface.

*Table 5.1 Laboratory shaking table test arrangements*

| Test No. | Targeted degrees of saturation Sr (%) | Ground condition | Seepage flow condition | Bio-cementation |
|---|---|---|---|---|
| Test 1 (TL1) | 100 | Leveled | - | - |
| Test 2 (TL2) | 96 | Leveled | - | - |
| Test 3 (TL3) | 90 | Leveled | - | - |
| Test 4 (TL4) | 90 | Leveled | Upward | - |
| Test 5 (TL5) | 90 | Leveled | Upward | Yes |
| Test 6 (TS1) | 100 | Sloping | - | - |
| Test 7 (TS2) | 90 | Sloping | - | - |
| Test 8 (TS3) | 90 | Sloping | Upward | - |
| Test 9 (TS4) | 90 | Sloping | Upward | Yes |

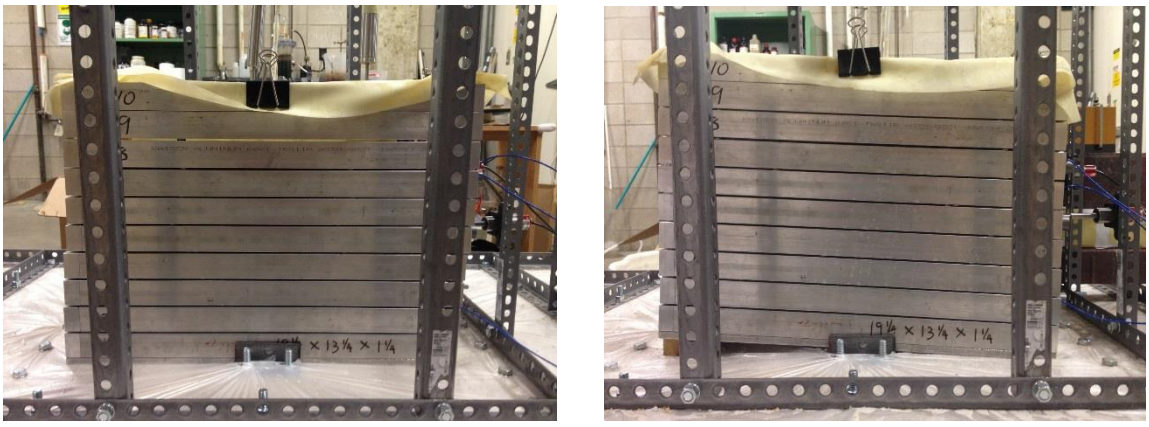

(a) Leveled ground (b) Sloping ground

*Figure 5.8 Laminar box pre-test condition (a) leveled ground; (b) sloping ground*

To evaluate the stability of the biogas bubbles trapped in sand under a certain seepage condition, there was an upward flow applied to the sand specimen in Test 4, 5, 8 and 9 ($S_r$ = 90% in those four tests). When the desaturation process was over and the desired degree of saturation achieved, a peristaltic pump was used to supply a steady upward flow through the modified laminar box drainage system as shown in Figure 5.2. According to a report from USGS (Alley *et al.* 1999), a velocity of 1 foot per day or greater is a high rate of movement for ground water, and ground water velocities can be as low as 1 foot per year or even 1 foot per decade. To simulate the ground water flow, distilled water was pumped into the laminar box through four openings from the bottom drainage layer in a considerable low rate for 24 hours.

The combined biodesaturation and bioclogging method was applied to Test 5 and Test 9. The objective of the two tests was to examine the effectiveness of the combined biodesaturation and bioclogging method under either a hydrostatic or an upward seepage condition. It should be noted that a low calcite content of 1% by mass was used and the purpose was only to form a barrier in the pores between sand particles to retain some gas bubbles, rather than to reinforce the sand to increase its shear resistance. The same seepage condition used for Test 4 was applied when the bioclogging process had finished. Cyclic motions were applied using the shaking table and the response of sand was monitored. The testing results were analyzed and compared with those of Test 4 where the test was conducted under the same conditions, but without bioclogging treatment.

### 5.3.2 Test procedures

The silica sand was washed through distilled water and oven-dried afterwards to remove fines and other impurities before used for all the tests. Prior to preparing sand deposits in the laminar box, the shaker was first mounted onto the concrete floor. Back to the manual shaking table design (Figure 5.3), there were two wood boards connected though mild steel. The bottom board must be fixed and steady enough during shaking otherwise the whole system will be prone to slide in one direction as soon as the horizontal cyclic motion was applied.

Because the laminar box was stacked by a couple of layers of aluminum rings, gaps among those rings made it an unsealed container. Plastic sheets were reported to be used in previous studies to prevent soil or sand with water from leaking during dynamic loadings (Kagawa *et al*, 2004, Ghayoomi, 2011, He *et al*, 2013). However, usually thin regular plastic sheet was easy to be punched or torn by sand sample and thick plastic sheets have poor flexibility which might restrain the movement of soil sample. In this study, a latex membrane with a thickness of 1 mm was employed to separate the sand specimen from the laminar container. Because of its high flexibility, the latex membrane allows sand specimen to deform with less resist compare to plastic sheet. After assembling the laminar container, the membrane was tailored according to the inner size of the container and glued together by water-proof silicon grease. Four small holes were punched at both short sides of the bottom laminate ring to permits water flow through the laminar container wall and the membrane into sand sample. Compression fittings purchased from Swagelok® were used to seal all openings.

A 12 mm gravel layer was laid at the bottom of the laminar box as a drainage layer. Another 3 mm thickness of scouring pad separated gravels and the overlaying sand specimen. Figure 5.9 shows the drainage layer and the latex membrane prior to pouring the sand and water or substrate solution.

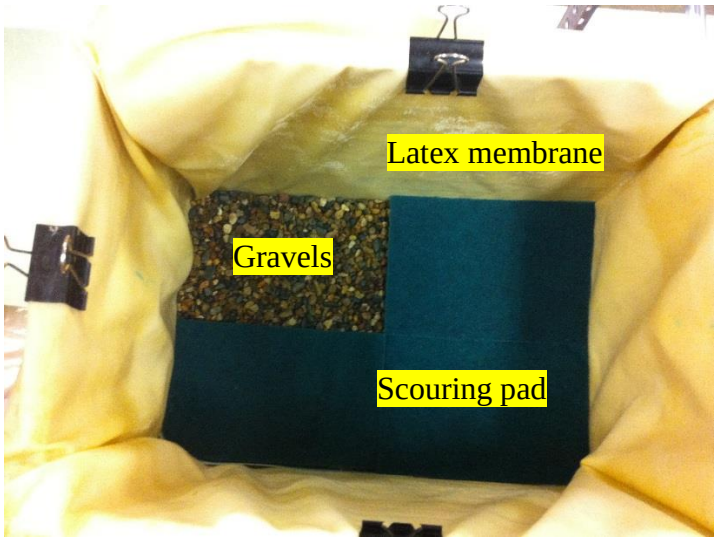


*Figure 5.9 Drainage layer and latex membrane*

Before spraying sand into the laminar box, two liters of inoculated enrichment denitrifying bacterial medium (for desaturated samples) or distilled water (for fully saturated samples) was poured into the box first. The volume of the nutrient solution was pre-determined based on the desired degree of saturation through phase calculation. It was convenient to adjust the concentration of nitrate and glucose according to a specific C:N ratio so that various initial degrees of saturation of the sand specimen could be achieved properly. Keep other nutrient content in the bacterial medium to be constant in all tests while only adjust the carbon and nitrogen source content to avoid disturb from other nutrient compounds.

The wet sedimentation method was adopted for the sand specimen preparation in this study. As shown in Figure 5.10a, dry sand was rained down slowly into the laminar box through a funnel. The funnel was moved back and forth by following a zigzag path (Figure 5.10b) in order to form a uniform and low relative density sand deposit. The process was carefully carried out to avoid large air bubbles trapped in sand.

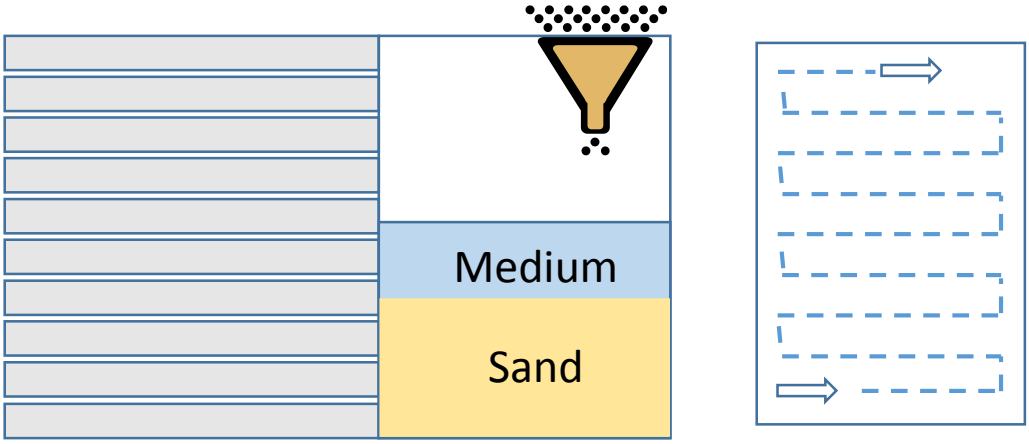


(a) Wet sedimentation (b) Sand spray

*Figure 5.10 Schematic of sand preparation method*

A pre-determined sand mass and nutrient was divided into three portions equally. They were introduced into the laminar box by sequence. For each portion, as the sand surface height hit the water level, raining process was stopped. And another portion of nutrient solution flew into the box through siphon under a low hydraulic gradient of 0.1. After that, the sand raining process resumed until the last portion of sand mass was laid down to the laminar box. Upon completion of laying all three portions of sand, the sand surface was leveled and the height of the specimen was measured to evaluate the actual soil parameters of void ratio, relative density and degree of saturation. The water table was about 1-1.5 cm above the sand surface at final in all tests. The thickness of the sand specimen was about 22

to 25 cm depending on the sand mass and thus gave a relative density about 25-30%. Figure 5.11 shows a photo of pre-shaking test set-up. The initial water surface height was recorded. As the denitrification process went on, the water level rose as well due to the occupation of pore voids by those gas bubbles generated within the sand specimen. The raised water level can be seen as an indicator to calculate the volume of biogas trapped in the sand and thus the concurrent degree of saturation can be predicted as well.

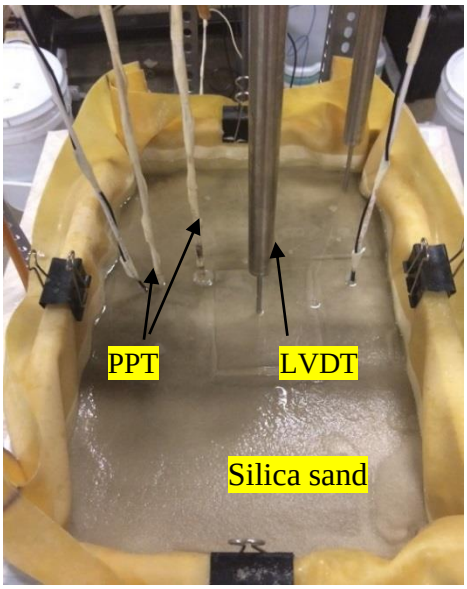


*Figure 5.11 Pre-shaking test setup*

When the denitrification process had reached the desired degree of saturation, various magnitude of cyclic loadings were applied to the shaking table in an order of from low acceleration to high acceleration, for instance, from 0.05g (0.5m/s$^2$) to 0.25g (2.5m/s$^2$). If a low acceleration load did not trigger the liquefaction and the settlement of the sand deposit was tiny and negligible, a following level of acceleration load was applied. Each shaking stage took about 20 seconds in a frequency of 1 to 1.5 Hz. A time interval of five minutes existed between adjacent shakings to allow the complete dissipation of excess pore water

pressure generated during the shaking. The vertical deformation of the sand deposit after every shaking was recorded for updating the current value of void ratio and relative density.

For tests with seepage flow in the sand specimen, as mentioned in the test arrangement section, a flow stream was introduced into the sand specimen via a peristaltic pump from the bottom of the laminar box after the denitrification process. The flow rate was same as the one used in 1 m column biogas stability test described previously. It was proved that under such a low flow rate, the amount of biogas generated in pore void would not be driven away by the flow. The continuous flow lasted 48 hours. Figure 5.12 demonstrates the seepage flow system. The same system was employed to deliver UPB suspension as well as calcium chloride and urea solution for MICP process. The UPB suspension was made from freeze-dried biomass power (1g/L). In order to produce 1% (w/w) of calcite, 4L of 1M calcium chloride and urea solution was used in both Test 5 and Test 9. Several sand samples taken from different positions of the sand specimen after tests were kept for calcite content determination.

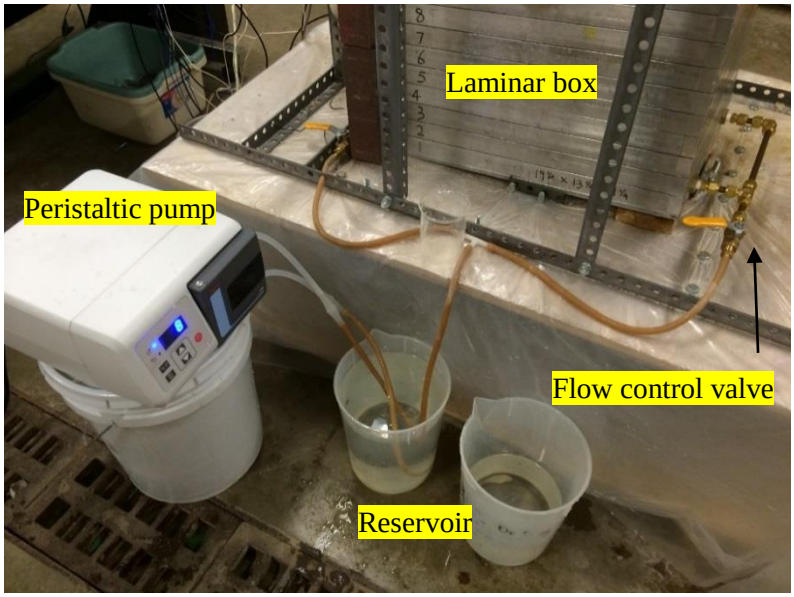


*Figure 5.12 Seepage flow supply system*

### 5.3.3 Monitoring the denitrification process

There were two methods used to monitor the variation of degrees of saturation. One was to measure the height change of the water surface. Because the sand specimen was assumed fully saturated after deposit. All pore voids were filled with nutrient solution or distilled water. Nitrogen gas has poor solubility in the atmospheric pressure condition. It would occupied space and excluded the nutrient solution or water. Measuring the risen height of water surface thus was a reasonable approach to estimate the volume of nitrogen gas generated within the sand specimen. Another method was to measure the reduction in nitrate concentration. Based on the reaction in the denitrification process, the amount of nitrogen gas produced can be estimated. According to the nitrate conversion rate results given in Table 3.1, a roughly 80% conversion rate could be expected. The amount of nitrate added into the nutrient solution which delivered to the sand was pre-determined so that the generation of nitrogen gas can be expected and controlled.

Figure 5.13 presents the monitored variation in the degree of saturation of the sand over time. The data show that all three desired degrees of saturation were reached according to the observation from the monitoring methods mentioned above. The calculated degree of saturation based on the consumption of nitrate (or the variation in nitrate concentration) presented by hollow data points is slightly higher than the degree of saturation calculated from monitored water level increase (solid data points). However, the difference is not significant. The increase in pH values during the denitrification process shown in Figure 5.14 is higher than those measured in the gas generation tests. It might be due to the high

concentration of nitrate. An alkaline ambient after denitrification was also found in other studies (Šimek and Cooper 2002; Saleh-Lakha *et al*. 2009; Saggar *et al*. 2012).

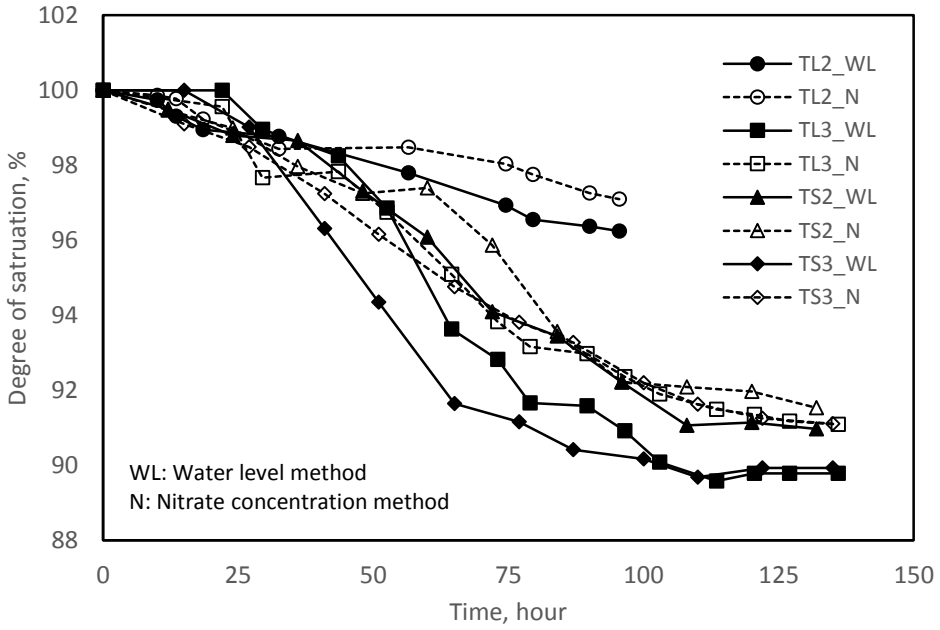


*Figure 5.13 Variation of degree of saturation during denitrification process in the laminar box*

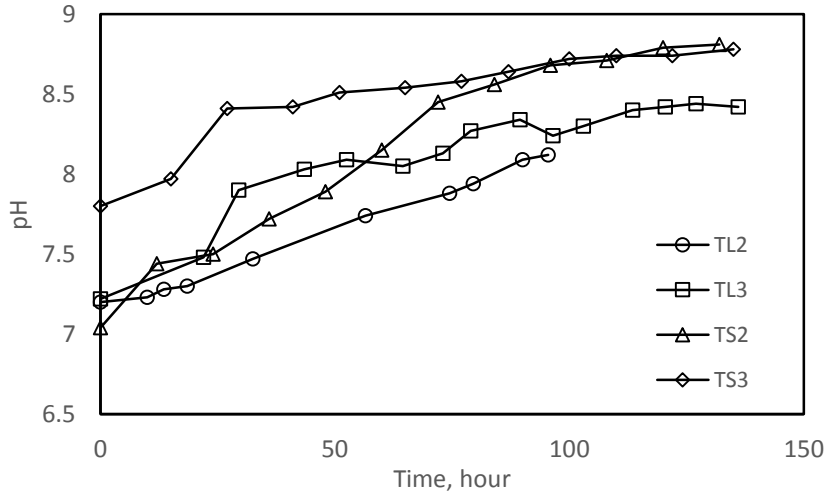


*Figure 5.14 Change of pH values during denitrification process in the laminar box*

## 5.4 Test Results

### 5.4.1 Overview

To study the behavior of biogas desaturated sand under cyclic loading, nine tests with different testing setups were conducted. An overview of the major test results is given in Table 5.2 and Table 5.3 for both leveled ground (TL) and sloping ground (TS), respectively. For each test set, acceleration response of the laminar box, excess pore water pressure, vertical and lateral displacement of the sand specimen were recorded and analyzed. Seepage conditions were also considered at both leveled ground and sloping ground circumstance. Relationships among pore pressure ratio, relative density and volumetric strains were analyzed to investigate the effectiveness of the biogas desaturation method as a liquefaction mitigation option. The seismic behavior of sand specimen treated with combined biogas and bioclogging technique was also studied.

*Table 5.2 Laboratory shaking table test results (Leveled ground)*

| | | Acceleration (g) | Void Ratio | Relative Density (%) | Volumetric Strain (%) | Pore Pressure Ratio | |
|---|---|---|---|---|---|---|---|
| | | | | | | 2/3 Depth | 1/3 Depth |
| Test TL1 $S_r$ = 100% | Test 1a | 0.05 | 0.737 | 20.99 | 0.22 | 0.068 | 0.091 |
| | Test 1b | 0.10 | 0.691 | 36.31 | 2.72 | 0.594 | 0.906 |
| | Test 1c | 0.15 | 0.613 | 62.23 | 4.82 | 0.595 | 0.952 |
| | Test 1d | 0.15 | 0.588 | 70.78 | 1.62 | 0.479 | 0.483 |
| | Test 1e | 0.15 | 0.580 | 73.46 | 0.51 | 0.098 | 0.168 |
| | Test 1f | 0.20 | 0.534 | 88.65 | 2.97 | 0.410 | 0.809 |
| Test TL2 $S_r$ = 96% | Test 2a | 0.05 | 0.732 | 22.62 | 0.33 | 0.006 | 0.009 |
| | Test 2b | 0.10 | 0.723 | 25.76 | 0.55 | 0.321 | 0.399 |
| | Test 2c | 0.15 | 0.666 | 40.63 | 3.40 | 0.300 | 0.378 |
| | Test 2d | 0.15 | 0.652 | 49.31 | 0.85 | 0.084 | 0.120 |
| | Test 2e | 0.15 | 0.646 | 51.32 | 0.37 | 0.046 | 0.060 |
| | Test 2f | 0.20 | 0.601 | 66.42 | 2.83 | 0.198 | 0.234 |
| Test TL3 $S_r$ = 90% | Test 3a | 0.05 | 0.733 | 22.26 | 0.09 | 0.005 | 0.017 |
| | Test 3b | 0.10 | 0.730 | 23.49 | 0.21 | 0.037 | 0.224 |
| | Test 3c | 0.15 | 0.706 | 31.29 | 1.37 | 0.032 | 0.200 |
| | Test 3d | 0.15 | 0.699 | 33.82 | 0.45 | 0.018 | 0.030 |
| | Test 3e | 0.15 | 0.696 | 34.74 | 0.16 | 0.009 | 0.023 |
| | Test 3f | 0.20 | 0.670 | 43.19 | 1.52 | 0.022 | 0.074 |
| Test TL4 $S_r$ = 90% Seepage | Test 4a | 0.05 | 0.728 | 24.02 | 0.15 | 0.035 | 0.055 |
| | Test 4b | 0.10 | 0.713 | 29.03 | 0.88 | 0.133 | 0.237 |
| | Test 4c | 0.15 | 0.663 | 45.81 | 3.03 | 0.202 | 0.387 |
| | Test 4d | 0.15 | 0.654 | 48.55 | 0.5 | 0.118 | 0.166 |
| | Test 4e | 0.15 | 0.652 | 49.44 | 0.16 | 0.052 | 0.046 |
| | Test 4f | 0.20 | 0.632 | 56.12 | 1.23 | 0.193 | 0.253 |
| Test TL5 $S_r$ = 90% Bioclogging | Test 5a | 0.05 | 0.723 | 25.83 | 0.08 | 0.028 | 0.035 |
| | Test 5b | 0.10 | 0.721 | 26.50 | 0.12 | 0.010 | 0.024 |
| | Test 5c | 0.15 | 0.699 | 33.81 | 1.29 | 0.058 | 0.131 |
| | Test 5d | 0.15 | 0.690 | 36.54 | 0.49 | 0.036 | 0.090 |
| | Test 5e | 0.15 | 0.687 | 37.71 | 0.21 | 0.025 | 0.073 |
| | Test 5f | 0.20 | 0.675 | 41.65 | 0.70 | 0.118 | 0.172 |

*Table 5.3 Laboratory shaking table test results (Sloping ground)*

| | | Acceleration (g) | Void Ratio | Relative Density (%) | Volumetric Strain (%) | Pore Pressure Ratio | |
|---|---|---|---|---|---|---|---|
| | | | | | | 2/3 Depth | 1/3 Depth |
| Test TS1 Sr = 100% | Test 1a | 0.05 | 0.734 | 21.83 | 0.15 | 0.035 | 0.055 |
| | Test 1b | 0.10 | 0.698 | 33.99 | 2.15 | 0.562 | 0.600 |
| | Test 1c | 0.15 | 0.602 | 65.86 | 5.97 | 0.602 | 0.583 |
| | Test 1d | 0.15 | 0.578 | 74.06 | 1.56 | 0.561 | 0.500 |
| | Test 1e | 0.15 | 0.566 | 77.95 | 0.74 | 0.097 | 0.084 |
| | Tetst 1f | 0.20 | 0.550 | 83.21 | 1.02 | 0.694 | 0.629 |
| Test TS2 Sr = 90% | Test 2a | 0.05 | 0.736 | 21.38 | 0.18 | 0.028 | 0.035 |
| | Test 2b | 0.10 | 0.724 | 25.32 | 0.69 | 0.035 | 0.061 |
| | Test 2c | 0.15 | 0.649 | 50.35 | 4.55 | 0.134 | 0.425 |
| | Test 2d | 0.15 | 0.640 | 53.35 | 0.55 | 0.067 | 0.084 |
| | Test 2e | 0.15 | 0.635 | 55.12 | 0.32 | 0.011 | 0.061 |
| | Test 2f | 0.20 | 0.590 | 69.97 | 2.80 | 0.701 | 0.238 |
| Test TS3 Sr = 90% Seepage | Test 3a | 0.05 | 0.734 | 22.10 | 0.09 | 0.005 | 0.017 |
| | Test 3b | 0.10 | 0.720 | 26.77 | 0.82 | 0.091 | 0.121 |
| | Test 3c | 0.15 | 0.662 | 46.15 | 3.50 | 0.245 | 0.325 |
| | Test 3d | 0.15 | 0.633 | 55.76 | 1.77 | 0.074 | 0.106 |
| | Test 3e | 0.15 | 0.627 | 57.64 | 0.35 | 0.045 | 0.059 |
| | Test 3f | 0.20 | 0.597 | 67.82 | 1.91 | 0.404 | 0.368 |
| Test TS4 Sr = 90% Bioclogging | Test 4a | 0.05 | 0.739 | 20.45 | 0.15 | 0.035 | 0.055 |
| | Test 4b | 0.10 | 0.733 | 22.33 | 0.33 | 0.005 | 0.041 |
| | Test 4c | 0.15 | 0.725 | 25.05 | 0.47 | 0.071 | 0.130 |
| | Test 4d | 0.15 | 0.718 | 27.22 | 0.38 | 0.004 | 0.007 |
| | Test 4e | 0.15 | 0.713 | 28.98 | 0.31 | 0.026 | 0.067 |
| | Test 4f | 0.20 | 0.612 | 62.61 | 6.26 | 0.074 | 0.146 |

### 5.4.2 The leveled ground condition

5.4.2.1 Acceleration response

Selection of an appropriate and consistent shaking magnitude for each test is one of the critical factors for obtaining reliable results in shaking table test. The motion often required to be considerable to initiate liquefaction of the sand deposit without the cost of stability of the shaking table system. Too vigorous shaking might put the laminar box and the shaker at risk. Historical earthquake records show that most earthquakes that caused severe damage usually has frequencies ranging from 1 to 2 Hz (Prasad *et al*., 2004; He and Chu, 2014). In this study, the shaking started at 1 Hz and the frequency gradually increased to 1.5 Hz. In general there were 30 cycles during the shaking period for each shaking level represented by acceleration magnitude. Typical acceleration responses measured at the base of the shaking table during cyclic motions are presented in Figure 5.15. The desired peak accelerations were 0.1g, 0.15g and 0.2g depending on the level of ground shaking required.

The induced accelerations were measured at three different positions. One was at the base of the laminar box. The other two located at the height of 10 cm and 18 cm above the base, respectively. Figure 5.16 plots the induced accelerations for fully saturated sand or biogas desaturated sand under leveled ground conditions for an input cyclic load of 0.15g magnitude. It is clear that except the base, at both the mid layer and the upper layer, the induced acceleration in biogas desaturated sand is much less than those in the fully saturated sand. It can be seen in Figure 5.16a that the induced peak acceleration at the upper layer of the fully saturated sand was more than twice of the input acceleration. However, as shown in Figure 5.16b, a different peak acceleration response at the upper layer of the biogas desaturated sand was observed.

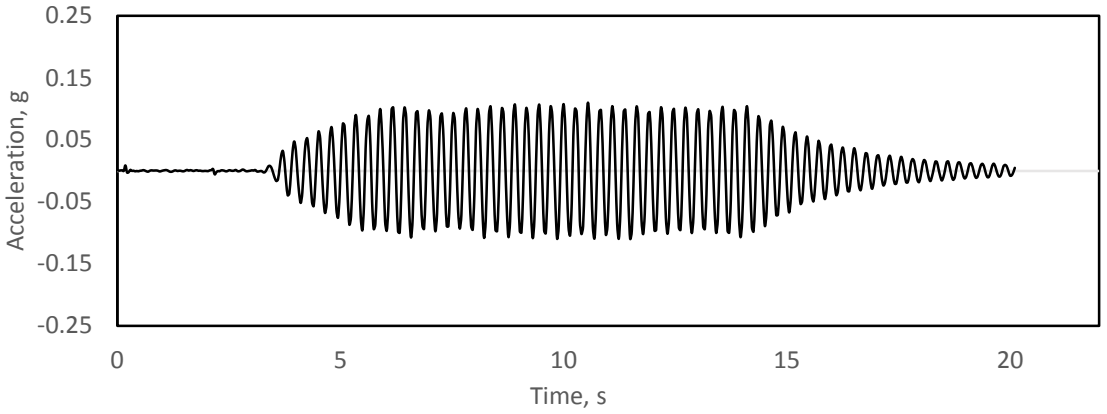


*(a) Input acceleration a = 1.0 m/s²*

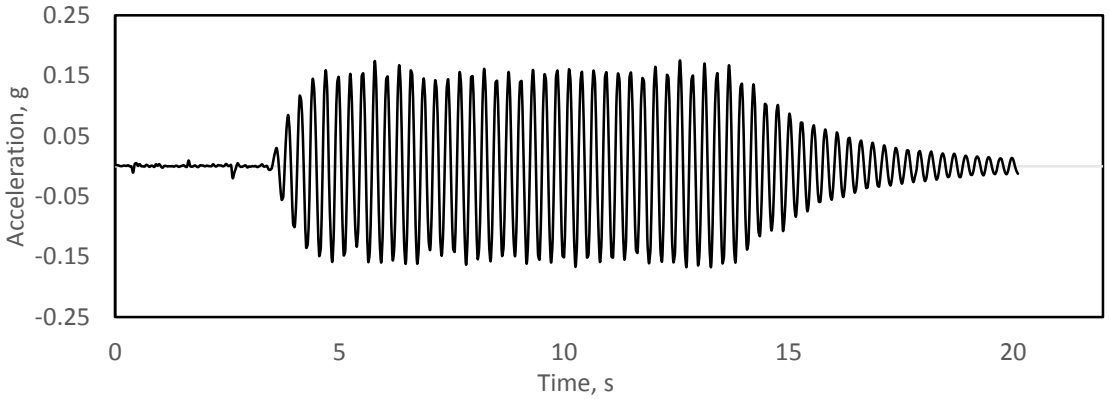


*(b) Input acceleration a = 1.5 m/s²*

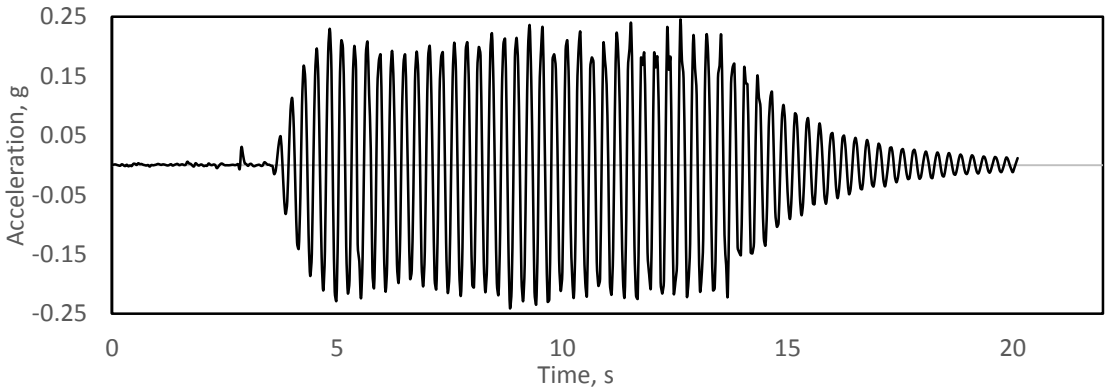


*(c) Input acceleration a = 2.0 m/s²*

*Figure 5.15 Typical acceleration inputs on the shaking table system*

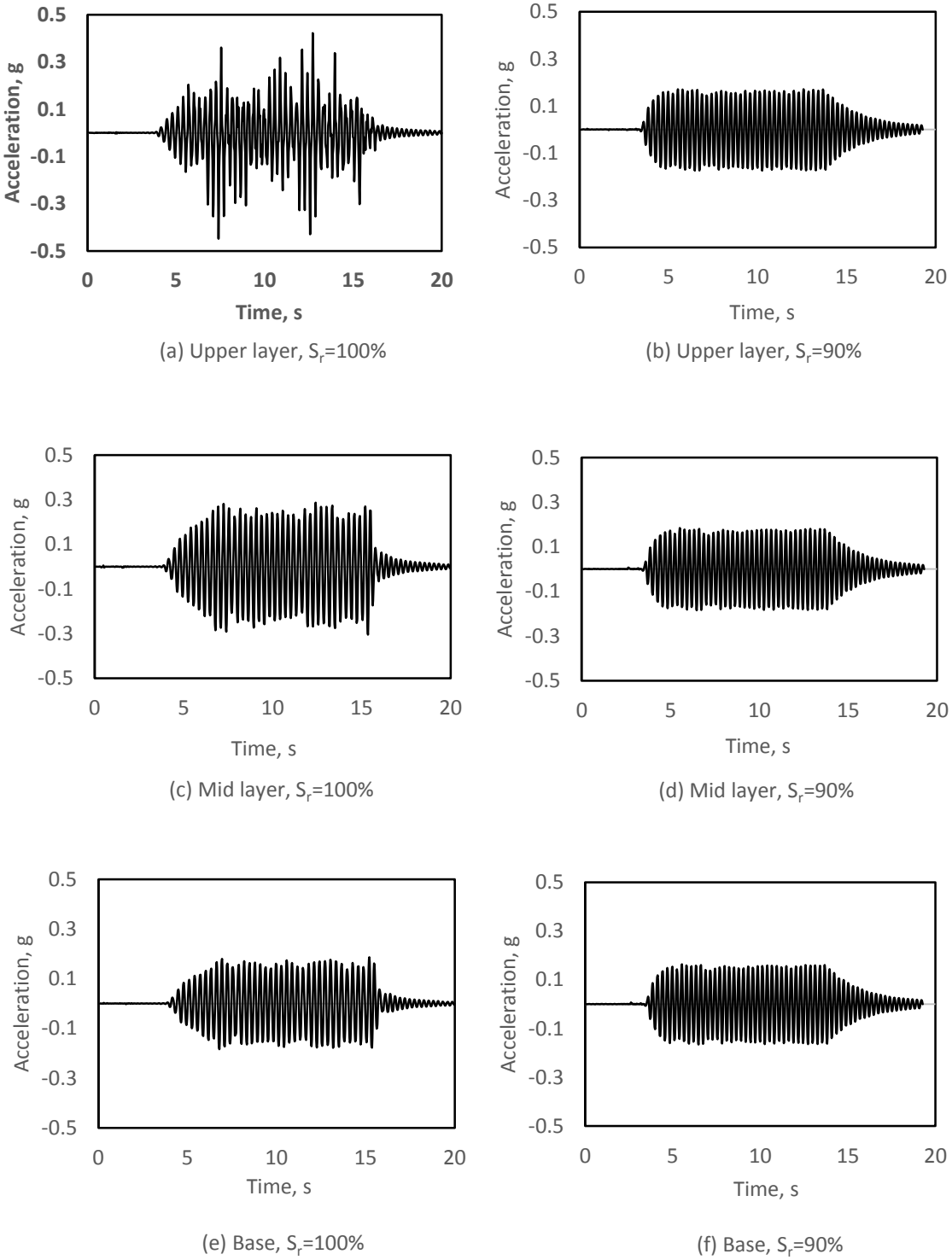


*Figure 5.16 Typical acceleration responses in sand specimens with different degrees of saturation (leveled ground)*

It is noticed that when the sand is fully saturated, the induced acceleration pattern became scattered from the base of the sand specimen to its surface. However, the magnification effect of the induced acceleration in biogas desaturated (Sr = 90%) sand was not as significant as that for fully saturated sand. Amplification ratio which is defined as the acceleration measured at the sand to that at the shaking table is used in the following discussion. Figure 5.17 illustrates the variation of amplification ratio as the change of degree of saturation and the intensity of shaking. The accelerations at the upper part of the sand specimen were amplified compared to the input acceleration. The data pattern has an overall magnifying trend in the peak induced acceleration by the increasing the degree of saturation.

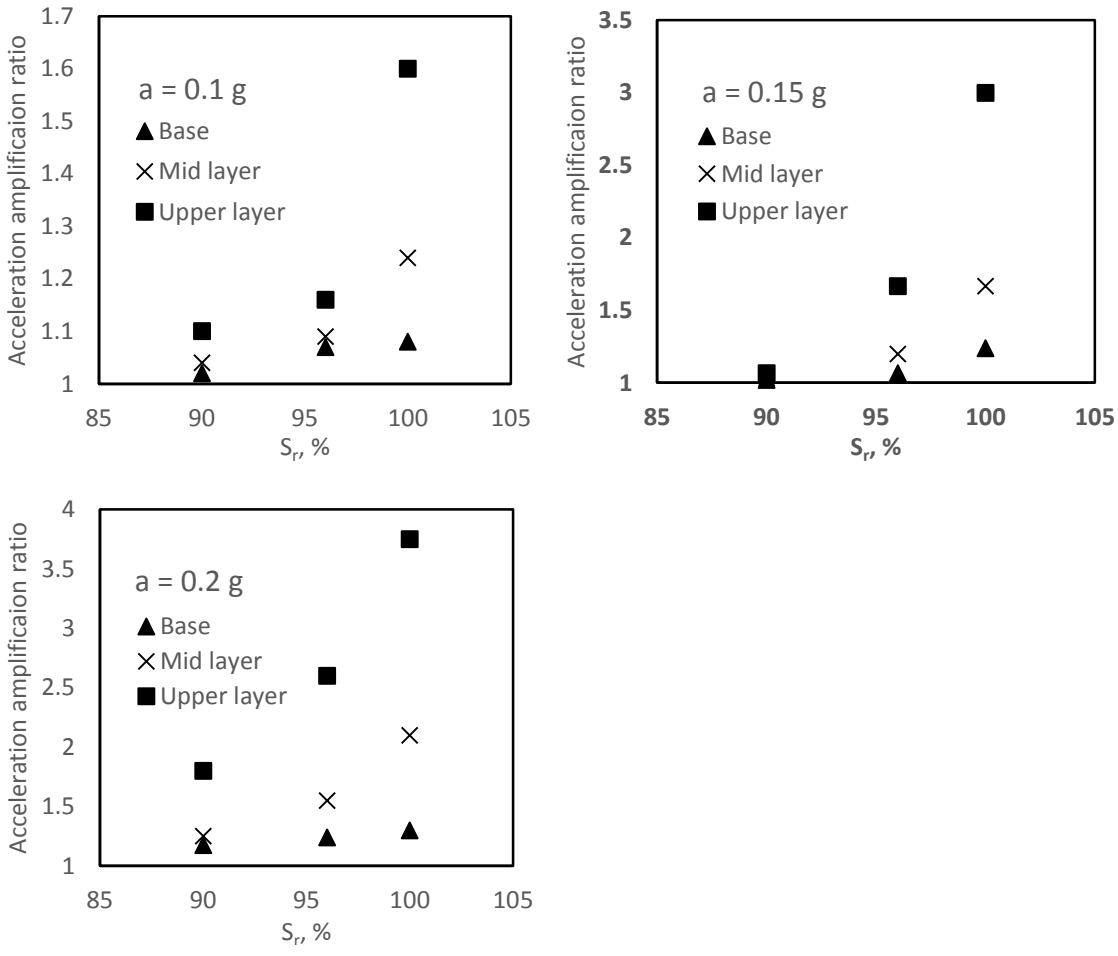


*Figure 5.17 Acceleration amplification ratio versus degree of saturation (leveled ground)*

5.4.2.2 Pore water pressure

Pore water pressure variations during shaking are presented in Figure 5.18. The pore pressures are plotted in terms of water head in Figure 5.18. The input acceleration was 0.1g (0.15 m/s$^2$). The pore pressure head at the surface and the mid part of the fully saturated sand increased by about 2.5 and 4 cm, respectively. However, as the degree of saturation was reduced by the biogas to 96%, only about 1cm increase in the pore pressure head was observed both at the surface and at the mid part of the sand specimen. For the sand specimen with 90% degree of saturation, less than 0.5cm increase in the pore pressure head was measured. The trend strongly suggests that the excess pore water pressure generation in sand is largely confined as the slight reduction of degree of saturation.

Figure 5.19 shows the development of pore pressure ratio in sand with different degrees of saturation under the same input acceleration of a = 1.5 m/s$^2$. $R_u$ is defined as the ratio of maximum excess pore pressure generated by the cyclic load to the initial effective overburden stress. The pore pressure increased during the cyclic loading and dissipated afterwards. For fully saturated sand, there was a considerable amount of increase in excess pore pressure as the shaking took place. The pore pressure ratio at both the mid and surface positions exceeded 0.5 which indicates that the liquefaction occurred. The pore pressure generated in Test TL2 were substantially lower than that in Test TL1, even though the reduction in $S_r$ (96%) was quite small. When $S_r$ dropped to 90%, the increase in pore pressure becomes insignificant. The maximum $R_u$ ratio in the biogas desaturated sample ($S_r$ = 90%) was less than a tenth of that in the fully saturated ones.

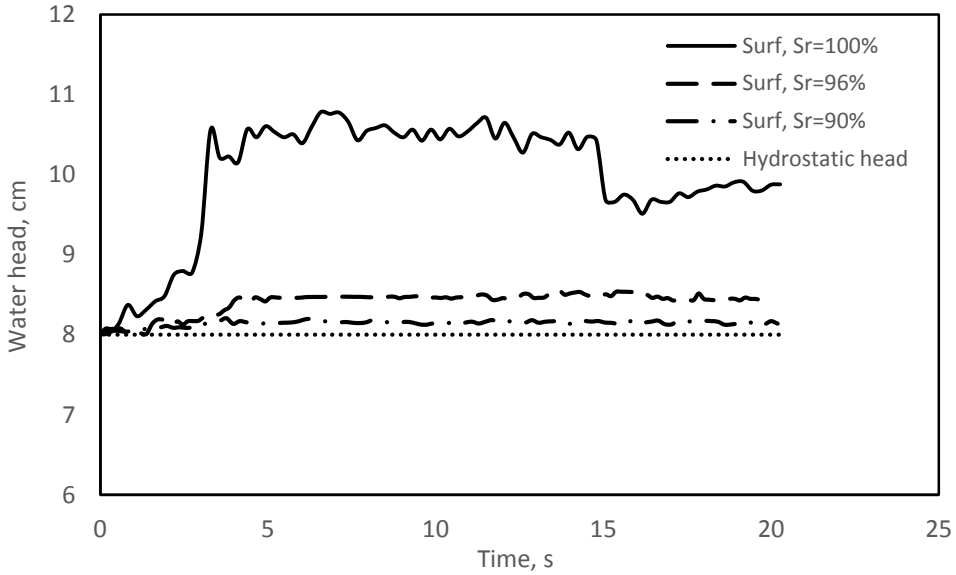


*(a) Surface position*

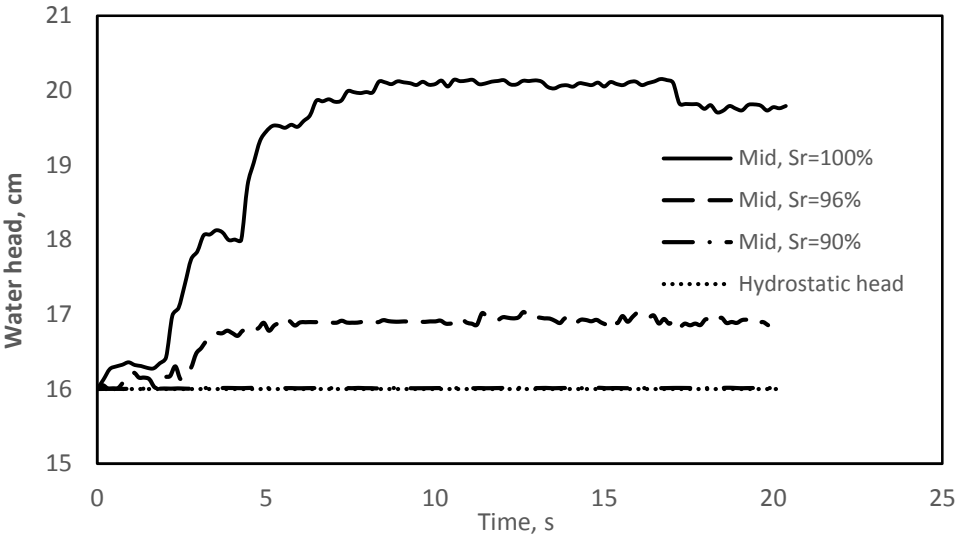


*(b) Mid position*

*Figure 5.18 Pore pressure response to cyclic load in the leveled ground ($a=1.5m/s^2$)*

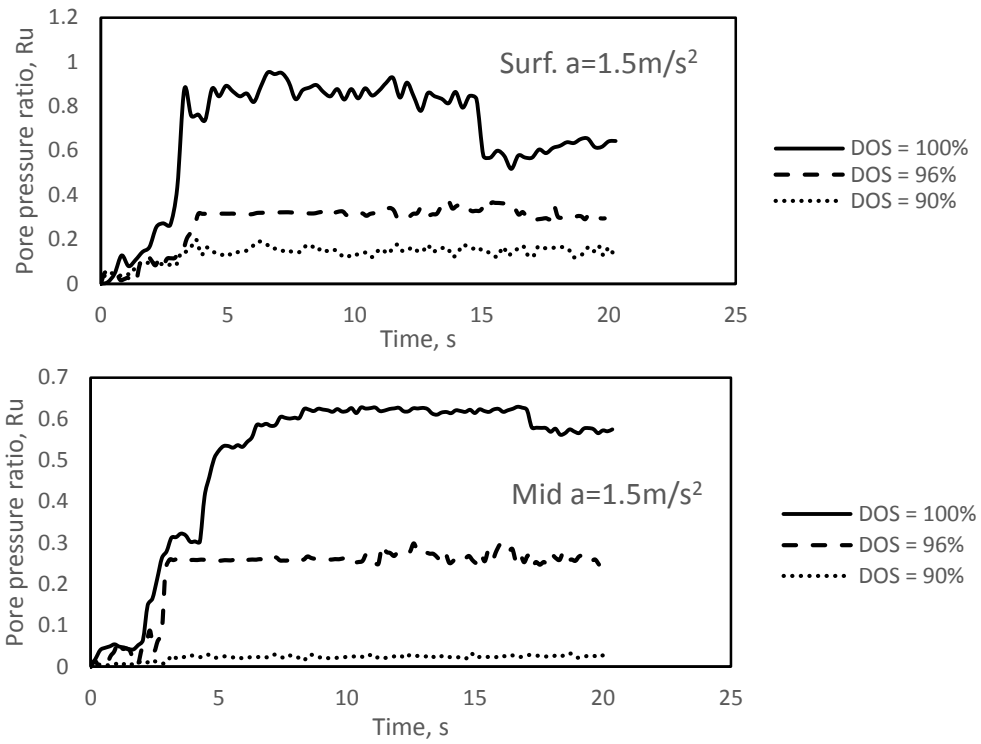


*Figure 5.19 Pore pressure ratio development in the leveled ground ($a=1.5m/s^2$)*

5.4.2.3 Settlement or vertical strain

The measured cumulative settlements of the sand surface were recorded by a LVDT installed on top of the laminar box. For sand specimens with different degree of saturation, Figure 5.20 presents an overview of settlements developed under various input accelerations in the leveled ground condition. All settlements were normalized as vertical strain by dividing the initial height of the sand specimen under an assumption that the sample deformed one dimensionally.

There was a significant difference in the vertical volumetric strain between the saturated and the biogas desaturated sand specimen as shown in Figure 5.20. When the sample was fully saturated, considerable settlement occurred which indicated that the sand sample liquefied. As shown in Figure 5.20, more than 8 percent vertical strain took place

after an acceleration of 1.5 m/s$^2$ or 2 m/s$^2$ was imposed. Although there was a slight reduction of 4 percent in the degree of saturation in Test TL2, more than half of the vertical strain was prevented compared to that occurred in the fully saturated sample. When the degrees of saturation dropped to 90 percent, the volumetric strain caused by the ground shaking were mostly within only 1%. This is clear evidence that the biogas desaturated sand had strong resistance to liquefaction. This finding corroborates the description of Tokimatsu and Seed (1987), who reported that volumetric strains observed in non-liquefiable soils were usually less than 1%.

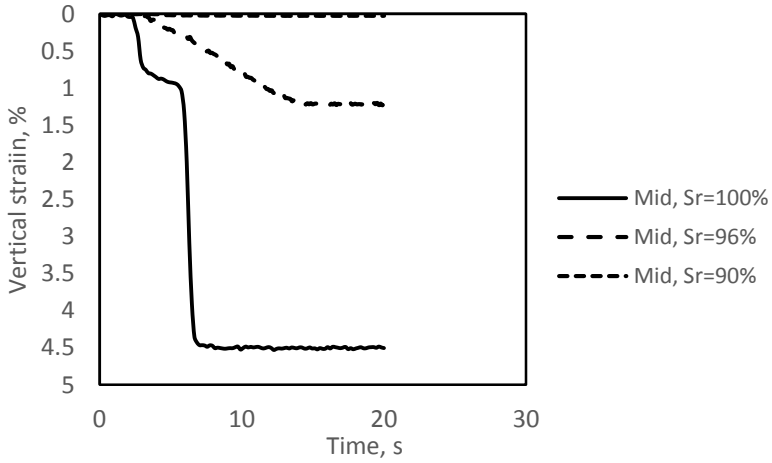


(a) a = 1 m/s$^2$

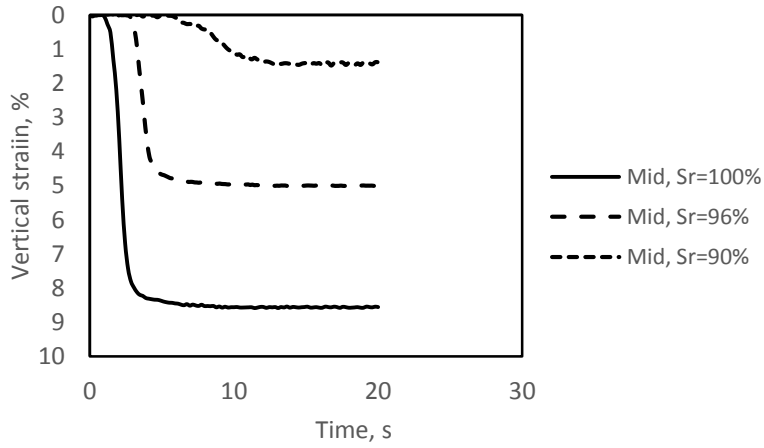


(b) a = 1.5 m/s$^2$

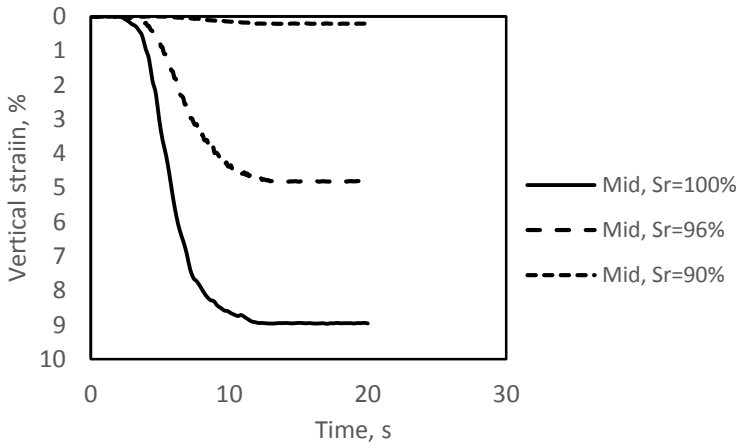


(c) a = 2 m/s$^2$

*Figure 5.20 Volumetric strain development in the leveled ground*

5.4.2.4 Lateral spreading or lateral strain

Two LVDTs were installed at a height of 10 and 18 cm from the base of the laminar box, respectively, to measure the lateral displacement or lateral spreading of the laminate ring which represents the lateral movement of the relevant sand specimen. Figure 5.21 illustrates the changes of lateral strain responses to various magnitudes of shaking. Here the lateral strain was obtained from dividing lateral displacement by the height where it measured. All of the lateral displacements measured were relative movements which equal to the difference in the movements between the laminate rings and the base of the box.

A reduction in the degree of saturation would decrease the amount of lateral spreading. When the sand specimen was or close to a fully saturated status, as shown in Figure 5.21 (a) and (c), the peak value of lateral spreading arrived early and then gradually decayed as the shaking carried on. However, Figure 5.21 (b) and (d) demonstrates that the decay effect was not significant when the shaking magnitude increased to a higher value of

0.2g. The lateral spreading in biogas desaturated sand was barely enlarged of 1 percent at both the upper and mid sand layer which was much less than that in fully saturated sand.

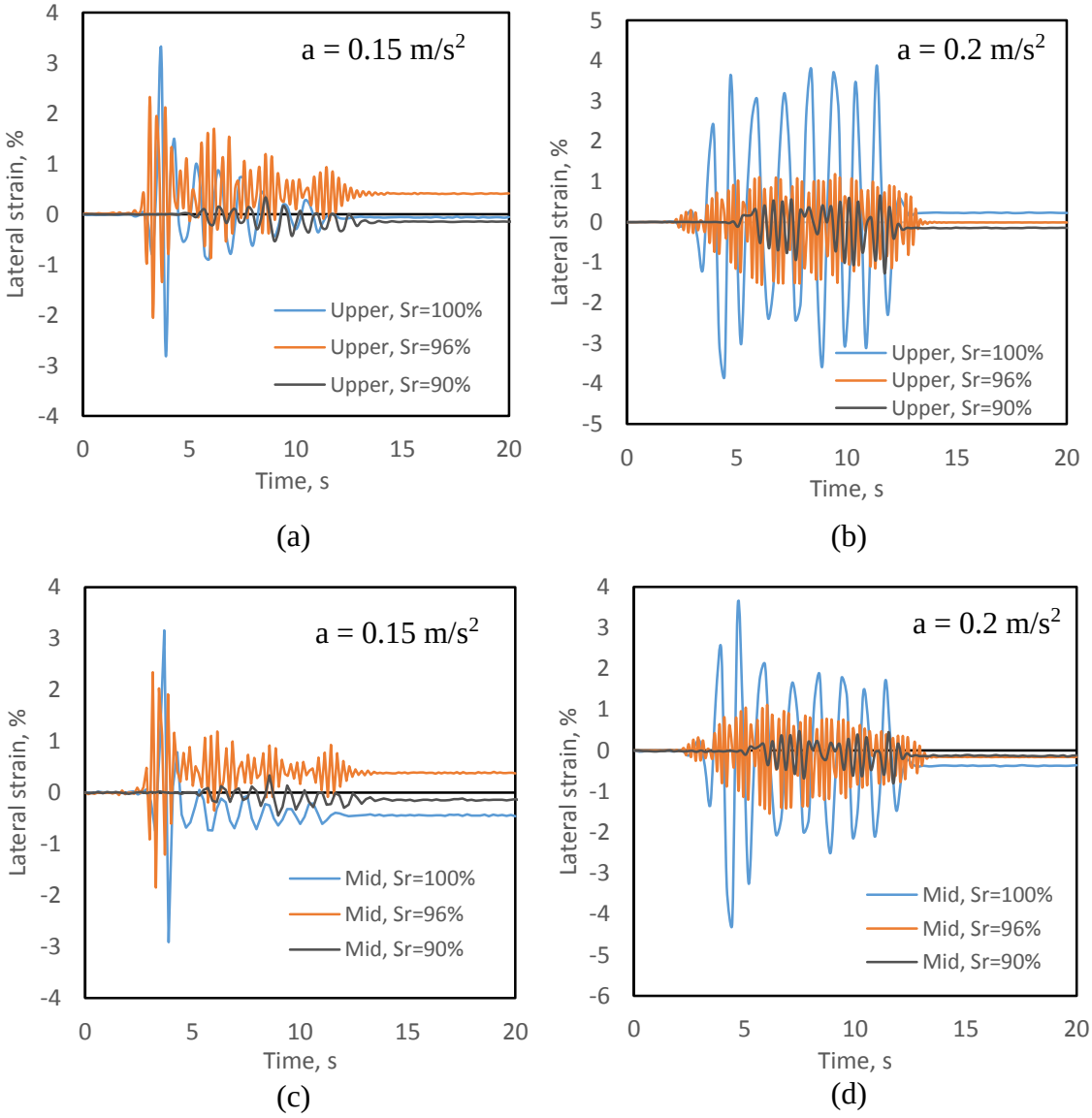


*Figure 5.21 Lateral strain development during shaking in the leveled ground*

The maximum lateral spreading measured along the sand specimen depth is depicted in Figure 5.22. The origin point in the axis X represents the static position, the positive value means the laminates moving forward, and the negative value implies moving backward. This

effect observed under various magnitudes of shaking. The profiles of lateral spreading for the biogas desaturated sand are inclined to the original axis (x=0) which indicates the movement of sand specimen in both forward and backward direction were largely limited.

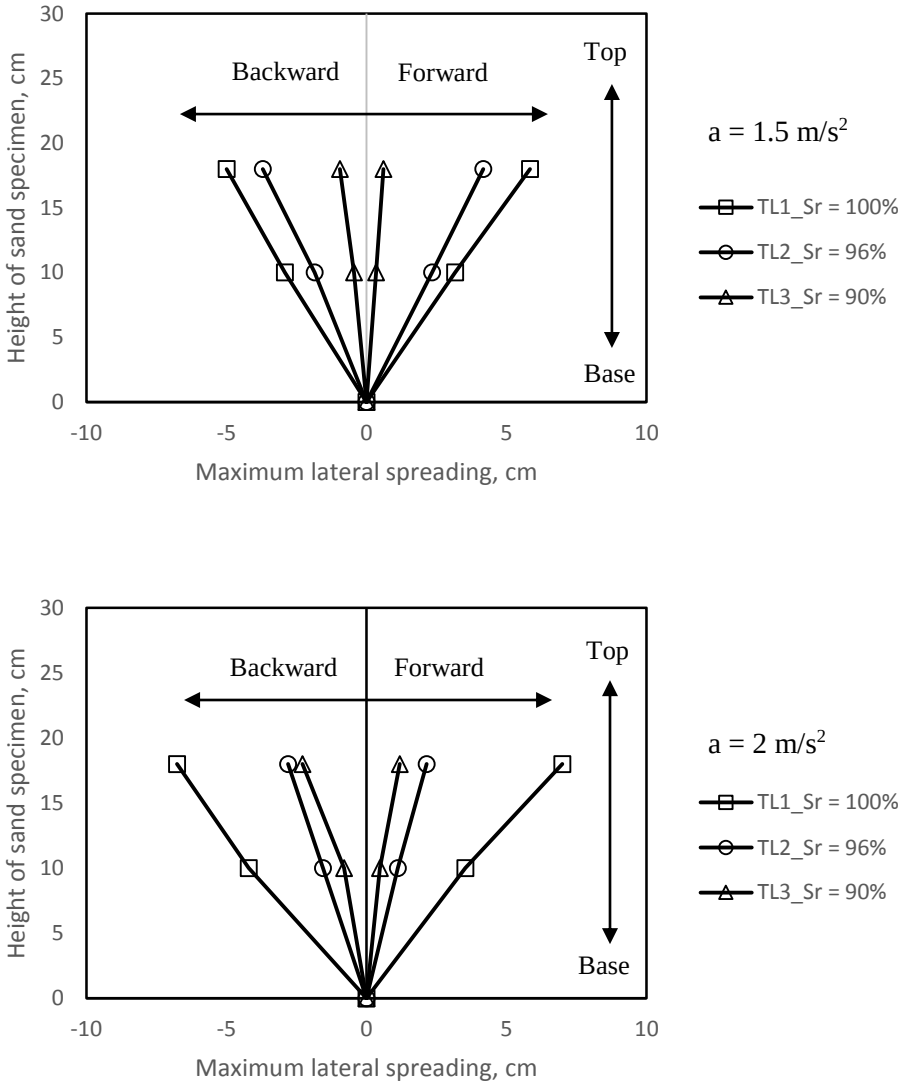


*Figure 5.22 Maximum lateral spreading measurement (leveled ground)*

5.4.2.5 Upward seepage and MICP effect

There was a slow rate of upward seepage introduced into sand in both Tests TL4 and TL5 to investigate the stability of biogas generated through the denitrification process and its influence to the cyclic response of sand specimen. The combined biodesaturation and bioclogging method was applied to Test TL5. The amount of calcium carbonate generated was 1 percent of dry sand mass. The test results are presented in Figures 5.23, 5.24 and 5.25 for pore pressure ratio, vertical strain and lateral strain, respectively. The applied input acceleration was 1.5 m/s$^2$.

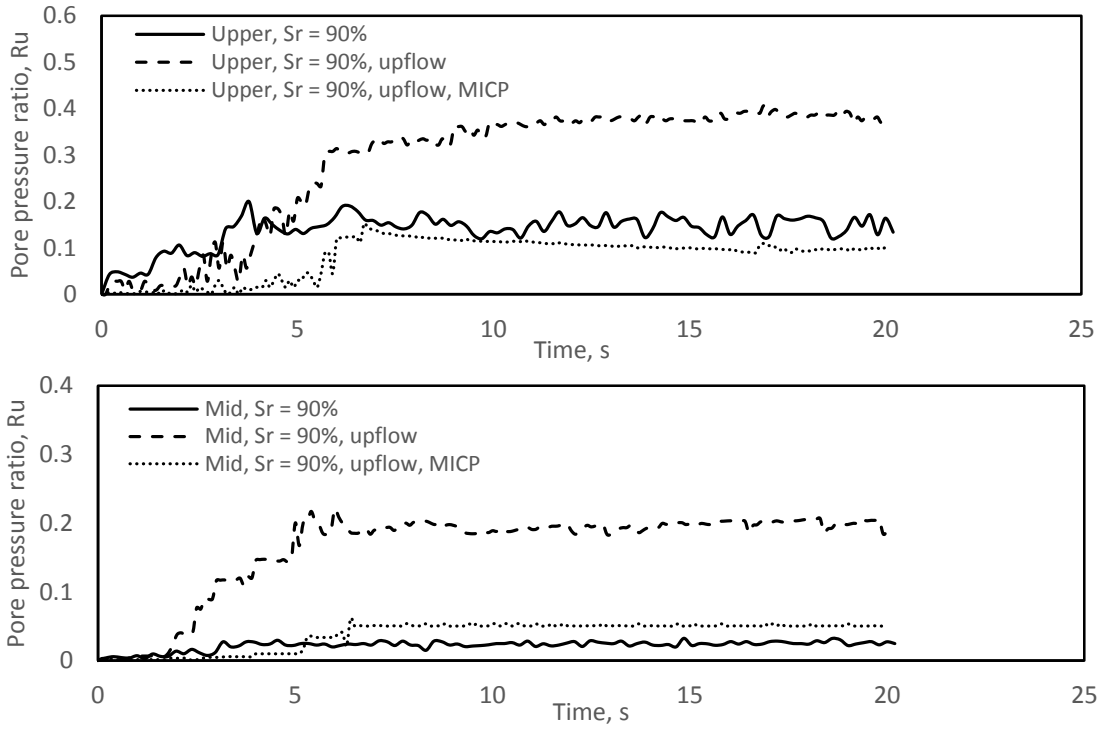


*Figure 5.23 Pore pressure ratio development in the leveled ground (a=1.5m/s$^2$)*

It can be seen from curves in Figure 5.23 that the pore pressure ratio $R_u$ shifted a lot when an upward seepage was applied. The pore pressure response to the same acceleration under seepage was more than triple of that without seepage at both mid and upper sand layers.

It seems that the biogas treated sand specimen partially lost its resistance to the cyclic loading and generated more excess pore pressure. This effect suggests that the upward stream might have carried some biogas bubbles with it and flew out of sand specimen. The stream flowed through the pore void caused redistribution of gas bubbles trapped and created areas where the degree of saturation raised again. Excess pore pressure was easily generated in those area since fully saturation was achieved. Interestingly, the MICP treated sand specimen was observed to behave distinctively even the same upward seepage existed. The pore pressure ratio was maintained in a low level which was quite similar to the pore pressure response in the condition without seepage.

The vertical strain development was presented in Figure 5.24. Originally, only 1.5 percent of vertical strain was induced as the 0.15g acceleration applied on the sand specimen. However, after upward stream flew through the specimen, nearly 3 percent vertical strain took place. If the same seepage applied to MICP treated sand specimen, such an increase in vertical strain disappeared. It seems that the MICP treated sand was not affected by the upward stream.

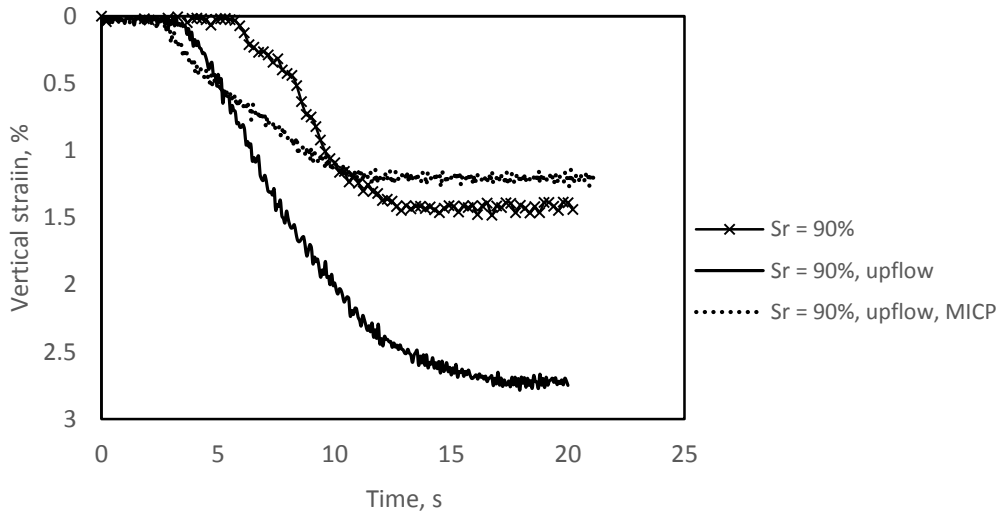


*Figure 5.24 Vertical strain development in the leveled ground ($a=1.5m/s^2$)*

For the lateral spreading perspective, the same trend was found as the pore pressure ratio and vertical strain variation. Figure 5.25 shows the pattern of lateral strain was enlarged in the upward flow condition at the same degree of saturation. There was a similarity in the amplification effect between the upper layer and mid layer of the sand specimen. The introduced MICP seemed to confine the amplification tendency and decreased lateral strain into within 0.5 percent. It is worth pointing out that comparing the vertical strain developed in fully saturated sand under the same shaking magnitude, all those difference among seepage and MICP treatment circumstances were not significant and negligible.

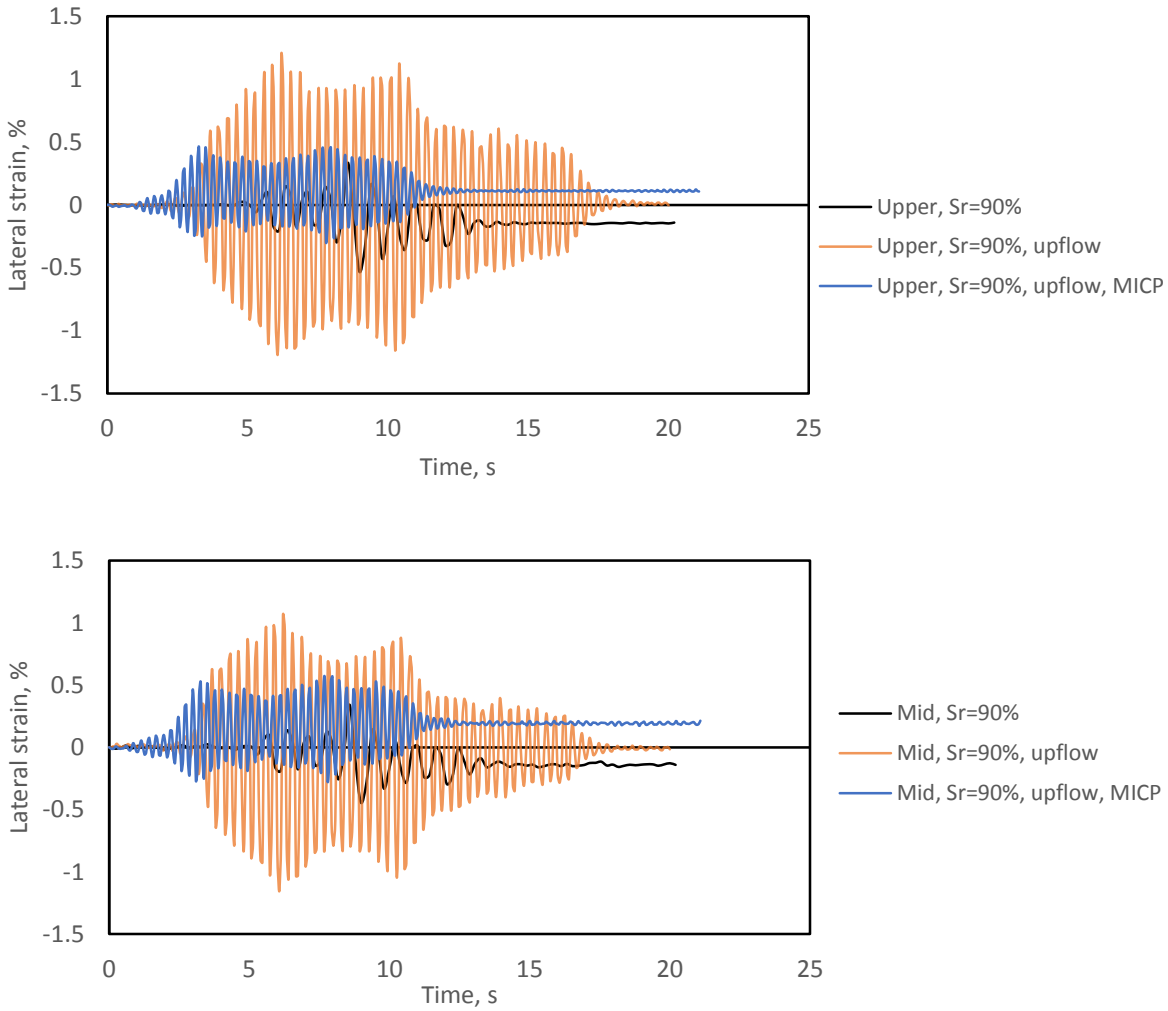


*Figure 5.25 Lateral strain development in the leveled ground ($a=1.5m/s^2$)*

### 5.4.3 The sloping ground condition

5.4.3.1 Acceleration response

The magnitude and order of cyclic loadings applied to tests conducted in the sloping ground condition were the same as those in the leveled ground condition. All acceleration responses in the sloping ground condition shared similar trends with those in the leveled ground condition. Take results obtained when induced acceleration was 1.5 $m/s^2$ as examples, Figure 5.26 describes acceleration responses in base, mid layer and upper layer of the sand specimen. The upper layer of the fully saturated sand specimen easily generated considerable magnitude of acceleration whereas the biogas desaturated sand specimen exhibited a better resistance to the shaking which produced a smaller and steadier response to the same load. Compare with results of the leveled ground condition, Figure 5.26 (a) and (b) implied that the intensity of upper layer shaking was stronger in the sloping ground condition regardless of the degree of saturation.

The acceleration amplification ratio in the sloping ground condition is demonstrated in the Figure 5.27. Obviously, when the degree of saturation decreased to 90%, the amplification affect was largely confined to a small range of 1 to 1.5. As the shaking intensity raised, the pattern of amplification ratio, particular in fully saturated sand, became more scattered. The amplification of acceleration occurred at the upper layer of the sand was responsible for higher strains and pore pressure generation during the cyclic motion. The results will be discussed further in the later part of this chapter.

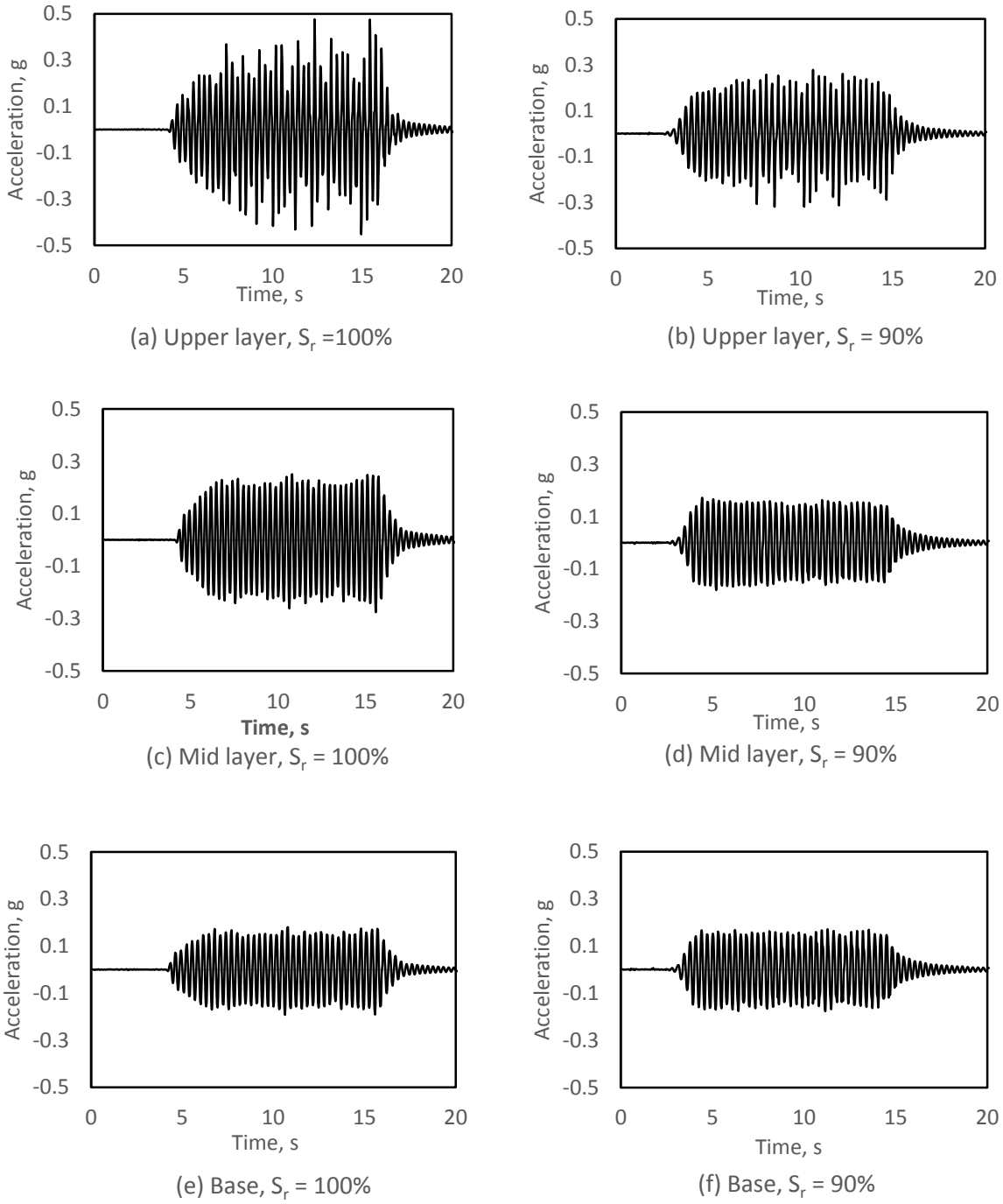


*Figure 5.26 Typical acceleration responses in sand specimens with different degrees of saturation (sloping ground)*

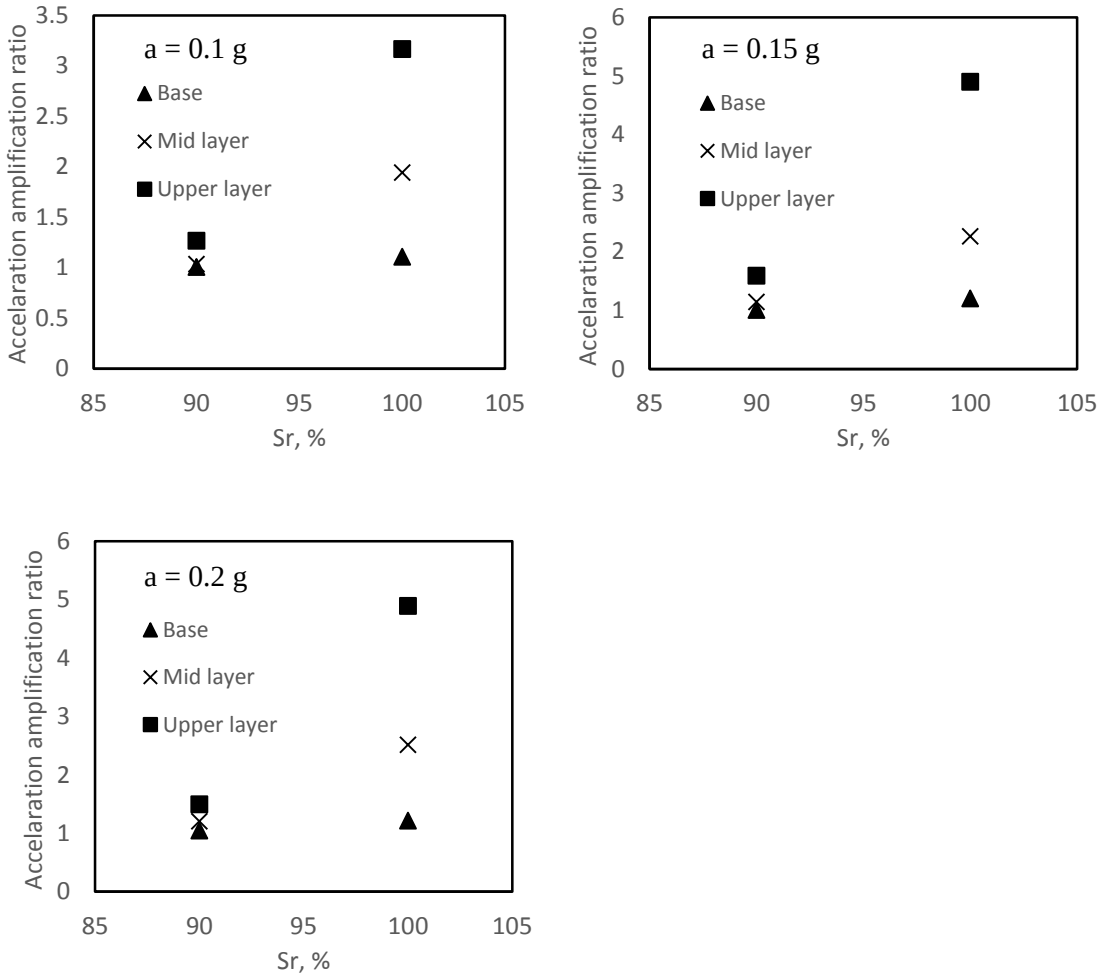


*Figure 5.27 Acceleration amplification ratio versus degrees of saturation (sloping ground)*

5.4.3.2 Pore water pressure

Four sets of shaking table test were conducted in the sloping ground condition. The pore pressure response to the cyclic loading in a sloping ground is shown in Figure 5.28. When the degree of saturation dropped from 100 percent to 90 percent, the increase in pore pressure head was declined sharply from more than 30 percent to less than 5 percent. The corresponding pore pressure ratio was illustrated in Figure 5.29. Similar patterns were found also developed in the leveled ground condition. The phenomenon strongly confirmed that a

slightly reduction of degree of saturation can considerably restrain the generation of excess pore water pressure caused by cyclic loading even in a sloping ground. The nitrogen gas produced through the denitrification process was able to stay in the sand and take effect when a shaking force was applied.

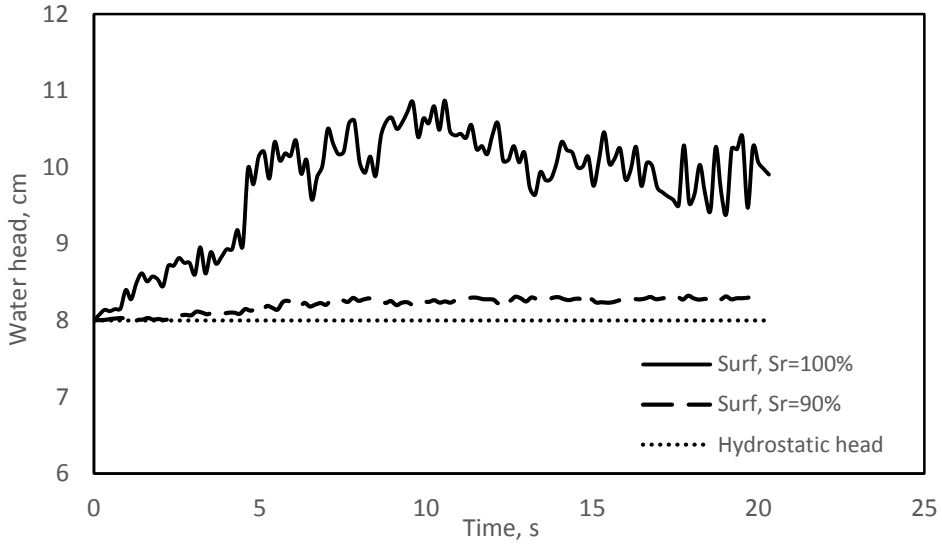


*(a) Surface position*

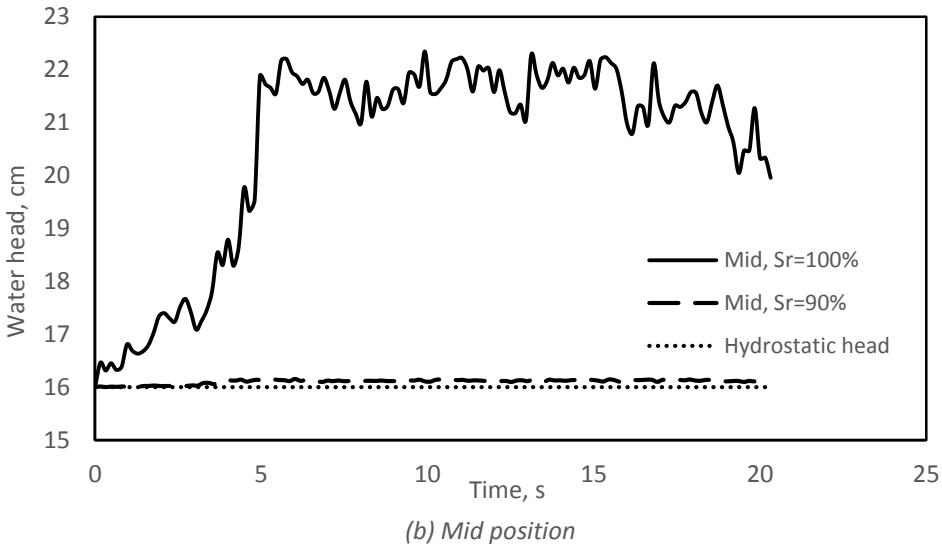


*(b) Mid position*

*Figure 5.28 Pore pressure response to cyclic load in the sloping ground ($a=1.5m/s^2$)*

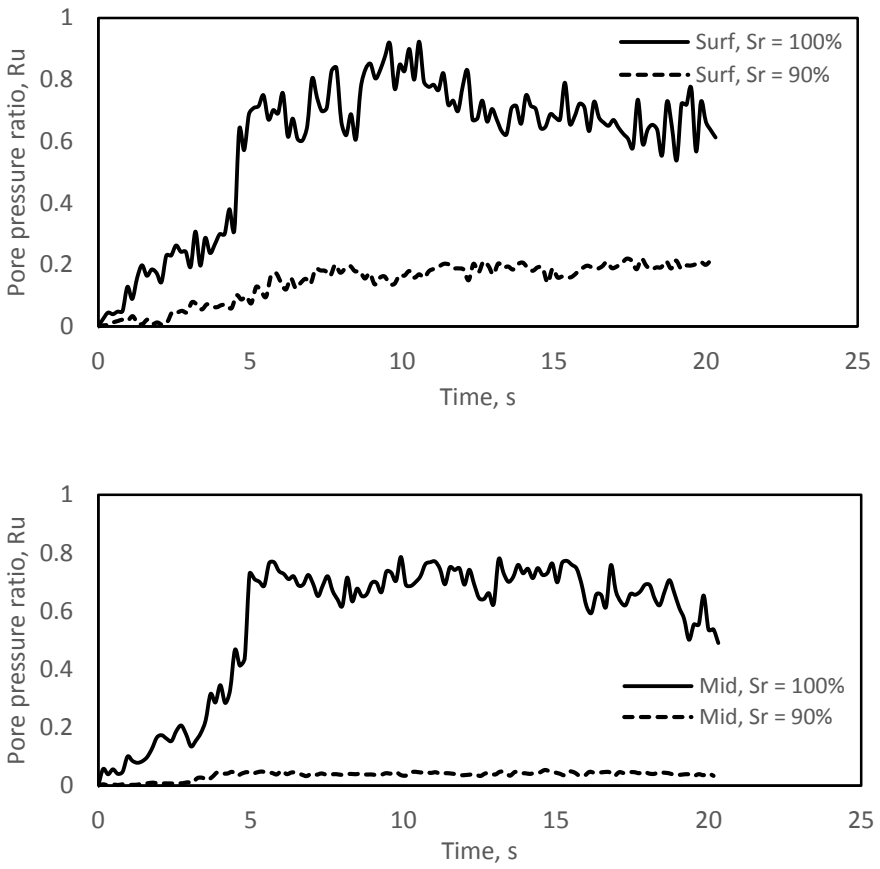


*Figure 5.29 Pore pressure ratio development in the sloping ground (a = 1.5m/s$^2$)*

5.4.3.3 Settlement or vertical strain

The settlement data recorded in the test TS1 and TS2 were converted into vertical strain and plotted against time in Figure 5.30. The difference of vertical strain developed in fully and biogas desaturated sand was significant again. Only a tenth of settlement was found in TS2 compare to that occurred in TS1 when the shaking was mild. Although a more intense shaking led to distinct settlement in desaturated sand, the value was still remarkably low against ones in the fully saturated sand. When a high acceleration of 2 m/s$^2$ was imposed, an immediate vertical strain developed and kept on increasing before reaching a steady stage at both TS1 and TS2 which was not the case in corresponding leveled ground condition test

TL2 and TL3. This phenomenon reveals that the sloping condition was much easier to cause large settlement or vertical strain when a drastic shaking was applied.

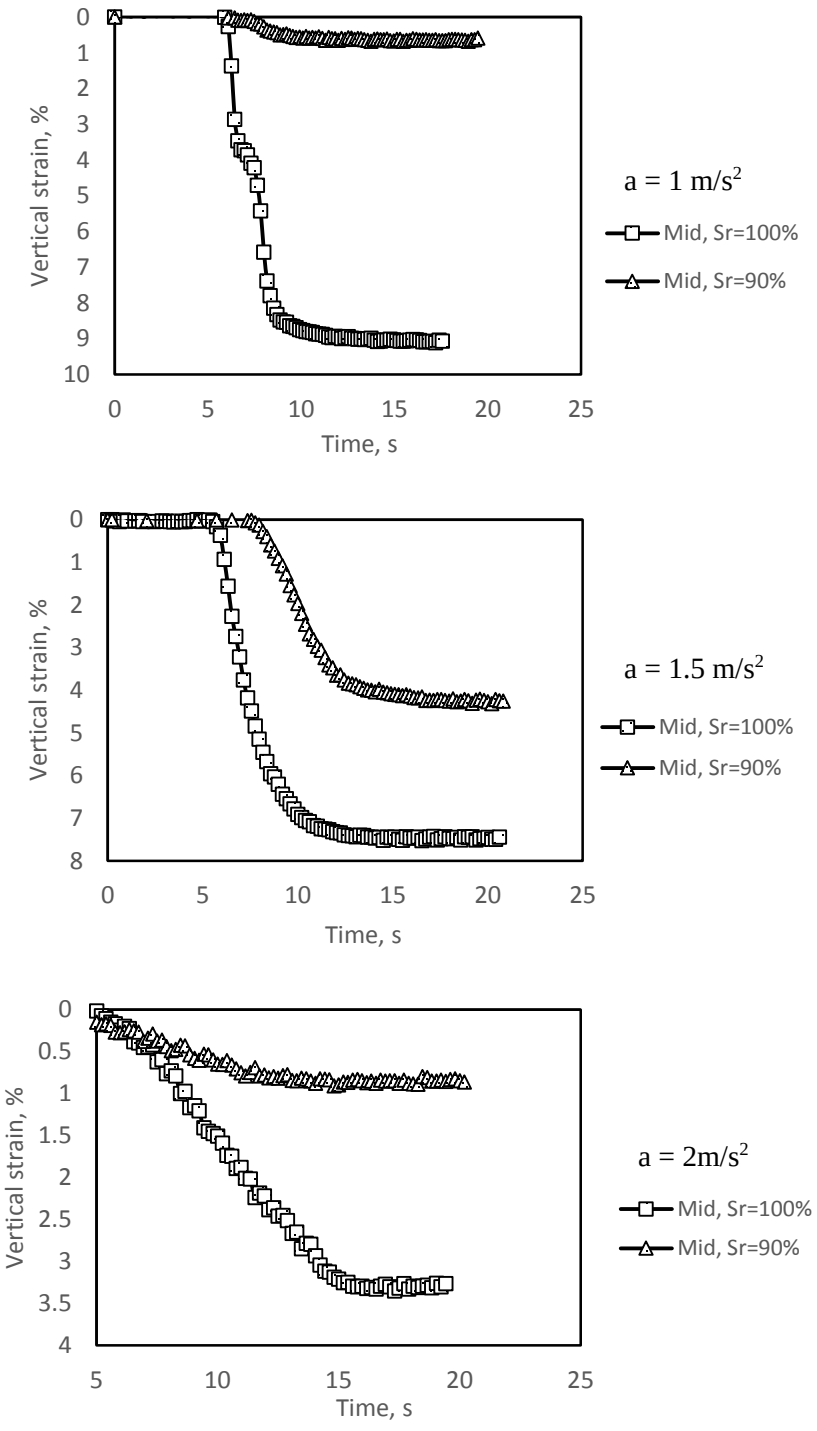


*Figure 5.30 Volumetric strain development in the sloping ground*

5.4.3.4 Lateral spreading or lateral strain

The lateral displacements occurred in shaking tests under the sloping ground condition were also normalized to lateral strains and plotted against time in Figure 5.31. Overall, these results show that the patterns of lateral spreading respond to applied shaking in both saturated and biogas desaturated ($S_r$ = 90%) were similar. Except that the reaction from biogas desaturated sand was much smaller than its counterpart in fully saturated sand. Interestingly, the lateral strain developed in the sloping ground condition was not bounced back to zero after shaking which the laminar box did in the leveled ground condition. In other words, the shaking caused some lateral deformation that remained as unrecovered when it struck on a sloping ground. This phenomenon was also observed by other researchers in several shaking table tests (Youd *et al*. 2001; Wartman *et al*. 2005; Dobry *et al*. 2011). Some of them described it as 'permanent deformation' (Dobry *et al*. 2011). Figure 5.31 (a) (b) (c) and (d) show a dramatic change in lateral response behavior between the non-destructive shaking event and the strong shaking event. The permanent deformation at both upper and mid layer of sand specimen was negligible. Only close to 0.5 percent of lateral strain when a low magnitude of shaking (a = 1m/s$^2$) was applied. However, as the input acceleration increased to 1.5 m/s$^2$ in the successive shaking, a much more lateral strain up to 3 percent had occurred. Apparently, liquefaction had been triggered in fully saturated sand under this magnitude of shaking and it was also confirmed by the measured pore pressure ratio and vertical strain data. The large lateral strain seems to be ascribed to a slope slide since the sand deposit liquefied. The permanent displacement developed in the strongest shaking (a = 2 m/s$^2$) was not as big as the previous test because the slope had already slid and the tilt effect was hugely released or the sand specimen was no longer in a sloping ground condition.

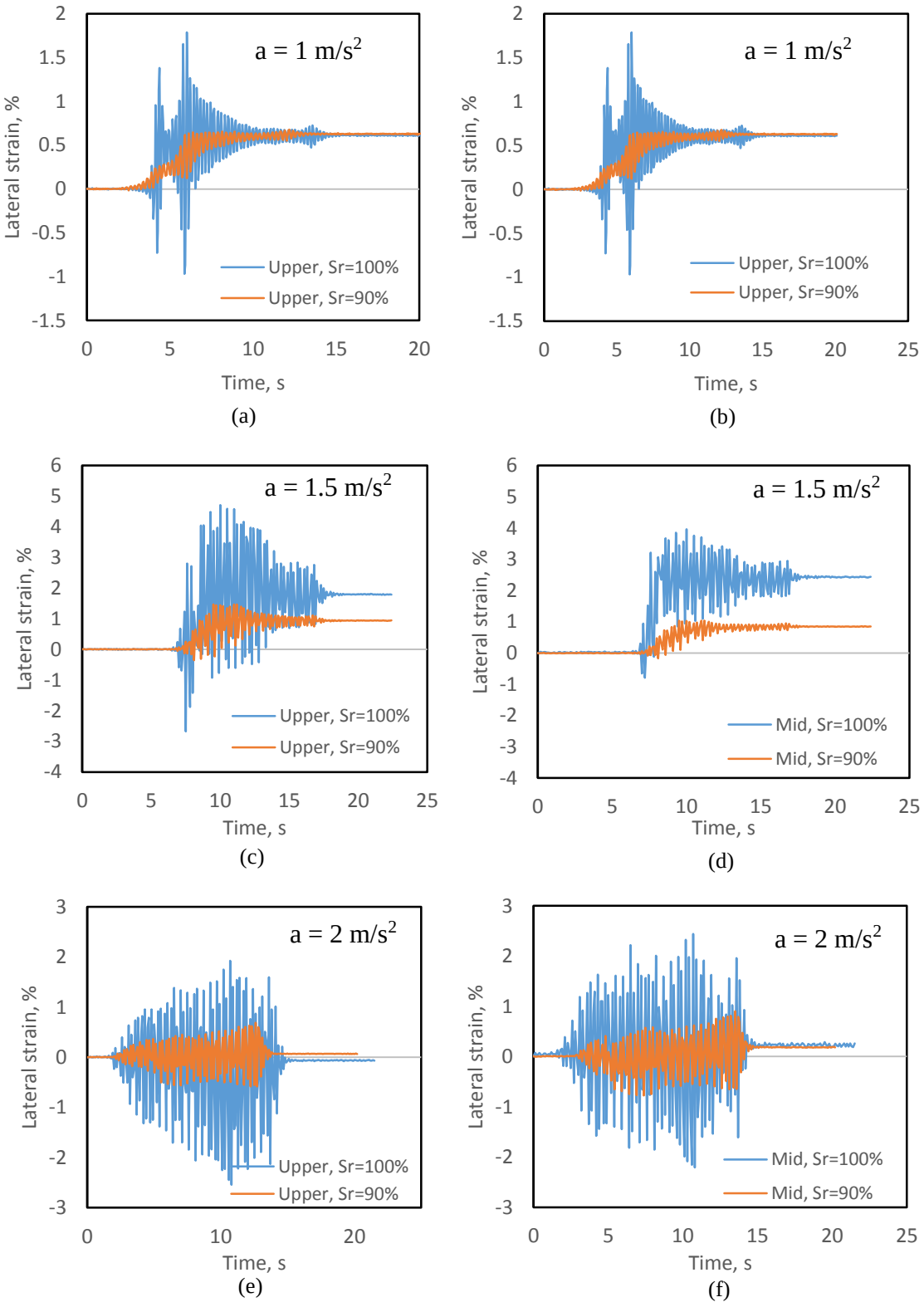


*Figure 5.31 Lateral strain development in the sloping ground*

Figure 5.32 demonstrates the maximum lateral spreading measured in shaking events under the slope ground condition. It can be seen that the lateral spreading in the upper layer was obviously bigger than the mid layer in all shaking events. As shown in Figure 5.32 (a) and (b), the data suggests that the sand specimen was more likely to move forward than backward which was reasonable since the shaking direction was consistent with the slop heading direction. In that case, the upper sand layer was easily pushed ahead when the shaking stroke and contributed more displacement in the lateral direction. However, in Figure 5.32 (c) the forward displacement seemed to be confined and the backward one became dominate. As explained before this might due to the slid occurred in last shaking event erased the tilting angle and the sloping ground effect no longer existed. The permanent deformation developed in such a circumstance was not prominent as that in previous shaking events.

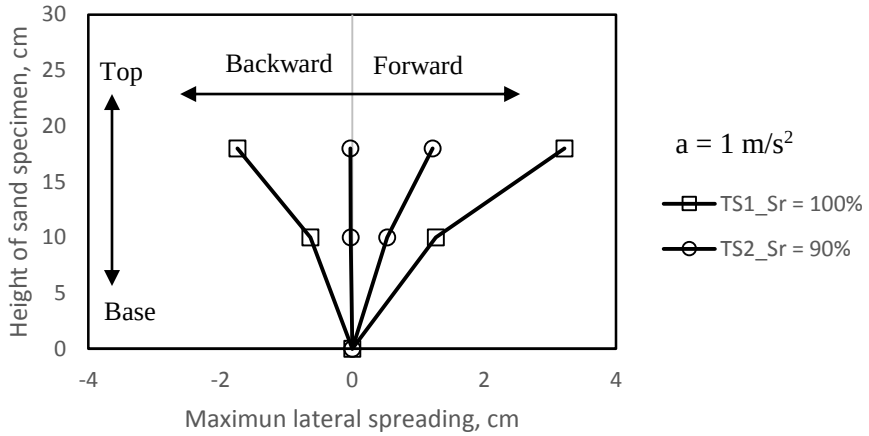


(a)

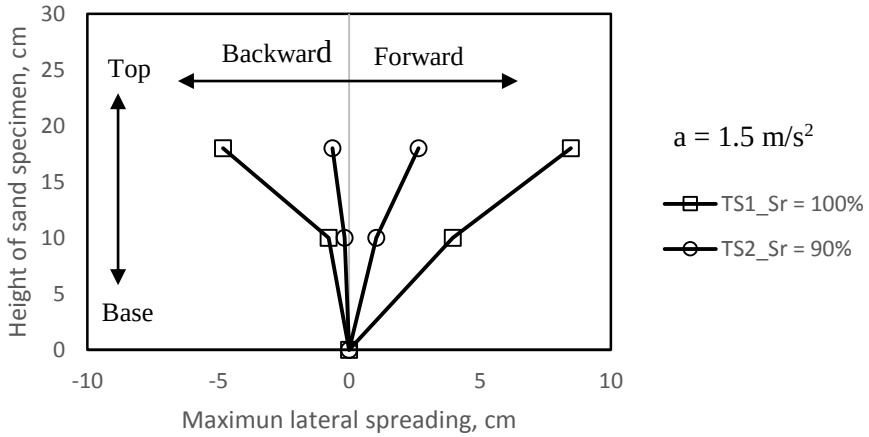


(b)

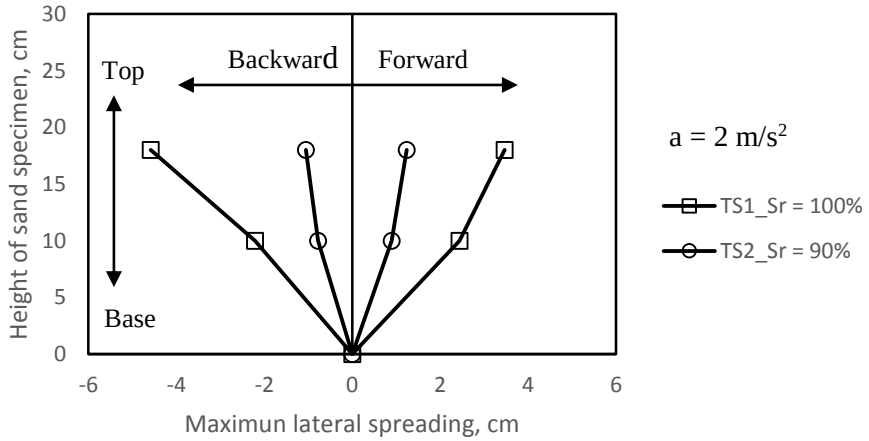


(c)

*Figure 5.32 Maximum lateral spreading measurement (sloping ground)*

5.4.3.5 Upward seepage and MICP effect

Figure 5.33 illustrates pore pressure ratio change at the upper and mid layer of the sand specimen under a shaking acceleration of 1.5 m/s$^2$. The measured pore pressure change at different test conditions shared a similar trend. As anticipated, the one with the upward seepage produced the largest $R_u$ value – 0.34 and 0.33 in the upper and mid layer of sand slope, respectively. After the bioclogging process, the sand specimen underwent upward seepage responded to the same shaking with a much less excess pore pressure. For a comparison for the upper layer, the pore pressure ratio is the smallest for the test treated with the combined biodesaturation and bioclogging method as shown in Figure 5.33. At the mid layer of the sand slope, the pore pressure ratio for the sand treated by the combined method is still among the lowest. Thus, the combined method seems to be more effective as far as the resistance to liquefaction is concerned.

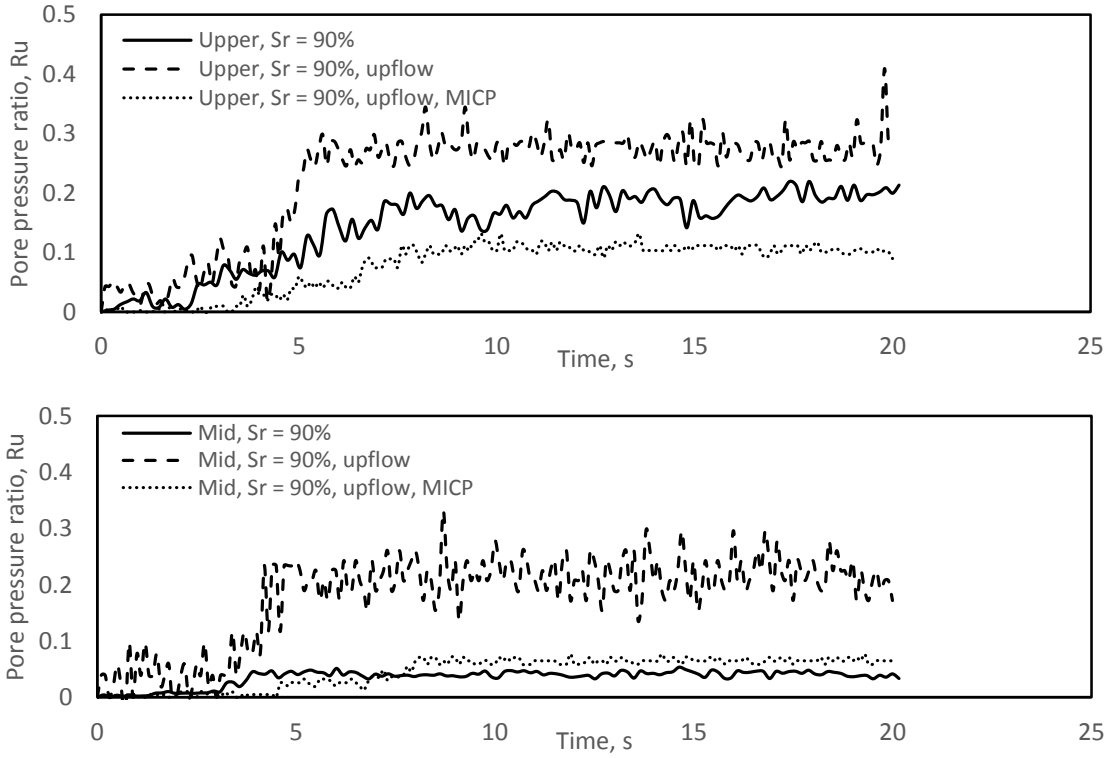


*Figure 5.33 Pore pressure ratio development in sand with seepage and bioclogging*

The vertical strain versus time curves for three tests (TS2, TS3 and TS4) are shown in Figure 5.34. Comparing the settlement data between the tests with and without an upward seepage, about 1 percent extra vertical strain was observed in the test with the upward seepage. The most striking observation from Figure 5.34 is that the vertical strain developed in the test treated by the combined method is much less than other tests. However, this is not the case for the leveled ground condition as shown in Figure 5.20. It is speculated that as the shaking causes the top sand to slide towards the tip of the slope and created a large sand displacement at both the lateral and vertical directions. However, the bioclogging provides a bond among sand grains and limited the lateral movement so that the sliding tendency was largely reduced especially in the upper layer of the sand slope. As a result, less vertical strain was developed as the slope was more stable after the bioclogging treatment.

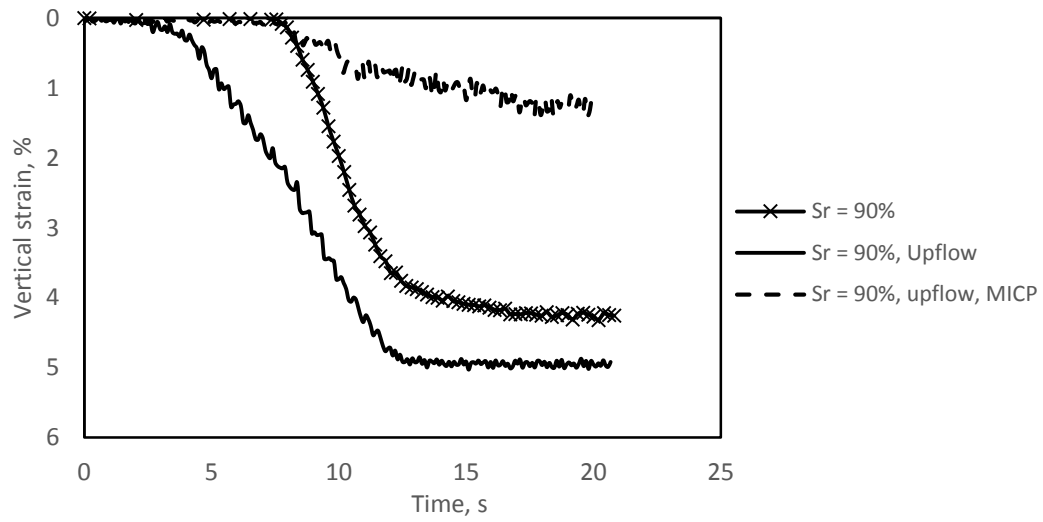


*Figure 5.34 Vertical strain development in sand with seepage and bioclogging*

The lateral strain variation in tests with different seepage and bioclogging conditions are shown in Figure 5.35. Unsurprisingly, a larger lateral strain occurred in the test without bioclogging treatment (Test TS3). In addition to the bigger permanent deformation, the

lateral strain was also larger compared with other tests as the amplitude of curves shown in Figure 5.35. For the test using the combined method, although it underwent the same upward seepage flow, the lateral strain was still insignificant compared with the test without upward seepage. Especially on the upper layer of the sand, only one-fifth of permanent deformation was observed in MICP treated desaturated sand comparing with clean desaturated sand. These observations seem to suggest that the bioclogging effect also helps to increase the liquefaction resistance and reduce deformation due to the bonding effect MICP provided.

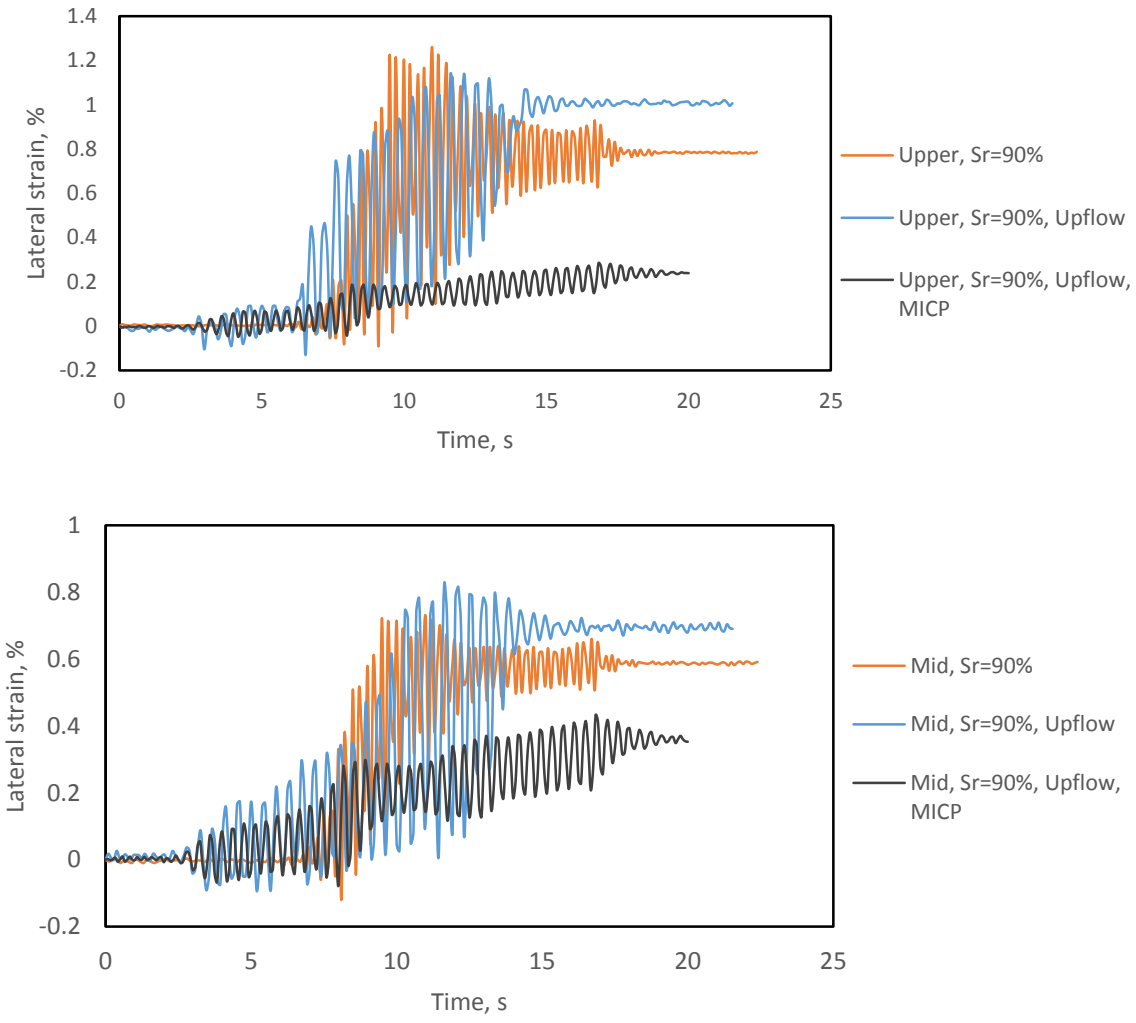


*Figure 5.35 Lateral strain development in sand with seepage and bioclogging*

## 5.5 Comparison and Discussion

The relationship between the volumetric strain and the pore pressure ratio is also established in Figure 5.36 using the model testing data. It can be seen that the volumetric strains gradually increased with the pore water pressure development. Most of volumetric strains are within 2 percent if the pore pressure ratio is kept below 0.2. When the pore pressure ratio is close to or bigger than 0.5, significant volumetric strain has developed. This phenomenon is consistent with previous studies (Lee and Albaisa 1974; Tokimatsu and Seed 1987; Okamura and Teraoka 2006).

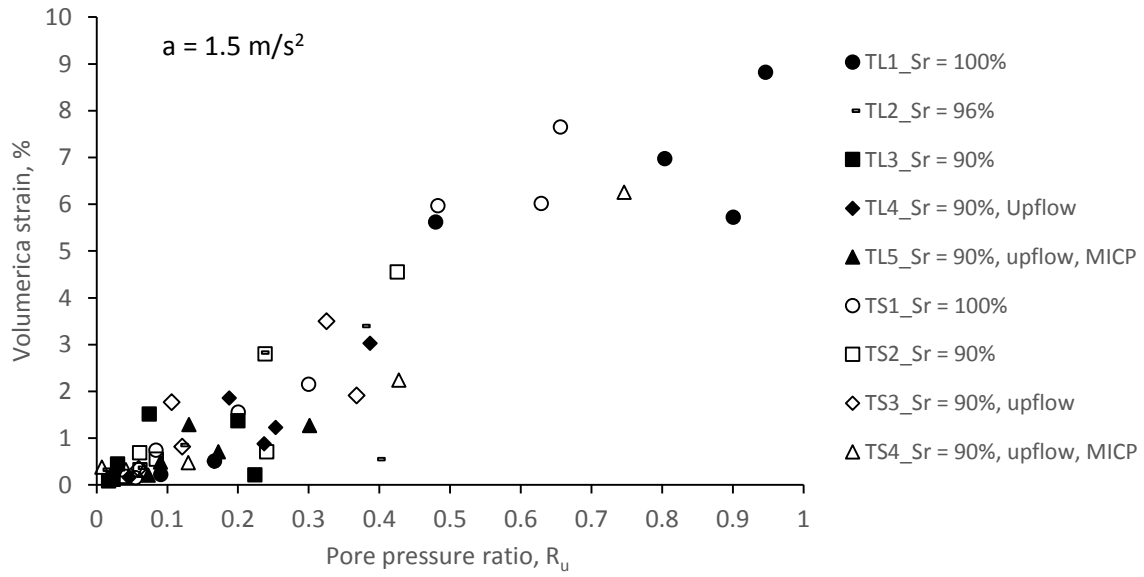


*Figure 5.36 Volumetric strain versus pore pressure ratio*

The volumetric strain versus relative density curves are plotted in Figure 5.37 for all tests. The data obtained from tests using a sloping ground are shown in open data points. It can be seen that larger volumetric strain is developed in sloping ground than in leveled ground. This is the case for both fully saturated and biogas desaturated sand at different relative densities states.

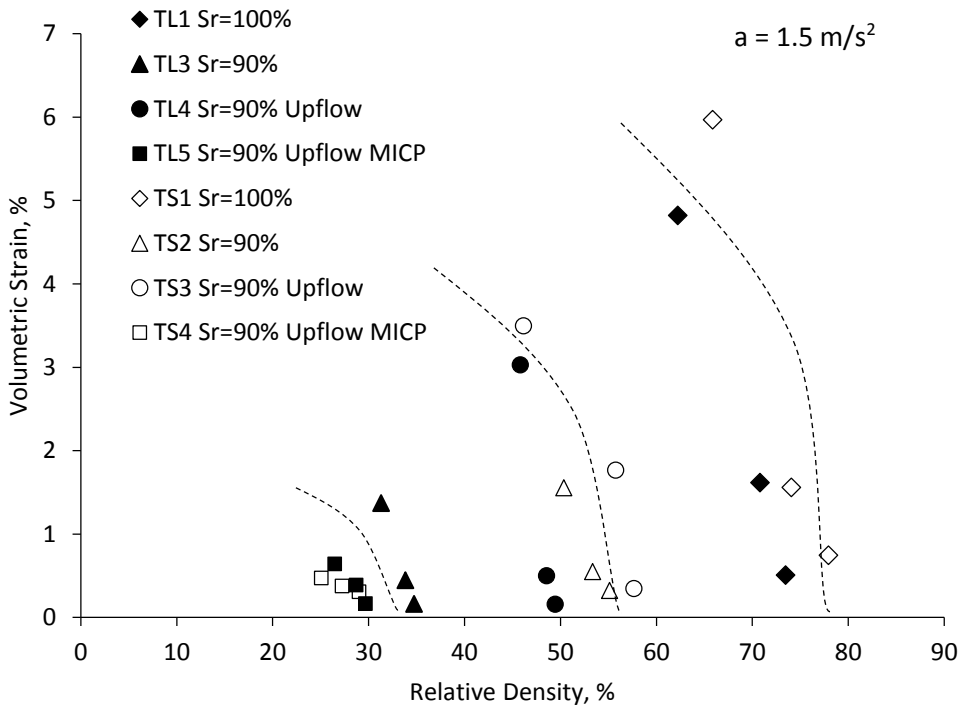


*Figure 5.37 Volumetric strain against relative density*

The pore pressure ratio against relative density of sand is plotted in Figure 5.38. The solid data points represent the tests conducted on a leveled ground. The open data points indicate the tests performed on a sloping ground. Envelope curves can be drawn based on different ranges of relative density. Usually a high pore pressure is generated when the relative density is small. It can be seen from Figure 5.38 that there is a trend that high pore pressure ratio is more readily achieved in the fully saturated sand, irrespective of whether the ground is leveled or inclined. The data located at the outer dashed curve presents the behavior of the fully saturated sample. During the first shaking, pore pressure ratio exceeds 0.5 when the relative density is slightly less than 40 percent. As the soil is densified to a relative high density, for example, more than 70 percent, the pore pressure ratio is reduced to 0.1. For biogas desaturated sand at a low relative density within the 20 to 40 percent, the pore

pressure ratio is less than 0.1 or 0.2 at the middle and upper depths. Therefore, a reduction of the degree of saturation through biogas desaturation is effective to increase the liquefaction resistance of the sand.

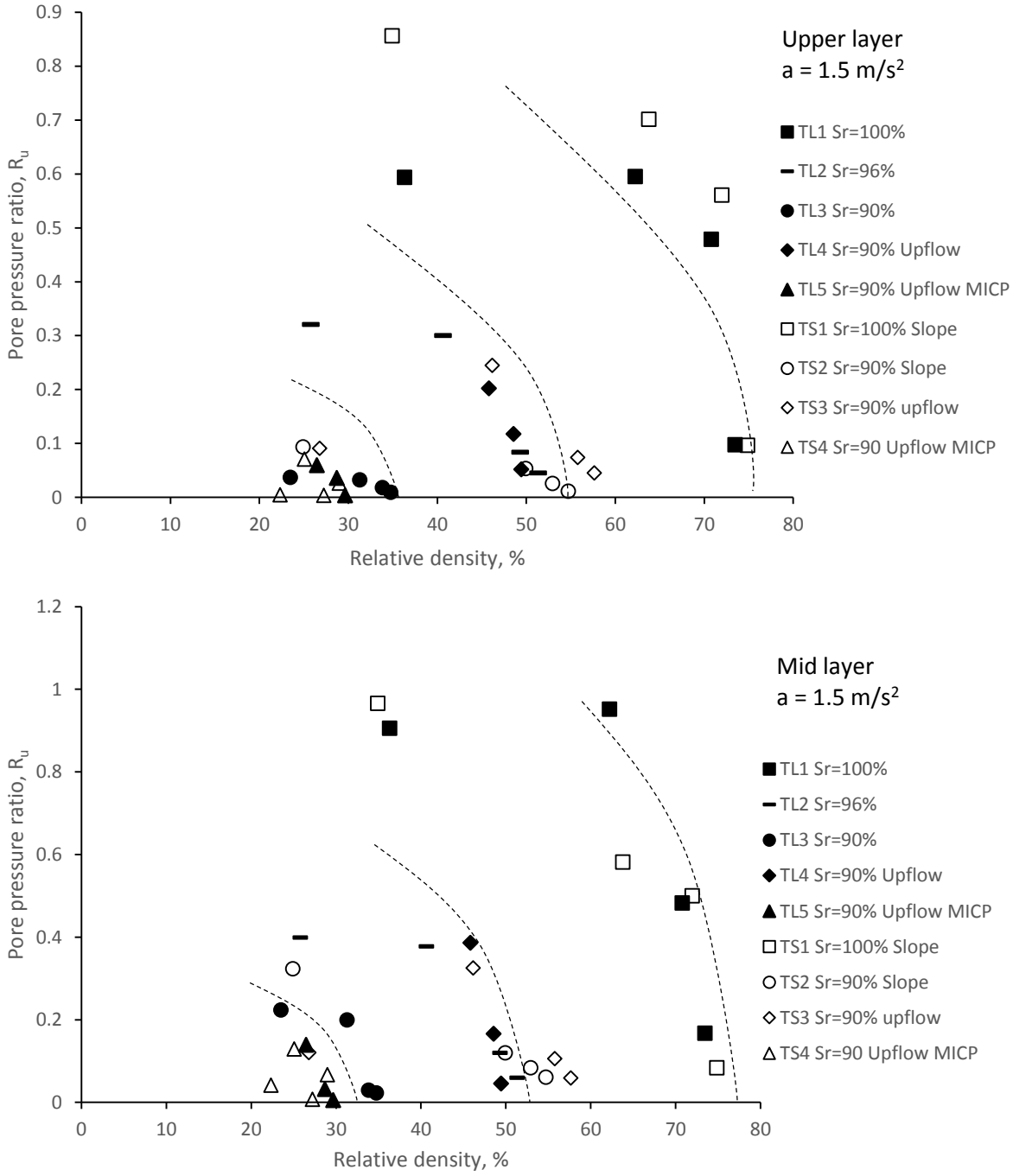


*Figure 5.38 Pore pressure ratio against relative density*

The above observations are consistent with other studies (Ghayoomi 2011; He *et al*. 2013) and they support further the conclusions that the excess pore pressure generation in biogas desaturated sand specimen is much lower than that in the fully saturated sand and the volume change due to pore pressure dissipation in biogas desaturated sand is also lower than that in the saturated sand.

Although it is not always the case, the pore pressure ratio is commonly lower in the sand in the mid layer than that produced in the shallow position. This may be explained by the higher effective stress level at the mid layer. In the model tests, the liquefaction was initially triggered at the surface and then progressed down. Similar observations were also made in other studies (He *et al*. 2011; Montoya 2012).

## 5.6 Conclusions

The model testing results presented in this chapter provides to study the seismic responses of biogas desaturated sand. Nine shaking table tests were conducted under different test conditions. An instrumented laminar box was used to contain silica sand specimens with initial degree of saturation of 100, 96 and 90 percent. A series of cyclic loading were applied to simulate earthquake circumstances. Upward seepage was also applied to sand specimens treated using biogas desaturation and the combined biodesaturation and bioclogging methods to investigate the stability of gas bubbles in sand under the flow condition. The following conclusions can be draw from the study:

1) The enrichment culture cultivated from soils is able to generate nitrogen gas bubbles in loosely packed sand specimens and reduce the degree of saturation.

2) The shaking table results show that liquefaction occurred for saturated sand specimens at loose state under a = 0.5 m/s$^2$ shaking magnitude and at medium dense states under a = 1.5 m/s$^2$ shaking magnitude. Liquefaction does not occur under the same condition for biogas desaturated sand samples with a degree of saturation of 90 to 95 percent. The pore pressure ratio developed in biogas desaturated sand ($S_r$ = 90%) is only a tenth of that in fully saturated sand.

3) The volumetric strain increases with the increase in pore pressure ratio at a given acceleration. When the pore pressure ratio is smaller than 0.2, the volumetric strain development is less than 1 percent. The key to mitigation of liquefaction is to limit the generation of excess pore pressure. Compared with the lateral strain observed in both the fully saturated and the biogas desaturated sand, it is obviously that the biogas desaturation method can also reduce the development of lateral spreading.

4) Liquefaction is more prone to occur in sloping ground than in leveled ground. For sand with a 90 percent degree of saturation, the pore pressure ratio in the sloping ground is almost doubled as compared with the one in the leveled ground at the same position. Nevertheless, the pore pressure ratio is still far less than that generated in the fully saturated sand. For sloping ground, a permanent displacement is developed after shaking. The amount of the permanent displacement developed in biogas desaturated sand ($S_r$ = 90%) is only a quarter to half of that in fully saturated sand.

5) Upward seepage affects the stability of the biogas bubbles in sand. For two otherwise identical tests, the pore pressure ratio and volumetric strain become more than twice as big in the test subjected to an upward seepage. The combined biogas and bioclogging method can reduce the migration of gas bubbles and thus lower the increase

effect of the sand degree of saturation caused by seepage flow. The testing data also suggest that the bioclogging process also builds the bonding in sand grains and thus helps in reducing the ground settlement as well as the lateral displacement.

# CHAPTER 6

# UNDRAINED SHEAR BEHAVIOR OF BIOGAS DESATURATED SAND

## 6.1 Introduction

Monotonic triaxial compression tests were used in this study to assess liquefaction potential. The aim of the study is to assess the effect of biogas desaturation on the liquefaction potential of sand. In this chapter, fully saturated sand specimens with various relative densities were first desaturated by biogas ($N_2$) generated via the denitrification process and then used for isotropic or $K_0$ consolidated compression tests under the undrained condition.

## 6.2 Material and Equipment

### 6.2.1 Test material

All laboratory triaxial test specimens were prepared using the same silica sand which meets ASTM C778 standard. The sand has a specific gravity of 2.65 and a mean grain size ($D_{50}$) of 0.36 mm. The maximum and minimum void ratio are 0.87 and 0.52, respectively. Details about sand information can be found in Section 4.2.1.

### 6.2.2 Automated triaxial testing system

The major test equipment used in this study is the GeoTAC TruePath$^{TM}$ Automated Stress Path System (Figure 6.1), which consists of an axial load frame, cell and pore

pressure/volume controller (pump), a triaxial cell, measurement instrumentation (external load cell, axial LVDT, pore pressure sensor), data acquisition, control module (TestNet) and control software package. This automated load triaxial system is designed and fabricated by Trautwein Soil Testing Equipment Company in Houston, Texas. The whole system setting up is provided in Figure 6.2.

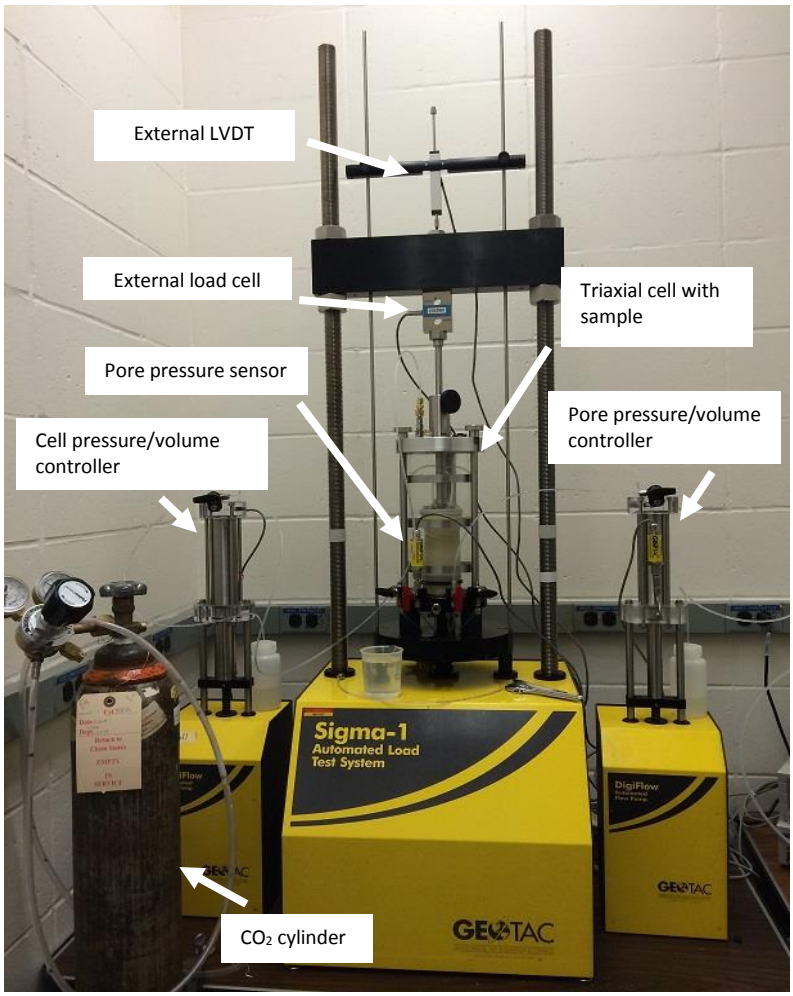


*Figure 6.1 GeoTAC True Path triaxial testing system*

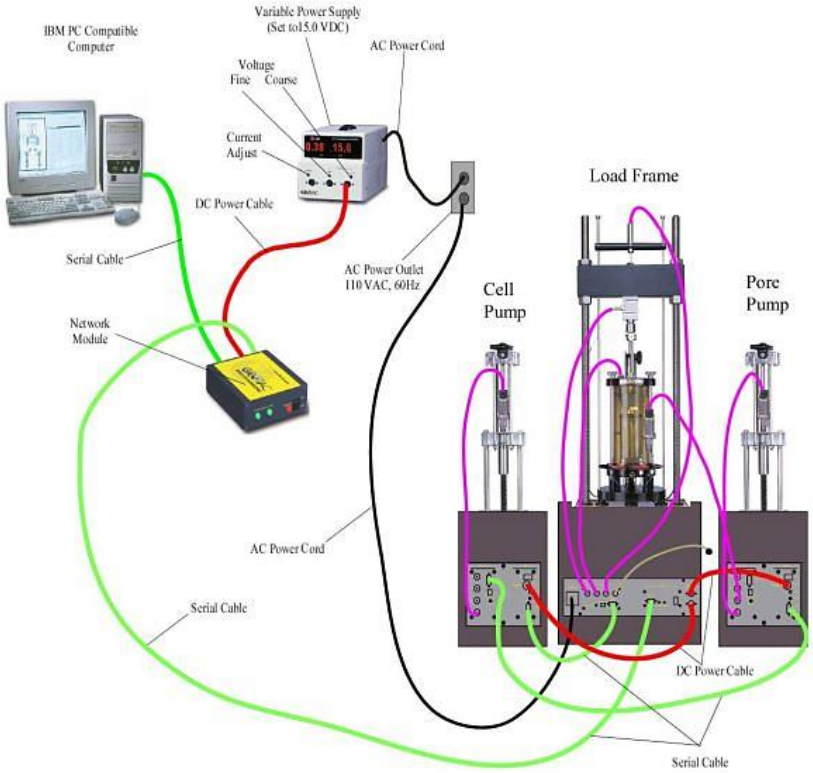


*Figure 6.2 TruePath Automated Stress Path System set up (GeoTAC, 2004)*

## 6.3 Testing Methodologies

### 6.3.1 Specimen preparation

In order to obtain homogeneous samples with a uniform distribution of void ratio, it is essential to employ an appropriate specimen preparation method. Different methods of sample reconstitution have been known to create different fabrics and would result in different response to load. As shown in Figure 6.3, Ishihara (1993) summarized three most common sand sample preparation methods for conventional triaxial tests.

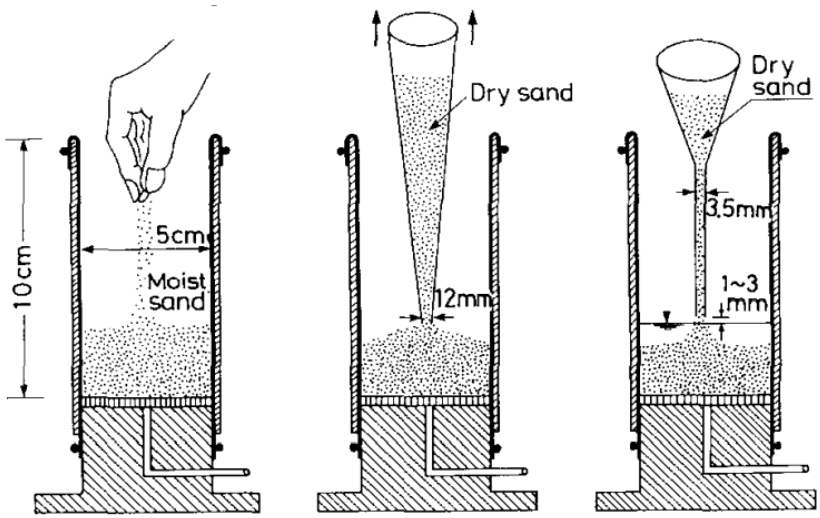


*Figure 6.3 Methods of sample preparation (adopted from Ishihara 1993)*

*Moist tamping method:* Pre-weighed, oven-dried portions of sand are mixed with de-aired water at a water content of 5%. Place them into a mold in several (usually five to six) layers and tamp each layer with a small flat-bottom tamper. The tamping energy imposed on each layer determines the establishment of loose or dense sample. If the tamping energy is small, the sample is usually thought to have a loose structure. In such a condition, the capillary force between sand particles would result in a very loose structure well in excess of the maximum void ratio of the dry sand. If a dense sample is required, a larger amount of tamping energy will be applied. One of the advantage to use the moist tamping method is that it is able to produce a sample within a wide range of void ratio.

*Air Pluviation method:* Oven-dry sand is spread into a mold by using a funnel with zero height of fall. The filling rate is kept constant until the mold fulfilled with the dry sand. Tapping energy is applied to sample by hitting the wall of the mold. The sample prepared

from this method is usually denser than that produced from the moist tamping method and shows a slightly different behavior in the subsequent loading.

*Water sedimentation method:* In this technique, sand is mixed with de-aired water and poured through a funnel in several layers. The sand is deposited continuously under water without causing appreciable segregation. If a denser sample is to be prepared, compacting energy is applied by hitting the wall of the mold stepwise during the process of sample placement.

Liquefaction mainly occurs in loose to medium dense sand. Thus, the moist tamping method was adopted to prepare loose sand specimens by following the following procedure. A 365 grams of sand was mixed with 18 grams of de-aired water (5 percent of moisture content). Then the sand sample was divided into five equivalent portions and placed into a split mold in five layers. The split mold had a dimension of 50 mm of inner diameter and 120 mm of height which can be seen from Figure 6.4. For each layer, tamping was gently applied with a small flat-bottomed tamper. The amount of tamping energy for each layer was carefully controlled. After the sample is enclosed by the membrane with the top cap, a 10 kPa vacuum pressure was applied via a vacuum pump. The mold was then disassembled and the dimensions of the specimen were taken and the initial void ratio ($e_o$) was calculated. The triaxial cell was then assembled and filled with distilled water. A cell pressure of 20 kPa was applied to contain the sample. Figure 6.5 shows an image of a sand specimen prepared by the moist tamping method.


*Figure 6.4 Sand sample preparation tool kit*

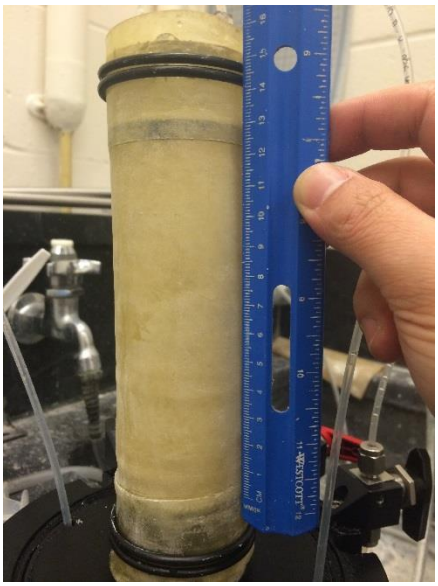

*Figure 6.5 A sand specimen prepared by moisture tamping method*

### 6.3.2 Saturated and biogas desaturated sand samples

Once the sample was assembled, carbon dioxide ($CO_2$) was used to percolate the specimen from the bottom to the top in a period of 15 to 20 minutes. The top drainage line

was immersed in a beaker of distilled water to monitor the bubbling of gas. The pressure of $CO_2$ was adjusted to a relatively low value to avoid disturbing sand fabric.

After percolating $CO_2$ gas through the specimen, de-aired water was then introduced into sand for saturation if a fully saturated sand sample was required. For biogas desaturated sand samples, denitrification solution included enrichment denitrifying bacteria and nutrient was used. The gravity driven fluid (de-aired water or denitrification solution) slowly flew into the sand sample through the bottom drainage port from a container sat on top of the load frame. The whole flush process lasted 60 minutes with a hydraulic head of about 0.5m. This upward flow was expected to replace and dissolve a part of $CO_2$ gas in the sample. The amount of fluid allowed to pass through the sample was roughly estimated to be 2 to 3 times the volume of voids.

In order to obtain desaturated sample with a known degree of saturation, the denitrification solution component was carefully determined. In a unit volume of denitrification solution, twenty percent was enriched denitrifying bacteria suspension and the rest 80 percent was nutrient solution. The nutrient recipe was same as mentioned in Chapter 3. Only the nitrate and carbon source content was adjusted according to the desired degree of saturation. The monitoring of gas generation process was accomplished by using a graduated tube connected with the top drainage port of the triaxial cell. The tube was prefilled with a small amount of distilled water and all tubing connected with the sand sample were de-aired. As the denitrification process took place, the water level in the tube increased because the nitrogen gas was extremely difficult to dissolve in water in a low ambient pressure circumstance. The increase amount of water in the graduated tube could thus be seen as the

amount of nitrogen gas generated in sand sample. Figure 6.6 shows an image of monitoring of denitrification process prior to the compression test.

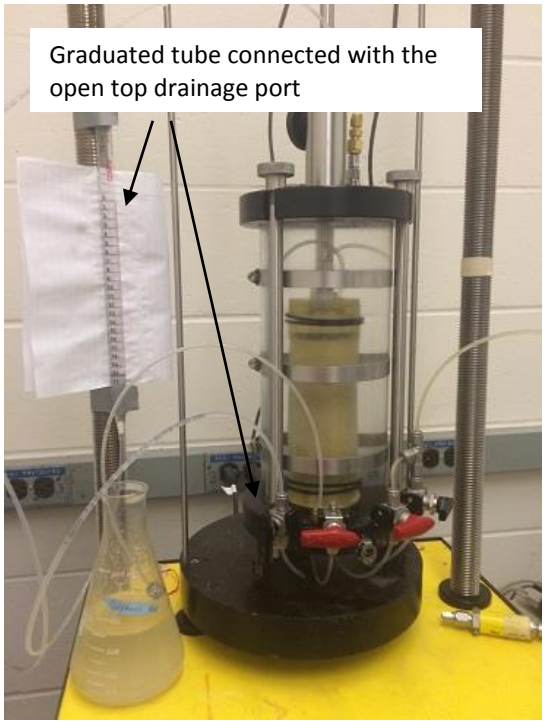


*Figure 6.6 Monitoring of denitrification process in a triaxial test*

Because the back pressure used in saturation stage was only 100 kPa. All nitrogen gas bubbles were assumed stay steady and cannot dissolved in water under such a low pressure. Thus the degree of saturation of biogas desaturated sample could be estimated through the following equation.

$$S_r = \frac{\Delta V}{V_v} = \frac{G_s \Delta V}{G_s V - M_s} \tag{6.1}$$

where $\Delta V$ is the water volume change in the graduated tube, $G_s$ is the specific gravity of sand and $M_s$ is the dry mass of sand.

### 6.3.3 Calculation of void ratio

Depending on the void ratio at the time of sample preparation, the sample in a triaxial test can be very loose and highly contractive or be dense and dilative when the shear load was applied. There are two primary methods to evaluate the void ratio of a specimen.

6.3.3.1 Void ratio based on initial sample dimension

Directly calculate void ratio based on sample's diameter and height is a simple way to obtain void ratio. Careful measurement was required to minimize the discrepancy, for example, taking multiple circumference instead of diameter may help improve the accuracy. The change of height during the percolation of $CO_2$ and de-aired water through the specimen should also be considered. Based on the volume change during setup and saturation, and subsequent changes in volume during consolidation, the void ratio at the beginning of shear can be determined.

6.3.3.2 Void ratio based on post-test moisture content

The second method of evaluating void ratio was reckoned from the moisture content of the post-shearing specimen. In this method, the specimen is carefully disassembled after shearing and all sands along with water inside is collected for moisture content test. The void ratio at the end of the test, $e_f$ can be calculated from the following formula

$$e_f = \frac{M_w}{M_s} G_s \tag{6.2}$$

where $e_f$ is the specimen void ratio at the end of test, $M_w$ is the mass of pore fluid in the tested specimen, $M_s$ is the dry mass of the sand and $G_s$ the specific gravity of sand. In a saturated undrained test, the void ratio does not change during the shearing stage. So the void ratio after the consolidation equals to the final void ratio after shearing. For biogas desaturated

sand case, the determination of void ratio was more complex. Because of the undrained condition, the volume of water retained in sand sample after shearing is still the same as pre-shearing. However, the void ratio of the specimen changed during the test due to the varied degree of saturation. The void ratio at the beginning of shear was calculated from the final volume of water retained in the specimen, the final dry mass of the specimen, and the initial degree of saturation.

### 6.3.4 Triaxial testing procedure

6.3.4.1 Back pressure saturation

A high back pressure is normally used for the saturation of triaxial samples. In this study, this approach is not suitable as we need to maintain the gas bubbles there for desaturation purpose. To be consistent for all the tests, a back pressure of 100 kPa was used for all the tests. Sample saturation was achieved using the $CO_2$ method in which $CO_2$ gas was flushed slowly into the samples followed by water flushing to replace or dissolve $CO_2$ in the sample. All samples were fully saturated initially. If samples needed to be desaturated using biogas, the denitrification process was introduced subsequently. The denitrification solution comprised of denitrifying bacteria suspension and denitrification nutrient in a volume ratio of 20 percent to 80 percent. The solution was introduced into the specimen from a container on top of the load frame. The falling head of solution was estimated to be 0.5 meter. The solution passed through the sand sample was estimated to be 5 times of the pore volume to ensure as much as bacteria suspension and nutrients flew into the sand specimen.

When the denitrification process finished, drainage channels were closed except the one connected with a back pressure source. A pore pressure/volume controller (Figure 6.7)

was employed to keep a constant effective confining pressure (the cell pressure minus the back pressure) of 10 kPa during the whole saturation process. After the saturation process, *B* value was checked to evaluate the degree of saturation. To perform a *B* value test, the drainage line to the pore pressure/volume controller was shut off. Increase the cell pressure by 20 kPa. Wait half a minute and then measure the associated change in pore pressure caused by the change of the confining pressure. The Skempton's pore pressure parameter *B* is calculated by the following equation

$$B = \frac{\Delta u}{\Delta \sigma_3} \tag{6.3}$$

Where Δu is the change in pore pressure resulting from the increase in cell pressure. $\Delta\sigma_3$ is an incremental change in confining pressure (cell pressure). Typically, a *B* value above 0.98 means the sample is fully saturated.


*Figure 6.7 Pore pressure/volume controller*

6.3.4.2 Consolidation

Typically there are two types of consolidation, isotropic and anisotropic. In the isotropic consolidation, the sample is subjected to an equal all-round pressure ($\sigma_h = \sigma_v$), which causes it to consolidate laterally as well as axially. It is usually accomplished by increasing the cell pressure while maintaining a constant back pressure, thereby increasing the effective stress. Because pore water pressure is measured it is sometimes referred to as a pore pressure dissipation test. In contrast, during the anisotropic consolidation, an axial load is applied to the sample during consolidation in order to maintain the ratio of the horizontal and vertical principal stresses ($\sigma_h / \sigma_v$) at a constant value. A special case of anisotropic consolidation test with no lateral yield which corresponds to the conditions in the regular oedometer consolidation test is called $K_0$ consolidation test. The ratio of the principal effective horizontal stress to effective vertical stress ($\sigma_h^{'} / \sigma_v^{'}$) is equal to $K_0$. During $K_0$ consolidation, the ratio of volumetric strain to axial strain is kept at a constant value of 1 ($d\varepsilon_v / d\varepsilon_1 = 1$) so that no lateral strain developed in the soil. This condition applies to the consolidation in-situ of a wide stratum of soil under its own weight. $K_0$ may not remain constant at all stress levels.

Isotropic consolidated specimens were consolidated to an effective stress of 100 kPa in a stress rate of 200 kPa/hour and $K_0$ consolidated specimens were also consolidated to the same effective stress of 100 kPa in a rate of 2.5 %/hour. The volume of water driven out of the sample was measured from the change in the pore pump volume before and after consolidation and hence the post-consolidation void ratio ($e_c$) was readily obtained through the following equation

$$e_c = (V_v - \Delta V_c) / V_s \tag{6.4}$$

where $V_v$ is the volume of voids, $\Delta V_c$ is the volume change during consolidation recorded by the pore pressure/volume controller, and $V_s$ is the volume of dry sands.

6.3.4.3 Shearing

Monotonic triaxial compression testing follows an effective stress path controlled by increasing the effective major principal stress while maintaining the effective minor principal stress to be constant. Upon the completion of consolidation, each specimen was subjected to monotonic axial compression using a deformation-controlled loading in a strain rate of 5 %/hour. Both top and bottom drainage channels connected to the sand specimen was closed during shearing to maintain an undrained condition. Pore pressure measurements were taken by a pressure sensor directly connected to the sand specimen through another bottom drainage valve. Each test had a maximum axial strain of 20 percent limit. Figure 6.8 shows a sand specimen before and after shearing.


(a) Before shearing (b) Before shearing

*Figure 6.8 Sand specimen pre- and post-shearing*

## 6.4 Results and Discussion

### 6.4.1 Testing Program

A summary of the triaxial testing program is given in Table 6.1. In this laboratory program, undrained triaxial compression tests were performed on biogas desaturated loose and medium dense sand samples. To better understand the liquefaction potential of sand, tests are analyzed within the framework of critical state soil mechanics. Specimen results for both the saturated and biogas desaturated sand are presented within this framework. Critical state soil mechanics states that the deviator stress, *q*, the effective mean normal stress, *p'*, and the void ratio, *e*, are uniquely related in the region between the normally consolidated state and the critical state (Roscoe *et al*. 1958). These parameters are defined as follows:

$$p' = \frac{1}{3}(\sigma_1' + 2\sigma_3') \tag{6.5}$$

$$q = (\sigma_1' - \sigma_3') \tag{6.6}$$

### 6.4.2 Degree of saturation and pore pressure coefficient B-value

The biogas bubble generated through the denitrification process in sand sample fluid direct affects the degree of saturation. Adjusting the nitrate and carbon source content can successfully control the finial degree of saturation as described in previous chapters. Based on the nitrate source content and fluid volume which assumed to be equal as the pore volume, total amount of nitrate source input can be obtained. According to the biogas generation test results in Chapter 3, a biogas conversion rate of 0.8 was applied to calculate the final gas bubble volume in sand.

*Table 6.1 Summary of the triaxial testing program*

| Test No. | Nitrate source ($KNO_3$) content (mM) | Estimated degree of consolidation (%) | Consolidation type | Initial void ratio | Initial relative density (%) | B-value | Pore pressure ratio | Peak value (kPa) | |
|---|---|---|---|---|---|---|---|---|---|
| | | | | | | | | p’ | q |
| CIU1* | 0 | 100 | Isotropic | 0.749 | 17.0 | 0.99 | 0.87 | 68.98 | 50.37 |
| CIU2* | 15 | 95.2 | Isotropic | 0.742 | 19.3 | 0.55 | 0.69 | 76.28 | 68.27 |
| CIU3* | 22 | 92.5 | Isotropic | 0.740 | 20.0 | 0.42 | 0.64 | 92.99 | 86.29 |
| CIU4* | 30 | 89.1 | Isotropic | 0.745 | 18.3 | 0.39 | 0.30 | 125.26 | 149.03 |
| $CK_0U1L^{\#}$ | 0 | 100 | $K_0$ | 0.737 | 21.0 | 0.99 | 0.95 | 72.14 | 46.53 |
| $CK_0U2L$ | 10 | 97.2 | $K_0$ | 0.732 | 22.7 | 0.75 | 0.93 | 71.82 | 52.75 |
| $CK_0U3L$ | 20 | 95.6 | $K_0$ | 0.728 | 24.0 | 0.46 | 0.85 | 72.84 | 56.43 |
| $CK_0U4L$ | 30 | 92.5 | $K_0$ | 0.730 | 23.3 | 0.39 | 0.69 | 73.23 | 53.12 |
| $CK_0U5L$ | 40 | 89.4 | $K_0$ | 0.734 | 22.0 | 0.32 | 0.65 | 74.16 | 55.91 |
| $CK_0U1D$ | 0 | 100 | $K_0$ | 0.679 | 40.3 | 0.98 | - | 281.33 | 372.80 |
| $CK_0U2D$ | 10 | 96.8 | $K_0$ | 0.682 | 39.3 | 0.52 | - | 243.94 | 319.46 |
| $CK_0U3D$ | 20 | 92.6 | $K_0$ | 0.685 | 38.3 | 0.35 | - | 208.76 | 290.81 |
| $CK_0U4D$ | 40 | 87.2 | $K_0$ | 0.677 | 41.0 | 0.31 | - | 210.50 | 271.96 |

* Test data from Hansen (2015) # L: Loose D: Medium Dense

Usually, the pore pressure coefficient *B* value is used to evaluate the saturation in triaxial tests. The theoretical relationship of *B* value and degree of saturation has been proposed as an equation 2.8. Based on previous study results and values obtained in this research, relationship between *B* value and degree of saturation can be plotted in Figure 6.9. Most of the data points are close to the theoretical curve within a small range of scatter. It shows that the pore pressure coefficient *B* value obtained from biogas desaturated sample after the saturation stage can be used to well quantify with the theoretical degree of saturation curve.

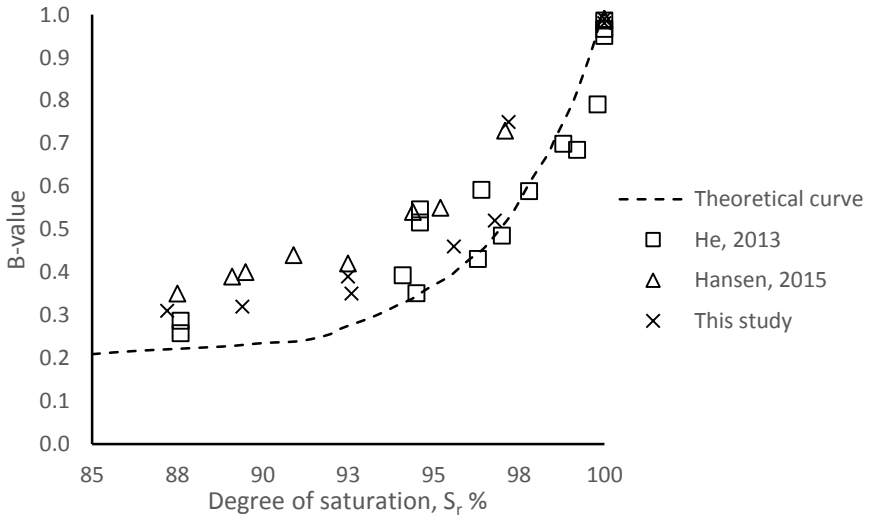


*Figure 6.9 Relationship between B-value and degree of saturation*

### 6.4.3 Undrained shear behavior of biogas desaturated sand

The isotropic consolidated biogas desaturated sand response to undrained shearing is illustrated in Figure 6.10. Except the degree of saturation, all other test conditions, such as initial void ratio, effective confining stress and the sand specimen preparation method for four tests are similar. Figure 6.10(a) shows the stress path of four tests which yield to

distinctive response. As the degree of saturation slightly decreased from 100 to 89.1 percent, the potential for liquefaction also largely reduced. The shear stress and excess pore pressure against axial strain were plotted in Figure 6.10(b) and (c), respectively. Specimen CIU1, which was fully saturated, exhibited the lowest shear strength and the highest excess pore pressure when subjected to undrained loading. The excess pore pressure had reached more than 80 kPa which surpassed 80 percent of effective confining stress (100 kPa) led to a strain softening behavior. As the degree of saturation decreased, the shear strength increased with a reduction of excess pore pressure generation. When the degree of saturation dropped blew 90 percent in specimen CIU4, a strain hardening behavior was observed and the excess pore pressure folded to less than a quarter of the value generated in the fully saturated sand specimen.

The laboratory evaluation of *in situ* usually employs $K_0$ consolidation process. Figure 6.11 and Figure 6.12 show the compression curve and the development of $K_0$ value during the consolidation stage, respectively. There were two groups of sand in $K_0$ consolidation process. One group of loose sand with an initial void ratio of 0.68 ($D_r$ = 22%) and the other group of medium dense sand with an initial void ratio of 0.77 ($D_r$ = 40%) were anisotropic consolidated. For each group, the effective consolidation pressure, void ratio, and relative density were similar. Again, the only difference among specimens in the same group was the degree of saturation.

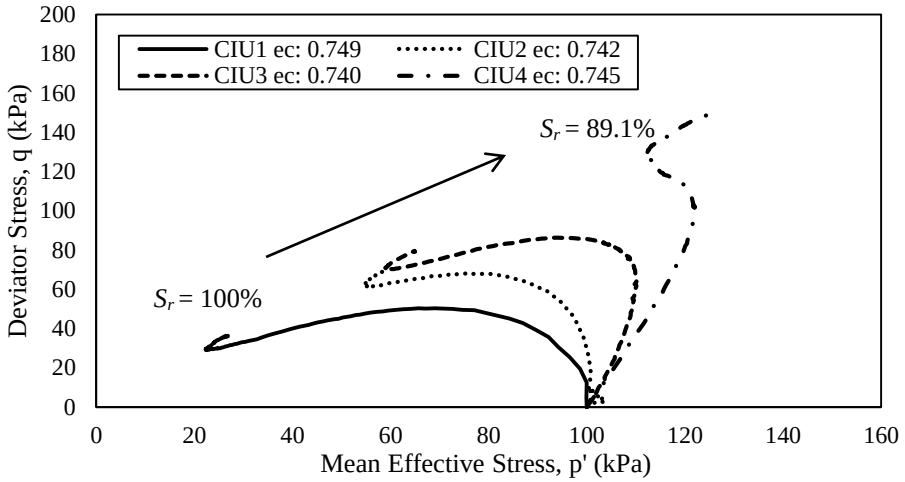


(a) Effective stress path

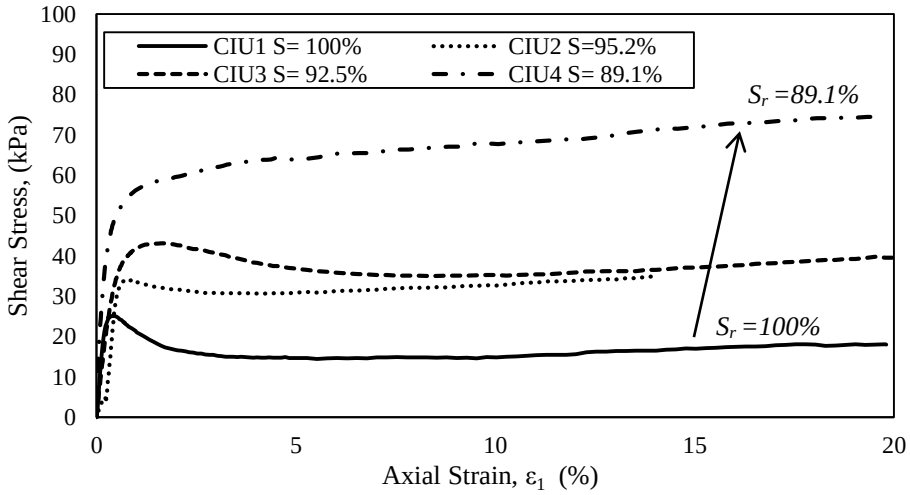


(b) Shear stress response

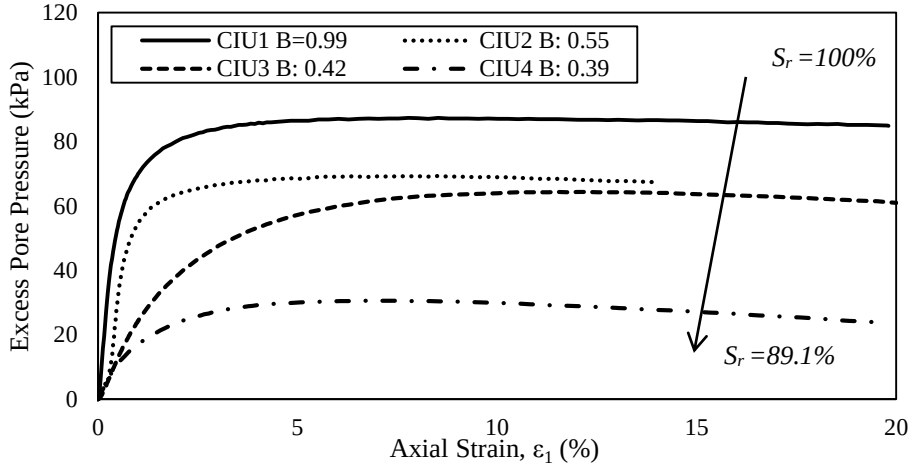


(c) Pore pressure response

*Figure 6.10 Undrained behavior of isotropic consolidated biogas desaturated sand (Hansen, 2015)*

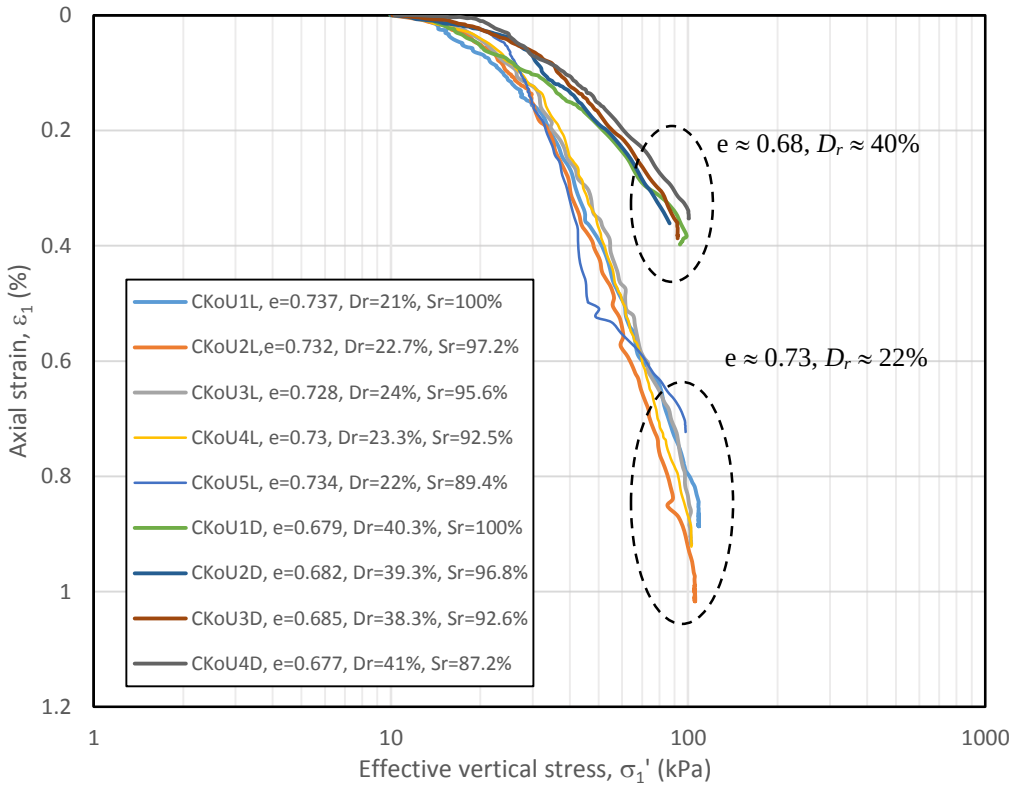


*Figure 6.11 Axial strain versus effective vertical stress during $K_0$ consolidation*

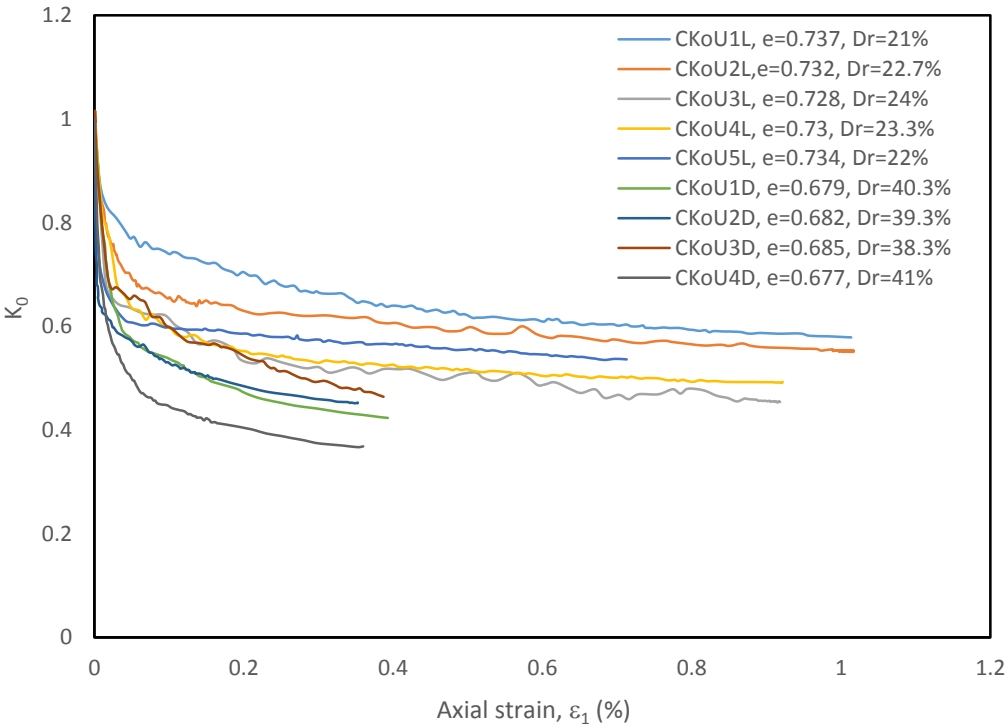


*Figure 6.12 $K_0$ value of anisotropic consolidation*

It can be seen from Figure 6.11(a) that medium dense sand specimens all yield with a small strain close to 0.4% as the effective vertical stress reached the target of 100 kPa, regardless of variations in the degree of saturation. However, there were significance among loose sand specimens. The largest strain observed was 1 percent from a specimen with an initial void ratio of 0.732 ($S_r$ = 97.2%). The smallest strain found in the same $K_0$ consolidation stage was only 0.72 percent in a specimen with the same initial void ratio (e = 0.73) but a much lower degree of saturation ($S_r$ = 89.4%). It seems that the content of biogas bubbles plays an important role in compression behavior of loose sand in the $K_0$ consolidation. Figure 6.12 describes $K_0$ values against the axial strain for all sand specimens. Loose sand apparently had a higher $K_0$ than medium dense sand. Due to the distinction among degrees of saturation, the biogas desaturated sand developed different $K_0$ values at the end of the consolidation stage which indicated their stress status might also be different at the beginning of the undrained shear stage.

The undrained shear responses of the $K_0$ consolidated biogas desaturated loose sand at a relative density of about 22 percent is shown in Figure 6.13. All test specimens exhibits a strain softening behavior. The deviator stress almost immediately plunged after shear loading applied. The fully saturated sand specimen held the lowest deviator stress (45 kPa) after $K_0$ consolidation yet generated the highest excess pore pressure (55 kPa). Due to variation in initial degrees of saturation, biogas desaturated sand specimens ended with stress status slightly different from each other. However, the difference was not significant. As the degree of saturation decreased, the excess pore pressure generation was also confined. Figure 6.13(c) reveals that the lowest excess pore pressure observed when the degree of saturation

fell into 89.4 percent. It was less than 40 kPa which reduced almost 30 percent from the highest value obtained from a fully saturated sand specimen.

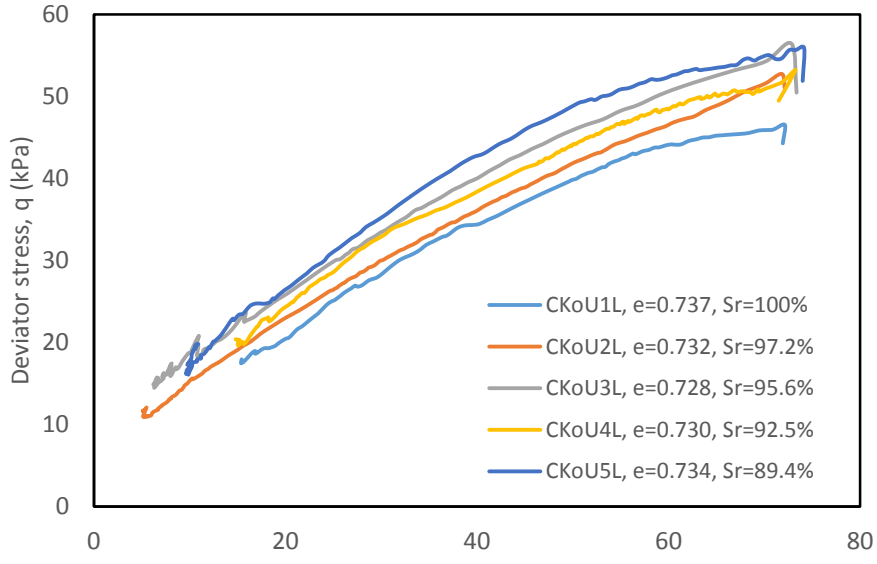


(a) Effective stress path

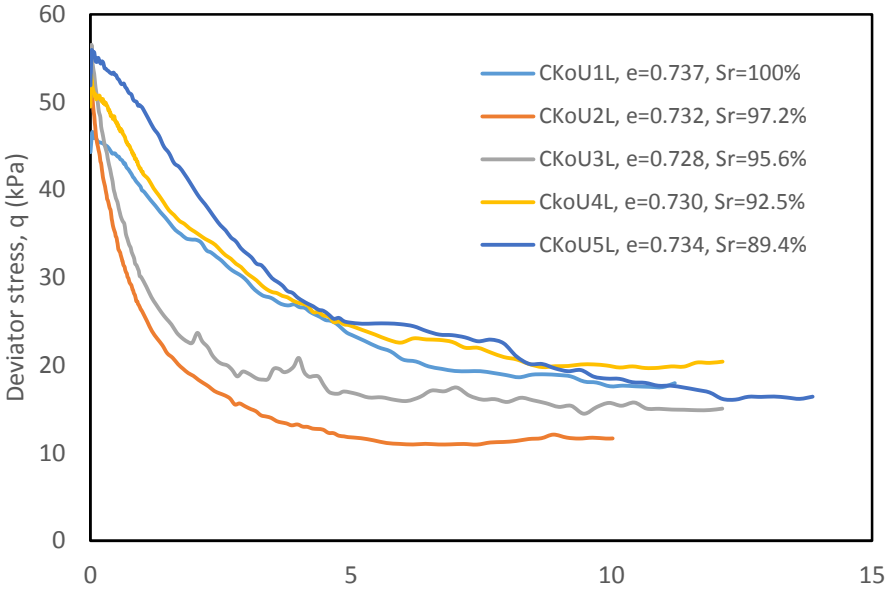


(b) Deviator stress response

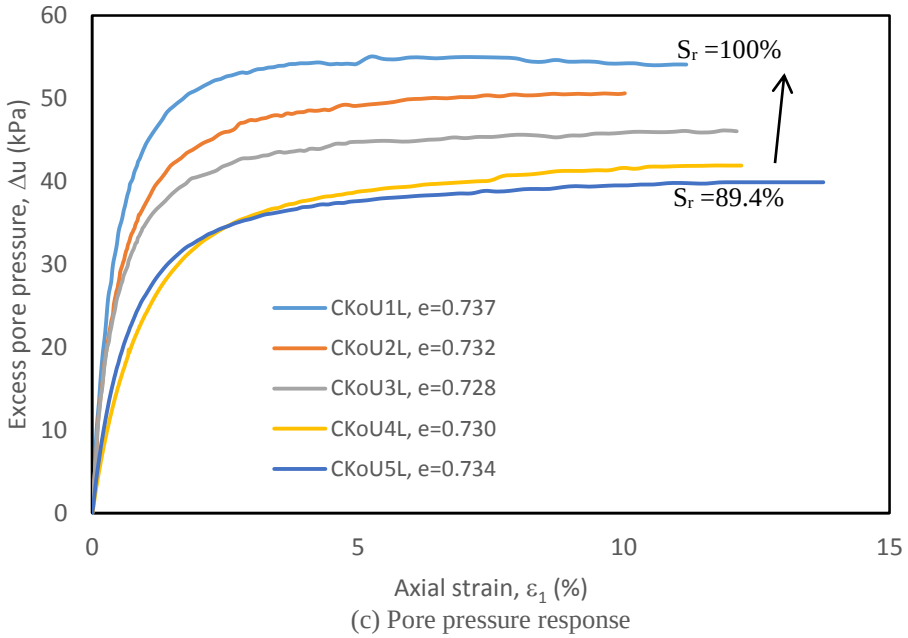

(c) Pore pressure response

*Figure 6.13 Undrained shear behavior of $K_0$ consolidated loose biogas desaturated sand*

Undrained shear behavior of $K_0$ consolidated medium dense biogas desaturated sand was demonstrated in Figure 6.14. The medium dense sand specimens were also prepared by using the moist tamping method. The initial relative density was about 40%. From the effective stress path figure and the deviator stress response, unlike loose sand, there was no strain softening behavior observed. Instead, a slight strain hardening dominated in four specimens. Excess pore pressure increased first and then turned to negative values as the axial strain developed. The fully saturated sand carried the highest deviator stress up to 370.8 kPa and also generated the biggest negative pore pressure (-120.31 kPa). As shown in Figure 6.14(b), the final deviator stress decreased with the reduction of the degree of saturation. Interestingly, Figure 6.14(c) which was an amplification of the dash circle in Figure 6.14(b) illustrates that when the axial strain was small, for instance, less than 0.1 percent, the deviator stress increase in fully saturated sand was the lowest. The deviator stress increase in biogas desaturated sand was much faster and it yielded at a higher stress level than fully

saturated sand. Excess pore pressure change in small strain is shown in Figure 6.14(e). Within the positive excess pore pressure range, the same phenomenon in the loose sand case was found again that the excess pore pressure decreased when the degree of saturation dropped from 100 percent to 87.2 percent. Which indicated that biogas bubbles trapped in both loose and medium dense sand specimens were able to restrict the generation of excess pore pressure when the undrained shearing was applied.

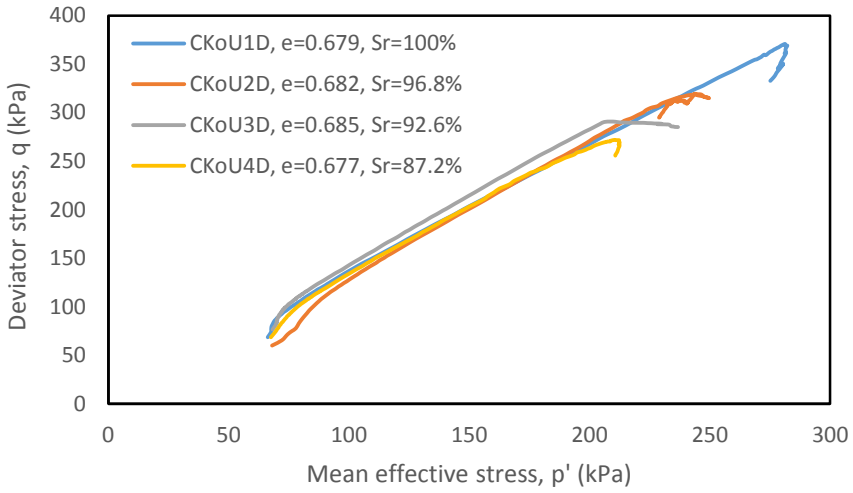


(a) Effective stress path

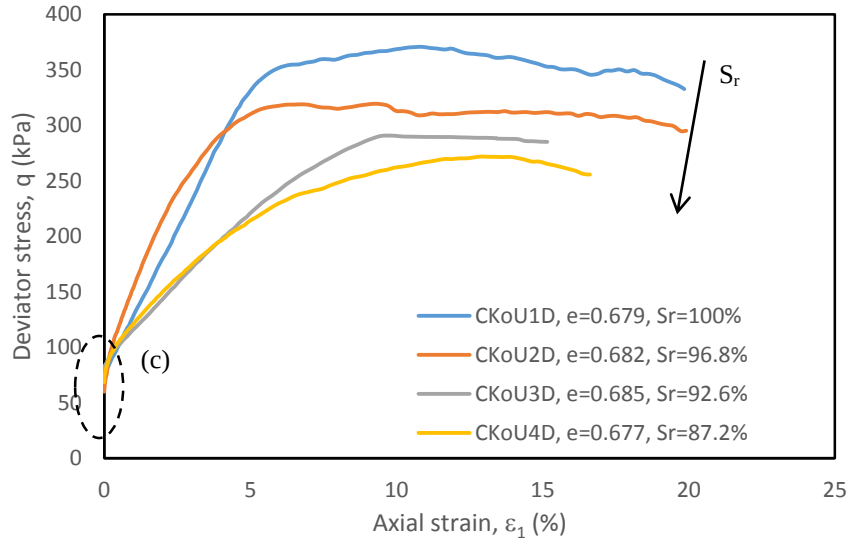


(b) Deviator stress response

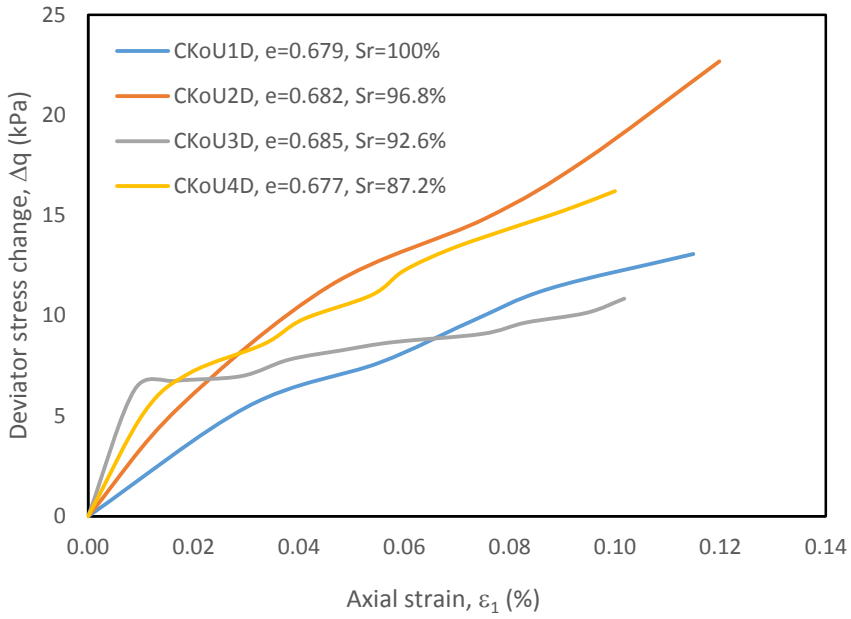


(c) Deviator stress change in a small strain

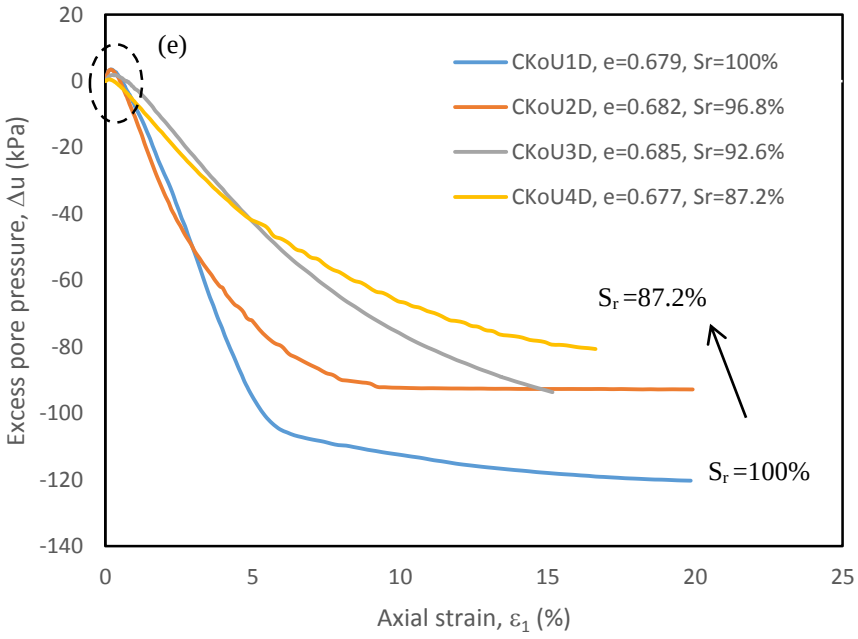


(d) Pore pressure response

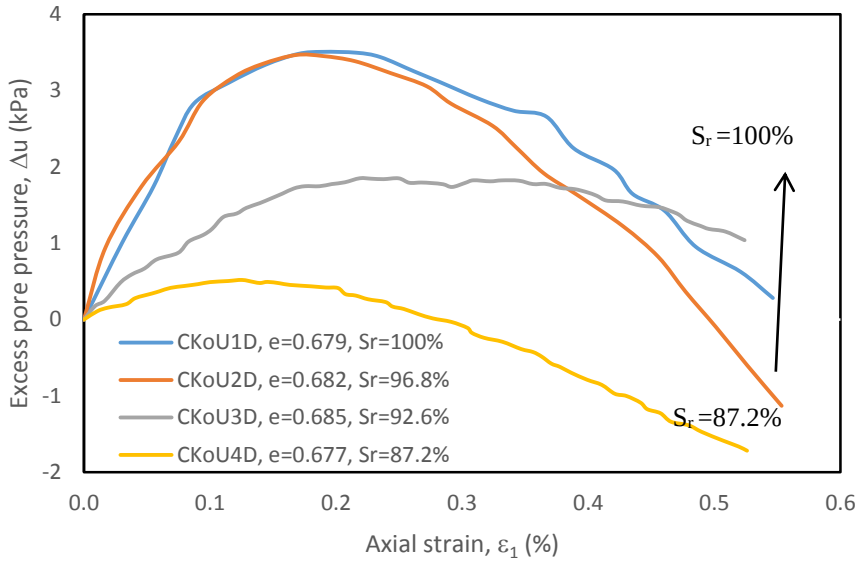


(e) Excess pore pressure in a small strain

*Figure 6.14 Undrained shear behavior of $K_0$ consolidated medium dense biogas desaturated sand*

### 6.4.4 Discussion

The undrained shear results of isotropic consolidated sand in Figure 6.10 shows that biogas desaturated loose sand can shift from completely strain softening to strain hardening behavior as the degree of saturation reduced. In other words, the liquefaction potential was largely decreased as the reduction of degree of saturation. The peak deviator stress increased almost three times, from 50 kPa to about 150 kPa when the degree of saturation dropped from 100 percent to less than 90 percent. These results are consistent with data obtained in previous studies (Grozic 2000; He and Chu 2014). Referring to the $K_0$ consolidation case, the biogas desaturated loose sand exhibited a similar behavior as isotropic consolidated loose sand contained biogas. Reduce the degree of saturation from 100 percent to roughly 90 percent, the peak deviator stress increased more than 30 percent. However, there is a lack of transition from strain softening to strain hardening in the series of tests shown in Figure 6.13.

One possible reason could be that the degree of saturation was not low enough or the undrained behavior was affected by the initial shear stress. It should be noted that the initial shear stresses were different in different tests as a result of the $K_0$ consolidation.

Figure 6.15 demonstrates the normalized undrained shear strength ratio ($q_{peak} / 2p_0^{'}$) of biogas desaturated sand specimens with different degrees of saturation. As long as the sand had a similar initial void ratio, the shear strength improved at both cases of isotropic consolidation and $K_0$ consolidation when the degree of saturation reduced. Especially for isotropic consolidated sand, the shear strength increased remarkably from 0.3 to 0.75 when the degree of saturation dropped below 90 percent. In the $K_0$ consolidated test group, the improvement of shear strength was not as significant as in the isotropic consolidation case. The normalized shear strength ratio only increased less than 15 percent (0.32 to 0.38) from the fully saturated sand to the 90 percent saturated sand. The biggest improvement occurred when the degree of saturation was 95.6 percent. These findings indicate that the shear strength of biogas desaturated sand was sensitive to the type of consolidation process. A slight difference in stress status would yield with distinct results.

Except shear strength, pore pressure ratio is another important indicator for liquefaction resistance. Pore pressure ratio $R_u$ is defined as the ratio of the maximum excess pore pressure to the initial effective confining stress. If the $R_u$ = 1, then the sample loses all effective stress and completely liquefies. A lower pore pressure ratio usually means a higher liquefaction resistance. The pore pressure ratio $R_u$ generated in undrained shear tests were plotted against the degree of saturation in Figure 6.16. For sand specimens with a void ratio about 0.7, a tendency towards lower value of $R_u$ was found as a result of decrease in the degree of saturation. When the sand was fully saturated, the pore pressure ratio was close to

unity for both CIUC and $CK_0UC$. A 10 percent of reduction in degree of saturation caused $R_u$ fell to a lower value. The reduction of $R_u$ was dramatic in the CIUC group. In terms of the improvement of liquefaction resistance, unlike the small increase in normalized undrained shear strength ratio, $K_0$ consolidated biogas desaturated sand exhibited a bigger boost in reduction of pore pressure ratio.

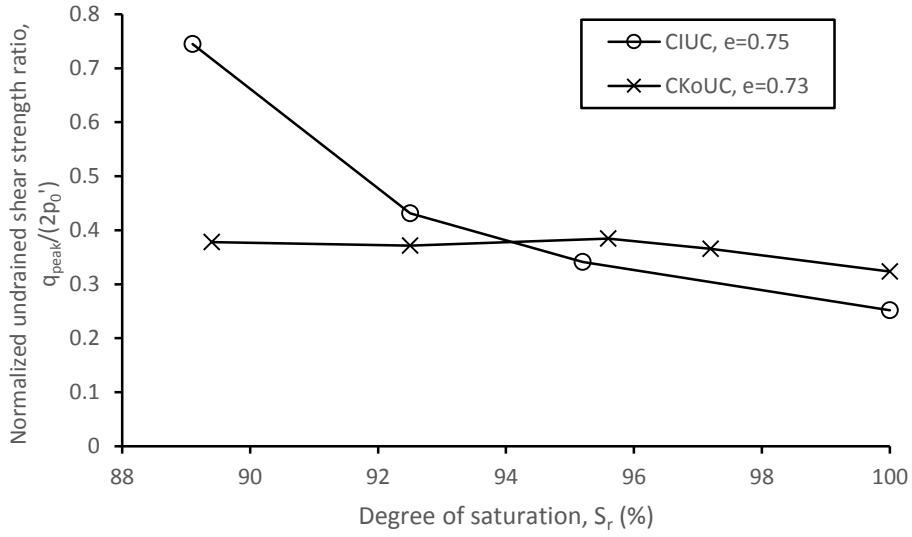


*Figure 6.15 Normalized undrained shear strength ratio against degree of saturation*

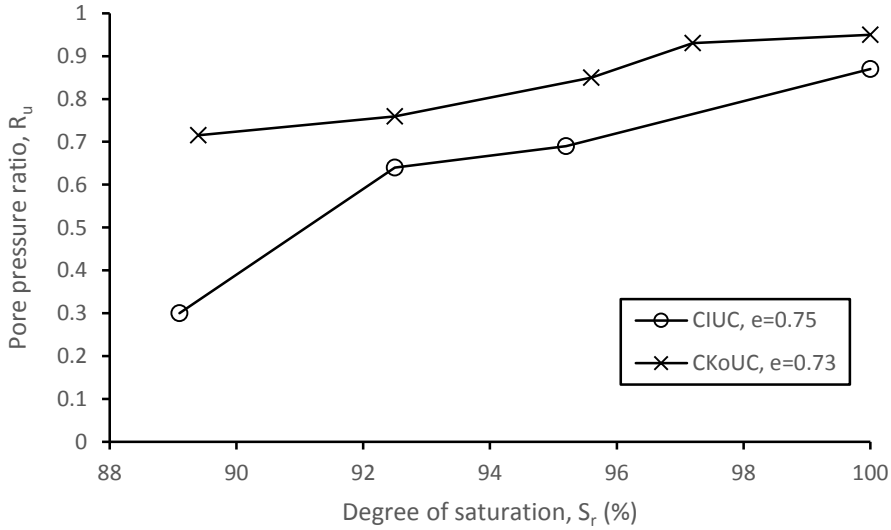


*Figure 6.16 Pore pressure ratio against degree of saturation in undrained shear test*

## 6.5 Conclusions

A laboratory study on the undrained shear behavior of biogas desaturated sand was carried out using undrained triaxial compression tests. Both fully saturated sand and biogas desaturated sand specimens were tested. Desaturation was achieved using nitrogen gas produced via the denitrification process. Both isotropic and anisotropic $K_0$ consolidation were employed to consolidate sand specimens with an effective vertical stress of 100 kPa. All sand specimens were prepared by the moist tamping method to create a similar sand packing structure and control the initial void ratio. The denitrification process was successfully employed to produce triaxial sand specimens with varied degrees of saturation. The presence of biogas in sand affect the undrained shear strength and excess pore pressure behavior.

For loose sand specimens, the liquefaction potential decreased as the degree of saturation dropped below 100 percent. The liquefaction potential continued to decrease with the reduction in degree of saturation. This phenomenon was more significant when the sand specimens were isotropic consolidated. As the normalized shear strength increased three times and the pore pressure ratio folded two-thirds when the degree of saturation dropped from 100 to less than 90 percent. In the $K_0$ consolidated tests, the improvement to liquefaction resistance reflected well in terms of decrease in pore pressure ratio. However, the increase in the undrained shear strength with a reduction in degree of saturation was not substantial. This could possibly due to the reduction in the degree of consolidation was not sufficient or the effect of initial stresses achieved at the end of $K_0$ consolidation.

For biogas desaturated medium dense sand in the undrained shear condition, it was observed that only the excess pore pressure seemed to be affected by the degree of saturation.

Strain hardening was found in all $K_0$ consolidated medium dense sand specimens. The liquefaction potential was low in such a case.

# CHAPTER 7

# CONCLUSIONS AND RECOMMENDATIONS

## 7.1 Conclusions

An effort to apply microbial geotechnologies in sand as a liquefaction mitigation approach has been made in this research. The combined biodesaturation and bioclogging method employs both microbial denitrification process and microbial urea hydrolysis process to produce biogas and calcium carbonate precipitation, respectively. The microbial activities and their creations improve the engineering property of sand. Selective bacteria were cultivated through engineered procedures to serve the bio-desaturation purpose. Element tests using small size triaxial specimens as well as laboratory model tests using big sand columns and a shaking table system were carried out. The following conclusions can be made from this study:

1) To optimize the process of biogas generation, batch experiments were conducted to investigate the preferred conditions for the growth of denitrifying bacteria. Biogas ($N_2$) generation test results show that by using nitrate and glucose as electron acceptor and electron donor, respectively, can obtain a high nitrate to nitrogen gas conversion rate (80%) when a proper N:C ratio (1:2.5) was chosen.

2) A technique of producing freeze dried UPB was developed. The dry biomass can dissolve in one percent sodium chloride solution for injection or spray usage. Laboratory bench scale sand column cementation test results suggest the shear strength of sand increased

considerably to more than 2 MPa when the calcite content reaches 10 percent. At the same time, permeability of sand almost dropped one magnitude.

3) Experimental sand column tests show that biogas trapped within saturated sand remains in the sand under the hydrostatic condition. When a seepage flow exists, even under a small hydraulic gradient, gas bubbles will be carried out by the flow in 10 days. The downward flow is able to move gas bubbles out of sand voids quicker than the upward flow does when the hydraulic gradient is 0.1. The permeability of biogas desaturated sand is smaller than fully saturated sand in all hydraulic gradients condition tested. As the biogas generated from the denitrification process accumulate, the degree of saturation decreases from 100 percent, and the permeability also gradually reduces.

4) Long term flow tests for sand columns treated using the combined biodesaturation and bioclogging method under a hydraulic gradient of 0.1 for up to 40 days with either upward or downward flow indicate that the combined method is effective in enhancing the stability of the bubbles because of the formation of calcite crystals in sand to act as a sealing wall or barrier to reduce the flow rate. The permeability decreases significantly as the bioclogging takes place. The combined biogas and bioclogging method can help to stabilize the gas bubbles in sand.

5) The biogas distribution in a long sand column test is affected by the effective overburden stresses. Water head readings from piezometers at different positions of the sand column shows a linear relationship from top to bottom when the sand is fully saturated. As the degree of saturation reduced, nonlinear relationship is found between piezometers located at the bottom layer of sand column, which indicates that more biogas exists in that area and imposes a more intense affect to the flow rate than those trapped in the upper layer. The gas

bubbles generated at deep area could be tiny and immobile due to a high effective overburden stress. In the shallow layer of sand, because of low effective overburden stress, biogas bubbles have a better chance to collide and gather to form aggregations which is easy to be removed by a seepage flow.

6) CT images demonstrate that the more biogas generated in sand, the lower degree of saturation can be achieved. When the degree of saturation is below 90 percent, tiny gas bubbles are more likely to merge and form big aggregations. SEM images reveals that for biocemented sand with low calcium carbonate concentration (0.8%, w/w), majority of the calcite precipitation is formed as single crystal on the top of sand grain.

7) The shaking table results show that the liquefaction occurs only in fully saturated loose sand under an acceleration of a = 1.5 $m/s^2$. Liquefaction does not happen when the sand sample is desaturated by the biogas method to a degree of saturation of 90 percent. The pore pressure ratio in biogas desaturated sand is only tenth of that in fully saturated sand.

8) Liquefaction is more prone to happen in sloping ground than in leveled ground. For sand with a 90 percent degree of saturation, the pore pressure ratio in the sloping ground is almost as twice as the one in the leveled ground at the same position. Nevertheless, the pore pressure ratio is still far more less than that generated in the fully saturated sand. The amount of lateral spreading is largely confined in the biogas desaturated sand sample. The permanent lateral displacement developed in the biogas desaturated sand with a 90 percent degree of saturation is only a quarter to half of that in fully saturated sand.

9) When the sand sample is treated with the combined biodesaturation and bioclogging method, pore pressure ratio and volumetric strain are reduced even seepage flow

exists in both leveled ground and sloping ground conditions. The testing data suggests that the bioclogging process also increases the bonding in sand grain and thus helps in reducing the ground settlement and lateral displacement.

10) For loose sand in the undrained compression test, the liquefaction potential decreases as the degree of saturation drops below 100 percent. This phenomenon is observed in both isotropic and $K_0$ consolidated sand specimens. For isotropic consolidated sand, the undrained shear strength increases and the pore pressure reduces as the reduction in degree of saturation. When the sand is $K_0$ consolidated, the increase in the shear strength is not substantial as in the isotropic case. This could be due to the reduction in the degree of saturation is not sufficient or the effect of initial stresses achieved at the end of $K_0$ consolidation.

## 7.2 Recommendations

With sustainability becoming an increasingly important driver for all activities, including the geotechnical practice, it is to be expected that there will be considerable developments in research activity on those cost-competitive and energy-saving techniques. The combined biodesaturation and bioclogging method holds a promising potential for the reduction of liquefaction susceptibility and the damage due to seismic loading. Some recommendations and suggestions for further studies on this topic are proposed as follows:

1) Large scale shaking table tests or centrifuge tests can be carried out to investigate the engineering behavior of biogas desaturated sand.

2) Non-destructive technique such as soil wave method (S-wave and P-wave) can be employed to detect gas content in sand. It provides an effective way for the monitoring of the generation of biogas and biocement or biogrout, especially in large scale tests or *in situ* tests.

# REFERENCES


Akunna, J. C., Bizeau, C., and Moletta, R. (1993). "Nitrate and nitrite reductions with anaerobic sludge using various carbon sources: glucose, glycerol, acetic acid, lactic acid and methanol." *Water Research*, 27(8), 1303-1312.

Al Qabany, A., Mortensen, B., Martinez, B., Soga, K., and DeJong, J. (2011). "Microbial carbonate precipitation: correlation of S-wave velocity with calcite precipitation." *Geo-Frontiers 2011, 3993-4001*.

Al Qabany, A., Soga, K., and Santamarina, C. (2012). "Factors affecting efficiency of microbially induced calcite precipitation." *Journal of Geotechnical and Geoenvironmental Engineering*, 138(8), 992-1001.

Alef, K., and Nannipieri, P. (1995). *Methods in Applied Soil Microbiology and Biochemistry*, Academic press, London.

Alley, W., Reilly, T., and Franke, O. (1999). "Sustainability of ground-water resources: US Geological Survey." *U.S. Geological Survey Circular 1186*, USGS, Denver, Colorado.

Altun, S., and Goktepe, A. B. (2006). "Cyclic stress-strain behavior of partially saturated soils." *Unsaturated Soils 2006*, Geotechnical Special Publication No. 147, 497-507.

Amaratunga, A., and Grozic, J. (2009). "On the undrained unloading behaviour of gassy sands." *Canadian Geotechnical Journal*, 46(11), 1267-1276.

Amidi, S., and Wang, J. (2015). "Surface treatment of concrete bricks using calcium carbonate precipitation." *Construction and Building Materials*, 80, 273-278.

Anderle, M., Bersani, M., Vanzetti, L., and Pederzoli, S. (2006). "Macromolecules in Cultural Heritage." *Macromolecular Symposia*, 238(1), v-viii

Arah, J., and Smith, K. (1990). "Factors influencing the fraction of the gaseous products of soil denitrification evolved to the atmosphere as nitrous oxide." *Soils and The Greenhouse Effect. New York, John Wiley & Sons*, 475-480.

Atkinson, J., and Bransby, P. (1978). *The Mechanics of Soils: An Introduction to Critical State Soil Mechanics*, McGraw-Hill, New York, USA.

Avalakki, U., Strong, W., and Saffigna, P. (1995). "Measurement of gaseous emissions from denitrification of applied N-15. 2. Effects of temperature and added straw." *Australian Journal of Soil Research*, 33(1), 89-99.

Banagan, B. L., Wertheim, B. M., Roth, M. J. S., and Caslake, L. F. (2010). "Microbial strengthening of loose sand." *Letters in Applied Microbiology*, 51(2), 138-142.

Bang, S., Lippert, J., Yerra, U., Mulukutla, S., and Ramakrishnan, V. (2010). "Microbial calcite, a bio-based smart nanomaterial in concrete remediation." *International Journal of Smart and Nano Materials*, 1(1), 28-39.

Bang, S. S., Bang, S., Frutiger, S., Nehl, L. M., and Comes, B. L. (2009). "Application of novel biological technique in dust suppression." *Proc., Transportation Research Board 88th Annual Meeting*, Washington DC, USA.

Bäuerlein, E. (2003). "Biomineralization of unicellular organisms: an unusual membrane biochemistry for the production of inorganic nano - and microstructures." *Angewandte Chemie International Edition*, 42(6), 614-641.

Been, K., and Jefferies, M. G. (1985). "A state parameter for sands." *Géotechnique*, 35(2), 99-112.

Bishop, A. (1973). "The influence of an undrained change in stress on the pore pressure in porous media of low compressibility." *Géotechnique*, 23(3), 435-442.

Black, D. K., and Lee, K. L. (1973). "Saturating laboratory samples by back pressure." *Journal of the Soil Mechanics and Foundations Division*, 99(1), 75-93.

Blauw, M., Lambert, J. W. M., and Latil, M. N. (2009). "Biosealing: a method for in situ sealing of leakages." *Proc., Proceedings of the International Symposium on Ground Improvement Technologies and Case Histories, ISGI'09*, 125-130.

Bouwer, H. (2002). "Artificial recharge of groundwater: hydrogeology and engineering." *Hydrogeology Journal*, 10(1), 121-142.

Bremner, J., and Blackmer, A. M. (1978). "Nitrous oxide: emission from soils during nitrification of fertilizer nitrogen." *Science*, 199(4326), 295-296.

Bremner, J., and Shaw, K. (1958). "Denitrification in soil. II. factors affecting denitrification." *The Journal of Agricultural Science*, 51(01), 40-52.

Brignoli, E., Gotti, M., and Stokoe, K. H. (1996). "Measurement of shear waves in laboratory specimens by means of piezoelectric transducers." *ASTM geotechnical testing journal*, 19(4), 384-397.

Carlson, C. A., and Ingraham, J. L. (1983). "Comparison of denitrification by Pseudomonas stutzeri, Pseudomonas aeruginosa, and Paracoccus denitrificans." *Applied and Environmental Microbiology*, 45(4), 1247-1253.

Casagrande, A. (1936). "The determination of the pre-consolidation load and its practical significance." *Proc., Proceedings of the international conference on soil mechanics and foundation engineering*, Harvard University Cambridge, 60-64.

Casagrande, A. (1971). "On liquefaction phenomena." *Geotechnique*, 21(3), 197-202.

Castro, G. (1969). "Liquefaction of sands." PhD thesis, Division of Engineering and Applied Mechanics, Havard University

Chaney, R. C. (1978). "Saturation effects on the cyclic strength of sands." *Proc., Proceedings of the ASCE Geotechnical Engineering Division Specialty Conference*, ASCE, 342-358.

Cheng, L., and Cord-Ruwisch, R. (2012). "In situ soil cementation with ureolytic bacteria by surface percolation." *Ecological Engineering*, 42(0), 64-72.

Cheng, L., Cord-Ruwisch, R., and Shahin, M. A. (2013). "Cementation of sand soil by microbially induced calcite precipitation at various degrees of saturation." *Canadian Geotechnical Journal*, 50(1), 81-90.

Cho, C., Burton, D., and Chang, C. (1997). "Denitrification and fluxes of nitrogenous gases from soil under steady oxygen distribution." *Canadian Journal of Soil Science*, 77(2), 261-269.

Cho, G. C. (2001). "Unsaturated soil stiffness and post-liquefaction shear strength." PhD thesis, Georgia Institute of Technology.

Chu, J., Ivanov, V., Stabnikov, V., He, J., Li, B., and Naemi, M. (2012). "Biocement: green building-and energy-saving material." *Advanced Materials Research*, 347, 4051-4054.

Chu, J., Ivanov, V., Stabnikov, V., and Li, B. (2013). "Microbial method for construction of an aquaculture pond in sand." *Géotechnique*, 63(10), 871-875.

Chu, J., and Leong, W. (2001). "Pre-failure strain softening and pre-failure instability of sand: a comparative study." *Géotechnique*, 51(4), 311-321.

Chu, J., Leroueil, S., and Leong, W. (2003). "Unstable behaviour of sand and its implication for slope instability." *Canadian Geotechnical Journal*, 40(5), 873-885.

Chu, J., Lo, S.-C., and Lee, I. K. (1993). "Instability of granular soils under strain path testing." *Journal of Geotechnical Engineering*, 119(5), 874-892.

Chu, J., Stabnikov, V., and Ivanov, V. (2012). "Microbially induced calcium carbonate precipitation on surface or in the bulk of soil." *Geomicrobiology Journal*, 29(6), 544-549.

Chu, J., and Wanatowski, D. (2008). "Instability conditions of loose sand in plane strain." *Journal of Geotechnical and Geoenvironmental Engineering*, 134(1), 136-142.

Chu, J., and Wanatowski, D. (2009). "Effect of loading mode on strain softening and instability behavior of sand in plane-strain tests." *Journal of Geotechnical and Geoenvironmental Engineering*, 135(1), 108-120.

Čuhel, J., Šimek, M., Laughlin, R. J., Bru, D., Chèneby, D., Watson, C. J., and Philippot, L. (2010). "Insights into the effect of soil pH on $N_2O$ and $N_2$ emissions and denitrifier community size and activity." *Applied and Environmental Microbiology*, 76(6), 1870-1878.

Davies, M., McRoberts, E., and Martin, T. "Static liquefaction of tailings–fundamentals and case histories." *Proceedings Tailings Dams ASDSO/USCOLD*, 233-255.

DeJong, J. T., Fritzges, M. B., and Nusslein, K. (2006). "Microbially Induced Cementation to Control Sand Response to Undrained Shear." *Journal of Geotechnical and Geoenvironmental Engineering*, 132(11), 1381-1392.

DeJong, J. T., Soga, K., Banwart, S. A., Whalley, W. R., Ginn, T. R., Nelson, D. C., Mortensen, B. M., Martinez, B. C., and Barkouki, T. (2011). "Soil engineering *in vivo*: harnessing natural biogeochemical systems for sustainable, multi-functional engineering solutions." *Journal of The Royal Society Interface*, 8(54), 1-15.

DeJong, J. T., Soga, K., Kavazanjian, E., Burns, S., Paassen, L. A. V., Qabany, A. A., Aydilek, A., Bang, S. S., Burbank, M., Caslake, L. F., Chen, C. Y., Cheng, X., Chu, J., Ciurli, S., Esnault-Filet, A., Fauriel, S., Hamdan, N., Hata, T., Inagaki, Y., Jefferis, S., Kuo, M., Laloui, L., Larrahondo, J., Manning, D. A. C., Martinez, B., Montoya, B. M., Nelson, D. C., Palomino, A., Renforth, P., Santamarina, J. C., Seagren, E. A., Tanyu, B., Tsesarsky, M., and Weaver, T. (2013). "Biogeochemical processes and geotechnical applications: progress, opportunities and challenges." *Géotechnique*, 63(4), 287-301.

Dendooven, L., Bonhomme, E., Merckx, R., and Vlassak, K. (1998). "Injection of pig slurry and its effects on dynamics of nitrogen and carbon in a loamy soil unter laboratory conditions." *Biology and Fertility of Soils*, 27(1), 5-8.

Dendooven, L., Splatt, P., Pemberton, E., Ellis, S., Anderson, J., Jarvis, S., and Pain, B. (1997). "Controls over denitrification and its gaseous products in a permanent pasture soil." *Gaseous Nitrogen Emissions from Grasslands.*, 19-25.

Dhami, N. K., Reddy, M. S., and Mukherjee, A. (2013). "Biomineralization of calcium carbonates and their engineered applications: a review." *Frontiers in microbiology*, 4.

Dobry, R., Ladd, R., Yokel, F. Y., Chung, R. M., and Powell, D. (1982). "Prediction of pore water pressure buildup and liquefaction of sands during earthquakes by the cyclic strain method." US Department of Commerce, National Bureau of Standards, Vol 38.

Dobry, R., Thevanayagam, S., Medina, C., Bethapudi, R., Elgamal, A., Bennett, V., Abdoun, T., Zeghal, M., Shamy, U. E., and Mercado, V. M. (2011). "Mechanics of lateral spreading observed in a full-scale shake test." *Journal of Geotechnical and Geoenvironmental Engineering*, 137(2), 115-129.

Douglas, S., and Beveridge, T. J. (1998). "Mineral formation by bacteria in natural microbial communities." *FEMS microbiology ecology*, 26(2), 79-88.

Eseller-Bayat, E. E. (2009). "Seismic response and prevention of liquefaction failure of sands partially saturated through introduction of gas bubbles." PhD thesis, Northeastern University, Boston, Massachusetts.

Fageria, N., and Baligar, V. (2008). "Ameliorating soil acidity of tropical Oxisols by liming for sustainable crop production." *Advances in Agronomy*, 99, 345-399.

Fauriel, S., and Laloui, L. (2012). "A bio-chemo-hydro-mechanical model for microbially induced calcite precipitation in soils." *Computers and Geotechnics*, 46(0), 104-120.

Ferris, F., Stehmeier, L., Kantzas, A., and Mourits, F. (1996). "Bacteriogenic mineral plugging." *Journal of Canadian Petroleum Technology*, 35(8), 56-61.

Finn, W. (1981). "Liquefaction potential: developments since 1976." *First International Conference on Recent Advances in Geotechnical earthquake Engineering and Soil Dynamics (1981: April 26-May 3; St. Louis, Missouri)*, Missouri S&T (formerly the University of Missouri--Rolla).

Fioravante, V., and Capoferri, R. (2001). "On the use of multi-directional piezoelectric transducers in triaxial testing." *ASTM Geotechnical Testing Journal*, 24(3), 243-255.

Firestone, M., Smith, M., Firestone, R., and Tiedje, J. (1979). "The influence of nitrate, nitrite, and oxygen on the composition of the gaseous products of denitrification in soil." *Soil Science Society of America Journal*, 43(6), 1140-1144.

Fortin, D., Ferris, F., and Beveridge, T. (1997). "Surface-mediated mineral development by bacteria." *Reviews in Mineralogy and Geochemistry*, 35(1), 161-180.

Fourie, A., Hofmann, B., Mikula, R., Lord, E., and Robertson, P. (2001). "Partially saturated tailings sand below the phreatic surface." *Géotechnique*, 51(7), 577-585.

Fredlund, D. G., and Rahardjo, H. (1993). *Soil mechanics for unsaturated soils*, John Wiley & Sons.

Fujita, Y., Ferris, F. G., Lawson, R. D., Colwell, F. S., and Smith, R. W. (2000). "Subscribed content calcium carbonate precipitation by ureolytic subsurface bacteria." *Geomicrobiology Journal*, 17(4), 305-318.

Fujita, Y., Taylor, J. L., Gresham, T. L. T., Delwiche, M. E., Colwell, F. S., McLing, T. L., Petzke, L. M., and Smith, R. W. (2008). "Stimulation Of Microbial Urea Hydrolysis In Groundwater To Enhance Calcite Precipitation." *Environmental Science & Technology*, 42(8), 3025-3032.

Gebauer, D., Gunawidjaja, P. N., Ko, J. Y. P., Bacsik, Z., Aziz, B., Liu, L., Hu, Y., Bergström, L., Tai, C.-W., Sham, T.-K., Edén, M., and Hedin, N. (2010). "Proto-calcite and proto-vaterite in amorphous calcium carbonates." *Angewandte Chemie International Edition*, 49(47), 8889-8891.

Ghayoomi, M. (2011). "Seimically induced settlement of partially-saturated sand." PhD thesis, University of Colorado at Boulder, Boulder, Colorado.

Ghayoomi, M., McCartney, J., and Ko, H.-Y. (2011). "Centrifuge test to assess the seismic compression of partially saturated sand layers." *ASTM Geotechnical Testing Journal*, 34(4), 321-331.

Gomez, M. G., Martinez, B. C., DeJong, J. T., Hunt, C. E., Major, D. W., and Dworatzek, S. M. (2014). "Field-scale bio-cementation tests to improve sands." *Ground Improvement*, Ahead of Print.

González, J. M., and Saiz-Jiménez, C. (2005). "Application of molecular nucleic acid-based techniques for the study of microbial communities in monuments and artworks." *International Microbiology*, 8(3), 189.

Gower, L. B. (2008). "Biomimetic model systems for investigating the amorphous precursor pathway and its role in biomineralization." *Chemical Reviews*, 108(11), 4551-4627.

Grozic, J. L., Robertson, P. K., and Morgenstern, N. R. (2000). "Cyclic liquefaction of loose gassy sand." *Canadian Geotechnical Journal*, 37(4), 843-856.

Harkes, M. P., van Paassen, L. A., Booster, J. L., Whiffin, V. S., and van Loosdrecht, M. C. M. (2010). "Fixation and distribution of bacterial activity in sand to induce carbonate precipitation for ground reinforcement." *Ecological Engineering*, 36(2), 112-117.

He, J., and Chu, J. (2014). "Undrained Responses of Microbially Desaturated Sand under Monotonic Loading." *Journal of Geotechnical and Geoenvironmental Engineering*, 140(5), 04014003.

He, J., Chu, J., and Ivanov, V. (2013). "Mitigation of liquefaction of saturated sand using biogas." *Geotechnique*, 63(4), 267-275.

Higo, Y., Oka, F., Morishita, R., Matsushima, Y., and Yoshida, T. (2014). "Trinarization of μX-ray CT images of partially saturated sand at different water-retention states using a region growing method." *Nuclear Instruments and Methods in Physics Research Section B: Beam Interactions with Materials and Atoms*, 324, 63-69.

Inagaki, Y., Tsukamoto, M., Mori, H., Nakajiman, S., Sasaki, T., and Kawasaki, S. (2011). "A centrifugal model test of microbial carbonate precipitation as liquefaction countermeasure." *Jiban Kogaku Janaru*, 6(2), 157-167.

Ishihara, K. (1993). "Liquefaction and flow failure during earthquakes." *Geotechnique*, 43(3), 351-415.

Ishihara, K. (1996). "Soil behaviour in earthquake geotechnics." *Clarendon Press*, Oxford University Press.

Ishihara, K., Tatsuoka, F., and Yasuda, S. (1975). "Undrained deformation and liquefaction of sand under cyclic stresses." *Soils and foundations*, 15(1), 29.

Ivanov, V., and Chu, J. (2008). "Applications of microorganisms to geotechnical engineering for bioclogging and biocementation of soil in situ." *Reviews in Environmental Science and Bio/Technology*, 7(2), 139-153.

Ivanov, V., Chu, J., Stabnikov, V., He, J., and Naeimi, M. (2012). "Iron-based Bio-grout for soil improvement and land reclamation." *Proc. 2nd Int. Conf. Sustainable Construction Mater. Technol, Ancona* Special, 415-420.

Iwasaki, T. (1986). "Soil liquefaction studies in Japan: state-of-the-art." *Soil Dynamics and Earthquake Engineering*, 5(1), 2-68.

Jansson, C., and Northen, T. (2010). "Calcifying cyanobacteria—the potential of biomineralization for carbon capture and storage." *Current Opinion in Biotechnology*, 21(3), 365-371.

Jonkers, H. M., Thijssen, A., Muyzer, G., Copuroglu, O., and Schlangen, E. (2010). "Application of bacteria as self-healing agent for the development of sustainable concrete." *Ecological Engineering*, 36(2), 230-235.

Kagawa, T., Sato, M., Minowa, C., Abe, A., and Tazoh, T. (2004). "Centrifuge simulations of large-scale shaking table tests: case studies." *Journal of Geotechnical and Geoenvironmental Engineering*, 130(7), 663-672.

Kantzas, A., Stehmeier, L., Marentette, D., Ferris, F., Jha, K., and Maurits, F. (1992). "A novel method of sand consolidation through bacteriogenic mineral plugging." In *Annual Technical Meeting*, Petroleum Society of Canada.

Keeney, D., Fillery, I., and Marx, G. (1979). "Effect of temperature on the gaseous nitrogen products of denitrification in a silt loam soil." *Soil Science Society of America Journal*, 43(6), 1124-1128.

Kester, R. A., De Boer, W., and Laanbroek, H. J. (1997). "Production of NO and $N_2O$ by pure cultures of nitrifying and denitrifying bacteria during changes in aeration." *Applied and Environmental Microbiology*, 63(10), 3872-3877.

Knowles, R. (1982). "Denitrification." *Microbiological Reviews*, 46(1), 43.

Koning, H. L. (1963). "Some observations on the modulus of compressibility of water." *Proceedings of the European Conference on Soil Mechanics and Foundation Engineering*, 1, 33-36.

Kramer, S. L. (1996). "Geotechnical earthquake engineering." Vol. 80, Prentice Hall Upper Saddle River, NJ: Prentice Hall.

Kutter, B. L. (2012). "Effects of capillary number, bond number, and gas solubility on water saturation of sand specimens." *Canadian Geotechnical Journal*, 50(2), 133-144.

Lade, P. V. (1993). "Initiation of static instability in the submarine Nerlerk berm." *Canadian Geotechnical Journal*, 30(6), 895-904.

Lade, P. V., and Hernandez, S. B. (1977). "Membrane penetration effects in undrained tests." *Journal of the Geotechnical Engineering Division*, 103(2), 109-125.

Lade, P. V., Nelson, R. B., and Ito, Y. M. (1987). "Nonassociated flow and stability of granular materials." *Journal of Engineering Mechanics*, 113(9), 1302-1318.

Lade, P. V., Nelson, R. B., and Ito, Y. M. (1988). "Instability of granular materials with nonassociated flow." *Journal of Engineering Mechanics*, 114(12), 2173-2191.

Lade, P. V., and Pradel, D. (1990). "Instability and plastic flow of soils. I: experimental observations." *Journal of Engineering Mechanics*, 116(11), 2532-2550.

Lawes, G. (1987). "Scanning electron microscopy and X-ray microanalysis." John Weiley and Sons Inc., New York, NY

Lee, C., Lee, J. S., Lee, W., and Cho, T. H. (2008). "Experiment setup for shear wave and electrical resistance measurements in an oedometer." *Geotechnical Testing Journal*, 31(2), 149-156.

Lee, K. L., and Albaisa, A. (1974). "Earthquake induced settlements in saturated sands." *International Journal of Rock Mechanics and Mining Sciences & Geomechanics Abstracts*. 11(8), Pergamon.

Li, B. (2014). "Geotechnical properties of biocement treated sand and clay." PhD thesis, Nanyang Technological University, Singapore.

Lorant, G. (2012). "Seismic design principles." *National Institute of Building Sciences. Available [online]*, 01-10.

Luo, J., White, R., Ball, P. R., and Tillman, R. (1996). "Measuring denitrification activity in soils under pasture: optimizing conditions for the short-term denitrification enzyme assay and effects of soil storage on denitrification activity." *Soil Biology and Biochemistry*, 28(3), 409-417.

Martin, G. R., Seed, H. B., and Finn, W. (1975). "Fundamentals of liquefaction under cyclic loading." *Journal of the Geotechnical Engineering Division*, 101(5), 423-438.

Martinez, B., DeJong, J., Ginn, T., Montoya, B., Barkouki, T., Hunt, C., Tanyu, B., and Major, D. (2013). "Experimental optimization of microbial-induced carbonate precipitation for soil improvement." *Journal of Geotechnical and Geoenvironmental Engineering*, 139(4), 587-598.

Meng, G. (2010). "The strength and deformation behaviour of a residual soil in Singapore." PhD thesis, Nanyang Technological University, Singapore.

Mitchell, A. C., Dideriksen, K., Spangler, L. H., Cunningham, A. B., and Gerlach, R. (2010). "Microbially enhanced carbon capture and storage by mineral-trapping and solubility-trapping." *Environmental Science & Technology*, 44(13), 5270-5276.

Mitchell, J. K., and Santamarina, J. C. (2005). "Biological considerations in geotechnical engineering." *Journal of Geotechnical and Geoenvironmental Engineering*, 131(10), 1222-1233.

Montory, B. M., and DeJong, J. T. (2015). "Stress-Strain Behavior of Sands Cemented by Microbially Induced Calcite Precipitation." *Journal of Geotechnical and Geoenvironmental Engineering*, 141(6), 04015019.

Montoya, B. M., Dejong, J. T., and Boulanger, R. W. (2013). "Dynamic response of liquefiable sand improved by microbial-induced calcite precipitation." *Géotechnique*, 63(4), 302-312.

Montoya, B. M., Gerhard, R., DeJong, J. T., Wilson, D. W., Weil, M. H., Martinez, B. C., and Pederson, L. (2012). "Fabrication, operation, and health monitoring of bender elements for aggressive environments." *ASTM Geotechnical Testing Journal*, 35(5), 728-742.

Mostafa, M., and Van Geel, P. J. (2007). "Conceptual models and simulations for biological clogging in unsaturated soils." *Vadose Zone Journal*, 6(1), 175-185.

Mycielski, R., Blaszczyk, M., Jackowska, A., and Olkowska, H. (1982). "Denitrification of high concentrations of nitrites and nitrates in synthetic medium with different sources of organic carbon. II. ethanol." *Acta Microbiologica Polonica*, 32(4), 381-388.

Nägele, W., and Conrad, R. (1990). "Influence of soil pH on the nitrate-reducing microbial populations and their potential to reduce nitrate to NO and $N_2O$." *FEMS Microbiology Letters*, 74(1), 49-57.

NCR (2006). "Geological and geotechnical engineering in the new millennium: Opportunities for research and technological innovation." Washington, DC, USA: National Research Council.

Okamura, M., Ishihara, M., and Oshita, T. (2003). "Liquefaction resistance of sand deposit improved with sand compaction piles." *Soils and foundations*, 43(5), 13.

Okamura, M., Ishihara, M., and Tamura, K. (2006). "Degree of saturation and liquefaction resistances of sand improved with sand compaction pile." *Journal of Geotechnical and Geoenvironmental Engineering*, 132(2), 258-264.

Okamura, M., and Soga, Y. (2006). "Effects of pore fluid compressibility on liquefaction resistance of partially saturated sand." *Soils and Foundations*, 46(5), 695-700.

Okamura, M., Takebayashi, M., Nishida, K., Fujii, N., Jinguji, M., Imasato, T., Yasuhara, H., and Nakagawa, E. (2009). "In-situ test on desaturation by air injection and its monitoring." *Japanese Society of Civil Engineering*, 65, 756-766.

Okamura, M., Takebayashi, M., Nishida, K., Fujii, N., Jinguji, M., Imasato, T., Yasuhara, H., and Nakagawa, E. (2011). "In-Situ desaturation test by air injection and its evaluation through field monitoring and multiphase flow simulation." *Journal of Geotechnical and Geoenvironmental Engineering*, 137(7), 643-652.

Okamura, M., and Teraoka, T. (2006). "Shaking table tests to investigate soil desaturation as a liquefaction countermeasure." *Geotechnical Special Publication*, 145, 282.

Onal Okyay, T., and Frigi Rodrigues, D. (2014). "Optimized carbonate micro-particle production by *Sporosarcina pasteurii* using response surface methodology." *Ecological Engineering*, 62, 168-174.

Phillips, A. J., Gerlach, R., Lauchnor, E., Mitchell, A. C., Cunningham, A. B., and Spangler, L. (2013). "Engineered applications of ureolytic biomineralization: a review." *Biofouling*, 29(6), 715-733.

Poulos, S. J., Castro, G., and France, J. W. (1985). "Liquefaction evaluation procedure." *Journal of Geotechnical Engineering*, 111(6), 772-792.

Prasad, S., Towhata, I., Chandradhara, G., and Nanjundaswamy, P. (2004). "Shaking table tests in earthquake geotechnical engineering." *Current Science*, 87(10), 1398-1404.

Qabany, A. A., and Soga, K. (2013). "Effect of chemical treatment used in MICP on engineering properties of cemented soils." *Géotechnique*, 63(4), 331-339.

Rad, N. S., and Lunne, T. (1994). "Gas in soil. I: detection and η-profiling." *Journal of Geotechnical Engineering*, 120(4), 697-715.

Rebata-Landa, V., and Santamarina, J. C. (2012). "Mechanical effects of biogenic nitrogen gas bubbles in soils." *Journal of Geotechnical and Geoenvironmental Engineering*, 138(2), 128-137.

Rebstock, D., Wienbroer, H., and Huber, G. (2010). "Liquefaction and reconsolidation in a 1-g shake-box testing device." *Physical Modelling in Geotechnics, Two Volume Set*, CRC Press, 1427-1432.

Robertson, P., Sasitharan, S., Cunning, J., and Sego, D. (1995). "Shear-wave velocity to evaluate in-situ state of Ottawa sand." *Journal of Geotechnical Engineering*, 121(3), 262-273.

Robertson, P., and Wride, C. (1998). "Evaluating cyclic liquefaction potential using the cone penetration test." *Canadian Geotechnical Journal*, 35(3), 442-459.

Robertson, P. K. (1994). "Suggested terminology for liquefaction." *47th Canadian Geotechnical Conference, Halifax, Canada, September*, 277-286.

Robertson, P. K., and Fear, C. E. (1995). "Liquefaction of sands and its evaluation." *Proceedings of the 1st International Conference on Earthquake Geotechnical Engineering*, Tokyo.

Rocker, K. (1968). "The liquefaction behavior of sands subjected to cyclic loading." Master thesis, Massachusetts Institute of Technology, Massachusetts, USA.

Roden, E. E., Leonardo, M. R., and Ferris, F. G. (2002). "Immobilization of strontium during iron biomineralization coupled to dissimilatory hydrous ferric oxide reduction." *Geochimica et Cosmochimica Acta*, 66(16), 2823-2839.

Roscoe, K. H., Schofield, A., and Wroth, C. (1958). "On the yielding of soils." *Géotechnique*, 8(1), 22-53.

Rusu, C., Cheng, X. H., and Li, M. (2011). "Biological clogging in Tangshan sand columns under salt water intrusion by Sporosarcina pasteurii." *Advanced Materials Research*, 250, 2040-2046.

Saggar, S., Jha, N., Deslippe, J., Bolan, N. S., Luo, J., Giltrap, D. L., Kim, D. G., Zaman, M., and Tillman, R. W. (2012). "Denitrification and $N_2O$:$N_2$ production in temperate grasslands: processes, measurements, modelling and mitigating negative impacts." *Science of The Total Environment*, 465, 173-195.

Saleh-Lakha, S., Shannon, K. E., Henderson, S. L., Goyer, C., Trevors, J. T., Zebarth, B. J., and Burton, D. L. (2009). "Effect of pH and temperature on denitrification gene expression and activity in *Pseudomonas mandelii*." *Applied and environmental microbiology*, 75(12), 3903-3911.

Sangadji, S., and Schlangen, E. (2012). "Self healing of concrete structures - novel approach using porous network concrete." *Journal of Advanced Concrete Technology*, 10(5), 185-194.

Seed, H. B. (1979). "Soil liquefaction and cyclic mobility evaluation for level ground during earthquakes." *Journal of the Geotechnical Engineering Division*, 105(2), 201-255.

Seed, H. B., and Booker, J. R. (1977). "Stabilization of potentially liquefiable sand deposits using gravel drains." *Journal of the Geotechnical Engineering Division*, 103(7), 757-768.

Seed, H. B., Idriss, I., and Arango, I. (1983). "Evaluation of liquefaction potential using field performance data." *Journal of Geotechnical Engineering*, 109(3), 458-482.

Seed, H. B., and Idriss, I. M. (1971). "Simplified procedure for evaluating soil liquefaction potential." *Journal of the Soil Mechanics and Foundations Division*, 97(9), 1249-1273.

Senbayram, M., Chen, R., Budai, A., Bakken, L., and Dittert, K. (2012). "$N_2O$ emission and the $N_2O/(N_2O + N_2)$ product ratio of denitrification as controlled by available carbon substrates and nitrate concentrations." *Agriculture, Ecosystems & Environment*, 147, 4-12.

Shen, J., and Cheng, X. "Laboratory investigation on restoration of Chinese ancient masonry buildings using microbial carbonate precipitation." *1st BioGeoCivil Engineering Conference*, Delft.

Sherif, M. A., Tsuchiya, C., and Ishibashi, I. (1977). "Saturation effects on initial soil liquefaction." *Journal of the Geotechnical Engineering Division*, 103(8), 914-917.

Šimek, M., and Cooper, J. (2002). "The influence of soil pH on denitrification: progress towards the understanding of this interaction over the last 50 years." *European Journal of Soil Science*, 53(3), 345-354.

Šimek, M., Jíšová, L., and Hopkins, D. W. (2002). "What is the so-called optimum pH for denitrification in soil?" *Soil Biology and Biochemistry*, 34(9), 1227-1234.

Smith, M. S., and Tiedje, J. M. (1979). "Phases of denitrification following oxygen depletion in soil." *Soil Biology and Biochemistry*, 11(3), 261-267.

Soleimani, S., Van Geel, P. J., Isgor, O. B., and Mostafa, M. B. (2009). "Modeling of biological clogging in unsaturated porous media." *Journal of Contaminant Hydrology*, 106(1-2), 39-50.

Stabnikov, V., Naeimi, M., Ivanov, V., and Chu, J. (2011). "Formation of water-impermeable crust on sand surface using biocement." *Cement and Concrete Research*, 41(11), 1143-1149.

Stevens, R., and Laughlin, R. (1998). "Measurement of nitrous oxide and di-nitrogen emissions from agricultural soils." *Nutrient Cycling in Agroecosystems*, 52(2-3), 131-139.

Stewart, T. L., and Fogler, H. S. (2001). "Biomass plug development and propagation in porous media." *Biotechnology and Bioengineering*, 72(3), 353-363.

Stocks-Fischer, S., Galinat, J. K., and Bang, S. S. (1999). "Microbiological precipitation of $CaCO_3$." *Soil Biology & Biochemistry*, 31(11), 1563-1571.

Su, D., Ming, H. Y., and Li, X. S. (2013). "Effect of shaking strength on the seismic response of liquefiable level ground." *Engineering Geology*, 166, 262-271.

Suwal, L. P., and Kuwano, R. (2013). "Disk shaped piezo-ceramic transducer for P and S wave measurement in a laboratory soil specimen." *Soils and Foundations*, 53(4), 510-524.

Swerts, M., Merckx, R., and Vlassak, K. (1996). "Denitrification, $N_2$-fixation and fermentation during anaerobic incubation of soils amended with glucose and nitrate." *Biology and Fertility of Soils*, 23(3), 229-235.

Tamura, S., Tokimatsu, K., A., A., and M., S. (2002). "Effects of air bubbles on B-value and P-wave velocity of a partly saturated sand." *Soils and Foundations*, 42(1), 121-129.

Terzaghi, K., Peck, R. B. (1948). *Soil mechanics in engineering practice*, John Wiley & Sons.

Thevanayagam, S., Kanagalingam, T., Reinhorn, A., Tharmendhira, R., Dobry, R., Pitman, M., Abdoun, T., Elgamal, A., Zeghal, M., and Ecemis, N. (2009). "Laminar box system for 1-g physical modeling of liquefaction and lateral spreading." *ASTM Geotechnical Testing Journal*, 32(5), 438-449.

Tokimatsu, K., and Seed, H. B. (1987). "Evaluation of settlements in sands due to earthquake shaking." *Journal of Geotechnical Engineering*, 113(8), 861-878.

Tsukamoto, Y., Ishihara, K., Nakazawa, H., Kamada, K., and Huang, Y. (2002). "Resistance of partly saturated sand to liquefaction with reference to longitudinal and shear wave velocities." *Soils and Foundations*, 42(6), 93-104.

Ueng, T. S., Wang, M. H., Chen, M. H., Chen, C. H., and Peng, L. H. (2006). "A large biaxial shear box for shaking table test on saturated sand." *ASTM Geotechnical Testing Journal*, 29(1), 1-8.

Valle-Molina, C., and Stokoe, K. H. (2012). "Seismic measurements in sand specimens with varying degrees of saturation using piezoelectric transducers." *Canadian Geotechnical Journal*, 671-685.

Van der Star, W., Van Wijngaarden, W., Van Paassen, L., Van Baalen, L., and Zwieten, G. (2011). "Stabilization of gravel deposits using microorganisms." *Proceedings of the 15th European Conference on Soil Mechanics and Geotechnical Engineering, Athens, Greece, 5-9 October 2011*, IOS Press.

Van Meurs, G., Van Der Zon, W., Lambert, J., Van Ree, D., Whiffin, V., and Molendijk, W. (2006). "The challenge to adapt soil properties." *Proceedings of the 5th ICEG: Environ. Geotechnics: Opportunities, Challenges and Responsibilities for Environmental Geotechnics*, 2, 1192-1199.

Van Paassen, L. (2011). "Bio-mediated ground improvement: from laboratory experiment to pilot applications." *Geo-Frontiers 2011 - Advances in Geotechnical Engineering*, ASCE, 4099-4108.

Van Paassen, L., Harkes, M., Van Zwieten, G., Van der Zon, W., Van der Star, W., and Van Loosdrecht, M. (2009). "Scale up of BioGrout: a biological ground reinforcement method." *Proceedings of the 17th International Conference on Soil Mechanics and Geotechnical Engineering*, 2328-2333.

Van Paassen, L., Pieron, M., Mulder, A., Van der Linden, T., Van Loosdrecht, M., and Ngan-Tillard, D. (2009). "Strength and deformation of biologically cemented sandstone." *International Society for Rock Mechanics*, ISRM Regional Symposium – EUROCK 2009, 29-31 October, Cavtat, Croatia.

van Paassen, L. A., Daza, C. M., Staal, M., Sorokin, D. Y., van der Zon, W., and van Loosdrecht, M. C. M. (2010). "Potential soil reinforcement by biological denitrification." *Ecological Engineering*, 36(2), 168-175.

Van Tittelboom, K., De Belie, N., De Muynck, W., and Verstraete, W. (2010). "Use of bacteria to repair cracks in concrete." *Cement and Concrete Research*, 40(1), 157-166.

Viggiani, G., Lenoir, N., Bésuelle, P., Di Michiel, M., Marello, S., Desrues, J., and Kretzschmer, M. (2004). "X-ray microtomography for studying localized deformation

in fine-grained geomaterials under triaxial compression." *Comptes Rendus Mécanique*, 332(10), 819-826.

Warren, L. A., Maurice, P. A., Parmar, N., and Ferris, F. G. (2001). "Microbially mediated calcium carbonate precipitation: implications for interpreting calcite precipitation and for solid-phase capture of inorganic contaminants." *Geomicrobiology Journal*, 18(1), 93-115.

Warthmann, R., Van Lith, Y., Vasconcelos, C., McKenzie, J. A., and Karpoff, A. M. (2000). "Bacterially induced dolomite precipitation in anoxic culture experiments." *Geology*, 28(12), 1091-1094.

Wartman, J., Seed, R., and Bray, J. (2005). "Shaking table modeling of seismically induced deformations in slopes." *Journal of Geotechnical and Geoenvironmental Engineering*, 131(5), 610-622.

Weier, K., Doran, J., Power, J., and Walters, D. (1993). "Denitrification and the dinitrogen/nitrous oxide ratio as affected by soil water, available carbon, and nitrate." *Soil Science Society of America Journal*, 57(1), 66-72.

Weil, M. H., DeJong, J. T., Martinez, B. C., and Mortensen, B. M. (2012). "Seismic and resistivity measurements for real-time monitoring of microbially induced calcite precipitation in sand." *ASTM Geotechnical Testing Journal*, 35(2), 12.

Whiffin, V. S., van Paassen, L. A., and Harkes, M. P. (2007). "Microbial carbonate precipitation as a soil improvement technique." *Geomicrobiology Journal*, 24(5), 417-423.

Whitman, R., and Lambe, P. (1986). "Effect of boundary conditions upon centrifuge experiments using ground motion simulation." *ASTM Geotechnical Testing Journal*, 9(2), 61-71.

Whitman, W. B., Coleman, D. C., and Wiebe, W. J. (1998). "Prokaryotes: the unseen majority." *Proceedings of the National Academy of Sciences*, 95(12), 6578-6583.

Wijngaarden, W. K., Vermolen, F. J., Meurs, G. A. M., and Vuik, C. (2012). "A mathematical model and analytical solution for the fixation of bacteria in biogrout." *Transport in Porous Media*, 92(3), 847-866.

Xia, H., and Hu, T. (1991). "Effects of saturation and back pressure on sand liquefaction." *Journal of Geotechnical Engineering*, 117(9), 1347-1362.

Yamamoto, S., Alcauskas, J. B., and Crozier, T. E. (1976). "Solubility of methane in distilled water and seawater." *Journal of Chemical and Engineering Data*, 21(1), 78-80.

Yamamoto, Y., Hyodo, M., and Orense, R. P. (2009). "Liquefaction resistance of sandy soils under partially drained condition." *Journal of Geotechnical and Geoenvironmental Engineering*, 135(8), 1032-1043.

Yamamuro, J. A., and Lade, P. V. (1997). "Instability of granular materials at high pressures." *Soils and Foundations*, 37(1), 41-52.

Yang, J. (2002). "Non-uniqueness of flow liquefaction line for loose sand." *Géotechnique*, 52(10), 757-760.

Yang, J., Savidis, S., and Roemer, M. (2004). "Evaluating liquefaction strength of partially saturated sand." *Journal of Geotechnical and Geoenvironmental Engineering*, 130(9), 975-979.

Yang, J., Savidis, S., Sato, T., and Li, X. (2003). "Influence of vertical acceleration on soil liquefaction: new findings and implications." *Proceeding Soil and Rock America*, 1.

Yasuhara, H., Okamura, M., and Kochi, Y. (2008). "Experiments and predictions of soil desaturation by air-injection technique and the implications mediated by multiphase flow simulation." *Soils and Foundations*, 48(6), 791-804.

Yegian, M., Eseller-Bayat, E., Alshawabkeh, A., and Ali, S. (2007). "Induced-partial saturation for liquefaction mitigation: experimental investigation." *Journal of Geotechnical and Geoenvironmental Engineering*, 133, 372.

Yoshimi, Y., Richart, F., and Prakash, S. (1978). "Soil dynamics and its application to foundation engineering. State-of-the-art report: Proc 9th International Conference on Soil Mechanics and Foundation Engineering, Tokyo, 1977, V2, P605-650." *International Journal of Rock Mechanics and Mining Sciences & Geomechanics Abstracts*, 15(2), p. A28.

Yoshimi, Y., T., K., and Kohji, T. (1989). "Liquefaction resistance of a partially saturated sand." *Soils and Foundations*, 29(3), 157-162.

Youd, T. L., and Hoose, S. (1977). "Liquefaction susceptibility and geologic setting." *Proceedings of 6th World Conference on Earthquake Engineering, New Delhi, India*, 37-42.

Youd, T. L., Idriss, I. M., Andrus, R. D., Arango, I., Castro, G., Christian, J. T., Dobry, R., Finn, W. D. L., Harder, L. F., Hynes, M. E., Ishihara, K., Koester, J. P., Liao, S. S. C., Marcuson, W. F., Martin, G. R., Mitchell, J. K., Moriwaki, Y., Power, M. S., Robertson, P. K., Seed, R. B., and Stokoe, K. H. (2001). "Liquefaction resistance of soils: summary report from the 1996 NCEER and 1998 NCEER/NSF workshops on evaluation of liquefaction resistance of soils." *Journal of Geotechnical and Geoenvironmental Engineering*, 127(10), 817-833.

Yu, X., Qian, C., Xue, B., and Wang, X. (2015). "The influence of standing time and content of the slurry on bio-sandstone cemented by biological phosphates." *Construction and Building Materials*, 82, 167-172.

Zhou, Y.-G., Chen, Y.-M., and Shamoto, Y. (2010). "Verification of the soil-type specific correlation between liquefaction resistance and shear-wave velocity of sand by dynamic centrifuge test." *Journal of Geotechnical and Geoenvironmental Engineering*, 136(1), 165-177.